GREEN SYNTHESIS OF LOW DIMENSIONAL MATERIALS FOR THE ADVANCED TECHNOLOGIES

THESIS SUBMITTED FOR THE AWARD OF THE DEGREE OF

Doctor of Philosophy

In
Applied Physics

By
Surya Pratap Goutam
Enrolment No.: 587/11

Under the Supervision of
Dr. Anil Kumar Yadav

Department of Applied Physics
School for Physical Sciences
Babasaheb Bhimrao Ambedkar University, Lucknow,
U.P., (India) – 226025

2018

This Thesis is

Dedicated to my

Parents and my

teachers

DECLARATION

I declare that the thesis entitled **"Green Synthesis of Low Dimensional Materials for the Advanced Technologies"** has been prepared by me under the supervision of Dr. Anil Kumar Yadav, Assistant Professor, Department of Applied Physics, School for Physical Sciences, Babasaheb Bhimrao Ambedkar University, Lucknow. No part of this thesis has formed the basis for the award of any degree, diploma or fellowship previously. Further, I declare that the material embodied in the present work is based on original research work and the indebtedness to others has been duly acknowledged at relevant places. This is also declared that the thesis is essentially free from all kinds of plagiarism.

Surya Pratap Goutam

(Surya Pratap Goutam)

Department of Applied Physics
School for Physical Sciences
Babasaheb Bhimrao Ambedkar University
Vidya Vihar, Raebareili Road,
Lucknow, (U.P.), India-226025

Date: 24/09/2018
Place: Lucknow

CERTIFICATE

This is to certify that the thesis titled **"Green Synthesis of Low Dimensional Materials for the Advanced Technologies"** submitted by **Mr. Surya Pratap Goutam** is an original research work and has not been previously submitted in part or full for the award of any other degree or diploma to this or any university.

The thesis submitted to Babasaheb Bhimrao Ambedkar University, Lucknow satisfies all the requirement as stipulated in *Doctor of Philosophy (Ph.D.) Regulations -1999 as amended in 2010* and it is fit for submission and evaluation for the award of the degree of Doctor of Philosophy of the University.

Date: 24/09/2018

Supervisor

24/9/18

Head of Department

ACKNOWLEDGEMENT

Many people have helped me to accomplish this thesis work, and I owe my gratitude to all of them.

First and foremost I would like to thank my advisor, Dr. Anil Kumar Yadav, without whose guidance and advice this dissertation would not be what it is today. His patience and support rescued me from despair on countless occasions.

I am also thankful to Prof. Devesh Kumar, Head, DAP, Babasaheb Bhimrao Ambedkar University (BBAU), Prof. Bal Chandra Yadav, Dr. Ramesh Chandra, Dr. Devendra Singh and Dr. Khem Bahadur Thapa for their constant support, blessings and co-operation that helped me to accomplish my thesis with determination.

I wish to express my gratitude to all members of National Centre of Experimental Mineralogy and Petrology (NCEMP), University of Allahabad, India especially Dr. Kamlesh Pandey, Dr. M.M. Dwivedi for offering their expertise. I am also grateful to the Director, Birbal Sahni Institute of Palaeobotany (BSIP), Lucknow for FESEM analysis; Dr. Richa Kothari, Assistant Professor, DES, BBAU for providing PTR from Solar Energy Laboratory for Experimental Studies; Director, Centre for Biomedical Research (CBMR), Sanjay Gandhi Post-Graduate Institute of Medical Sciences (SGPGIMS), Lucknow for kindly providing the liquid nitrogen for BET analysis; Dr. Subhash Awasthi, Incharge CETP, Unnao (India) for kindly providing the secondary treated TWW sample.

I am also thankful to Prof. Gajanan Pandey, Prof. Rajesh Kumar, Dr. Ram Naresh Bhargava, Mr. Gaurav Saxena, Mr. Amar Jyoti Das, Mr. Asok Gautam and Mrs.

Varunika Singh for their unrestricted support for the experimental requirements. I would like to thank all of my friends, especially Mr. Diptarka Roy, Mr. Raj Kamal Shastri, Mr. Asheesh Kumar, Mr. Utkarsh Kumar, Mr. Krishan Pal, Mr. Ratindra Gautam, Miss. Yash Kaur, Miss. Ruchi Mishra, Mr. Narendra Kumar, for their encouragement.

I would love to mention the appreciation to my brothers: Vimal Kumar Gautam and sisters: Uma Kumari Gautam; Anupam Gautam and Madhu Gautam for their thoughtful care and concerns for me.

Last, but certainly not least, my deepest thanks go to my parents (Mr. Omkar Singh and Mrs. Sadavati Devi) for supporting and encouraging me to achieve my goal. I am forever grateful to them for showing me the value of education.

This thesis work was financially supported by University Grant Commission (UGC), Government of India (GOI), New Delhi, India.

Surya Pratap Goutam

(Surya Pratap Goutam)

ABSTRACT

In the process of global efforts to reduce harmful chemicals and waste on this beautiful planet earth, there is always need to explore a method which is simple, cost-effective, non-toxic, biocompatible and productive, and could lead to the advancement in the nanoparticles (NPs) synthesis process. Plant-mediated synthesis of nanomaterials is a green chemistry approach that connects plant resources with nanotechnology.

To work in this direction, several crystalline metal oxide low dimensional materials in the form NPs (TiO_2, CuO, ZnO and Fe_2O_3) were synthesized in the present study at room temperature using green synthesis route for the environmental and biomedical applications. Further, green synthesized nanoparticles were characterized by using Scanning electron microscopy (SEM), Energy dispersive X-ray spectroscopy (EDS), Field Emission Scanning Electron Microscope (FESEM), Transmission electron microscopy (TEM), X-ray powder diffraction (XRD), Brunauer-Emmett-Teller (BET) analysis, Dynamic light scattering (DLS), Ultraviolet-Visible spectroscopy (UV-Vis), Fourier transform infrared spectroscopy (FTIR), and Photoluminescence spectroscopy for the investigation of their structural, morphological, elemental composition, functional groups and optical properties.

A study conducted on TiO_2 reveal a successful synthesis of nanoparticles using leaf extract of *Jatropha curcas L.* Obtained results confirmed the anatase phase of the spherical TiO_2 NPs with average crystalline size 13 nm, and also unfold the presence of phytochemicals in leaf extract, which might involve in the capping/stabilization of NPs. The surface area of the green synthesized TiO_2 NPs was determined by the Brunauer-

Emmett-Teller (BET) analysis whereas pore volume and pore size distribution were determined by the Barrett-Joyner-Halenda (BJH) analysis. Further, the green synthesized TiO_2 NPs were applied for the first time to testify its potential for the simultaneous removal of chemical oxygen demand (COD) and chromium (Cr) from secondary treated tannery wastewater (TWW) and 82.26% removal of COD and 76.48% removal of Cr from TWW was achieved upon the photocatalytic treatment.

Further, investigations on copper oxide demonstrate the formation of copper oxide nanoparticles by using leaf extract of *Jatropha Curcas L.* for the cytotoxicity test in hepatocellular liver carcinoma cell line HepG2. XRD result gives crystalline size as 45 nm while FTIR spectra reveal phytochemicals present in Jatropha curcas L. leaf extract play a significant role in the reduction/stabilization of cupric chloride ions. The cell viability assay showed that copper oxide nanoparticles exhibited to cancer cell killing ability without any evil effect on hepatocytes.

Coriandrum sativum leaf extract mediated synthesis of Zinc oxide and Iron oxide nanoparticles have been carried out for the antibacterial applications. TEM results demonstrated the presence of spherical nanoparticles ZnO of average particle size 40 nm, whereas dynamic light scattering examination shows average particle size of 55 nm, which were well supported by crystalline size 60 nm. Furthermore, FESEM analysis confirmed the successful synthesis of spherical shaped iron oxide NPs. Herein, Agar well diffusion method was used to assess the antimicrobial activity of synthesized nanoparticles against bacteria Escherichia coli. It was observed the interplay between the membrane biology of the pathogen and chemical and physical properties of medium appears to be a most important aspect of bactericidal properties.

Overall, the work reported in this thesis, clearly demonstrates that the green synthesis method provides progression over chemical and physical method and synthesized materials will not be used only in environmental applications but also in the development of nanoparticles based antimicrobial drugs for drug delivery advantageously.

Keywords: Green synthesis, Metal oxide nanoparticles; Wastewater Treatment; Antibacterial activity

PREFACE

"For a successful technology, reality must take precedence over public relations, for nature can not be fooled". **-Richard P. Feynman**

There has been remarkable growth over the globe in the synthesis of materials using 'green chemistry principles' in recent years. The term 'green chemistry' was postulated by Paul Anastas and John Warner, which refers to 'The use of a set of principles that minimize or eradicates the use or generation of hazardous solvents and chemicals in the synthesis, chemical analysis and application of chemical products. The motivation among the scientific community for the green synthesis as eco-friendly alternatives to chemical and physical methods is mainly because it is simple, inexpensive, efficient, more eco-friendly, non-toxic and require relatively lower processing temperatures. An extensive observation of literature shows that the research reported on the green synthesis of metal oxide nanoparticles (TiO_2, CuO, ZnO and Fe_2O_3) for environmental and biomedical applications such as water, wastewater treatment and antimicrobial activity are rarely available. This is the main cause which has given birth to my research problem for the doctoral work on such an important problem. In this context, we have synthesized TiO_2, CuO, ZnO and Fe_2O_3 metal oxide low dimensional materials in the form of nanoparticles with the objectives of their distinct environmental and biomedical applications by subjecting these nanoparticles to structural, morphological and optical characterizations. The results obtained from these studies have been systematically analyzed and discussed

to understand the structural, morphological and optical properties with the suitable background information.

The whole thesis comprises seven chapters.

C**hapter-1** is devoted to the general background about nanoscience and nanotechnology, role and importance of metal oxide nanoparticles in nanoscience and nanotechnology, their valuable properties and applications. Moreover, details of various synthesis techniques and a comprehensive review of research work carried out with birds eye view on green synthesis are described**.**

Chapter-2 presents a brief discussion of the characterization techniques employed in this study to characterize the synthesized materials. These include Scanning electron microscopy, Field emission scanning electron microscope, Transmission electron microscopy, Energy dispersive X-Ray spectroscopy, X-ray powder diffraction, Ultraviolet-visible spectroscopy, Fourier transform infrared spectroscopy and Dynamic light scattering analysis.

Chapter-3 is focused on the green synthesis of TiO_2 nanoparticles using leaf extract of Jatropha curcas L. and study of its characterization for the photocatalytic degradation of tannery wastewater. It also accounts for examination of the potential of green synthesized TiO_2 NPs for the simultaneous removal of chemical oxygen demand (COD) and chromium (Cr) from secondary treated tannery wastewater.

In Chapter-4, synthesis and characterization of copper oxide nanoparticles using leaf extract of Jatropha Curcas L. has been considered for the cytotoxicity test in hepatocellular liver carcinoma cell line HepG2. Morpho-structural and optical properties of nanoparticles were also explained.

Chapter- 5 deals about the synthesis of zinc oxide nanoparticles using *Coriandrum sativum* leaf extract and their structural and optical properties. Obtained results along with the antibacterial activity of NPs against the test bacteria E. coli have been discussed. The synthesized zinc oxide exhibited potential antibacterial activity.

In **Chapter- 6,** preparation of iron oxide nanoparticles using leaf extract of *Coriandrum sativum* is delineated in this chapter. Characterization of the synthesized sample was carried out by X-ray Diffraction (XRD), field scanning electron microscopy (FESEM), EDX, UV-Visible and FTIR spectroscopy. Moreover, the antibacterial activity of iron oxide nanoparticles has been studied.

Finally **Chapter- 7** describes the many salient results out of the research work, future prospects and scope of the thesis work.

LIST OF ABBREVIATIONS

AFM	Atomic force microscopy
ANOVA	Analysis of variance
As	Arsenic
ATSDR	Agency for Toxic Substances and Disease Registry
BET	Brunauer-Emmett-Teller
BJH	Barrett-Joyner-Halenda
BOD	Biochemical oxygen demand
CASTP	Conventional activated sludge treatment process
CETP	Common Effluent Treatment Plant
CETP	Common Effluent Treatment Plant
CNTs	Carbon nanotubes
CO	Carbon mono oxide
Co_3O_4	Cobalt(II,III) oxide
COD	Chemical oxygen demand
Cr	Chromium
Cr_2O_3	Chromium(III) oxide
$CrSO_4$	Chromous sulfate
Cu	Copper
Cu_2O	Cuprous oxide
CuO	Copper(II) oxide
CuO	Cupric oxide
CV	Cyclic voltammetry
DD	Double distilled
DLS	Dynamic light scattering
DNA	Deoxyribonucleic acid
DRS	Diffuse reflectance spectra
DSC	Differential scanning calorimetry/thermogravimetric analysis
E. Coli	*Escherichia coli*
EBT	Eriochrome Black T
EDDS	Ethylenediamine-N, N'-disuccinic acid
EDS	Energy Dispersive X-ray Spectroscopy
EDTA	Ethylenediaminetetraacetic acid
Emu	Electromagnetic unit
EPMA	Electron probe micro analyzer
EPR	Electron paramagnetic resonance
Fe_2O_3	Iron(III) oxide
Fe_3O_4	Iron(II,III) oxide
$FeCl_3$	Iron(III) chloride
FESEM	Field-emission Scanning Electron Microscope
FTIR	Fourier Transform Infrared
FWHM	Full width at half maximum
h ν	Photon energy
ICP-AES	Inductively coupled plasma atomic emission

	spectroscopy
JCLE	Jatropha curcus leaf extract
JCPDS	Joint Committee on Powder Diff raction Standards
KHz	Kilohertz
LSE	Lagerstroemia speciosa leaf extract
LTs	Leather tanneries
MCB)	Mono chlorobenzene
MG	Malachite Green
MHT	Magnetic Hyperthermia Therapy
MHz	Megahertz
mL	Mili Litre
mM	Mili mole
MO	Methyl orange
MRI	Magnetic resonance imaging
MTT	3-(4,5-dimethylthiazol-2-yl)-2,5-diphenyltetrazolium bromide
N_2	N_2
NADH	Nicotinamide adenine dinucleotide
Ni	Nickel
Nm	Nanometer
NNI	National Nanotechnology Initiative
NOx	Oxides of nitrogen
NPs	Nanoparticles
Pb	Lead
PTR	Parabolic trough reactor
PVD	Physical Vapour Deposition
RNA	Ribonucleic acid
ROS	Chemical element species
SAED	Selected Area Electron Diffraction
SEM	Scanning Electron Microscopy
SnO_2	Tin(IV) Oxide
SOx	Oxides of
SQUID	Superconducting quantum interference device
TDS	Total dissolved solids
TEM	Transmission Electron Microscopy
TGA	Thermogravimetric analysis
$TiCl_4$	Titanium chloride
TiO_2	Titanium dioxide
TWW	Tannery wastewater
USEPA	U.S Environmental Protection Agency
UV-Vis	Ultraviolet-Visible
Vd	Vanadium
VSM	Value stream mapping
VSM	Vibrating sample magnetometry
WWTPs	Wastewater treatment plants
XRD	X-Ray Diffraction

ZnO	Zinc oxide
α	Absorption Coefficient
B	Bita
γ	Gama
δ	Delta
Θ	Theta
λ	Wavelength
μM	Micro mole
ε	Dielectric Constant

LIST OF TABLES

LIST OF FIGURES

TABLE OF CONTENTS

Chapter: 1

Introduction

1.1. Nanoscience and Nanotechnology

Dreams and imagination of the mankind have been often causing the evolution of new science and technology. In the last few decades, enormous attention has been paid across the world on the research and development of nanomaterials in numerous fields with vital impacts on both fundamental science and industry, due to their unique physical and chemical properties. Nanoscience and nanotechnology have been considered to revolutionize the world of materials and to cause enormous impacts on the life of mankind in all sphere in the near future through innovative transformations. Nanoscience could be defined as an understanding of physical phenomena, properties, manipulation and control of materials within the size range 1-100 nm [1, 2]. At this size range, atoms and molecules behave differently and material properties may be different and surprising from those of the bulk materials. The word 'nano' comes from the Greek word 'Nanos' meaning a "dwarf", which means tiny or extremely small [1]. One-nanometer is an International system of a unit of length, equal to 10^{-9} meter. Nanoscale has different aspects in physics, chemistry and biology exclusively. Generally, in physics, nanoscale is related with the quantum behavior of electrons in nanostructures of materials. Sols, gels and emulsions are focused states of materials at the nanoscale in chemistry, whereas in biology RNA, DNA and subcellular organelles are treated as nanostructures and associated with Nanoscience [2]. Nanotechnology is the term which simply means the creation and exploitation of nanomaterials. In a broader sense, it concerns itself with the design, fabrication and applications of nanostructures and nanomaterials [1, 2]. Although, there are numerous views about the term

nanotechnology what exactly it is. Most of the researchers use U.S. National Nanotechnology Initiative (NNI) definition, which states that "nanoscience and nanotechnology are research and technology development at the atomic, molecular and macromolecular levels in the length scale of approximately the 1-100 nanometer range, to provide a fundamental understanding of phenomena and materials at the nanoscale, and to create and use structures, devices and systems that have novel properties and functions because of their small and/or intermediate size". The difference between nanoscience and nanotechnology primarily indicates the conceptual distinction between the term the science and technology. The different delineations of the nanotechnology specify that it should not be viewed as a single technique that affects particular areas, but as an interdisciplinary field of research which encompasses physics, chemistry, material science, engineering and biology. Though extensive interest in nanotechnology is recent, the emergence of nanotechnology and the exact time period of the modern development of nanotechnology are still difficult to define. Nevertheless, its entire concept is not new, and time span for the start of nanotechnology is explained by the very fact that it has its backgrounds within the distant past when individuals used it without an understanding of it. The Lycurgus Cup is a rare example of nanotechnology. It was created in the 4^{th} century by the dichroic glass in roman, which shows a different colour depending on whether or not light is passing through it. This glass appears red when the light drops on it from behind and appears green when the light drops on it from in front. It's been declared as the most spectacular glass of the period, that we all know to possess existed [3-7].

Moreover, the beginning of modern nanotechnology is attributed to the famous lecture of Richard Feynman titled "There's Plenty of Room at the Bottom" delivered in 1959 at the session of the American Physical Society [8, 9]. In the lecture, he envisioned the

possibility of manipulating matter at the atomic and molecular level and foreseen that ‘’It would be possible to put the 24 volumes of Encyclopaedia Brittanica on the head of a pin’. His novel idea revealed new ways of thinking amongst researchers and scientist. Almost 15 years after Feynman’s legendary talk, N. Taniguchi from Tokyo Science University coined the term “Nanotechnology” first time at the international conference on industrial production in Tokyo in 1974 for the explanation of the super skinny process of materials with nanometer accuracy and also the creation of nano-sized mechanisms [9]. The golden era of nanotechnology arose in the 1980s with the discovery of the advanced microscopic tool scanning tunnelling microscope in 1981 which enabled the observation at the level of atom and molecule, fullerenes in 1985, and with the publication of the book ‘Engines of Creation: The Coming Era of Nanotechnology’ by E. Drexler of Massachusetts Institute of Technology in 1986 [10], who was inspired from the lecture of Feynman. Drexler idea of nanotechnology is often termed ‘‘molecular nanotechnology.’’ Further, within the late 1980s to the first half of 1990s variety of important discoveries and inventions had been done which created an important impact on the furtherance of nanotechnology. The beginning of the 21st century witnessed an outstanding progression and enormous interest in the nanoscience and nanotechnology. Since then many radical advancements has been observed in several fields arising from the practice of nanoscience and nanotechnology.

1.2. Low Dimensional Materials

Low dimensional materials are essentially nanomaterials; refer to the materials with at least one of the three spatially dimensions reduced to nanoscale i.e. between 1 nm to 100 nanometers [11]. In other words, nanomaterials can be understood as the materials, which are characterized by at least in one of three dimensions by nanometer scale including both the sample of a material as a whole and its structural elements [12]. Low

dimensional materials exhibit superior and unique properties which do not exist in their bulk counterparts thus enable unprecedented prospects in a wide range of applications. The uniqueness of the structural features and properties of low dimensional materials is attributed to two major effects; firstly to the large surface area to volume ratio owing to their small size which brings out new physical and chemical properties in comparison to their bulk counterparts, and secondly size-dependent quantum confinement effects [12-15].

1.2.1. Classification of low dimensional materials

Various types of low dimensional materials have been reported in the literature depending on their source, dimension, size, shape and properties. On the basis of reduced dimensionality, low dimensional materials are usually classified as two dimensional: Quantum well, thin films, one dimensional: nanowires and nanotubes and zero-dimensional: quantum dots [16-18]. Furthermore, nanoparticles (NPs) are defined as the minute objects with three external dimensions in the range 1 nm – 100 nm. Nanoparticles act as a bridge between atomic/molecular structures and bulk materials.Nanoparticles can be broadly categorized into organic nanoparticles (fullerenes, dendrimers, micelles,) and inorganic nanoparticles. Inorganic nanoparticles comprise ceramics, metal (noble metals, iron, nickel etc.) and metal oxides nanoparticles (ZnO, TiO_2, CuO, iron oxides etc.) etc. These nanoparticles may be single crystal, polycrystalline and amorphous with all possible morphologies like spheres, cubes and platelets. If the nanoparticles are single crystalline, they are often referred to as nanocrystals. They have generated immense attention because of their superior properties with a variety of functions dissimilar to corresponding bulk materials. Size-dependent properties of nanoparticles are usually related with the quantum confinement effect, which occurs when any of the dimensions of material is reduced compared to de

Broglie wavelength, and to relatively higher surface to volume ratio [19-22]. Likewise, dimensional and material based classifications, nanoparticles can be further distinguished by their source of production. They have been reported to produce naturally in the atmosphere either by biological species or through human activities. The different types of intentionally produced or man-made nanoparticles, such as quantum dots, nanowires, nanotubes, nanorods, nanocrystals, nanoribbons, dendrimers, liposomes and polymeric micelles are produced by engine exhaust and smoke, paints and coatings, cosmetics and personal care products, textiles etc., sometimes forest fires, volcanic eruptions, or are synthesized through various physical, chemical, biological methods [23, 24].

1.2.2. Metal oxide nanomaterials

Metal oxide nanomaterials are most exciting material for the research and technological applications due to their outstanding physical, chemical, optical, thermal, electrical, electronic, properties [25]. Metal oxides play a vital role in a variety of applications and near about one third of the consumer product from the nanotechnology market is represented by metal oxide nanoparticles [26]; and some important applications of metal oxide nanoparticles are found in magnetic storage media [27], targeted drug delivery [28, 29], magnetic resonance imaging (MRI) [30-32], hyperthermia and cancer therapy [33-37], water remediation [38], magnetic ferrofluids [39, 40], magnetic refrigeration [41], microelectronic devices [42], sensors [43], fuel cells [44], coatings [45], catalysts [46], optoelectronic devices [47] etc. Metal oxide nanoparticles exhibit metallic, semiconducting or insulating behaviour due to the difference in electronic structure. Wide bandgap semiconducting oxides, such as SnO_2, ZnO and TiO_2 are useful for a number of applications, including transparent conducting oxides, gas sensors, and optical components [48]. The metal elements are capable to form a variety

of oxide compounds, which can adopt a large number of structural geometries with an electronic structure that can exhibit various interesting properties [49]. Oxides have long been used in a variety of technological applications, for example, almost all catalysts involve an oxide as active phase, promoter (or support) which allows the active components to disperse on. In the chemical and petrochemical industries, products worth billions of dollars are generated every year through processes that use metal oxide catalysts. For the control of environmental pollution, catalysts or sorbents that contain oxides are employed to remove the CO, NOx, and SOx species formed during the combustion of fossil-derived fuels [49].

1.2.2.1. Titanium dioxide nanoparticles

Titanium dioxide (TiO_2) NPs mainly exists in three phases: anatase, brookite and rutile. Rutile phase is a most stable phase in bulk, but for the solution-phase fabrication of TiO_2 NPs, anatase phase is the most stable and favorable phase of TiO_2 NPs. At the nanoscale, TiO_2 NPs shows quantum confinement which directs the movement of electrons and holes in semiconductor nanomaterials [50]. TiO_2 nanoparticles have the ability to solve the several serious environmental and pollution problems. These NPs are also playing a tremendous role in energy crisis through the effective application of solar energy based on photovoltaic and photocatalytic water-splitting devices and also have several elements adsorbent capacity [51]. It is the second most popular nanomaterial in shopper product, behind silver nanoparticles [52]. TiO_2 is used in sunscreens due to its ability to block UV radiation while remaining transparent on the skin; and its photocatalytic sterilizing properties also make it useful as an additive in construction materials.

1.2.2.2. Copper oxide nanoparticles

Copper oxide is a very valuable p-type semiconductor with a narrow band gap (1.85 eV) in bulk size [53]. Copper has two forms of oxides, namely cuprous oxide (Cu_2O) and cupric oxide (CuO) with energy band gap ~2.2 eV and 1.2 eV respectively [54]. NPs of copper oxide have unique and very valuable applications in the field of electronics and optoelectronics [55] and can be used in the development of semiconductors, supercapacitors, near-infrared filters, in magnetic storage media, sensors, catalysis etc. [56-58]. Nowadays, copper oxide (CuO) nanoparticles are getting much attention among the researchers because they may be used in biomedical applications due to their valuable biolytic and antimicrobial properties [59, 60]. CuO NPs are capable materials for the fabrication of solar cells and water pollution remediation due to their effective photoconductive and photochemical properties [61].

1.2.2.3. Zinc oxide nanoparticles

Zinc oxide is a wide band gap semiconductor of the II-VI group with the centrosymmetric type of structure. The native doping of the semiconductor (due to oxygen vacancies or zinc interstitials) is an n-type semiconductor [62]. Among various semiconducting materials, Zinc oxide is an idiosyncratic photonic n-type semiconductor with a wide band gap of 3.37eV and a high exciton binding energy (60 meV) at room temperature [63]. Zinc oxide shows the tetrahedral structure in its most common form, wurtzite. In tetrahedral structure each ion is enclosed by four ions of opposite charge which points towards the corners of a tetrahedron. Because of this type of structure two important properties piezoelectricity and pyroelectricity are the characteristic of zinc oxide [62]. The wide band gap of zinc oxide NPs has many benefits like enabling high temperature and power operations, reducing electronic noise, making sustenance in large electronic noise, making sustenance in large electric

fields possible and raising breakdown voltages. Those properties are used in emerging applications for transparent electrodes in liquid crystal displays, in energy-saving or heat-protecting windows and in electronics as thin film transistors and light-emitting diodes [64, 65]. ZnO NPs are a promising candidate for various applications, such as nanogenerators, gas sensors, biosensors, solar cells, photodetectors and photocatalysts, transparent electrodes in liquid crystal displays, in energy-saving or heat-protecting windows. Apart from this, bio-safe characteristics of ZnO make it very attractive for biomedical applications [66, 67].

1.2.2.4. Iron oxide nanoparticles

Iron oxides are common natural compounds and can also easily be synthesized in the laboratory up to the particle diameter in between approximately 1 and 100 nm. Various compounds of iron exist in the hydrosphere, the lithosphere and in the atmosphere as contaminants. Iron is a biocompatible element but some iron complexes can cause unsafe to humans and environment protection [68, 69]. Iron oxides exist in 16 different forms including oxides, hydroxides, and oxide-hydroxides. All these forms of iron oxides same on the base of composition of Fe, O, and/or OH occurs due to the aqueous reactions under various redox and pH conditions only differs by valency of iron. The two main forms of iron oxide nanoparticles consisting of magnetite (Fe_3O_4) and its oxidized form maghemite (γ-Fe_2O_3) have attracted extensive interest due to their superparamagnetic properties and find applications in magnetic data storage, biosensing, drug delivery, catalysis, sensors, and high-sensitivity biomolecular magnetic resonance imaging (MRI) for medical diagnosis and therapeutics etc.[70]. Eight iron oxides are known [69], among these iron oxides, hematite (α-Fe_2O_3), magnetite (Fe_3O_4) and maghemite (γ- Fe_2O_3) are very promising

and popular candidates due to their polymorphism involving temperature-induced phase transition [71].

1.3. Techniques for Nanomaterials Synthesis

Synthesis of metal oxide NPs is one of the fundamental benchmarks and is a rapidly growing area of research in the field of nanotechnology because it permits the control of particle size, shape, size distributions, and composition. There are various methods for the synthesis of nanoparticles. These routes of preparation are broadly grouped under two methods: Top-down and Bottom-up approach [72]. The top-down approach includes the physical processes such as milling, crushing etc. where larger bulk particles are systematically break up into small to smaller particles without atomic level control, as a result, nanoparticles are formed. Top-down approaches have a negative impact on the surface structure due to crystallographic imperfections created during the formation of the nanostructure, which is a major limitation of this approach as the chemistry of the surface and other valuable properties are mainly dependent on the surface structure [23,73]. On the other hand, in a bottom-up approach, nanoparticles are formed by self-assembly or putting together the smaller entities similar to the building a brick house [74]. Therefore, by controlling the chemical reactions and environment of a growing particle, desired size, shape and composition of the nanoparticles depending on the specific requirements can be achieved [23]. Many of these techniques can be tailored to be performed in gas, liquid, solid state phase, hence the applicability of bottom-up strategies to a wide range of end products. The bottom-up approach includes chemical and biological processes of production of NPs such as laser pyrolysis, sol-gel, plasma spraying process, aerosol-based prosses, green synthesis method etc. The bottom-up approach is very fabulous and far better as compared to a top-down approach to fabricate nanomaterials with uniform structures and distributions with less defects [75].

Different techniques employed to synthesize nanomaterials are discussed briefly, and for better understanding have been shown systematically in the Fig. 1.1.

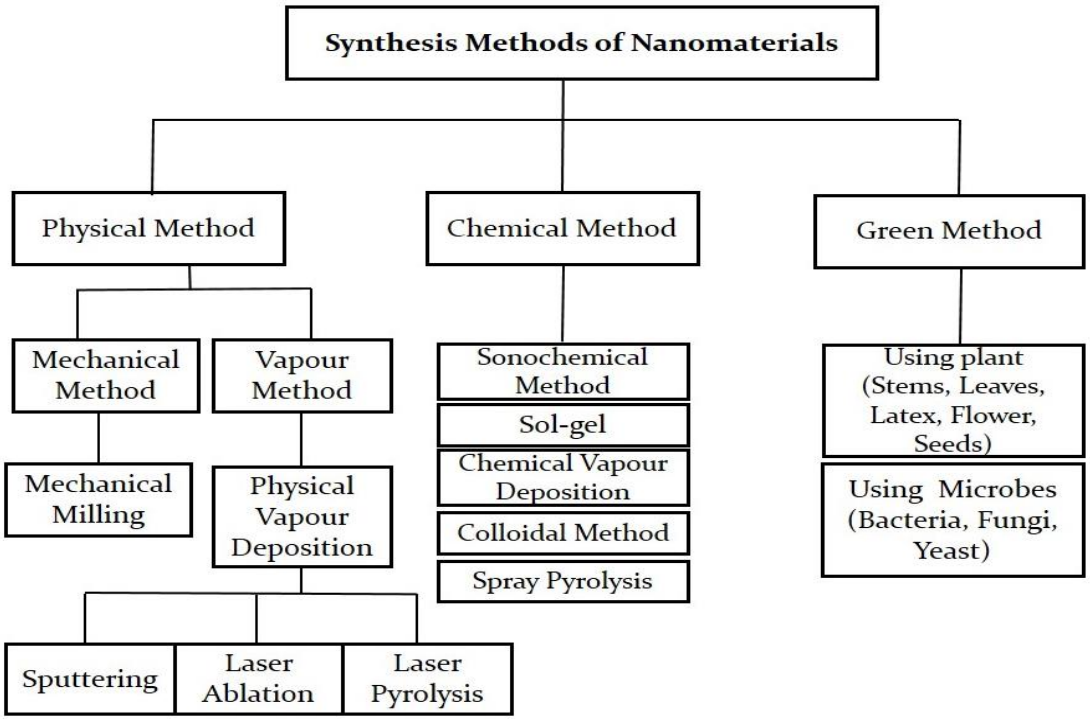

Fig. 1.1: Methods of nanomaterials synthesis

1.3.1. Sonochemical method

A chemical reaction occurs in the sonochemical method due to the irradiation of powerful ultrasound in the frequency range 20 KHz to 10 MHz through a probe submerged directly in the reaction solution.This method provides an extraordinary route to known materials without using high temperatures, high pressures, or long reaction times [76]. It has been used for the preparation of nanomaterials such as metal alloy, metal oxide and metal composites [77].

1.3.2. Mechanical milling method

Mechanical milling is a top-down approach for the synthesis of nanomaterials and nanocomposites on large scale. In mechanical milling, a high energy mill is required for milling the powder charge, and fine particles are produced from the bulk materials

during a collision with one another by the introduction of an agitator medium or high-speed air jets to produce enormous pressure and friction together [78]. However, the method suffers from drawbacks, such as very high energy consumption, structural defects, chemical disorders, and elastic strain introduced to parent bulk material during the whole process. Ball milling is an appropriate example of mechanical milling [79].

1.3.3. Physical vapor deposition

Physical Vapor Deposition (PVD) is a technique to deposit thin layers of material, typically in the range of a few nanometers to several micrometers. In this method nanostructures are produced at gas phase using a focused beam of electrons that heat the parent bulk material [80]. This method does not depend on any catalytic interaction during the synthesis process and there is no chemical reaction occurs from the start to the end of the process during the formation of final production from parent entity. Two most common PVD techniques are: thermal evaporation and sputtering. Thermal evaporation is a deposition technique that relies on vaporization of source material by heating the material using appropriate methods in a vacuum. Sputtering is a plasma-assisted technique that creates a vapor from the source target through bombardment with accelerated gaseous ions (typically Argon). In both methods, the resulting vapor phase is subsequently deposited onto the desired substrate through a condensation mechanism [81].

1.3.4. Laser ablation

Laser ablation is a technique in which, the material is removed from a solid surface by irradiating it with a laser beam to generate nanostructures under high vacuum system [80]. When the laser flux is low, the material is heated by the absorbed laser energy and evaporates and at high laser flux, the material is characteristically converted to a plasma. Commonly, laser ablation is achieved using pulsed laser and continuous wave

if the laser beam is sufficiently high. Laser pulses can vary over a very wide range of duration (milliseconds to femtoseconds) and fluxes, and can be precisely controlled. This makes laser ablation very valuable for both research and industrial applications [83].

1.3.5. Laser pyrolysis

Laser pyrolysis is a laser supported deposition technique where the vaporized reactant material is decomposed by using a potent laser beam in some inert gas environment. In this method, the reactant vapor atoms interact with inert gas atoms under collision, then deposited on a substrate to grow nanostructured film [84]. It is a very suitable gas-phase approach for the synthesis of a wide range of NPs at laboratory scale.

1.3.6. Sol-gel

The sol-gel method is a bottom-up method for producing solid materials from small molecules. It is a wet chemical technique to synthesize NPs by gelation follows by precipitation and calcination, respectively. Usually, the gel is organized from the stabilized sols where sols are often present in the form of colloidal aggregates of small metal oxy-hydroxy particles in an aqueous solvent [85, 86]. Hydrolysis and condensation play a pivotal role in a controlled way during gelation of the system. The relative rates of hydrolysis and condensation depend on various physical and chemical parameters such as temperature, pH, the concentration of metal ions precursor solution etc. The change in pH value affects the surface properties of the synthesized material remarkably, which occur due to the change in porosity of gel. As usual for the preparation of nanostructures, metal alkoxides are taken as precursors in some organic solvent. Sometimes in place of alkoxide, chelate also can use to be a precursor, which has the ability to stabilize the metal cations. Chelating facilitates mainly for the preparation of multicomponent gel, for example TiO_2-SiO_2 mixed gel, etc. [85]. The

sol-gel process is a cheap and low-temperature process that permits the good control of the product's chemical composition, especially metal oxide nanoparticles [86].

1.3.7. Chemical vapor deposition

Chemical vapor deposition technique is used to generate a highly pure nanostructural thin film having high performance. In this method, the precursor is deposited on the surface of a substrate by heating followed by evaporation to generate vapor, and the deposition occurs through a chemical reaction under vacuum in such a way to create a difference of chemical properties between precursor material and product. After exposing the surface of the substrate to the vaporized precursor, primarily a template is formed on the surface, thereafter nanostructures are formed on that template [85]. The formation of the nanostructure is always influenced by the reaction temperature, the reaction rate and also the precursor concentration during the deposition occurrence [88]. Overall, this method facilitates the uniform coating of nanostructures on the substrate surface, though there is some restriction due to the higher temperature requirement in the process.

1.3.8. Colloidal method

The colloidal method is a chemical precipitation method where different ionic solutions are mixed up to get precipitated by the adjustment of the reagent's concentration, capping agents and also by using the temperature and pressure in a controlled way [89]. This method has requirement of stabilizer to prevent agglomeration that arises mainly due to the presence of Vander Walls forces between colloidal NPs and can be stabilized electrically or sterically by Coulombic repulsions and adsorption of surfactants onto the NPs surfaces respectively [89]. This method is very popular to produce metal and metal oxide nanoparticles and useful in various organic and pharmaceutical fields.

1.3.9. Spray pyrolysis

Spray pyrolysis is a chemical deposition technique which is extensively used for the preparation of nanomaterial thin film. The formation of thin film depends on numerous parameters such as the spray rate, the temperature of the substrate, the concentration of chemical solution etc. The deposition efficiency can be improved by controlling the sizes of droplets and their distribution on the substrate during spraying [90]. It is a very easy approach to prepare nanostructures on the substrate as a film by taking facilities for doping of several elements with any proportions in spraying solution. There are no limitations on quality, dimension and surface properties of the substrate and thus, the method has certain positive impacts compared with the others vapor deposition techniques to have opportunities for industrialization [91].

1.3.10. Green synthesis for nanoparticles fabrication

Conventional methods of synthesis are bound with various limitations such as expensive equipment, generation of hazardous, toxic chemicals, the requirement of high temperature and pressure etc. [92]. Due to these drawbacks of conventional methods, researchers and scientist have been focusing on the biological systems and giving preference towards green approaches. In recent years, the development of efficient green chemistry methods for synthesis of metal NPs has become a major focus of researchers and scientist. They have investigated in order to find an eco-friendly alternative for the production of well defined NPs. It is an environment-friendly, cost-effective process to synthesize nanostructural material to have adjustable structures, morphologies and particle size distributions [93]. Recent progress displays an important role in biological synthesis for the production of nanomaterials. Green synthesis methods employ organisms like plant, bacteria, fungi etc., for the synthesis of nanomaterials, and it has become a very quickly rising area of research due to their less

or non-toxic nature, environment-friendly behavior and low cost of preparation. For the plant-mediated synthesis method, the plants are used to synthesize nanoparticles that have excessive potential in heavy metal accumulation mechanism and detoxification [94]. Production of metal NPs using plant organisms is one of the most considered methods. Plants organisms seem to be the best candidates and they are suitable for large-scale biosynthesis of NPs [95].

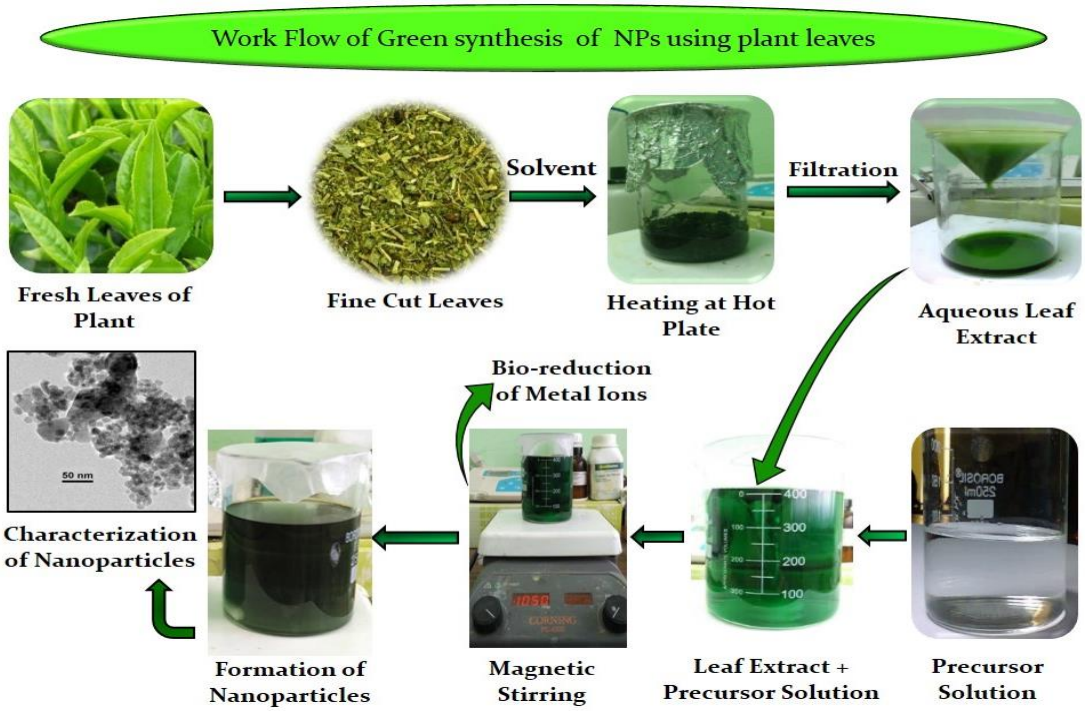

Fig. 1.2: The general process of green synthesis of nanomaterial using plant leaf

Plant extract can be prepared from leaves, stems, flower, seeds of various plants. The extract contains biomolecules such as protein, amino acid, enzymes, vitamins, terpenoids, flavonoids, alkaloids, phenolic acids, etc., which act as capping and reducing agents that can reduce metal ions during the bioreduction process to produce nanoparticles or nanostructures with different shapes and sizes [95,96].

1.4. Applications of Nanoparticles

Metal oxide NPs have been extensively used in various fields like electronics, water/ wastewater treatment, cancer therapy, sensing, antibacterial activity and cosmetics. etc.

1.4.1. Electronics

In the field of electronics, nanotechnology is playing an important role to overcome the disadvantage as high cost of fabrication of integrated circuits and physical size [97]. Currently, nanotechnology is covering a diverse set of electronic devices with effective and valuable characteristic behavior and improve the capabilities of electronic components as reducing the size of the material to the nanoscale.In nanotechnology, nanoelectronics has various approaches like nanomaterial electronics, molecular electronics, nanofabrication, nanophotonics and nanoionics etc [97]. Quantum dots are being used for producing more vibrant colors due to their more energy efficient behavior of ultra-high definition displays and televisions.

1.4.2. Water/wastewater treatment

Currently, the scarcity of drinking water resources and to develop the effective treatment of wastewater is a major challenge for the globe. It is an immediate need to develop the advanced wastewater treatment technology with high efficiency and low cost [98]. Nanotechnology for water and wastewater treatment is gaining momentum globally. The unique properties of nanomaterials and their convergence with current treatment technologies present pronounced opportunities to revolutionize the water and wastewater treatment. Currently, dyes degradation from wastewater is the most emerging area of research. The concentration of synthetic dyes in wastewater above permissible levels in wastewater may cause toxic effects on the human health as well as environment. These synthetic dyes are non-biodegradable, toxic and easily incorporated in the food chain. Various approaches have been using to remove dyes

from different industrial effluents. There are three techniques very popular for the wastewater treatment nowadays: nano-sorbents, nano-catalysts, nanomembranes and nanofiltration. The nanosorbent approach is the most influencing approach for dye removal because of its efficient nature [99]. NPs also have been using for the removal of heavy metal ions from wastewater [100]. Various metal oxide nanoparticles and other NPs with unique morphological and structural properties are using as adsorbents to develop the wastewater treatment approach and to enhance the efficiency and adsorption capacities of removing contaminants from wastewater [100].

1.4.3. Cancer therapy

In recent years, Nanotechnology is offering efficient and versatile tools for cancer detection and treatment [101]. Nanotechnology is an emerging area of research with wide applications in cancer treatment against cancer with early diagnosis, medicine, prediction and prevention and provides the advancement of cancer therapy [102]. Devices at the nanoscale are 100 to 1,000-fold smaller than cancer cells so they can be easily transferred through leaky blood vessels and interact with targeted tumor-specific proteins both on the surface and inside the cancer cells [103]. Currently, there are only three approaches are available for cancer therapies which have a risk to damage normal tissues. Cancer nanotechnology provides an increased probability of survival and decreased risk to the patient by offers the means to target chemotherapies directly and selectively to cancerous cells and neoplasms, guide in surgical resection of tumors, and enhance the therapeutic efficacy of radiation-based and other current treatment modalities.

1.4.4. Sensing

Various nanoelements such as metal oxide NPs, nanotubes and nanowires can be used as a sensor. Due to the small size of nanoelements, a very few gas molecules are

sufficient to change the electrical properties of the sensing element [104]. Sensing by using nanosensors is mainly targeted to small, inexpensive sensors that can sniff out chemicals. Nanosensors are very small and inexpensive which can easily identify the chemical vapor and can be used in the applications as sensors in industrial plants that use chemicals in manufacturing to detect the release of chemical vapors, throughout an airport, to check for vapors given off by explosive devices or any facility with security concerns. These sensors can also be used in the detection of escaped hydrogen. Nanosensors can also be used in air quality monitoring to improve the tracking of air pollution sources [104].

1.4.5. Antimicrobial activity

Bacterial infections are a major cause of morbidity and mortality yet, whether numerous potent antibiotics are available nowadays. High incidence of bacterial infection and the growing resistance of bacteria to conventional antibiotics induced urgent need to develop additional antibacterial means which would be helpful to solve the problem of multidrug-resistant bacterial strains and biofilm-associated infections. Nanoparticles have been gaining too much interest among researchers and scientist for the development in the field of antimicrobial chemotherapy. Three things are the center of focus for the study of NPs as an antibacterial agent which are the mode of action, NPs effect on drug-resistant bacteria, and the risks attendant on their use as antibacterial agents [105]. Nanomaterials with their unique properties at nanoscale getting great interest as a process to kill or reduce the activity of several microorganisms [106].

1.4.6. Cosmetics

Nowadays, nanotechnology has found new applications in various fields, nanocosmetics are one of the emerging application of nanotechnology which is gaining great interest in the field of cosmetics. Many cosmetic products like sunscreen,

moisturizers, hair care products and makeup have been using with improved performance using nanotechnology. The enhanced properties of nanomaterials such as solubility, color and transparency from their bulk size greatly influencing to cosmetic industries. Various nanomaterials like metal oxide nanoparticles (ZnO, TiO_2 etc.) being employed in cosmetics [107,108]. Researchers and scientist who are working on nano cosmetics also focusing on the potential risks caused by nanoparticles both to human life and also to the environmental safety, and they are also trying to reduce toxic effects of nanoparticles.

1.5. Review of Literature

Carvalho et al., successfully synthesized iron oxide NPs (maghemite 7 nm and magnetite 20 nm.) using two approaches reduction-precipitation method under air and precipitation method in a controlled atmosphere. In this research work, the author established the relationship between the composition of iron oxide nanoparticles and their size, structural, morphological and magnetic properties of the synthesized material. They described that, In $Fe_{3-x}O_4$, when X will decrease the particle size of the nanoparticles will increase. The result shows the compatibility with core-shell structure model where a magnetic core is surrounded by an oxidized magnetite layer and found that the magnetite core dimension depends on the average particle size. Results, also show that the reduction precipitation method allows obtaining smaller particles than the classical precipitation process [109]. Periyathambi et al., successfully synthesized the iron oxide nanoparticles and fibrin functionalized iron nanoparticles for developing them as efficient and novel MRI contrast agents for early diagnosis of cancer. Acid leaching method was used in this work for the preparation of iron oxide nanoparticles and co-precipitation method was used for the preparation of fibrin functionalized iron nanoparticles and found the average size distribution 15 nm and 35 nm respectively.

Biocompatibility of synthesized nanoparticles was tested using Haemolysis and MTT assay. Further, MRI and VSM were used to analyze the magnetic property of fibrin functionalized iron nanoparticles, with the magnetic saturation value of 51.7 emu/g. In this study, as per the high compatibility and good magnetic property, fibrin functionalized iron nanoparticles were considered as effective MRI contrast agents and drug delivery agent [110]. Asmathunisha et al., reported a brief review on the biosynthesis of nanoparticles by marine organisms. In the review efficacy of nanoparticles in cancer treatments, the toxicity of nanoparticles prepared by various marine extracts on cancer cells and normal cells has to be largely studied. Various Marine microorganisms like bacteria (E. coli, Pseudomonas sp.), cyanobacteria (*Spirulina platensis, Oscillatoria willei, Phormidium tenue*), yeasts (*Pichia capsulata, Rhodospiridium diobovatum*), fungi (*Thraustochytrium sp., Penicillium fellutanum, Aspergillus niger*), and algae (*Navicula atomus, Diadesmis gallica, Stauroneis sp. Sargassum wightii, Fucus vesiculosus*) are rich sources of reducing agents and have reported for the synthesis of inorganic nanoparticles which were briefly described in this review [111]. Schrofel et al., reported a comprehensive review on the applications of biosynthesized metallic NPs. In this review several applications like catalytic applications, antimicrobial and biomedical applications were described which avail the benefits of biosynthesis over conventional methods (chemical or physical) of NPs syntheses. Biosynthesis of NPs provides the lower capital and operating expenses and reduced environmental impacts. Biocompatibility and stability of the NPs products synthesized by biological methods also described in this review [112]. Ahmed et al., briefly described the previously performed research work on the biogenic synthesis of ZnO NPs using plants and microbes and elaborate the critical mechanism behind the photosynthesis of ZnO NPs. This review described that how the nanotechnology

provides advancements in the field of medicine, science and engineering etc. This review paper also describes the limitations of conventional methods and advancement of the biogenic approach of the NPs synthesis. Further, the biogenic approach of ZnO nanoparticles synthesis defined as eco-friendly and considered it free of chemical impurities for effective biological applications. This study states that the use of plant extracts for ZnO nanoparticles synthesis is advantageous over the use of microorganisms due to no need of less toxic chemicals and difficult process of maintaining cell cultures [113]. Alagiri et al., successfully synthesized the α-Fe_2O_3 nanoparticles using Curcuma and tea leaves extract as a reducing and stabilizing agent. The crystal structure and particle size of α-Fe_2O_3 NPs using Curcuma and tea leaves extract were well described with the help of XRD analysis and the crystal structures were found rhombohedral and the particle sizes were found 4 and 5 nm respectively. Scanning electron microscopy (SEM) images revealed that the synthesized nanoparticles were spherical-like shaped with homogeneous size distribution. Raman spectroscopy was also performed to know the purity and properties of biologically synthesized α-Fe_2O_3 nanoparticles; the chemical composition of samples were analysed with the help of Fourier transform infrared spectroscopy. The absorption edge of synthesized nanoparticles using Curcuma and tea leaves were 561 and 551 nm and the band gap energy of were found at 2.2 eV and 2.25 eV. The photocatalytic activities of synthesized nanoparticles were measured by the degradation of methylene orange and found that the synthesized nanoparticles showed the excellent photocatalytic performance [114]. Anjum et al., reviewed the various reports on remediation of wastewater using various nanomaterials and unfold the challenges in the development and implementation of advanced wastewater treatment technologies with high efficiency and low capital requirement. This review demonstrated the potentiality of

nanomaterials for wastewater treatment and discussed the utilization of various classes of nano-materials for the wastewater treatment. As per variously reported literature in this review, it is clear that nanotechnology is one of the ideal options for advanced wastewater treatment approaches. This study also includes the investigation of various nanomaterials as nano-adsorbents, photocatalysts and nano-membranes. Nanoparticles as nano-adsorbents have efficient potential to remove heavy metals such as Cr, As, Hg, Zn, Cu, Ni, Pb and Vd from wastewater and as photocatalysts they may be used for treatment of both toxic pollutants and heavy metals, where the modification in catalyst material can provide the capability of using visible region of solar light instead of high cost artificial ultraviolet radiation. Nanoparticles as nanomembranes have been proven highly effective for reducing foulants, heavy metal and dyes in the filtration process of wastewater [99]. Arshadi et al., reports the synthesis of Co activated organo-functionalized SiO_2-Al_2O_3 mixed-oxides nanoparticles used as a scavenger of dyes such as methyl orange and then modified by Schiff base ligand. Si/Al-PAEA= SA@Co was also synthesized on the organo-functionalized mixed-oxides. Synthesized nanomaterials were characterized by transmission electron microscopy (TEM), Brunauer-Emmett-Teller (BET), Fourier transform infrared (FTIR), UV-Vis diffuse reflectance spectra (UV-Vis DRS), inductively coupled plasma atomic emission spectroscopy (ICP-AES), cyclic voltammetry (CV) and electron paramagnetic resonance (EPR). The heterogeneous Co ions were proved to be a potent adsorbent for the capture of methyl orange from aqueous media. Some removal conditions such as contact time, initial dye concentration, pH and adsorbent dosage on the removal efficiency of MO will influence the dye adsorption. Results of EPR and CV of Si/Al-PAEA = SA@Co confirmed that majority of the active sites of the nano-adsorbent are in the form of Co(II) ions. This study clearly suggested that the MO dye in contaminated

water could be efficiently removed with immobilized Co ions [99]. Behra and Giri successfully synthesized cuprous oxide (Cu_2O) nanoparticles (NPs) using Arka (*Calotropis gigantea*) leaves extract. Average crystallite size of synthesized nanoparticles was found 8.8 nm. With the help of illumination of visible light, the photo-bleaching activity of Cu_2O NPs was studied on the aqueous methylene blue (MB) dye. This study shows that as per absorption spectra that a red shift in its peak position as a function of irradiation time is proposing that oxide particles are degrading the organic dye in an aqueous medium. In the vibration spectra of MB in presence of Cu_2O NPs suggest that the surface adsorption of MB over NP's surfaces due to the red shift in the C-H stretching band (2954, 2926, and 2855 cm^{-1}) of methylene group and C-N stretching band (1343 and 1226 cm^{-1}). Absorption spectra shown that % decomposition of MB dye decreases non-linearly in the presence of Cu_2O NPs and it was found 90% after light exposure for 120 min. This study also confirm that the Cu_2O NPs can be reclaimed and they will maintain their original catalytic activity because XRD crystallite size of the particles hardly alters after implying adsorption of MB dye on the surface. Existence of interfacial interaction between MB dye and Cu_2O NPs, which is responsible for photodegradation of MB dye in presence of oxide NPs suggested by the characterization techniques XPS, FTIR, and zeta potential. Dynamic quenching mechanism in this system also introduced by a linear Stern-Volmer plot. In presence of Cu_2O NPs extensive quenching in the emission intensity of MB molecules was observed which was attributed to the existence of a charge transfer-type interaction between oxide NP and MB molecules as transference of non-bonding electron (n) occurs from S-atom of MBH molecules to the surface of oxide NPs [115]. Bagheri et al., synthesized titanium dioxide NPs in anatase phase via a sol-gel process using with and without freshly water-soluble egg white proteins. Egg white proteins work as a

gelling agent which provide long-term stability for nanoparticles by preventing the particles from agglomeration. Synthesized nanoparticles characterized by XRD, TEM, FTIR, UV-Vis and thermogravimetric analysis (TGA). The sizes of titanium dioxide NPs with and without using egg white solution are were found at 12.55 ± 3.42 nm and 21.45 ± 4.21 nm, respectively. This study confirmed that egg white solution is a suitable gelling agent for preparing titanium dioxide NPs by using sol-gel method [116].

Beyth et al., reviewed a paper on nano-antimicrobial materials as an alternative antimicrobial approach. This review emphasized the need to grow additional bactericidal resources significantly increased due to the growing concern concerning multidrug-resistant bacterial strains and biofilm-related infections. In this study, nanoparticles were suggested as the emerging materials for antimicrobial chemotherapy. This study also discussed the activities of nanoparticles as an antimicrobial means, their mode of action, nanoparticle effect on drug-resistant bacteria, and the risks attendant on their use as antibacterial agents. The small size of metal, organic, and additional nanoparticle are very appropriate for antimicrobial biological applications and have shown tremendous potential as bactericidal and fungicidal elements. Potential of nanoparticles also demonstrating as efficient antibiotic reagents. The efficiency of the nanoparticles is related to their size, shape and concentration. Various antimicrobial nanomaterials offer protracted antimicrobial activity with very less toxicity comparatively with small molecular antimicrobial agents which show the environmental toxicity [105]. Bhandare and Narayana reported a review on applications of nanotechnology in cancer and studied numerous reports on imaging and treatment. Nanotechnology in cancer treatment is a comparatively novel interdisciplinary area of comprehensive research which combines various fields like biology, chemistry, medicine and engineering. Submolecular interactions in NPs

propose unique and novel methods with a wide spectrum of applications in cancer treatment with various fields as prognostics, diagnostics, and therapeutics. NPs are constructed to transport myriad substances in a controlled and targeted way to malignant cells and minimize the damage to normal cells. NPs demonstrate the potential in both cancer diagnosis and therapy nanoparticles may be able to transport functions beneficial for diagnosis and treatment of cancer [101]. Biswas et al., reviewed the nanotechnology-based approaches in cancer therapeutics. Nanomedicine is playing a key role in the development of new delivery methods for optimum treatment outcome and offers many advantages over conventional drug delivery processes mainly for anticancer research. This review mainly focused on the identifying new delivery processes as well as progress in clinical trials by using nanotechnology and to study of various properties of NPs and their use in anticancer treatment [117]. Buzea et al., reported a review of scientific interest on nanoparticles, their origin, activity, and biological toxicity. NPs affect the human health, which is related with individual factors such as genetics and existing disease and nanoparticle chemistry their size, shape and electromagnetic properties. NPs show the toxicity due to their small size and they are also smaller than cells and cellular organelles which allows the nanoparticles to penetrate biological structures and disturbing their usual behaviour. Toxic effects of NPs includes the tissue inflammation, changed cellular redox balance to oxidation, which caused the cell death. This study suggested a balanced science-based method to minimize damage caused by nanomaterials which supporting sustained study and suitable development in industrial fields. It is described that nanotechnologies associated with health risks, so it is required for the smart handling of nanomaterials. This study also reveals the outcomes of life's long history of evolution with nanotechnology and described how the human body in particular has adapted to defend

itself against nanoparticulate interlopers [118]. Misra et al., reviewed the studies to describe the processes of cancer nanotechnology which can play a key role in the advancement of cancer therapy. Nanotechnology is the emerging application for cancer therapy and gaining significant attention through prediction, prevention and early diagnosis and medicine. Nanotechnology may play a significant role in the field of Target-specific drug therapy and processes of early diagnosis of pathologies [102]. Akhtar et al., investigated the cytotoxicity of ZnO NPs against three types of cancer cells (human hepatocellular carcinoma HepG2, human lung adenocarcinoma A549, and human bronchial epithelial BEAS-2B) and two primary rat cells (astrocytes and hepatocytes). This study describes that ZnO NPs induce selective killing of cancer cells and also resulted that ZnO NPs exert distinct effects on mammalian cell viability via killing of all three types of cancer cells while posing no impact on normal rat astrocytes and hepatocytes. Human liver cancer HepG2 cells have been used in this study to investigate the toxicity mechanisms of ZnO NPs. Authors demonstrated that ZnO NPs selectively induce apoptosis in cancer cells, which is likely to be mediated by reactive oxygen species via p53 pathway, through which most of the anticancer drugs trigger apoptosis and provides preliminary guidance for the development of liver cancer therapy using ZnO NPs [119]. Choudhary et al., reported the green synthesis of gold nanoparticles using Lagerstroemia speciosa leaf extract (LSE). It suggested on basis of UV-Vis spectroscopy and TEM that the morphology and size distribution of AuNPs depends on various parameter the pH of the gold solution, gold concentration, the volume of LSE, and reaction time and temperature. This study also described the role of polyphenolic functional groups as capping agents presented in the *Lagerstroemia speciosa* leaf extract (LSE) with the help of comparison between Fourier transform infrared spectroscopy (FT-IR) spectra of LSE and the synthesized AuNPs. It resulted

that the green synthesized AuNPs have strong and stable photocatalytic activity in the reduction of dyes methyl orange, methylene blue, bromocresol green, bromophenol blue and 4-nitrophenol under visible light in the presence of $NaBH_4$ and useful in environmental applications, particularly in the reduction of organic pollutants in wastewater [120]. Madhubala and Kalaivani successfully synthesized the Fe_3O_4@ZnO core-shell nanoparticles combination of phyto and hydrothermal synthesis at different concentrations of molar ratio. Synthesized nanoparticles have better morphology, small particles size of 45 nm and high crystallinity at molar ratio 1:20 than the 1:5 and 1:10. Thermo Gravimetric Analyzer (TGA) resulted that the prepared core-shell NPs are highly stable at higher temperatures. Synthesized core-shell NPs were also performed for the cytotoxicity test against vero cells with the help of MTT colorimetric assay, which shows the concentration of the core-shell nanoparticles has a great impact on the viability of cells and when the concentration of nanoparticle higher than the number of killed cells increases. This work suggested that lowest concentrations of Fe_3O_4@ZnO core-shell nanoparticles are applicable for the biomedical applications and due to its high stability this magnetic nanoparticle can be useful in the Magnetic Hyperthermia Therapy (MHT) for cancer treatment [121]. Das et al., reported a green method to synthesize Ag NPs at room temperature by using *Ocimum gratissimum* leaf extract for bioreduction of silver ions from silver nitrate salt. This study describes the need of antimicrobial agent for novel therapies against multi-drug resistant bacteria using green nanotechnology. Biosynthesis of Ag NPs has shown a stimulating effect against bacterial infection. Synthesized Ag NPs have a diameter of 31 nm with a polydispersity index of 0.65 and 15 mV zeta potential. Scanning and transmission electron microscopy were also performed which give the dry sizes of 18± 3 nm and 16 ± 2 nm respectively. This study resulted that the promising green biosynthesis of Ag NPs which shows the

potent antimicrobial activity against E. coli and S. aureus [122]. Davar et al., was performed green synthesis of ZnO NPs using lemon juice for the application as a novel photocatalyst. In the synthesis process, zinc acetate was used as precursor and effect of the addition of sucrose on the initial precursors was also investigated. Green synthesized samples were characterized using various techniques FE-SEM, XRD, FTIR, UV-Vis and photoluminescence (PL) spectroscopy. Mean particle size of the synthesized samples was found 21.5 nm and the sample was further used as photocatalyst and tested for the degradation of methyl orange, methyl red and methylene blue solutions. It revealed that the sample had shown good photocatalytic activity for the degradation of used all three organic dyes. Moreover, the sample was also performed for decolorization technique and the treatment of textile dyes and indicated that the sample was a promising photocatalyst for practical applications in the photocatalytic degradation of textile dye [123]. Devatha et al., reported the green synthesis of iron nanoparticles using various leaf extracts viz. *Mangifera indica, Murraya Koenigii, Azadiracta indica, Magnolia champaca* for the treatment of domestic waste water. Green synthesis of iron nanoparticles described as cost-effective and eco-friendly approach. Synthesized samples were characterized by SEM equipped with EDS, UV-Vis spectrophotometer and FTIR spectroscopy confirmed the formation of iron nanoparticles and presence of biomolecules which helped in capping the iron NPs. Iron nanoparticles synthesized using *Azadirachta indica* leaf extract showed satisfactory results compared to other leaf extracts for the treatment of domestic wastewater. To know the effectiveness of synthesizing Fe NPs using various leaf extracts, samples were performed for the treatment of domestic wastewater by analyzing various parameters like total phosphates, ammonia nitrogen and total COD. This research work showed that removal of total phosphates, ammonia nitrogen and

COD using *Azadirachta indica*-Fe NPs were found to be 98.1%, 84.3% and 82.4% respectively. This work also proves that *Azadirachta indica*-Fe NPs were found more effective for the treatment of domestic wastewater than other Fe NPs [124]. Dizaj et al., reported a review on the current research works on metal and metal oxide NPs in antimicrobial activity with their action mechanism. According to this review, reported literature shows that size of the nanoparticles play a very significant role to determine the antimicrobial effectiveness of the metal or metal oxides nanoparticles and could be advanced in the pharmaceutical and biomedical industries for sterilization of the medical devices. This study suggests that the therapy with the metal or metal oxide nanoparticles may be one of the possible beneficial strategies to overcome the current bacterial resistance to the antibacterial agents. Moreover, this study performed to unfold all the opportunities to minimize the toxicity of metal and metal oxide nanoparticles to apply as proper alternatives for antibiotics and disinfectants especially in the field of biomedical applications. This study described that the ion doping and polymer conjugates of nanoparticles could be helpful to decrease the related toxicity. Conclusively, this study remarks that metal or metal oxide nanoparticles with the minimized toxicity could be extensively used in the near future for removing numerous infectious disorders [125]. Dobrucka and Dugaszewska reported the synthesis of ZnO nanoparticles using *Trifolium pratense* flower extract to determine their antimicrobial efficacy against clinical and standard strains of *S. aureus* and *P. aeruginosa* and *E. coli.* ZnO nanoparticles synthesis using plants has been used as an alternative to conventional physical and chemical methods. Synthesized ZnO nanoparticles were characterized by various techniques X-ray diffraction (XRD), scanning electron microscopy (SEM), Energy dispersive X-ray analysis (EDX). UV–Vis absorption spectroscopy and Fourier transform infrared spectroscopy (FT-IR). Characterization

techniques confirm the size of synthesized nanoparticles in the range 60–70 nm and further this study shows the high activity of ZnO nanoparticles against S. aureus ATCC 4163, E. coli ATCC 25922, P. aeruginosa ATCC 6749, S. aureus and P. aeruginosa [126]. Ehrampoush et al., reported the green synthesis of iron oxide nanoparticles using tangerine peel extract for cadmium removal from aqueous solution. Concentrations of tangerine peel had an impact on the size of nanoparticles. It was found that when the concentration of tangerine peel extract was increased from 2 to 6 %, the average size of iron oxide nanoparticles decreased from 200 nm to 50 nm. Synthesized nanoparticles show the maximum removal of cadmium ions (90 %) occurred at pH of 4 and adsorbent dose of 0.4 g/100 ml and work as good adsorbent for the removal of cadmium from wastewater [127]. El-Kassas et al., reported the green synthesis of iron oxide nanoparticles (Fe_3O_4-NPs) by reduction of ferric chloride solution using brown seaweed water extracts. Extract of the two seaweeds *Padina pavonica* (*Linnaeus) Thivy and Sargassum acinarium (Linnaeus) Setchell* 1933 were used in this experimental research work. Brown seaweed extract contains sulphated polysaccharides which act as reducing and efficient stabilizer agent and play the main role in the reduction of ferric chloride solution. Particle sizes of the synthesized nanoparticles obtained in the range from 10 to 19.5 nm and 21.6 to 27.4 nm for P. pavonica and S. acinarium, respectively. Green synthesized Fe_3O_4-NPs had a high capacity for bioremoval of Pb (91%) by using the Brown seaweed *P. pavonica (Linnaeus) Thivy while that of S. acinarium (Linnaeus) Setchell* 1933 had a capacity of (78%) after 75 min [128]. Fu et al., reported the green synthesis of ZnO nanoparticles (NPs) using leaf extract of *Plectranthus amboinicus*. The synthesized NPs were characterized by different techniques such as XRD, SEM, EDX, UV-Vis spectroscopy, FTIR and photoluminescence spectroscopy. XRD crystalline nature of biosynthesized NPs as hexagonal wurtzite ZnO. SEM analysis

shows a rod shaped structure with the average size of particles 88 nm. Band gap energy of synthesized ZnO NPs was found 3.07eV with the help of UV-Vis diffuse reflectance spectrum analysis. The photocatalytic performance of biosynthesized ZnO NPs was investigated by photodegradation of methyl red (MR) under UV illumination and compared with hydrothermal synthesized ZnO NPs and P25. This research work has shown the biosynthesized ZnO NPs have a better photocatalytic activity towards degradation of methyl red than ZnO NPs synthesized by hydrothermal synthesized and P25 [129].

Grigore et al., presented a review of methods of synthesis, properties and biomedical applications of CuO nanoparticles. Synthesis process of nanoparticles influenced their properties, which cause variation in their biomedical applications. CuO nanoparticles can be used in effective antimicrobial action against a wide range of pathogens and also drug-resistant bacteria due to their great biological properties. This study also discussed that the nanosystems could represent efficient alternatives in the development of smart systems employed both for the finding of pathogens and for the treatment of infections. Application of CuO nanoparticles still limited in drug delivery formulations due to their enhanced toxicity, however other applications, such as topic formulations, dressings and coated textiles are of a great interest among the medical environments. Researchers and scientist are motivating the finest synthesis processes in order to decrease the toxicity of CuO NPs with improved efficiency in diagnosis and therapy for the advancement in their biomedical applications. [130]. Muthukumar and Manickam reported the green synthesis of iron oxide nanoparticles using aqueous leaf extract of *Amaranthus spinosus*. Leaf extract was used as reducing agents which were described as the rich source of amaranthine and phenolic compounds with high antioxidant. Operating parameters were analyzed during the synthesis process and properties of

synthesized nanoparticles such as optical and magnetic properties were investigated. The analytical techniques confirmed the synthesis of spherical shaped Fe NPs with a diameter in the range 54-270 nm and the surface area was of 54 m^2/g. Furthermore, synthesized nanoparticles show the ferromagnetism properties with a saturation magnetization of 92.12emu/g. Photoluminescence spectrum exhibited the strong emission band in the visible region at 431 nm with the intrinsic energy band gap at 1.9 eV. The photocatalytic and antioxidant activity of leaf extract mediated Fe NPs and $NaBH_4$ mediated Fe NPs were compared. Decolourization percentage were observed 75% and 69% against methyl orange and methylene blue by using extract mediated Fe NPs under the sunlight. Whereas extract mediated Fe NPs has shown 93% antioxidant efficiency [131]. Heiligtag and Niederberger reported a brief review of nanoparticle research and described the Size-related properties of nanoparticles and potential of NPs for innovative technological applications and challenges to researchers and scientists. This work focused on the reports which provided the descriptive overview of the current research work on nanoparticles for developing and emerging field. This review also highlighted the emerging nanomaterials, their effects, new models and concepts established to explain and understand the observed the results of experiments related to nanotechnology [132]. Hoag et al., reported a single step green synthesis of iron NPs using tea (Camellia sinensis) polyphenols without using extra surfactants as capping or reducing agents. Formation of iron NPs was recognized by color changes from pale yellow to dark greenish/black, due to the reaction between polyphenols and ferric nitrate occurs and also reaction occurred in few minutes at room temperature. Synthesized iron NPs were characterized using various characterization techniques. Synthesized nanoparticles were utilized to catalyze hydrogen peroxide for treatment of organic contamination and results were compared with Fe-EDTA and Fe-EDDS. This

experiment resulted that the highest rate of bromothymol blue degradation occurs with green tea mediated - nano-scale zero-valent iron-catalyzed H_2O_2 [133]. Hulkoti and Taranath reported the review on the use of consortium of diverse microorganisms belonging to both prokaryotes and eukaryotes for the synthesis of metallic NPs and metal oxide nanoparticles. The synthesis of NPs described as intracellular or extracellular. It was reported in various reports that NADH dependent nitrate reductive enzyme plays a vital role in the conversion of metallic ions into nanoparticles. There is still a need to improve synthesis approaches for better control of particle size and morphology. Less reduction time of biosynthesis of nanoparticles make it more attractive and the ability to control size and shape would offer considerable advantage over physical and chemical approaches of synthesis. Currently, the efforts of the scientific community on improving particle synthesis efficiency and exploring their biomedical applications. This study resulted that the implementation of biosynthesis large scale production of nanoparticles and their commercial applications in medicine and health care will take place [134]. Khan et al., reported a complete overview on the synthesis, properties and applications of NPs. Nanomaterials have various commercial and domestic applications including catalysis, environmental applications and medical applications. Properties of nanoparticles viz. reactivity and toughness are dependent on their unique size, shape and structure [135]. Ivask et al., reviewed the comprehensive and critical literature on the mechanism of toxic action of Ag, ZnO and CuO NPs to the selected ecotoxicological test organisms and mammalian cells in vitro. This study also describe the factors adjusting the toxic effect of nanoparticles and impact of the test media. There are three major phenomena which are mainly drive the toxicity of nanoparticles: (i) dissolution of nanoparticles, (ii) organism dependent cellular uptake of NPs and (iii) induction of oxidative stress and consequent cellular damages. To

design the more advance and efficient nano-antimicrobials using environment friendly approaches, More is more information on mechanisms is still needed [136]. Jassal et al., reported the novel green approach for the synthesis of potassium zinc hexacyanoferrate (K_2Zn_3 [Fe $(CN)_6$]2$9$H_2O$) (KZnHCF) nanocubes using *Sapindus mukorossi* as a natural surfactant and water as the solvent. The green synthesized nanoparticles were characterized by XRD, SEM, TEM, FTIR, thermo gravimetric techniques and BET surface area analysis. Synthesized nanoparticles were examined for their effect on the photocatalytic degradation of two synthetic dyes that is Eriochrome Black T (EBT) and Malachite Green (MG). In this research work degradation of Malachite Green (MG) and Eriochrome Black T (EBT) evaluated as 94.15% and 76.13%, respectively [137]. Gao et al., reported the biopolymer-mediated green synthesis of iron oxide nanoparticles for analysing their magnetic properties. Nanoparticles were synthesized using redox-based hydrothermal method and $FeCl_3 \cdot 6H_2O$ and urea were used as the starting materials. This research work resulted that biopolymer worked as reducing and stabilizing agent in the synthesis of iron oxide NPs. Synthesized NPs were confirmed the ferromagnetic behaviour from a direct current SQUID magnetometer [138]. Kuang et al., reported the green synthesis of Iron nanoparticles using tea extracts and synthesized NPs were applied as a catalyst for the Fenton-like oxidation of mono chlorobenzene (MCB). MCB were found degraded 69%, 53%, and 39% by Fe NPs synthesized using green tea extracts, oolong tea extracts, and black tea extracts respectively. In this research work, green synthesized Fe NPs using green tea extracts (GT-Fe NPs) have been shown the degradation. The synthesized Fe NPs remove the COD to 81% and 31% at optimal condition of dosages were 0.6 g/L GT-Fe NPs, 0.045 mol/L H_2O_2. The catalytic properties of the synthesized GT-Fe NPs indicate that Fe^{3+} and Fe^{2+} leached and consequently reduced iron sludge formation

[139]. Kumari et al., reported the green synthesis of silver nanoparticles using using zanthoxylum armatum leaves extract to experimentally perform the hazardous dyes degradation like safranine O, methyl red, methyl orange and methylene blue etc. This study described the water pollution in lakes, rivers and groundwater due to the discharge of hazardous dyes from textile industries. Green synthesized silver nanoparticles were characterized by XRD, TEM, SEM-EDX, DLS and SAED and evaluated the crystalline silver nanoparticles with particle size range 15- 50 nm. Further, study resulted that the presence of green synthesized silver nanoparticles as catalyst increases the efficiency of dyes degradation due to high surface area and accelerate migration rate of electrons/hole to the surface of silver nanoparticles [140]. Lata and Samadder reported a review on the challenges for the removal of arsenic from water using nanoparticles as adsorbents. Many researchers and individual are exploiting totally different nanoparticles as an adsorbent to get rid of water pollutants together with arsenic when modifying the properties of nanoparticles by up reactivity, biocompatibility, stability, charge density, multi-functionalities, and dispersibility. This study chiefly studied the potential of the nanoadsorbents for arsenic removal from contaminated water and also the challenges involved during this review evaluated the surface assimilation potency of the varied nanoparticles supported the size of nanoparticles, kinds of nano adsorbents, technique of synthesis, separation and regeneration of the nanoadsorbents [141]. Lu et al., reported a brief review on nanomaterials for their application in water and wastewater treatment. There are various reports have revealed that nanomaterials can play a very important role in water and wastewater treatment. This review mainly focused to the discussion on the metal oxide nanoparticles (TiO_2, ZnO, and iron oxides), zero-valent metal nanoparticles (Ag, Fe, and Zn), nanocomposites and carbon nanotubes (CNTs) for water and wastewater

treatment. This article suggested that the low cost is crucial to confirm their widespread applications in water and waste treatment, future analysis ought to be dedicated to up the economic potency of nanomaterials. The analysis and comparison of the performance of varied nanomaterials in water and waste product treatment area unit still in need of uniform or recognized standards. It's tough to match the performances of various nanomaterials and understand promising nanomaterials that merit more development [142]. Mahdavi et al., reported the green synthesis of iron oxide (Fe_3O_4) by reduction of ferric chloride solution with brown seaweed (BS, *Sargassum muticum*) aqueous extract which mainly contains sulphated polysaccharides as the main factor which acts as reducing agent and efficient stabilizer. Synthesized iron Oxide (Fe_3O_4) NPs were characterized by XRD, FTIR, FESEM, EDXRF, vibrating sample magnetometry (VSM) and TEM. The average size of synthesized nanoparticles were found 18 ± 4 nm with cubic shapes [143]. Matinise et al., reported the green synthesis of ZnO nanoparticles using *moringa oleifera* extract as a chelating agent for analyzing their physical properties and mechanism of formation. Various properties of synthesized material like crystalline structure, morphology, chemical composition, isothermal behaviour, optical properties and electrochemical activity were deliberate with the help of X-ray powder diffraction (XRD), High resolution transmission electron microscopy (HRTEM), FTIR, UV–Vis, Cyclic voltammetry (CV), Selected area electron diffraction (SEAD) and Differential scanning calorimetry/thermogravimetric analysis (DSC/TGA). Particle size of the synthesized nanoparticles were found in the range from 12.27and 30.51 nm [144]. Mudshinge et al., reported a review on nanoparticles as emerging carriers for drug delivery. This research work describes that in the drug delivery system, NPs mainly work to control and manipulate biomacromolecular constructs and supramolecular assemblies that are critical to living

cells in order to improve the quality of human health. This study described that the emerging nanotherapeutics/diagnostics can permit a deeper understanding of human longevity and human ills that embody cancer, disorder and genetic disorders. Development of drug delivery system being potential through the use of advanced material, improved management of particle size, and higher understanding of the interface between the biological and material surfaces, and their effects in vivo [145]. Mystrioti et al., reported a research paper on the comparative assessment of five plants of extracts Camellia sinensis (green tea, GT), Syzygium aromaticum (clove, CL), Mentha spicata (spearmint, SM), Punica granatum juice (pomegranate, PG) and Red Wine (RW) and juices for the green synthesis of iron NPs and their application for hexavalent chromium reduction. In this study, it was found that green tea, *punica granatum* juice and red wine mediated iron NPs are more effective for Cr(VI) reduction, reaching reduction rates as high as 500 mg Cr(VI) per g of iron in nanoparticles [146]. Aslan et al., reported the review on role of nanotechnology in cancer treatment. Cancer is a worldwide problem which is one of the main causes of mortality. This study describes that the nanomaterials as carriers can allow a chief drive to improve drug delivery in cancer. Nanocarriers primarily aimed to guard the drug from speedy degradation once general delivery and permitting it to achieve growth website at therapeutic concentrations, and with this they assist to avoid drug delivery to traditional sites the maximum amount as doable to scale back adverse effects. Structural and physical properties of nanomaterials like size, shape, charge and surface properties play a critical role to determine the biodistribution, pharmacokinetics, internalization and drugs safety [147]. Padil and cernik reported the green synthesis of copper oxide nanoparticles using gum karaya as a biotemplate for antibacterial application. Green synthesized CuO oxide nanoparticles were characterized by X-Ray diffraction,

Transmission electron microscopy, X-Ray photoelectron spectroscopy and Fourier transform infrared spectroscopy. Sizes of the green synthesized nanoparticles were found 4.8 ± 1.6 nm, 5.5 ± 2.5 nm, and 7.8 ± 2.3 nm with various concentrations 1 mM, 2 mM, and 3 mM of precursor $CuCl_2 \cdot 2H_2O$ respectively. At lowest concentration of precursor synthesized nanoparticles were found in smallest in size (4.8 ± 1.6 nm). The smaller size of the synthesized CuO NPs (4.8 ± 1.6 nm) was found to be yielding a maximum zone of inhibition compared to the larger size of synthesized CuO nanoparticles [148]. Peternela et al., reported the green synthesis of copper oxide nanoparticles using leaf extract of *Pomegranate* as a reducing and stabilizing agent for the application in the removal of multiple water pollutants. The inseminated carbons with CuO nanoparticles were characteriz ed morphologically and structurally. The analysis of XRD and SEM, after carbons modification, confirmed that the surface structure remained porous with CuO nanoparticles sizes between 40 nm and 78 nm. Impregnation of CuO nanoparticles favored to the nitrate removal from 0.93 mg/g to 4.09 mg/g. This study resulted that the green synthesized copper oxide nanoparticles on carbon activation have shown the sufficient impregnation time of 24 h [149]. Guzman et al., reported the synthesis of silver nanoparticles for antibacterial activity against gram-positive and gram-negative bacteria. This article describe the synthesis of Ag NPs synthesized by chemical reduction from aqueous solutions of silver nitrate and the mixture of hydrazine hydrate, wherein and sodium citrate worked as reductants and sodium dodecyl sulphate worked as a stabilizer. Characterization of the Ag NPs shows the narrow size distribution (from 40 to 60 nm) due to agglomerates of grains. Antibacterial activity of the synthesized Ag NPs was measured using the Kirby-Bauer method. Experimental results show the significant antibactericidal activity against *E. coli*, *Pseudomonas aeruginosa*, and *Staphylococcus aureus* [150]. Khairia reported the

green synthesis of zero-valent silver NPs using leaves extract of *ficus benjamina* for cadmium removal from the aqueous solution. Along with the Cd^{2+} removal efficiency of nanoparticles some other parameters like adsorbent dose, heavy metal concentration, pH, agitation speed and contact time were also analyzed. In this study, equilibrium data of removal have shown that the Freundlich isotherm model for the cadmium removal was best in the comparison of Langmuir isotherm models. Obtained results in this study might be helpful for designing and establishing a continuous treatment plant water and wastewater enriched in Cd(II) [151]. Quester et al., reported a review on biosynthesis and microscopic study of metallic NPs. This study provides a brief information regarding the biosynthesized nanoparticles as clean, non-toxic, and eco-friendly material for the application of industry and/or biomedicine. Silver and gold NPs were described as most studied metallic NPs due to their potential use in medical treatment. Most significant results were described in this work, which was focused on the use of organisms to produce metallic NPs as well as the microscopic analyses used to characterize the nanostructured material obtained, providing a valuable record for upcoming research in the field of nanotechnology. Numerous microorganisms, including plants, bacteria, yeast, fungi, and algae have been reported for the synthesis of different NPs like silver, gold, palladium, metal oxides etc. This study strongly recommended the biosynthesis of nanoparticles for the efficient applications in the field of antimicrobial activity or biological labeling systems [152]. Sadegh et al., reviews the role of nanomaterials as effective adsorbents and their present, past and future processes for heavy metal ions and dye removals from wastewater. Numerous nanomaterials have been studied with significant adsorption capacities of removing pollutants from wastewater. This review mainly focused on and highlighted to the promising future applications and opportunities of nanomaterials as adsorbents because of their unique

morphological and structural properties [100]. Santhosh Kumar et al., reported the green synthesis of zinc oxide nanoparticles (ZnO NPs) using *Passiflora caerulea* fresh leaf extract for the treatment of urinary tract infection. Synthesized NPs were characterized by XRD, SEM, EDAX, UV–Vis, FT-IR, and AFM, and test against the pathogenic culture showed a very good zone of inhibition compared with plant extract. In the green synthesis approach, oxidation and reduction process induced due to the presence of metabolites like terpenoids, flavonoids, and alkaloids in the leaf extract. Synthesized ZnO NPs nanoparticles were found in the range of 30–50 nm. This research work resulted in the significant antibacterial activity of green synthesized ZnO NPs against urinary tract infection [153]. Shittu and Ihebunna reported the green synthesis of silver NPs in the range of 50-114 nm using aqueous leave extract of *Piliostigma thonningii* for purification of laboratory simulated wastewater with optimization using the different conditions of silver nanoparticle formation such as time, temperature, and pH, the concentration of silver nitrate and volume of the aqueous extract. This study resulted that biosynthesized silver nanoparticles show efficient capability in the removal of heavy metal without subchronic adverse effects in experimental rats [154]. Sinha and Ahmaruzzaman reported the green synthesis of copper nanoparticles (Cu NPs) using the peel extracts of *Citrus grandis* where the peel extract of *Citrus grandis* worked as a reducing and stabilizing agent. Cu NPs were found spherical in shape with diameter 22-27 nm and average crystalline was 18 nm. The study resulted in the significant photocatalytic efficiency of the synthesized Cu NPs for the degradation of methyl red dye [155].

Sirelkhatim et al., reported a review of zinc oxide nanoparticles: Antibacterial Activity and their toxicity mechanism. ZnO is a biocompatible material which possesses photo-oxidizing and photocatalysis impacts on chemical and biological species. This review

represented the antibacterial drug activity of ZnO-NPs with testing strategies, the impact of ultraviolet illumination, ZnO particle properties, particle surface modification, and minimum repressing concentration. This study was represented the antiseptic and biological processes that primarily targeted on the production of reactive chemical element species (ROS) as well as peroxide (H_2O_2), OH- (hydroxyl radicals), and O_2-2 (peroxide). ROS has been described as the main factor for numerous mechanisms with cell wall harm due to ZnO-localized interaction, enhanced membrane permeability, internalization of NPs due to damage of proton cause force and uptake of toxic dissolved zinc ions [51]. Suarez-Cerda et al., reported the green synthesis of Ag-NPs using double delight petals extract of Rosa 'Andeli' for their kinetics and photocatalytic analysis. This research work also describes the effect of different concentrations of Rosa '*Andeli*' double delight petals aqueous extract (PERA) in the synthesis of silver nanoparticles (Ag-NPs). Synthesized Ag-NPs were characterized using TEM, SEM-EDS and UV-Vis spectroscopy. Green synthesized Ag-NPs were found spherical in shape with the size in the range of 0.5 to 1.4 nm. This study resulted that the Ag-NPs synthesis reaction followed the first order for metallic precursor (silver) and a second order for the reducing-stabilizing agent (PERA) and the photocatalytic activity of green synthesized Ag-NPs was found with the efficiency of 95% for degradation of commercial dye [156]. Sutradhar and Amin briefly reviewed the research work on nanotechnology in cancer drug delivery and selective targeting. NPs are rapidly being developed and trialed to overcome several limitations of traditional drug delivery systems and are coming up as a distinct therapeutics for cancer treatment. This review focuses on cell recognizing the ability of nanoparticles by various strategies having unique identifying properties that distinguish them from previous anticancer therapies. This study also discussed the specific drug delivery by

nanoparticles inside the cells demonstrating many successful types of research and how nanoparticles remove the side effects of conventional therapies with tailored cancer treatment [157]. Shanker et al., reported the synthesis of transition metal oxide nanoparticles (ZnO, CuO, Co_3O_4, NiO and Cr_2O_3) under the sunlight for the catalytic removal of organic colorants from the water. Synthesized NPs were found distinct morphologies with different sizes with the help of TEM: ZnO nanotubes <35 nm, nanorods CuO; 7-50 nm, Co_3O_4 nanorods, triangles and hexagons; 45-90 nm, NiO needle-shaped; 2-25 nm and Cr_2O_3 nanobeads ~17 nm. Synthesized transition metal oxide NPs were performed to analyze their potential for treatment of simulated water containing hazardous dyes: Alizarin Red S (ARS) + Methylene Blue (MB). This study resulted in the synthesized transition metal oxide NPs in presence of sunlight, can be used as significant adsorbents in wastewater treatment [158]. Wang et al., reviewed the antimicrobial activity of NPs in the present situation and for their future prospects. This study showed that the NPs are an efficient alternative of antibiotics to target bacteria. Reviewed research also focused on the antibacterial mechanisms of NPs against bacteria and discussed all the effective issues. This study resulted in the deep study of antibacterial mechanisms may contribute to the development of efficient antibacterial NPs as well as it can prevent the NP cytotoxicity [159]. Wang et al., reported the brief study on the application of nanotechnology in cancer therapy and imaging. This study discussed the developments in nanotechnology which can provide the new tools for cancer imaging and treatment for researchers and scientist. Nanotechnology provided the advancement in nanoscale devices which may be conjugated with various purposeful molecules at the same time, as well as antibodies, tumor-specific ligands, antitumor medication and imaging probes [103]. Wang et al., reported the green synthesis of Fe NPs using leaf extracts of eucalyptus for the treatment of eutrophic

wastewater. Synthesized Fe NPs were found spheroidal in shape with some polyphenols which bound to the surfaces of eucalyptus-Fe NPs as a capping/stabilizing agent. Reactivity of synthesized NPs was evaluated for the treatment of swine wastewater and it was found that 71.7% of total N and 84.5% of COD were removed, respectively. This study convincingly demonstrates the tremendous potential of green synthesized Fe NPs for in situ remediations of wastewater [160]. Seil and Webster reported a review of methods and literature on antimicrobial applications of nanotechnology. This study discussed that ZnO and silver nanoparticles provide a substantial reduction in bacteria feasibility and the particle diameter and surface charge are among the most relevant parameters, which determine the effectiveness of an antimicrobial nanoparticle. Future studies can observe additional physiologically relevant modes of microorganism introduction to and interaction with nanomaterials. In vitro, studies typically use liquid suspensions of microorganism in culture media that quickly turn out to be microorganism populations that are so much larger than physiologically relevant values. To raised perceive the flexibility of nanoparticles and nanomaterial surfaces to stop or treat infection, animal models of infection are necessary. During this method, the clinical potential of antimicrobial nanoparticles will additional accurately be determined [106]. Xin et al., reported the green synthesis of iron nanoparticles using the extract of tie guanyin tea for degradation of bromothymol blue. Green synthesized iron NPs were characterized by XRD, SEM, TEM, UV-Vis and FTIR. Iron NPs were found spherical in shape with an average size of 6.58 ± 0.76 nm. Moreover, the effect of concentration of iron nanoparticles and concentration of bromothymol blue on the kinetic rate constants during the degradation process was also studied in this research work. This study resulted in the high activity for bromothymol blue degradation with more than 90% of the dye removal. The highest reaction rate was achieved in the

presence of 2% H_2O_2 and 0.33 mM iron nanoparticles when the bromothymol blue was 150 mg/L which was shown with the help of catalytic kinetics [161]. Xu et al., briefly reviewed the use of iron oxide nanomaterials for wastewater treatment. Iron oxide nanomaterials can be used as nanosorbents and photocatalysts in the application of wastewater treatment for environmental clean-up. This study concludes that there is much interest in the use of engineered iron oxide NPs as an in-situ, relatively non-invasive tool in wastewater treatment. But before the widespread application, it is important to address uncertainties over the health impacts and environmental fate of nanomaterials [162]. Zhang et al., reviewed the development of nanomaterials for their current applications in water and wastewater treatment. The synthesis and physiochemical properties of various free nanomaterials, together with carbon-based mostly nanomaterial, metal and metal oxides nanoparticles in addition as metallic element nanoparticles, were targeted on their performance and mechanisms towards removal of assorted contaminants were mentioned during this analysis work. Nanomaterials show various merits, such as fast kinetics, high capacity, specific affinity towards targeted contaminants, enhanced photocatalytic response and strong antibacterial activity. Overall, the impacts and risks of the environmental nanomaterials targeted on, their synthesis via green chemistry to diminish their environmental impact ought to even be pursued in parallel [163]. *Pelargonium graveolens* extract reduces gold ions into nanoparticles of size 20-40 nm, *Trigonella foenum-graecum* extract can reduce gold ions into nanoparticles of size 15-25 nm [95,164]. Phenolate ions were capable of transferring electrons to the metal ions during nanoparticle formation [165]. For example, eugenol is the leading phenolic of *clove* extract which plays the foremost role in bio-reduction $AgNO_3$ and $HAuCl_4$ to form nanoparticles [166]. Flavonoids such as anthocyanin, flavonol, flavone, flavanone, isoflavonoid, chalcone etc. are also

composed of polyphenolic compounds that are capable of reducing the metal ions during the formation of nanoparticles. For example, *Ocimum basilicum* plant extract that contains flavonoids like as luteolin, apigenin etc. play a significant role in the formation of silver nanoparticles by reducing silver ions [167]. Amino acids are also found to be able to bind metal ions and reduce them into nanoparticles. It is observed that amino acids such as cysteine, arginine, methionine, lysine help to bind silver ions for the formation of silver nanoparticles [168].

Table 1.1: Application of Green Synthesized Nanoparticles in Environmental and Biomedical Applications.

Sr. No.	Nanoparticles	Biological materials	Biological agents	Characteristics	Application in dye removal and water and wastewater treatment	Ref.
1.	α-Fe_2O_3 NPs	Plant leaf extract	*Curcuma* and *Tea*	Crystallite size: using Curcuma (4 nm); using Tea (5 nm); Shape: spherical	Degradation of methylene orange	[109]
2.	Cuprous oxide (Cu_2O)	Plant leaf extract	*Calotropis gigantean*	Size: 8.8 nm; Shape: Octahedral, dodecahedra, and cubic	90 % MB dye removal after light exposure 120 minutes	[110]
3.	Au NPs	Plant leaf extract	*Lagerstroemia speciosa*	Size: 41 - 91 nm; Shape: hexagonal	Photocatalytic reduction of organic pollutants (methylene blue (MB), methyl orange (MO), bromophenol blue (BPB), and bromocresol green (BCG) dyes and nitro aromatic compound (4-nitrophenol (4-NP); Photocatalytic reduction of dyes with a reduction efficiency of ≥ 90%.	[115]
4.	Silver (Ag) NPs	Plant leaf extract	*Ocimumgratissimum*	Size:16 ± 2 nm; Shape: Triangular	Synthesized NPs were shown higher effective antibacterial activity against E. Coli	[117]
5.	ZnO NPs	Lemon juice	Lemon fruits	Size: ~ 21.5 nm; Shape: spherical	Photocatalytic degradation of dyes (methyl orange, methyl red and methylene blue)	[118]

6.	Fe NPs	Plants leaf extracts	*Azadiracta indica* (AI), *Magnolia champaca*(MC), *Mangifera indica* (MI) and *MurrayaKoenigii*(MK)	Size: (AI: 96 - 110 nm); (MC :99 - 129 nm); (MI and MK :100 - 150 nm); Shape: spherical	Treatment of domestic wastewater; AI- Fe NPs showed maximum removal efficiency (phosphates removal: 98.1%; ammonium nitrogen removal: 84.3%; and COD removal: 82.4%)	[119]
7.	Zinc Oxide (ZnO) NPs	Flower extract	*Trifoliumparatense*	Size: 60-70 nm	Synthesized NPs were shown high activity against S.aureous ATCC 4163, E. Coli ATCC 25922, P. aeruginosa 6749, S. aureous and P. aeruginosa.	[121]
8.	Iron oxide NPs	Peel extract	*Tangerine*	Size: ~ 50 nm; Shape: spherical	Treatment of contaminated solution (Cd removal: 90%)	[122]
9.	Fe_3O_4	Seaweeds (Algae)	*Padinapavonica (PP)* and *Sargassumacinarium (SA)*	Size: PP (10 - 19.5 nm) and SA (21.6 - 27.4 nm); Shape: spherical	Bioremoval of Pb removal using PP: 91%, Pb removal using SA: 78%	[123]
10.	ZnO NPs	Plant leaf extract	*Plectranthus amboinicus*	Average size: 88 nm; Shape: rod shape	Degradation of methyl red (MR)	[124]
11.	FeO NPs	Plant leaf extract	*Amaranthus spinosus*	Maximum particle size: 91 nm; Shape: spherical	Decolourization of dyes (methyl orange: 75% and methylene blue: 69%)	[126]
12.	Nano zero-valent iron (nZVI)	Tea extract	*Camellia sinensis*	Size: 5 - 15 nm; Shape: spherical	Degradation of bromothymol blue	[128]
13.	Potassium Zinc Hexacyanoferrate Nanocubes	Natural surfactant	*Sapindusmukorossi*	Size: 33 - 192 nm; Shape: cubic	Photocatalytic degradation of organic dyes (Malachite Green (MG): 94.15% and Eriochrome Black T (EBT): 76.13%)	[132]
14.	Fe NPs	Tea extract	Green Tea (GT), Oolong Tea (OT), and Black Tea (BT)	Size: GT-FeNPs (20 - 40 nm), Shape: irregular spherical	Treatment of wastewaters by removal of monochlorobenze	[134]

					ne (MCB) (MCB removal using GT: 69%, MCB removal using OT: 53%, and MCB removal using BT: 39%)	
15.	Ag NPs	Plant leaf extract	*Zanthoxylumarmatum*	Size: 15 - 50 nm; Shape: spherical	Degradation of dyes (degradation rate constant value of Safranine O: 1.02×10^{-3} Min^{-1}; degradation rate constant value of Methyl red: 1.03×10^{-3} Min^{-1}; degradation rate constant value of Methyl orange: 1.86×10^{-3} Min^{-1}; 10.degradation rate constant value of Methylene blue: 1.44×10^{-3} Min^{-1}	[135]
16.	Fe NPs	Plant extracts and juices	Extracts of *Camellia sinensis* (green tea, GT), *Syzygiumaromaticum* (clove, CL), *Menthaspicata* (spearmint, SM), *Punicagranatum* juice (pomegranate, PG) and Red Wine (RW)	Sizes: 50 - 60 nm; Shape: spherical	Reduction of hexavalent Cr	[141]
17.	Copper oxide (CuO) NPs	Gum	*Gum karaya*	Size: 4.8±1.6 nm; Shape: Spherical	Smaller size of synthesized NPs were shown higher antibacterial activity against E. Coli and S. aureous	[143]
18.	Copper oxide (CuO) NPs	Plant leaf extract	*pomegranate*	Size: 40-78 nm; Shape: Spherical	Impregnated carbons with CuO NPs were shown great removal of water pollutants mainly nitrate	[144]
19.	Ag NPs	Plant leaf extract	*Focus Benjamina*	Size: 60 - 105 nm	Maximum Cd removal from	[146]

					aqueous solution: 85%	
20.	Ag NPs	Plant leaf extract	*Piliostigma thonningii*	Size: 50 - 114 nm; Shape: spherical	Heavy metal removal activity (max. iron ion removal: 96.9%; max. copper removal: 89%; max. lead removal: 97.89%; max. magnesium removal: 93.6%)	[149]
21.	Cu NPs	Peel extract	*Citrus grandis*	Size: 22-27 nm; Shape: spherical	Degradation of methyl Red: 96%	[150]
22.	Ag-NPs	Petals extract	*Rosa* 'Andeli'	Size: 4 - 29 nm; Shape: spherical	Degradation of commercial dye Putnam sky blue 39 with an efficiency of 95%	[151]
23.	ZnO, CuO, Co_3O_4, NiO and Cr_2O_3	-	Sunlight Irradiation	Size: ZnO; <35 nm; CuO; 7 - 50 nm; Co_3O_4; 45-90 nm; NiO; 2 - 25 nm; Cr_2O_3: ~ 17 nm; Shape: ZnO (nanotubes); CuO (nanorods); Co_3O_4 (triangles and hexagons); NiO(needle-shaped) and Cr_2O_3 (nanobeads)	Treatment of simulated water containing hazardous dyes: removal dyes mixture (Alizarin Red S (ARS) + Methylene Blue (MB) (removal using Cr_2O_3: 88.24%; removal using > removal using ZnO: 87.96% > removal using CuO: 86.86% > removal usingNiO: 85.89% > removal using Co_3O_4: 80.35%	[153]
24.	Fe NPs	Plant leaf extracts	*Eucalyptus* sp.	Size: 20 - 80 nm; Shape: spheroidal	Treatment of eutrophic wastewater (N removal: 71.7%; P removal: 30.4%; and COD removal 84.5%)	[155]
25.	Iron NPs	Tea extract	*Tie Guanyin*	Size: 6.58 ± 0.76 nm; Shape: spherical	Degradation of dye (Bromothymol Blue removal: more than 90%)	[156]
26.	Au and Ag NPs	Plant stem extract	*Breyniarhamnoides*	Au: ~ 25 nm; Ag: ~ 64 nm; shape: spherical	Catalytic conversion of 4-nitrophenol (4-NP)	[169]

					to 4-aminophenol (4-AP)	
27.	AgNPs-Soil nanocomposite	Plant leaf extract	*Ocimumtenuiflorum*	Size: 20 - 40 nm; Average Size: 32.58 nm	Treatment of textile dye (turquoise blue dye removal: 96.8%)	[170]
28.	Reduced Graphene Oxide (RGO)/Fe_3O_4 Nanocomposites	Plant leaf extract	*Solanumtrilobatum*	Size:18 nm; Shape: spherical	Degradation of methylene blue: 95.9%	[171]
29.	Fe NPs	Plant leaf extracts	Green tea (*Camellia sinensis*) and Pomegranate (*Punicagranatum*)	-	95% color removal and almost 80% dissolved organic carbon removal From Textile Wastewater	[172]

References

[1] M. Wilson, K. Kannangara, G. Smith, M. Simmons, B. Raguse, Nanotechnology: Basic Science and Emerging Technologies, A CRC press company, Boca Raton new York Washington DC (2002).

[2] A. Dowling, Nanoscience and Nanotechnology: Opportunities and Uncertainties, a Report by the Royal Society & the Royal Academy of Engineering, London, July 2004.

[3] D.B. Harden, J. Toynbee, The Rothschild Lycurgus cup, Archaeologia. 97 (1959) 179-212.

[4] D.B. Harden, H. Hellenkemper, K. Painter and D. Whitehouse, Glass of the Caesars, Olivetti, Milan. (1987) 245-249.

[5] D.B. Harden, The Rothschild Lycurgus cup: addenda and corrigenda, Journal of Glass Studies. 5 (1963) 9-17.

[6] R.G. Chirnside, P. Proffitt, The Rothschild Lycurgus cup: an analytical investigation, Journal of Glass Studies. 5 (1963) 18-23.

[7] I.C. Freestone, N. Meeks, M. Sax and C. Higgitt, The Lycurgus cup- a Roman nanotechnology, Gold Bull. 40 (2007) 270-277.

[8] G. Timp (ed.): Nanotechnology (Springer, Berlin Heidelberg, New York, 1998), ISBN 978-1-4612-0531-9.

[9] R.P. Feynman, There's Plenty of Room at the Bottom, Eng. and Sci. 23 (5) (1960) 22-36

[10] M.C. Daniel, D. Astruc, Gold Nanoparticles: Assembly, Supramolecular Chemistry, Quantum-Size-Related Properties, and Applications toward Biology, Catalysis, and Nanotechnology, Chem. Rev. 104 (2004) 293-346.

[11] R. John Bosco Balaguru, B.G. Jeyaprakash, Introduction to Materials and Classification of Low Dimensional Materials, NPTEL – Elec. & Elec. Eng.-Sem. Nanodev. 1-18.

[12] G. Schmid, Nanoparticles: From Theory to Application, Wiley-VCH: Weinheim, Germany, 2004.

[13] M.A. El-Sayed, Some Interesting Properties of Metals Confined in Time and Nanometer Space of Different Shapes, Acc. Chem. Res.34 (4) (2001)257-264.

[14] D.L. Feldheim, C.A. Foss, Jr. Eds. Metal Nanoparticles: Synthesis, Characterization and Applications; Marcel Dekker: New York, 2002.

[15] M.C. Daniel, D. Astruc, Gold Nanoparticles: Assembly, Supramolecular Chemistry, Quantum-Size-Related Properties, and Applications toward Biology, Catalysis, and Nanotechnology, Chem. Rev. 104 (2004) 293-346.

[16] E. Roduner, Size matters: why nanomaterials are different, Chem. Soc. Rev. 35 (2006) 583-592.

[17] C. Suryanarayana, The structure and properties of nanocrystalline materials: Issues and concerns, JOM Journal of the Minerals, Metals and Materials Society. 54 (2002) 24-27.

[18] C. Suryanarayana, Recent developments in nanostructured materials, Adv. Eng. Mat. 7(11) (2005) 983-992.

[19] J. R. Heath, The chemistry of size and order on a nanometer scale, science. 270 (1995) 1315.

[20] C.B. Murray, R. Kagan, M.G. Bawendi, Self-Organization of CdSe Nanocrystallites into Three-Dimensional Quantum Dot Superlattices, Science. 270 (1995) 1335-1338.

[21] J.Z. Zhang, Ultrafast studies of electron dynamics in semiconductor and metal colloidal nanoparticles: effects of size and surface, Acc. Chem. Res.30 (10) (1997) 423-429.

[22] Y. Wang, N. Herron, Nanometer-sized semiconductor clusters: materials synthesis, quantum size effects, and photophysical properties, J. Phys. Chem. 95 (1991) 525-532.

[23] N.K. Thakkar, S.M. Snehit, Y.P. Rasesh, Biological synthesis of metallic nanoparticles, Nanomedicine: Nanotechnology, Bio. and Med. 6 (2010) 257-262.

[24] C. Bae, H. Yoo, S. Kim, K. Lee, J. Kim, M. M. Sung, H. Shin, Template-Directed Synthesis of Oxide Nanotubes: Fabrication, Characterization, and Applications, Chem. Mater.20(3) (2008) 756-767.

[25] M. Batzill, U. Diebold, The surface and materials science of tin oxide, Prog. in Surface Sci. 79 (2005) 47-154.

[26] A.D. Maynard, R.J. Aitken, T. Butz, V. Colvin, K. Donaldson, G. Oberdorster, M.A. Philbert, J. Ryan, A. Seaton, V. Stone, S.S. Tinkle, L. Tran, N.J. Walker, D.B. Warheit, Safe handling of nanotechnology, Nature. 444 (2006) 267-269.

[27] S.H. Sun, C.B. Murray, D. Weller, L. Folks, A. Moser, Monodisperse Fe-Pt nanoparticles and ferromagnetic Fe-Pt nanocrystal superlattices, Science. 287 (2000) 1989-1992.

[28] T.K. Jain, M.A. Morales, S.K. Sahoo, D.L. Leslie-Pelecky, V. Labhasetwar, Iron oxide nanoparticles for sustained delivery of anticancer agents, Mol. pharma. 2 (2005)194-205.

[29] C. Sun, J.S. Lee, M. Zhang, Magnetic nanoparticles in MR imaging and drug delivery, Adv. Drug Delivery Rev. 60 (2008) 1252-1265.

[30] E.H. Kim, H.S. Lee, B.K. Kwak, B.K. Kim, Synthesis of ferrofluid with magnetic nanoparticles by sonochemical method for MRI contrast agent, J. Magn. Magn. Mater. 289 (2005) 328-330.

[31] L. Babes, B. Denizot, G. Tanguy, J.J. Le Jeune, P. Jallet, Synthesis of Iron Oxide Nanoparticles Used as MRI Contrast Agents: A Parametric Study, J. Colloid Interface Sci. 212 (1999) 474-482.

[32] D.K. Kim, Y. Zhang, J. Kehr, T. Klason, B. Bjelke, M. Muhammed, Characterization and MRI study of surfactant-coated superparamagnetic nanoparticles administered into the rat brain, J. Magn. Magn. Mater. 225 (2001) 256-261.

[33] J.P. Fortin, F. Gazeau, C. Wilhelm, Intracellular heating of living cells through Neel relaxation of magnetic nanoparticles, Eur. Biophys. J. 37 (2008) 223-228.

[34] J.P. Fortin, C. Wilhelm, J. Servais, C. Menager, J.C. Bacri, F. Gazeau, Size-sorted anionic iron oxide nanomagnets as colloidal mediators for magnetic hyperthermia, J. Am. Chem. Soc. 129 (2007) 2628-2635.

[35] R. Hergt, R. Hiergeist, I. Hilger, W.A. Kaiser, Y. Lapatnikov, S. Margel, U. Richter, Maghemite nanoparticles with very high AC-losses for application in RF-magnetic hyperthermia, J. Magn. Magn. Mater. 270 (2004) 345-357.

[36] R. Hergt, S. Dutz, R. Muller, M. Zeisberger, Magnetic particle hyperthermia: nanoparticle magnetism and materials development for cancer therapy, J. Phys. Condens. Matter. 18 (2006) S2919-S2934.

[37] A. Jordan, R. Scholz, P. Wust, H. Schirra, T. Schiestel, H. Schmidt, R. Felix, Magnetic fluid hyperthermia (MFH): Cancer treatment with AC magnetic field induced excitation of biocompatible superparamagnetic nanoparticles, J. Magn. Magn. Mater. 194 (1999) 185-196.

[38] T. Tuutijarvi, J. Lu, M. Sillanpaa, G. Chen, Adsorption Mechanism of Arsenate on Crystal γ-Fe_2O_3 Nanoparticles J. Environ. Eng. 136 (2010) 897-905.

[39] K. Mosbach, L. Andersson, Magnetic ferrofluids for preparation of magnetic polymers and their application in affinity chromatography, Nature. 270 (1977) 259-261.

[40] S. Chikazumi, S. Taketomi, M. Ukita, M. Mizukami, H. Miyajima, M. Setogawa, Y. Kurihara, Physics of magnetic fluids, J. of Mag. and Mag. Mat. 65 (1987) 245-25.

[41] R.D. McMichael, R.D. Shull, L.J. Swartzendruber, L.H. Bennett, R.E. Watson, Magnetocaloric effect in superparamagnets, J. of Mag. and Mag. Mat. 111 (1992) 29-33.

[42] S. Schiller, U. Heisig, K. Goedicke, H. Bilz, K. Steinfelder, Methods and applications of plasmatron high rate sputtering in microelectronics, hybrid microelectronics and electronics, Thin Solid Films. 92 (1982) 81-98.

[43] R.S. Niranjan, Y.K. Hwang, D.K. Kim, S.H. Jhung, J.S. Chang, I.S. Mulla, Nanostructured tin oxide: Synthesis and gas-sensing properties, Mater. Chem. Phys. 92 (2005) 384-388.

[44] K. Eguchi, T. Setoguchi, T. Inoue, H. Arai, Electrical properties of ceria-based oxides and their application to solid oxide fuel cells, Solid State Ion. 52 (1992) 165-172.

[45] D.D. Hass, J.F. Groves, H.N.G. Wadley, Reactive vapor deposition of metal oxide coatings, Surface and Coatings Technol. 146 -147 (2001) 85-93.

[46] J.L. Graham, C.B. Almquist, S. Kumar, S. Sidhu, An investigation of nanostructured vanadia/titania catalysts for the oxidation of monochlorobenzene, Cat. Today. 88 (2003) 73-82.

[47] S.C. Lee, J.H. Lee, T.S. Oh, Y.H. Kim, Fabrication of tin oxide film by sol-gel method for photovoltaic solar cell system, Sol. Energy Mater. Sol. Cells. 75 (2003) 481.

[48] S. Lany, Semiconducting transition metal oxides, J. Phys.:Condens. Matter. 27 (2015) 283203.

[49] C.T. Dinh, T.D. Nguyen, F. Kleitz, T.O. Doa, Shape-Controlled Synthesis of Metal Oxide Nanocrystals, Controlled Nanofabrication: Advances and Applications Edited by Ru-Shi Liu Copyright © 2013 Pan Stanford Publishing Pte. Ltd. ISBN 978-981-4316-87-3 (Hardcover), 978-981-4364-51-5.

[50] D. Reyes-Coronado, G. Rodríguez-Gattorno, M.E. Espinosa-Pesqueira, C. Cab, R. de Coss, G Oskam, Phase-pure TiO_2 nanoparticles: anatase, brookite and rutile, Nanotechnol. (2008) 145605-145610.

[51] M.B. Hopkins, langmuir probe measurements in the gaseous electronics conference reference cell, J Res. Natl. Inst. Stand. Technol. 100(4) (1995) 415-425.

[52] M.E. Vance, T. Kuiken, E.P. Vejerano, S.P. Mc Ginnis, M.F. Hochella Jr, D. Rejeski, M.S. Hull, Nanotechnology in the real world: redeveloping the nanomaterial consumer products inventory, Beilstein J. of nanotechnol. 6 (1) (2015) 1769-1780.

[53] A. Rahnama, M. Gharagozlo, Preparation and properties of semiconductor CuO nanoparticles via a simple precipitation method at different reaction temperatures, Opt Quant Electron. 44 (2012) 313-322.

[54] F.G, U. Cvelbar, Copper oxide nanowires: a review of growth, nanotechnology. 23 (2012) 194001-194001.

[55] T.H. Tran, V.T. Nguyen, Copper oxide nanomaterials prepared by solution methods, some properties, and potential applications: a brief review, international scholarly research notices.14 (2014) 2014.

[56] Q. Zhang, K. Zhang, D. Xu, G. Yang, H. Huang, F. Nie, C. Liu, S. Yang, CuO nanostructures: Synthesis, characterization, growth mechanisms, fundamental properties, and applications. Prog. Mater. Sci. 60 (2014) 208-337.

[57] A.B. Devi, D.S. Moirangthem, N.C. Talukdar, N.R. Devi Singh, M.N. Luwang, Novel synthesis and characterization of CuO nanomaterials: biological applications, Chin. Chem. Lett. 25 (2014) 1615-1619.

[58] S. Dagher, Y. Haik, A.I. Ayesh, N. Tit, Synthesis and optical properties of colloidal CuO nanoparticles, J. Lumin. 151 (2014) 149-154.

[59] S. Nations, M. Long, M. Wages, J. D. Maul, C. W. Theodorakis, Cobb, G.P. Subchronic, chronic developmental effects of copper oxide (CuO) nanoparticles on Xenopus laevis, Chemosphere. 135 (2015) 166-174.

[60] M.E. Grigore, E.R. Biscu, A.M. Holban, M.C. Gestal, A.M. Grumezescu, Methods of synthesis, properties and biomedical applications of CuO nanoparticles, Pharmaceuticals. 9 (2016) 75.

[61] K.K. Dey, A. Kumar, R. Shanker, A. Dhawan, M. Wan, R.R. Yadav, A.K. Srivastava, Growth morphologies, Phase formation, optical and biological responses of nanostructures of CuO and their application as cooling fluid in high energy density devices, RSC Advances. 2 (2012) 1387-1403.

[62] A. Janotti, C.G. Van de Walle, Fundamentals of zinc oxide as a semiconductor, Rep. Prog. Phys. 72 (2009) 126501.

[63] Z.L. Wang, Zinc oxide nanostructures: growth, properties and applications, J. Phys.: Condens. Matter. 16 (2004) R829-R858.

[64] A.N. Ul Haq, A. Nadhman, I. Ullah, G. Mustafa, M. Yasinzai, I. Khan, Synthesis Approaches of Zinc Oxide Nanoparticles: The Dilemma of ecotoxicity, Journal of Nanomaterials. 2017 (2017) 1-14.

[65] D.P. Norton, Y.W. Heo, M.P. Ivill, K. Ip, S.J. Pearton, M.F. Chisholm, T. Steiner, ZnO: growth, doping & processing, mat. today. 7 (2004) 34-40.

[66] Y. Zhang, M.K. Ram, E.K. Stefanakos, D.Y. Goswami, Synthesis, characterization, and applications of ZnO nanowires, Journal of Nanomaterials, Article ID 624520, (2012) 22.

[67] Z.L. Wang, Zinc oxide nanostructures: growth, properties and applications, J. Phys.: Condens. Matter. 16 (2004) R829-R858.

[68] E.S. Gurzaua, C. Neagub, A. ElenaGurzaua, Essential metals-case study on iron, Ecotoxicology and Environmental Safety. 56 (2003) 190-200.

[69] R.M. Cornell, U. Schwertmann, The Iron Oixdes: Structures, Properties, Reactions, Occurences and Used, Weinheim: Wiley, (2003).

[70] L. Machala, R. Zboril, A. Gedanken, Amorphous Iron (III) Oxides A Review, J. Phys. Chem. B. 111 (2007) 4003-4018.

[71] W. Wu, Z. Wu, T. Yu, C. Jiang, W. S. Kim, Recent progress on magnetic iron oxide nanoparticles: synthesis, surface functional strategies and biomedical applications, Sci. Technol. Adv. Mater. 16 (2015) 023501.

[72] E.L. Hu, D.T. Shaw, Synthesis and Assembly, Nanostructure Sci Tech, Chapter-2 (1999) 15-33.

[73] N. Kumar, S. Kumbhat, Essentials in nanoscience and nanotechnology, published 2016 by John Wily & Sons, Inc, (2016) 31-74.

[74] M.Shah , D. Fawcett , S. Sharma , S. K. Tripathy, G. Eddy, J. Poinern, Synthesis of Metallic Nanoparticles via Biological Entities, Materials. 8 (2015) 7278-7308.

[75] P. Saravanan, R. Gopalan, V. Chandrasekaran Synthesis and characterisation of nanomaterials, Defence Sci. J. 58 (2008) 504-516.

[76] Y. Mizukoshi, T. Shuto, N. Masahashi, S. Tanabe, Preparation of superparamagnetic magnetite nanoparticles by reverse precipitation method: Contribution of sonochemically generated oxidants, Ultra. Sonochem. 16 (2009) 525-531.

[77] M. Sivakumar, A. Gedanken, W. Zhong, Y.H. Jiang, Y.W. Du, I. Brukental, D. Bhattacharya, Y. Yeshurunc, I. Nowik, Sonochemical synthesis of nanocrystalline $LaFeO_3$, J. of Mat. Chem. 14 (2004) 764-769.

[78] C.L. De Castro, B.S. Mitchell, Nanoparticles from mechanical attrition in synthesis, functionalization and surface treatment of nanoparticles Edited by M. I. Baraton (2002) American Scientific Publishers, ISBN: 1-58883-009-8.

[79] C.C. Koch, J.D. Whittenberger, Mechanical milling/alloying of intermetallics, Intermetallics. 4 (1996) 339-355.

[80] R. Janot, D. Guerard, Ball-milling in liquid media: Applications to the preparation of anodic materials for lithium-ion batteries, Progress in Mat. Sci. 50 (2005) 1-92.

[81] C.F. Powell, J.H. Oxley Jr, J.M. Blocher, Vapor Deposition; Wiley, New York, (1967).

[82] N. Ichinose, Y. Ozaki, S. Kashuu, Superfine particle technology, Springer-Verlag, ISBN- 13:978-1-4471-1810-7, (1992).

[83] V.P. Veiko, A.M. Skvortsov, C.T. Huynh, A.A. Petrov, Laser ablation of mono crystalline silicon under pulsed-frequency fiber laser, Sci. and Tech. J. of Information Technol., Mech. and Opt.15 (3) (2015) 426.

[84] S.K. Kulkarni, Nanotechnology: principles and practices, (2015).

[85] H.H. Kung, E.I. Ko, Preparation of oxide catalyst supports a review of recent advances, Chem Eng J. 64 (1996) 203-214.

[86] D.A.H. Hanaor, I. Chironi, I. Karatchevtseva, G. Triani, C.C. Sorrell, Single and mixed phase TiO_2 powders prepared by excess hydrolysis of titanium alkoxide, advances in applied ceramics. 111 (3) (2012) 149-158.

[87] L. Filipponi, D. Sutherland, Introduction to nanoscience and nanotechnologies (2010) http://nanoyou.eu/attachments/188_Module-1-chapter-1.pdf.

[88] C.S. Kim, K. Okuyama, K. Nakaso, M. Shimada, Direct measurement of nucleation and growth modes in titania nanoparticles generation by CVD method, J Chem Eng Japan 37: (2004) 1379-1389.

[89] J.H. Fendler, Colloid chemical approach to nanotechnology, Korean J Chem Eng. 18(1) (2001) 1-13.

[90] N.L. Tarwal, A.V.Rajgure, A.I. Inamdar, R.S. Devan, I.Y. Kim, S.S. Suryavanshi, Y.R. Ma, J.H. Kim, P.S. Patil, Growth of multifunctional ZnO thin films by spray pyrolysis technique, Sensors and Actuators A: Phy.199 (2013) 67-73.

[91] P.S. Patil, Versatility of Chemical spray pyrolysis technique, Mater. Chem. Phys. 59 (1999) 185-198.

[92] D. Sharma, S. Kanchi, K. Bisetty, Biogenic synthesis of nanoparticles: A review, Arabian J. of Chem. (2015).

[93] I. Khan, K. Saeed, I. Khan, Nanoparticles: Properties, applications and Toxicities, Arabian J. of Chem. (2017).

[94] S. Iravani, Green synthesis of metal nanoparticles using plants, Green Chem. 13 (2011) 2638.

[95] S.S. Shankar, A. Ahmd, R. Pasricha, M.J. Sastry, Bioreduction of chloroaurate ions by geranium leaves and its endophytic fungus yields gold nanoparticles of different shapes, Mater Chem. 13 (2003) 1822-1846.

[96] S.S. Shankar, A. Rai, A. Ahmad, M. Sastry, Rapid synthesis of Au, Ag, and bimetallic Au core–Ag shell nanoparticles using Neem (Azadirachta indica) leaf broth, J Colloid Interface Sci. 275 (2004) 496-502.

[97] Ting Zhu, Sylvain G. Cloutier, Ilia Ivanov, Kenneth L. Knappenberger Jr., Istvan Robel, and Fan Zhang, Nanocrystals for Electronic and Optoelectronic Applications, J. of Nanomat. 2012 (2012) 2.

[98] M. Arshadi, Adsorptive removal of an organic dye from aqueous solution with a nano-organometallic: Kinetic, thermodynamic and mechanism, Journal of Molecular Liquids. 211 (2015) 899-908.

[99] M. Anjum, R. Miandad, M. Waqas, F. Gehany, M. A. Barakat, Remediation of wastewater using various nano-materials, Arabian J. of Chem. (2016).

[100] H. Sadegh, Gomaa A.M. Ali, V.K. Gupta, A.S. Hamdy Makhlouf, R. Shahryari-ghoshekandi Mallikarjuna N. Nadagouda Mika Sillanpa, El_zbieta Megiel, The role of nanomaterials as effective adsorbents and their applications in wastewater treatment, J. Nanostruct. Chem. 7 (2017) 1-14.

[101] N. Bhandare, A. Narayana, Applications of Nanotechnology in Cancer: A Literature Review of Imaging and Treatment, J Nucl. Med. Radiat. Ther. (2014) 5:4.

[102] R. Misra, S. Acharya, S. K. Sahoo, Cancer nanotechnology: application of nanotechnology in cancer therapy, Drugery Discovery Today. 15 (2010) 19-20.

[103] X. Wang, L. Yang, Z. (Georgia) Chen, D.M. Shin, Application of nanotechnology in cancer therapy and imaging, CA: A Cancer J. Clin. 58 (2008) 97-110.

[104] F. Marquez, C. Morant, Nanomaterials for Sensor Applications, Soft Nanosci. Lett. 5 (2015) 1-2.

[105] N. Beyth, Y.H. Haddad, A. Domb, W. Khan, R. Hazan, Alternative antimicrobial approach: nano-antimicrobial materials, evidence-based complementary and alternative medicine volume, Article ID 246012, (2015) 16 pages.

[106] J.T. Seil, T.J. Webster, Antimicrobial applications of nanotechnology: methods and literature, Int. J. of Nanomed.7 (2012) 2767-2781.

[107] P.J. Lu, S.C. Huang, Y.P. Chen, L.C. Chiueh, D.Y.C. Shih, Analysis of titanium dioxide and zinc oxide, nanoparticles in cosmetics, J. of food and drug analysis. 23 (2015) 587-594.

[108] P.J. Lu, S.W. Fang, W.L. Cheng, S.C. Huang, M.C. Huang, H.F. Cheng, Characterization of titanium dioxide and zinc oxide nanoparticles in sunscreen powder by comparing different measurement methods, J. of food and drug analysis. 26 (2018) 11192-1200.

[109] M. D. Carvalho, F. Henriques, L.P. Ferreira, M. Godinho, M. M. Cruz, Iron oxide nanoparticles: the Influence of synthesis method and size on composition and magnetic properties, J. of Solid State Chem. 201 (2013) 144-152.

[110] P. Periyathambi, W. S. Vedakumari, S. Bojja, S. B. Kumar, T. P. Sastry, Green biosynthesis and characterization of fibrin functionalized iron oxide nanoparticles with MRI sensitivity and increased cellular internalization, Mat. Chem. and Phy. 148 (2014) 1212-1220.

[111] N. Asmathunisha, K. Kathiresan, A review on biosynthesis of nanoparticles by marine organisms, Colloids and Surfaces B: Bioint. 103 (2013) 283-287.

[112] A. Schrofel, G. Kratosova, I. Safarik, M. Safarikova, I. Raska, L.M. Shor, Applications of biosynthesized metallic nanoparticles - A review, Acta Biomat. 10 (2014) 4023-4042.

[113] S. Ahmed, Annu, S.A. Chaudhry, S. Ikram, A review on biogenic synthesis of ZnO nanoparticles using plant extracts and microbes: A prospect towards green chemistry, Journal of Photochemistry & Photobiology B: Bio. 166 (2017) 272-284.

[114] B. Ahmmad, K. Leonard, Md.S. Islam, J. Kurawaki, M. Muruganandham, T. Ohkubo, Y. Kuroda, Green synthesis of mesoporous hematite (α-Fe_2O_3) nanoparticles and their photocatalytic activity, Advanced Powder Technol. 24 (2013) 160-167.

[115] M. Behera, G. Giri, Inquiring the photo-catalytic activity of cuprous oxide nanoparticles synthesized by a green route on methylene blue dye, Int. J. Ind. Chem. 7 (2016) 157-166.

[116] S. Bagheri, K. Shameli, S. Bee A. Hamid, Synthesis and characterization of anatase titanium dioxide nanoparticles using egg white solution via sol-gel method, J. of Chem.. 2013 (2012) 5.

[117] A.K. Biswas, Md. R. Islam, Z.S. Choudhury, A. Mostafa, M.F. Kadir, Nanotechnology based approaches in cancer therapeutics, Adv. Nat. Sci.: Nanosci. Nanotechnol. 5 (2014) 043001.

[118] C. Buzea, I. Ivan, B. Pacheco, R. Kevin, Nanomaterials and nanoparticles: Sources and toxicity, Biointerphases. 2 (2007) MR17-MR71.

[119] M.J. Akhtar, M. Ahamed, S. Kumar , M.M. Khan, J. Ahmad, S.A. Alrokayan, Zinc oxide nanoparticles selectively induce apoptosis in human cancer cells through reactive oxygen species, Int. J. Nanomed. 7 (2012) 845-57.

[120] B.C. Choudhary, D. Paul, T. Gupta, S.R. Tetgure, V.J. Garole, A.U. Borse, D. J. Garole, Photo catalytic reduction of organic pollutant under visible light by green route synthesized gold nanoparticles, journal of environmental sci. 55 (2017) 236-246.

[121] V. Madhubala, T. Kalaivani, Phyto and hydrothermal synthesis of Fe_3O_4@ZnO core-shell nanoparticles using Azadirachta indica and its cytotoxicity studies, App. Surface Sci. 449 (2018) 584-590.

[122] B. Das, S.K. Dash, D. Mandal, T. Ghosh, S. Chattopadhyay, S. Tripathy, S. Das, S.K. Dey, D. Das, Somenath Roy, Green synthesized silver nanoparticles destroy multidrug resistant bacteria via reactive oxygen species mediated membrane damage, Arabian J. of Chem. 10 (2017) 862-876.

[123] F. Davar, A. Majedi, A. Mirzaei, Green Synthesis of ZnO nanoparticles and its application in the degradation of some dyes, J. Am. Ceram. Soc. 98 (2015) 1739-1746.

[124] C.P. Devatha, A. K. Thalla, S.Y. Katte, Green synthesis of iron nanoparticles using different leaf extracts for treatment of domestic wastewater, J. of Cleaner Prod. 139 (2016) 1425-1435.

[125] S.M. Dizaj, F. Lotfipour, M.B. Jalali, M.H. Zarrintan, K. Adibkia, Antimicrobial activity of the metals and metal oxide nanoparticles, Materials Science and Engineering: C. 44 (2014) 278-284.

[126] R. Dobrucka, J. Dugaszewska, Biosynthesis and antibacterial activity of ZnO nanoparticles using Trifolium pratense flower extract, Saudi J. of Bio. Sci. 23 (2016) 517-523.

[127] M.H. Ehrampoush, M. Miria, M.H. Salmani, A.H. Mahvi, Cadmium removal from aqueous solution by green synthesis iron oxide nanoparticles with tangerine peel extract, J. of Env. Health Sci. & Eng. (2015) 13:84.

[128] Y.E.K. Hala, M.A. Aly-Eldeen, S.M. Gharib, Green synthesis of iron oxide (Fe_3O_4) nanoparticles using two selected brown seaweeds: Characterization and application for lead bioremediation, Acta Oceanol. Sin. 35 (2016) 89-98.

[129] L. Fua, Z. Fu, Plectranthus amboinicus leaf extract–assisted biosynthesis of ZnO nanoparticles and their photocatalytic activity, Ceramics Int. 41 (2015) 2492-2496.

[130] M.E. Grigore, E.R. Biscu, A.M. Holban, M.C. Gestal, A.M. Grumezescu, Methods of Synthesis, Properties and Biomedical Applications of CuO Nanoparticles, Pharmaceuticals. 9 (2016) 75.

[131] H. Muthukumar, M. Manickam, Amaranthus spinosus leaf extract mediated FeO nanoparticles: Physicochemical traits, photocatalytic and antioxidant activity, Sustainable Chem. Eng. 3 (2015) 3149-3156.

[132] F.J. Heiligtag, M. Niederberger, The fascinating world of nanoparticle research, Mat. Today. 16 (2013) 262-271.

[133] G.E. Hoag, J.B. Collins, J.L. Holcomb, J.R. Hoag, M.N. Nadagouda, R.S. Varma, Degradation of bromothymol blue by 'greener' nano-scale zero-valent iron synthesized using tea polyphenols, J. Mater. Chem. 19 (2009) 8671-8677.

[134] N.I. Hulkoti, T.C. Taranath, Biosynthesis of nanoparticles using microbes-A review, Colloids and Surfaces B: Biointerfaces. 121 (2014) 474-483.

[135] I. Khan, K. Saeed, I. Khan, Nanoparticles: Properties, applications and toxicities, Arabian J. of Chem. (2017).

[136] A. Ivask, K. Juganson, O. Bondarenko, M. Mortimer, V. Aruoja, K. Kasemets, I. Blinova, M. Heinlaan, V. Slaveykova, A. Kahru, Mechanisms of toxic action of Ag, ZnO and CuO nanoparticles to selected ecotoxicological test organisms and mammalian cells in vitro: A comparative review, Nanotoxicology. 8 (2014) 57-71.

[137] V. Jassal, U. Shanker, B. S. Kaitha, S. Shankar, Green synthesis of potassium zinc hexacyanoferrate nanocubes and their potential application in photocatalytic degradation of organic dyes, RSC Adv. 5 (2015) 26141-26149.

[138] S. Gao, Y. Shi, S. Zhang, K. Jiang, S. Yang, Z. Li, E.T. Muromachi, Biopolymer-assisted green synthesis of iron oxide nanoparticles and their magnetic properties, J. Phys. Chem. C. 112 (2008) 10398-10401.

[139] Y. Kuang, Q. Wang, Z. Chen, M. Megharaj, R. Naidu, Heterogeneous Fenton-like oxidation of monochlorobenzene using green synthesis of iron nanoparticles, J. of Colloid and Int. Sci. 410 (2013) 67-73.

[140] J. Kumari, A. Singh, Green synthesis of nanostructured silver particles and their catalytic application in dye degradation, J. of Genetic Eng. and Biotech. 14 (2016) 311-317.

[141] S. Lata, S.R. Samadder, Removal of arsenic from water using nano adsorbents and challenges: A review, J. of Env. Mana. 166 (2016) 387-406.

[142] H. Lu, J. Wang, M. Stoller, T. Wang, Y. Bao, O. Hao, An Overview of Nano materials for Water and Wastewater Treatment, Adv. in Mat. Sci. and Eng. 2016 (2016)10.

[143] M. Mahdavi, F. Namvar, M.B. Ahmad, R. Mohamad, Green biosynthesis and characterization of magnetic iron oxide (Fe_3O_4) Nanoparticles Using Seaweed (Sargassum muticum) Aqueous Extract, Molecules. 18 (2013) 5954-5964.

[144] N. Matinise, X.G. Fukua, K. Kaviyarasua, N. Mayedwaa, M. Maaza, ZnO nanoparticles via Moringa oleifera green synthesis: Physical properties & mechanism of formation, App. Surface Sci. 406 (2017) 339-347.

[145] S.R. Mudshinge, A.B. Deore, S. Patil, C.M. Bhalgat Nanoparticles: Emerging carriers for drug delivery, Saudi Pharma. J. 19 (2011) 129-141.

[146] C. Mystrioti, T.D. Xanthopoulou, N. Papassiopi, A. Xenidis, Comparative evaluation of five plant extracts and juices for nanoiron synthesis and application for hexavalent chromium reduction, Sci. of the Total Env. 539 (2016) 105-113.

[147] B. Aslan, B. Ozpolat, A.K. Sood, G.L. Berestein, Nanotechnology in cancer therapy, J. Drug Target. 21 (2013) 904-913.

[148] V.V.T. Padil, M. Cernik, Green synthesis of copper oxide nanoparticles using gum karaya as a biotemplate and their antibacterial application, International J. of Nanomedicine. 8 (2013) 889-898.

[149] J. Peternela, M.F. Silva, M.F. Vieir, R. Bergamasco, A.M.S. Vieira, Synthesis and Impregnation of Copper Oxide Nanoparticles on Activated Carbon through Green Synthesis for Water Pollutant Removal, Mat. Res. 21 (2016) e20160460.

[150] M. Guzman, J. Dille, S. Godet, Synthesis and antibacterial activity of silver nanoparticles against gram-positive and gram-negative bacteria, Nanomedicine: Nanotechnol., Bio., and Med. 8 (2012) 37-45.

[151] M. Al-Qahtani Khairia, Cadmium removal from aqueous solution by green synthesis zero valent silver nanoparticles with Benjamina leaves extract, Egyptian J. of Aquatic Res. 43 (2017) 269-274.

[152] K. Quester, M. A. Borja, E. C. Longoria, Biosynthesis and microscopic study of metallic nanoparticles, Micron. 54 (2013) 1-27.

[153] J. Santhoshkumar, S.V. Kumar, S. Rajeshkumar, Synthesis of zinc oxide nanoparticles using plant leaf extract against urinary tract infection pathogen, Resource-Efficient Technol. 3 (2017) 459-465.

[154] K.O. Shittu, O. Ihebunna, Purification of simulated waste water using green synthesized silver nanoparticles of Piliostigma thonningii aqueous leave extract, Adv. Nat. Sci.: Nanosci. Nanotechnol. 8 (2017) 045003.

[155] T. Sinha, M. Ahmaruzzaman, Biogenic synthesis of Cu nanoparticles and its degradation behavior for methyl red, Mat. Lett. (2015).

[156] J. Suarez-Cerda, G. Alonso-Nunez, H. Espinoza-Gomez, L.Z. Flores-Lopez, Synthesis, kinetics and photo catalytic study of “ultra-small” Ag-NPs obtained by a green chemistry method using an extract of Rosa 'Andeli' double delight petals, Journal of Colloid and Int. Sci. 458 (2015) 169-177.

[157] K.B. Sutradhar, Md. L. Amin, Nanotechnology in Cancer Drug Delivery and Selective Targeting, ISRN Nanotechnol. 2014 (2014) 12.

[158] U. Shanker, V. Jassal, M. Rani, Catalytic removal of organic colorants from water using some transition metal oxide nanoparticles synthesized under sunlight, RSC Adv. 6 (2016) 94989-94999.

[159] L. Wang, C. Hu, L. Shao, The antimicrobial activity of nanoparticles: present situation and prospects for the future, International Journal of Nanomedicine. 12 (2017) 1227-1249.

[160] T. Wang, X. Jin, Z. Chen, M. Megharaj, R. Naidu, Green synthesis of Fe nanoparticles using eucalyptus leaf extracts for treatment of eutrophic wastewater, Sci. of the Total Env. 466-467 (2014) 210-213.

[161] H. Xin, X. Yang, X. Liu, X. Tang, L. Weng, Y. Han, Biosynthesis of Iron Nanoparticles Using Tie Guanyin Tea Extract for Degradation of Bromothymol Blue, J. of Nanotechnol. 2016 (2016) 8.

[162] P. Xu, G. M. Zeng, D.L. Huang, C.L. Feng, S. Hu, M.H. Zhao, C. Lai, Z. Wei, C. Huang, G.X. Xie, Z.F. Liu, Use of iron oxide nanomaterials in wastewater treatment: A review, Sci. of the Total Env.. 424 (2012) 1-10.

[163] Y. Zhang, B. Wu, H. Xu, H. Liu, M. Wang, Y. He, B. Pan, Nano materials-enabled water and wastewater treatment, Nano Impact. 3 (2016) 22-39.

[164] S.A. Aromal, D. Philip, Green synthesis of gold nanoparticles using Trigonella foenum-graecumand its size dependent catalytic activity. Spectrochimica Acta Part A: Mol Bio Spectro. 97 (2012) 1-5.

[165] A.I. Lukman, B. Gong, C.E. Marjo, U. Roessner, A.T. Harris, Facile synthesis, stabilization, and anti-bacterial performance of discrete Ag nanoparticles using Medicago sativa seed exudates, J Colloid Interface Sci. 353 (2010) 433-444.

[166] A. Singh, M. Talat, D. Singh, O.N. Srivastava, Biosynthesis of gold and silver nanoparticles by natural precursor clove and their functionalization with amine group, J Nanoparticle Res. 12 (2010) 1667-1675.

[167] N. Ahmad, S. Sharma, M.K. Alam, V.N. Singh, S.F. Shamsi, B.R. Mehta, A. Fatma Rapid synthesis of silver nanoparticles using dried medicinal plant of basil. Colloids Surf B: Bioint. 81 (2010) 81-86.

[168] L.C. Gruen, Interaction of amino acids with silver (I) ions. Biochim Biophys Acta, 386 (1975) 270-274.

[169] A. Gangula, R. Podila, M. Ramakrishna, L. Karanam, C. Janardhana, A.M. Rao, Catalytic Reduction of 4-Nitrophenol using Biogenic Gold and Silver

Nanoparticles Derived from Breynia rhamnoides, Langmuir. 27(2011)15268-15274

[170] P. Banerjee, S. Sau, P. Das, A. Mukhopadhyay, Green synthesis of silver - nanocomposite for treatment of textile dye, Nanosci. Technol. 1(2) (2014) 1-6.

[171] M. Vinothkannan, C. Karthikeyan, G.G. Kumar, A.R. Kim, D.J. Yoo, One-pot green synthesis of reduced graphene oxide (RGO)/Fe_3O_4 nanocomposites and its catalytic activity toward methylene blue dye degradation, Spectrochimica Acta Part A: Molecular and Bio. Spec. 136(2015) 256-264.

[172] Z.Y. Ozkan, M. Cakirgoz, E.S. Kaymak, E. Erdim, Rapid decolorization of Textile wastewater by green synthesized iron nanoparticles, Water Sci. technol. 77 (2) (2017) 511-517.

Chapter: 2

Experimental Techniques

2.1. Introduction

Nanomaterials act in a different way as the size varies with respect to the bulk. Hence, characterization of nanomaterials is important to analyze the varied physical, structural and optical properties. This chapter describes the assorted strategies of characterization of nanomaterials. Various characterization techniques have been using to identify the characteristics of nanomaterials such as, SEM, EDS, XRD, TEM, FTIR spectrum analysis, UV-Vis spectrum analysis, BET etc.

2.2. Characterization Techniques

2.2.1. Scanning electron microscopy

Scanning electron microscopy (SEM) is one of the most widely used characterization technique to obtain a high enlargement of three-dimension images for morphological and topographical studies of materials and surfaces on the scale of micrometer and submicrometer. SEM benefits from a large depth of field so most of the specimen surface is simultaneously in focus whatever the surface roughness [1]. SEM provides some advantages over TEM such that SEM permits non-destructive evaluation of the specimen whether the TEM is effectively a destructive technique because of the specimen preparation required. Easy specimen preparation process and consuming for specimen preparation time also provide the advantage of SEM over TEM [2]. The scanning electron microscope (SEM) uses a focused beam of high-energy electrons to generate a variety of signals in the form of electrons or photons at the surface region of solid specimens. SEM produces the three types of images: secondary electron images,

backscattered electron images, and elemental X-Ray maps [3]. The most common imaging mode collects secondary electrons that are ejected from the k-shell of the specimen atoms by inelastic scattering interactions with the energy less than 50 eV. Secondary electrons originate within the range of few nanometers from the specimen surface due to their lower energy [2, 4]. The emission of electrons from the specimen surface is typically confined to a neighborhood to the beam impact zone that allows pictures to be obtained at high resolution. These pictures, as seen on an electron beam tube, offer a 3-dimensional look because of the massive depth of field of the SEM furthermore because of the shadow relief of the secondary electrons distinction. The backscattering can seemingly occur in an exceedingly material of upper number and encompass high-energy electrons originating within the electromagnetic wave, that square measure mirrored or back-scattered out of the specimen interaction volume by elastic scattering interactions with specimen atoms with the energy larger than fifty work unit. Back-scattered electrons are used to detect contrast between areas with different chemical compositions [1, 2]. After the first electromagnetic wave collides with associated atom within the specimen and ejects a core electron from the atom, the excited atom then decays into its ground state and emit either a characteristic X-ray gauge boson or an Auger electron. Schematic diagram of SEM and the interaction between incident electrons and specimen have shown in Fig.2.1.

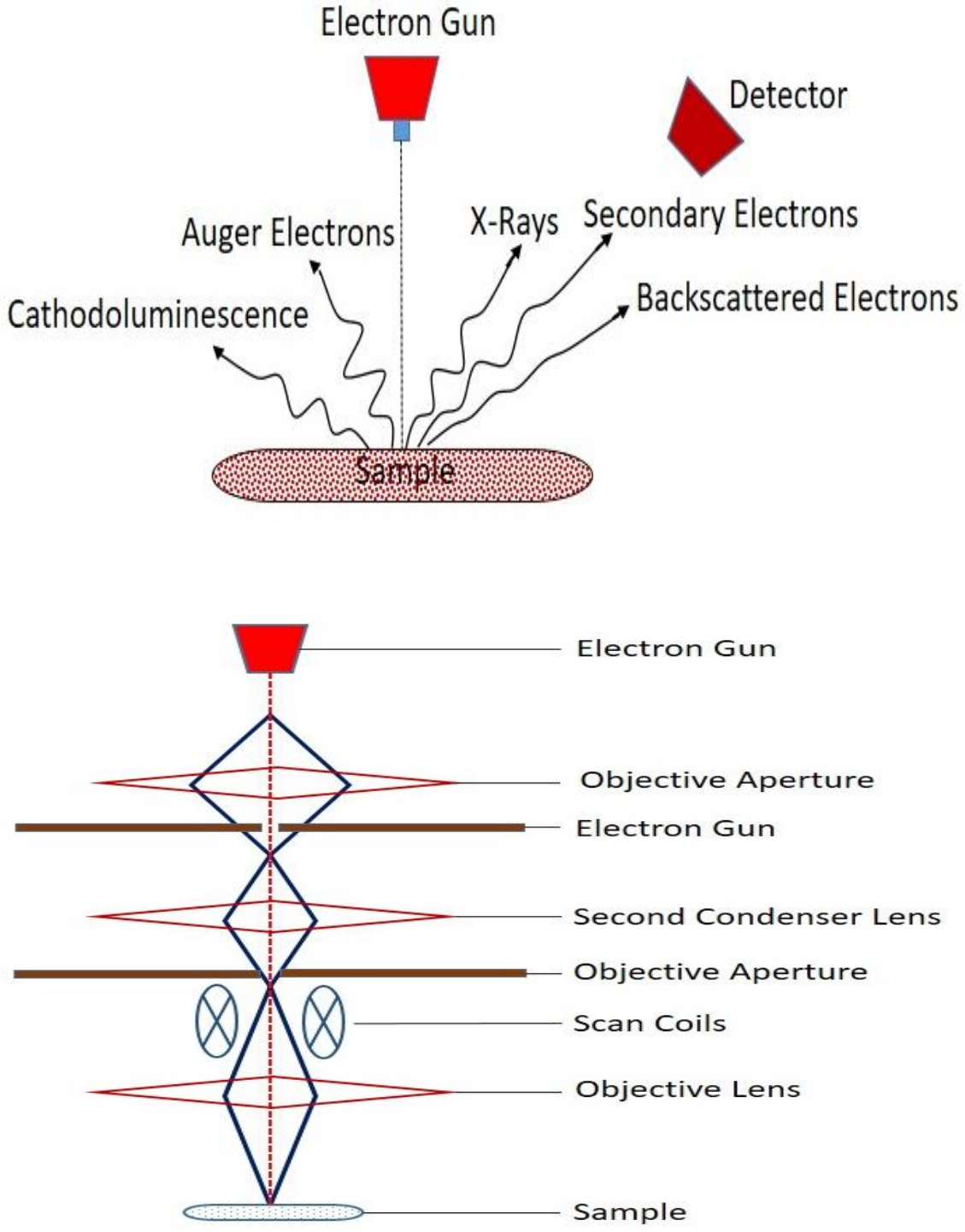

Fig. 2.1: Schematic diagram of the interaction between incident electrons and specimen and SEM

2.2.2. Energy dispersive X-Ray spectroscopy

Energy-dispersive X-Ray spectroscopy EDX, is an analytical technique used for the elemental analysis or chemical characterization of a sample. It relies on an interaction of some source of X-Ray excitation and a sample. Its characterization capabilities are due to the fundamental principle that is each element has a unique atomic structure allowing a unique set of peaks on its electromagnetic emission spectrum [5].

2.2.3. Field emission scanning electron microscope (FE-SEM)

The Field emission scanning electron microscope (FE-SEM) could be a terribly useful gizmo for high-resolution surface imaging within the fields of nanomaterials science. The field emission scanning microscope (FE-SEM) pictures a sample surface by formation scanning over it with a high-energy beam of electrons. In FE-SEM, the electrons interact with the atoms comprising the sample to supply signals that contain data regarding surface topography, composition and alternative properties. The work of the electron gun is to produce an outsized and stable current in a very little beam. There are two unit categories of emission source: a thermionic emitter and field electrode. Type of the emitter is the main distinction between the scanning microscope (SEM) and also the emission scanning microscope (FE-SEM). Field emission scanning electron microscopy (FE-SEM) provides topographical and elemental information at magnifications of 10x to 300,000x, with the virtually unlimited depth of field. Compared with convention scanning electron microscopy (SEM), field emission SEM (FE-SEM) produces clearer, less electrostatically distorted images. FE-SEM have various advantages like, low-voltage images with accelerating voltages ranging from 0.5 to 30 kilovolts, High-quality and there is no need for placing conducting coatings on insulating materials.

2.2.4. Transmission electron microscopy (TEM)

Transmission microscopy (TEM) is a powerful technique first developed within the 1930's to get data on morphology, size, crystal structure and defect structure of the crystalline materials [6]. In TEM, a beam of electrons is transmitted through the ultrathin specimen to form an image. An image is formed from the interaction of the electrons with the sample as the beam is transmitted through the specimen and the image is focused and magnified onto an imaging device. Electrons are typically generated in the associate microscope by a method referred to as emission from a filament, typically tungsten, within the same manner as a light bulb, or instead by field electron emission [7].TEMs are capable of imaging at a considerably higher resolution than light-weight microscopes due to the de Broglie wavelength of electrons. This permits the instrument's user to look at the fine detail whilst tiny as one column of atoms, that is tens of thousands times smaller than the slightest resolvable object during a microscope. TEM forms a significant analysis methodology during a variety of scientific fields, in each physical and biological sciences. TEM realize application in cancer analysis, virology, materials science further as pollution and semiconductor analysis. TEM image distinction is because of absorption of electrons within the material at smaller magnifications, because of the thickness and composition of the fabric. At higher magnifications complicated wave interactions modulate the intensity of the image, requiring professional analysis of ascertained pictures. Alternate modes of use afford the TEM to watch modulations in chemical identity, crystal orientation, leptonic structure and sample induced electron part shift in addition because the regular absorption based mostly imaging.

According to the theory, the utmost resolution, ‘d’ that one will get with a lightweight magnifier has been restricted by the wavelength of the photons that are being employed to probe the sample, λ and therefore the numerical aperture of the system, NA [8].

$$d = \frac{\lambda}{2\sin\alpha} \approx \frac{\lambda}{2NA} \qquad 2.1$$

Like all matter, electrons have both wave and particle properties (as theorized by Louis-Victor Diamond State Broglie), and their wave-like properties mean that a beam of electrons will be created to behave sort of a beam of the electromagnetic wave. The wavelength of electrons is found by leveling the Broglie equation to the mechanical energy of the associated electron. A further correction should be created to account for relativistic effects, as in TEM associate electron’s rate approaches the speed of sunshine, c [9].

$$\lambda_e = \frac{h}{\sqrt{2m_0E(1+\frac{E}{2m_0c^2})}} \qquad 2.2$$

Where, h is Planck's constant, m_0 is the rest mass of an electron and E is the energy of the accelerated electron.

The transmitted beam contains information regarding electron density, phase and periodicity and employed to make a picture. A TEM consists of many elements that embrace a vacuum system within which the electrons travel associate electron emission supply for generation of the electron stream, a series of magnetic attraction lenses, furthermore as electricity plates [10, 11].

TEM microscopic technique provides the advancement over the other technique because, with the help of this technique we can not only obtain the images of the sample but also diffraction patterns, which enable to make the detailed crystal structure analysis of the sample. With the help of diffraction analysis of material, one can find out size-

dependent changes in the lattice parameters, defects etc. in the sample. Moreover, it is also possible to analyze single particles at low dimensional scale. Schematic diagram of TEM has been shown in Fig.2.2.

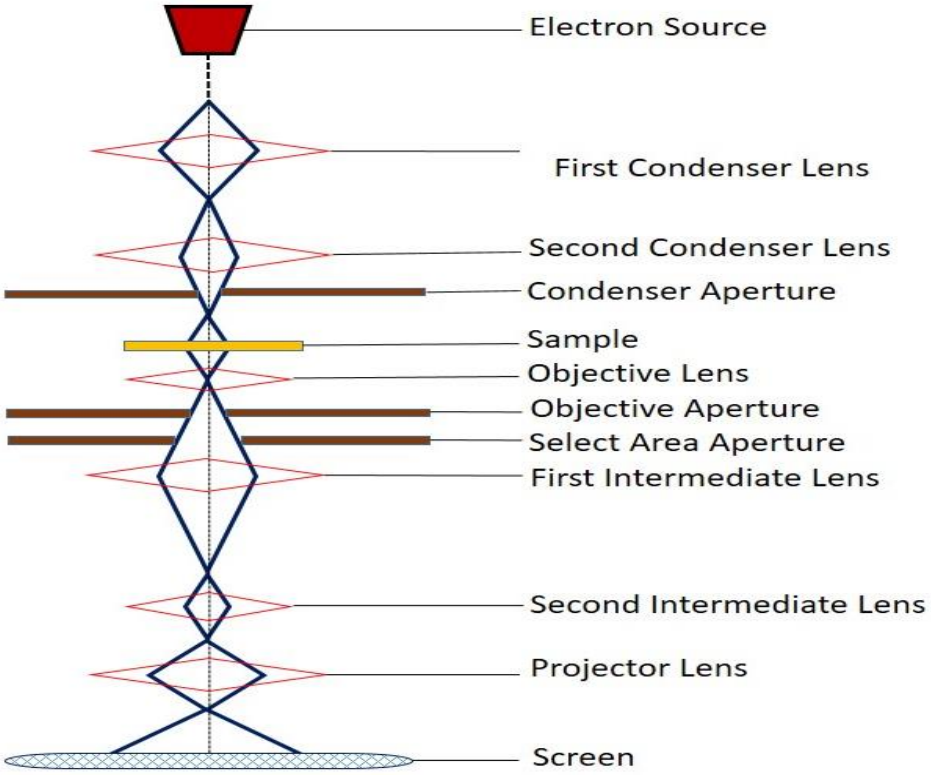

Fig. 2.2: Schematic diagram of TEM

2.2.5. X-Ray diffraction

X-Ray diffraction (XRD) is a very important technique that has been used to determine the crystal structure of solids, lattice constants, geometry, identification of unknown materials, the orientation of single crystals and defects. This technique is based on the constructive interference of monochromatic X-Rays and a crystalline sample. The XRD spectra are obtained by the measurement of the angles at which an X-Ray beam is diffracted by the crystalline phases in the specimen. In XRD, X-Rays are generated by a cathode ray tube than filtered to produce monochromatic radiation and collimated to concentrate and finally focused toward the specimen. The interaction of the incident

rays with the sample produces constructive interference (and a diffracted ray) when conditions satisfy Bragg's law. Bragg's equation relates the distance between two hkl planes and the angle of diffraction

$$2d \sin\theta = n\lambda \quad (2.3)$$

Where d is the interplaner spacing generating the diffraction, q is the diffraction angle, n is an integer and λ is the wavelength of the X-Rays.

Bragg's law tells about the wavelength of electromagnetic radiation to the diffraction angle and the lattice spacing in a crystalline sample and diffracted X-Rays are detected, processed, and counted. By scanning the specimen through a spread of 2θ angles, all attainable optical phenomenon directions of the lattice ought to be earned because of the random orientation of the small-grained material. When electrons have the appropriate energy to dislodge inner shell electrons of the target material, characteristic X-Ray spectra are made. These spectra encompass many parts; the foremost common being K_α and K_β. K_α consists, in part, of $K_{\alpha1}$ and $K_{\alpha2}$. $K_{\alpha1}$ features a slightly shorter wavelength and double the intensity of $K_{\alpha2}$. The precise wavelengths are characteristic of the target material (Cu, Fe etc.). Filtering, by foils or crystal monochromators, is needed to supply monochromatic X-Rays required for the optical phenomenon. $K_{\alpha1}$ and $K_{\alpha2}$ are sufficiently advance wavelength specified a weighted average of the two is employed. Copper is that the most typical target material for the single crystal optical phenomenon, with CuK_α radiation [12]. XRD broadening analysis has been widely used to determine the crystal size of nanoscale materials. The average size of the nanoparticles can be estimated using the Debye-Scherrer equation [13-14]:

$$d=0.89\lambda/\beta\cos\theta \quad (2.4)$$

Where d is the average mean diameter of NPs, λ is the wavelength of X-ray radiation source, 0.89 is a constant crystalline shape factor, θ is the Bragg's diffraction angle, and

β is the angular full width at half maximum (FWHM) of XRD peaks and 2θ is diffraction angle. Conclusively, with the help of analysis of XRD spectra, we can determine the unit cell parameters of the nanocrystalline materials, the degree of crystallinity, the uniqueness of nanocrystal structure and phase purity. Figure 2.2: Schematic representation of XRD and scattering of rays from different planes, in the same direction has been shown in Fig.2.3.

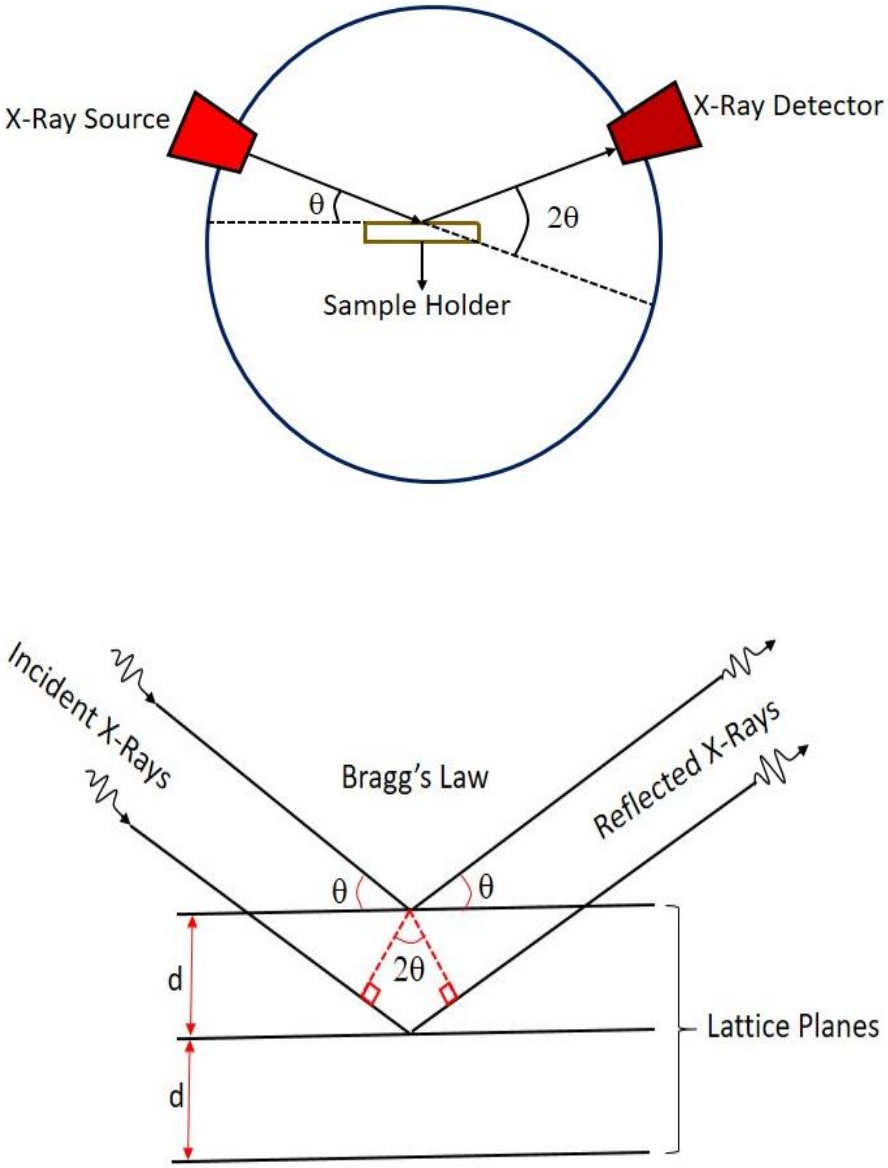

Fig. 2.3: Schematic representation of X-Ray diffraction and scattering of rays from different planes, in the same direction.

2.2.6. Fourier transform infrared (FTIR) spectroscopy

FTIR spectroscopy is an optical technique, use to analyze both organic and inorganic materials. The pictorial diagram of FTIR shown in Fig.2.4. In this spectroscopy, a light ray having wavelengths lying in between near-infrared to the far-infrared region is absorbed by molecules inside the materials, able to specify the presences of various bonds inside the molecules. The mechanism takes place inside the FTIR-spectrometer can be stated very easily. Under this process, a Fourier transformation of the interferogram is followed by the primary collection of sample's interferogram using a Michelson interferometer, to obtain the actual spectrum [15]. The infrared spectrum performs only if the vibrations among bonded atoms produces a permanent amendment within the dipole moment of the molecule. It is judicious to assume that a lot of polar a bond, a lot of intense are IR spectrum arise from the vibrations of the bond. The data regarding symmetry, structure, bond strength, inter and intramolecular interactions etc., are acquired by IR spectra. Intensity and spectral position of IR absorptions permit the identification of the structure of a presented molecule in the sample material. Using this technique, samples can be characterized in solid, liquid and gaseous phases. The entire spectrum of the polyatomic molecule may be divided into purposeful cluster region and also the fingerprint region. The purposeful cluster region is mostly thought-about from 4000 cm^{-1} to 1500 cm^{-1}. The fingerprint region exits among the wavenumber vary 1500 cm^{-1} to 400 cm^{-1}[16]. Generally, IR mass spectrometer is enclosed with a supply, a monochromator, and a detector. IR supply provides a continuing and high radiation energy output into the IR region. The foremost often used sources in the production of IR radiation are the Nernst Glower and the Globar [17]. In IR spectrum analysis, mainly the L-alanine doped deuterated triglycine sulphate (DLaTGS), deuterated triglycine sulphate (DTGS), mercury metal compound (MCT) detectors are usually used. FTIR

instrument contains the dispersive device, prism or grating monochromator, is replaced by Michelson interferometer. The beam splitter splits the radiation into two beams that are mirrored back from mirrors to beam splitter. The recombined beams produce interference at the beam splitter. If beam passes through the sample, absorptions cause gaps in distribution. One mirror of the measuring system is affected toward and far away from the splitter at a constant speed. The detector sees an interferogram (time domain signal) that is reborn into frequency domain spectrum by Fourier rework. FTIR spectroscopy has an advantage over the dispersive IR spectroscopy, mainly due to its capability of observation of all the wave numbers together within same measurement time, having with the same resolution and also with the help of same source and detector. Furthermore, FTIR is facilitated than a dispersive IR in such a manner that without the requirement of any slit to attain high resolution.

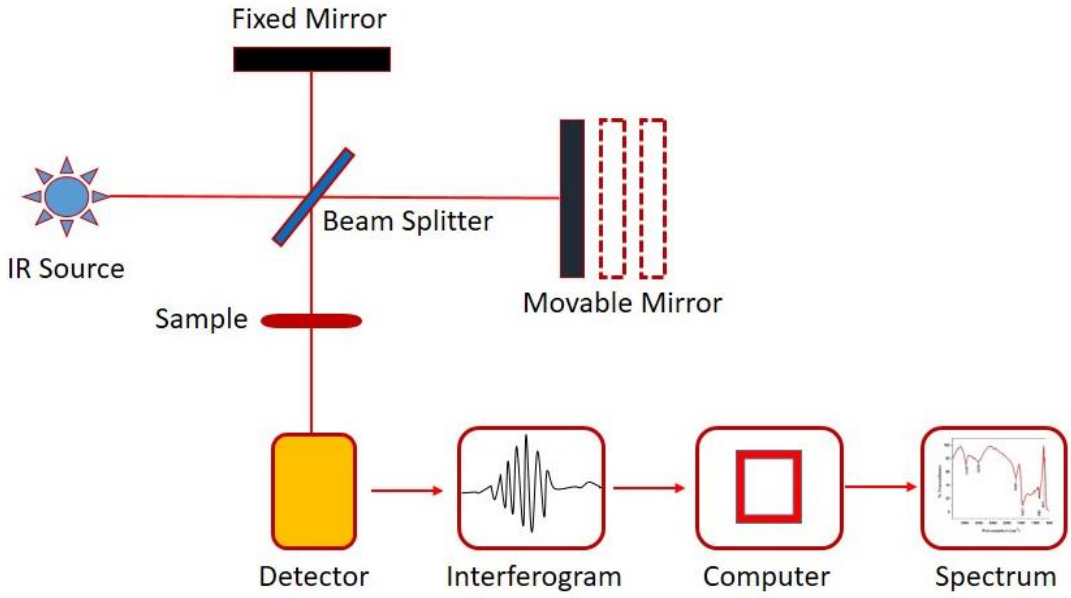

Fig. 2.4: The pictorial diagram of FTIR

2.2.7. Ultraviolet-visible spectroscopy

Ultraviolet-Visible spectroscopy (UV-Vis) refers to absorption spectroscopy or reflectance spectroscopy in the ultraviolet-visible spectral region. This means it uses light in the visible and adjacent ranges. In the UV-Vis spectroscopy, Light with wavelength from 400 nm to1100 nm is generated by a halogen lamp and a deuterium lamp. Amount of light that makes it through the sample is compared to the amount when the sample is not present. The absorption or reflectance in the visible range directly affects the perceived color of the chemicals involved. In this region of the electromagnetic spectrum, atoms and molecules undergo electronic transitions. Absorption spectroscopy is complementary to fluorescence spectroscopy, in that fluorescence deals with transitions from the excited state to the ground state, while absorption measures transitions from the ground state to the excited state. The absorption spectra and bandgap analysis of nanoparticles were attempted by UV-visible spectroscopy. UV-visible spectrum was recorded using a double beam spectrophotometer. The absorbance 'A' can be defined as

$$A=\varepsilon cx \qquad 2.5$$

Where, x = sample path length (cm), c = concentration (mol/L), ε = molar extinction coefficient ($mol^{-1}cm^{-1}$). With the help of absorption spectra we can also describe the particle size and size distribution of different materials in solution form. Usually a blue shift (decrease in wavelength) is associated with a decrease in particles size and vice-versa. Light with wavelength from 400 nm to1100 nm is generated by a halogen lamp and a deuterium lamp. Then the light is divided into two equal-intensity beams and passes through a prepared sample and a reference sample, respectively. A silicon photodiode is used to record the intensity of the transmitted light. The optical band gap of nanomaterials can be determined from Tauc relation [18]

$$\alpha(h\nu)=\beta(h\nu-E_g)^m \quad 2.6$$

where, α is the extinction coefficient, β is the constant and has different values for different transitions, E_g is the energy gap, hν is the photon energy and m denotes an exponent (m = 2) for an indirect allowed transition (plotted between α(hν)1/2 and hν); (m = 3) for an indirect forbidden transition (plotted between α(hν)1/3 and hν); (m = 1/2) for a direct allowed transition (plotted between $\alpha(h\nu)^2$ and hν); (m = 3/2) for a direct forbidden transition (plotted between α(hν)2/3 and hν) [19]. Schematic diagram of UV-Vis spectrophotometer has shown in Fig. 2.5.

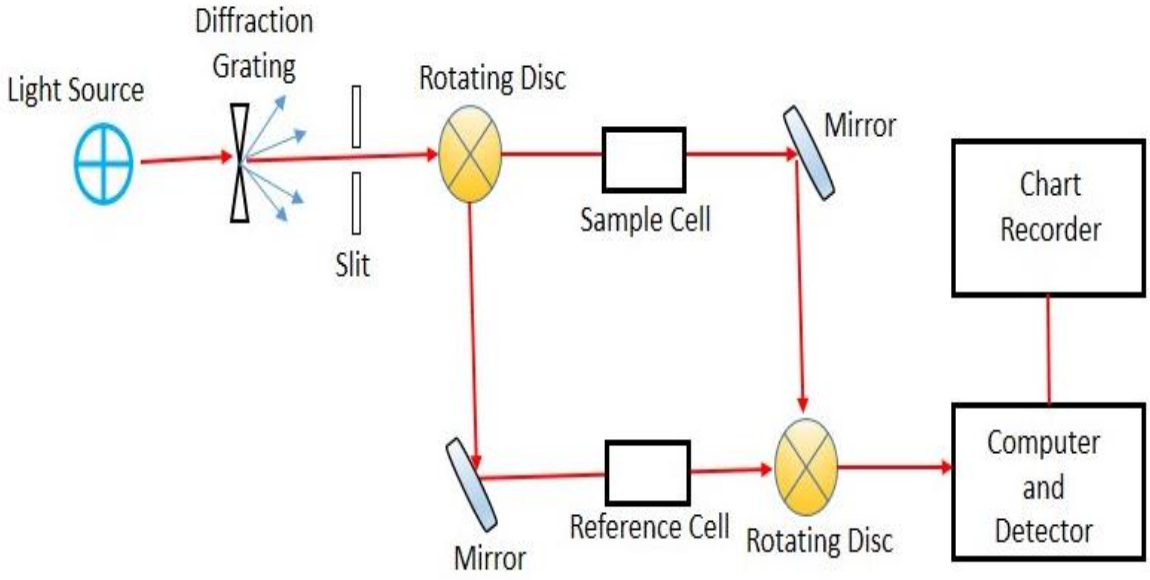

Fig. 2.5: Schematic diagram of UV-Vis absorption spectrophotometer

2.2.8. Dynamic light scattering (DLS)

DLS could be a very helpful technique in material science that may be used to confirm the size distribution profile of tiny particles in suspension in a solution [20]. In the scope of DLS, temporal fluctuations are measured by suggests of the intensity or photon auto-correlation perform. In the time domain analysis, the autocorrelation function (ACF) sometimes decays ranging from zero delay time, and quicker dynamics because of smaller particles cause quicker decorrelation of scattered intensity trace. It's been shown

that the intensity ACF is that the Fourier transform of the power spectrum, and so the DLS measurements are equally well performed within the spectral domain [21-22]

2.2.9. Brunauer-Emmett-Teller (BET)

Brunauer-Emmett-Teller (BET) theory aims to clarify the physical surface assimilation of gas molecules on a solid surface and is the idea for a very important analysis technique for the measurement of the particular expanse of materials. In 1938, author Brunauer, Paul Hugh Emmett, and Edward Teller printed the primary article concerning the BET theory within the Journal of the yankee Chemical Society [23]. The BET theory applies to systems of multilayer surface assimilation and typically utilizes probing gases that don't with chemicals react with material surfaces as adsorbates to quantify specific expanse. N is the most ordinarily utilized aerosolized adsorbate used for surface inquisitory by BET ways. For this reason, standard BET analysis is most frequently conducted at the boiling temperature of N_2 (77 K). Additional inquisitory adsorbates also are used, albeit with lower frequency, permitting the measure of expanse at completely different temperatures and measure scales. These have enclosed argon, carbonic acid gas, and water. Specific expanse may be a scale-dependent property, with no single true worth of specific expanse determinable, and so quantities of specific expanse determined through BET theory could rely on the adsorbate molecule used and its surface assimilation cross section [24]. BJH analysis can even be used to work out pore area and specific pore volume with the help of adsorption and desorption techniques. This method characterizes pore size distribution freelance of external space because of the particle size of the sample. The BET area examination is the augmentation of the Langmuir theory that's adsorption theory of monolayer to the multilayer adsorption with some hypothesis like gas molecules take absorb within the

infinite layers and therefore the adsorbable gas molecules will act with adjacent layer solely. The equation of BET is:

$$\frac{1}{v\left[\left(p_0/p\right)-1\right]}=\frac{c-1}{v_m c}\left(\frac{p}{p_0}\right)+\frac{1}{v_m c}$$

(2.7)

Where p_0 is saturation pressure of nitrogen gas as adsorbates at a temperature of surface assimilation, p is equilibrium pressure, v is that the total amount of gas absorbed and v_m is that the amount of gas absorbed on monolayer and c is that the BET constant. Where, the worth of c is

$$c=\exp\left(\frac{E_1-E_2}{RT}\right) \tag{2.8}$$

Where E_1 represents the heat of adsorption on the first layer and E_2 is for the second and higher layers and is equal to the heat of liquefaction.

Equation 2.7 is an equation of adsorption isotherm and plot a graph with the help of this equation against $1/v\ [(p/p_0)-1]$ vs. p/p_0. This plot is known as BET plot. To obtain linear relationship of this equation, the value of p/p_0 should be in the range $0.05<p/p_0<0.35$. The value of slope (S) and intercept (I) to measure the gas quantity (v_m) of the adsorbed monolayer gas and BET constant c used the following equation:

$$v_m=\frac{1}{S+I} \tag{2.9}$$

$$c=1+\frac{S}{I} \tag{2.10}$$

The total area (S_{total}) and specific surface area (S_{BET}) is measured with the help of the following equation:

$$S_{total}=\frac{\left(v_m N s\right)}{V} \tag{2.11}$$

$$S_{BET} = \frac{S_{total}}{a} \tag{2.12}$$

Where, v_m is the units of volume, N is Avogadro number, s is the cross section area of adsorbed gas and V is the molar volume of the adsorbate gas and a is the mass of the solid sample [23,24].

References

[1] K.D. Vernon-Parry, Scanning Electron Microscopy: an introduction, Centre for electronic materials, UMIST, analysis. 13 (2000) 40-44.

[2] G.I. Goldstein, , D.E. Newbury P. Echlin, D.C. Joy, C. Fiori, E. Lifshin, Scanning electron microscopy and X-ray microanalysis, New York: Plenum Press, ISBN 0-306-40768-X, (1981).

[3] L. Reimer, Scanning electron microscopy: physics of image formation and microanalysis, Second Edition, Meas. Sci. Technol. 11 (2000) 1826.

[4] Bo-H. Chung, S. J. Kim, M. S. Choi, D. Y. Jang, Design and fabrication of a scanning electron microscope (SEM) with an electrostatic column for process embedment, J. of the Korean Phy. Soc. 63 (2013) 1287-1290.

[5] J. Goldstein, D.E. Newbury P. Echlin, D.C. Joy, C.E. Lyman, P. Echlin, E. Lifshin, L. Sawyer, J.R. Michael, Scanning electron microscopy and X-Ray microanalysis, Springer, ISBN 978-0-306-47292-3 (2003).

[6] V.I. Klimov, Semiconductor and metal nanocrystals: synthesis and electronic and optical properties, CRC Press, (2003), ISBN 9780824747169 - CAT# DK5750.

[7] A. Hubbard, The Handbook of surface imaging and visualization, CRC Press, ISBN 0849389119 (1995).

[8] B. Fultz, J. Howe, Transmission electron microscopy and diffractometry of materials, Springer, ISBN 10: 3540738851 (2009).

[9] P.E. Champness, Electron diffraction in the transmission electron microscope, Garland Science, ISBN 1859961479 (2001).

[10] B. Fultz, J.M. Howe, Transmission electron microscopy and diffractometry of materials, Springer Science & Business Media, (2012), ISBN 978-3-642-29761-8.

[11] H. Kohl, L. Reimer, Transmission Electron Microscopy, Springer, (2008).

[12] A.A. Bunaciu, E.G. Udriştioiu, H.Y. Aboul-Enein, X-Ray diffraction: instrumentation and applications, Crit. Rev. in Analy. Chem. 45 (2015) 289-299.

[13] P. Debye and P. Scherrer, Interferenzen an regellosen Teilchen im Rontgenlicht Teil III, Phys. Zeitschr. 18 (1917) 291-301.

[14] G. K. Williamson, W. H. Hall, X- ray line broadening from field aluminium and wolfram, Acta Met. 1 (1953) 22-31

[15] C.E. Miller, T. Naes, A Pathlength Correction Method for Near-Infrared Spectroscopy, Appl. Spec. 44 (1990) 895-898

[16] V.N. Nikimin, B.Z. Volchek, Influence of Intermolecular and Intramolecular Order on the Infrared Absorption Spectra of Polymers, Russ. Chem. Rev. 37 (1968) 225-239.

[17] N. Colthup, LH-Daly and SE Wiberley, Introduction to infrared and raman spectroscopy, (1964).

[18] J.C. Tauc, The optical properties of solids, Amsterdam, North Holland, (1972) 372.

[19] R. Lopez, R. Gomez, Band-gap energy estimation from diffuse reflectance measurements on sol-gel and commercial TiO_2: a comparative study, J. Sol-Gel Sci. Technol. 61 (2012) 1-7.

[20] B.J. Berne, R. Pecora, Dynamic Light Scattering, Courier dover publications ISBN 0-486-41155-9 (2000).

[21] B. Chu, Laser Light Scattering, Annual Rev. of Physical Chem. 21(1) (1970) 145174.

[22] R. Pecora, Doppler Shifts in Light Scattering from Pure Liquids and Polymer Solutions, The J. Chem. Phys. 40 (1964) 1604.

[23] S. Brunauer, P. H. Emmett, E. Teller, (1938), Adsorption of Gases in multimolecular layers, J. American Chem. Soc. 60 (2) (1938) 309-319.

[24] D.A.H. Hanaor, M. Ghadiri, W. Chrzanowski, Y. Gan, Scalable surface area characterization by electro kinetic analysis of complex anion adsorption, Langmuir. 30 (50) (2014) 15143-15152.

Chapter: 3

Green Synthesis of TiO_2 Nanoparticles using Leaf Extracts of *Jatropha Curcas L.* For Photocatalytic Degradation of Tannery Wastewater

3.1. Introduction

Leather tanneries (LTs) are one of the key players in the economy of developing nations; however, these are also considered to be the major point source of environmental pollution caused by their potentially toxic and hazardous liquid waste, which creates a negative image of LTs in the society. The wastewater discharged from LTs is characterized by dark brown color, objectionable odour, high pH, chemical oxygen demand (COD), biochemical oxygen demand (BOD), total dissolved solids (TDS), chromium (Cr), sulphate, phosphate, nitrate and a variety of highly toxic organic chemicals and heavy metals [1-3]. In India, there are more than 2500 tanneries, which mostly rely on the chrome tanning process and afford approximately 15% of the total worldwide leather production [4]. In leather tanning, a huge amount of toxic chemicals such as chromium salts, vegetable and synthetic tannins, phenolic compounds, azo dyes, phthalates, polychlorinated biphenyls, pesticides, sulfonated oils etc., are being applied for the conversion of rawhide/skins into the commercial form of leather or leather products [1,5,6]. These chemicals are not fully taken up by the hide/skins and thus, finish up in tannery wastewater (TWW), which is a major source of well documented environmental (soil/water) pollution and severe health threats in living beings [7,8]. Moreover, in developing nations, TWW is also being used directly or indirectly by the local farmers for the irrigation of agricultural crops and this practice provides chances for the bioaccumulation of toxic metals at successively higher trophic levels in the food chain via human/animals consumption [9]. Moreover, TWW has

been well reported to contain high pollution parameters and toxic organic and inorganic pollutants in previous studies [1,5,6] and hence, responsible for the serious soil/water pollution and severe toxic effects in living beings [7,8] and thus, its adequate treatment is required prior to discharge in the environment.

The COD and Cr both are considered as the major pollution parameters to actually define the strength of the treated TWW. COD has been widely adopted as water quality criteria to measure the pollution profile of water and wastewaters. It represents the oxygen demand for both the biodegradable and non-biodegradable oxidizable pollutants in industrial wastewaters. The removal of Cr from TWW is a challenging task. TWW is highly rich in Cr because basic chromium sulfate ($CrSO_4$) is applied during the tanning process in LTs to produce the leather or leather products. Cr mainly exists in two forms i.e. Cr^{+3} and Cr^{+6}; however, Cr^{+6} is potentially toxic in nature due to its higher solubility in water and therefore, identified as a "priority pollutant" by U.S Environmental Protection Agency (USEPA) and Agency for Toxic Substances and Disease Registry (ATSDR). Cr^{+3} is commonly found in the environment, but it gets oxidized into Cr^{+6} in the presence of organic compounds [10]. The permissible limit for total Cr and Cr^{+6} in TWW are 2.0 mg L^{-1} and 0.01 mg L^{-1}, respectively. At high concentration, Cr^{+6} cause serious soil/water pollution and severe toxic, genotoxic and carcinogenic effects in living beings [11] and thus, its removal from TWW is a key requirement for the safety of public health and environment.

The conventional wastewater treatment plants (WWTPs), which mostly relied on the conventional activated sludge treatment process (CASTP) do not efficiently remove the color and other recalcitrant pollutants from TWW. The presence of poorly degradable tannins, recalcitrant metals like Cr and high salt concentration inhibit the biological treatment of TWW [1]. In addition, the high energy demand, operation, and

maintenance cost, post-treatment requirement for TWW and excess sludge production associated with CASTP also discredit its application at large scale. Moreover, several physicochemical treatment approaches (coagulation/flocculation and adsorption) are being applied for the treatment of TWW, but these use a huge amount of chemicals and thus, are environmentally destructive [5]. Further, the emerging treatment technologies such as membrane technologies, membrane bioreactors, anammox technology and oxidation processes are also available for the removal of recalcitrant organic pollutants and metals from TWW; however, the associated high operating cost, energy demand, and some other serious limitations make their large-scale applications uneconomical and thus, are of less preference in developing countries [1,6].

On contrary, nanotechnology offers a great potential for the development of next-generation water and wastewater treatment technologies and could replace the conventional wastewater treatment technologies. Nanoparticles (NPs) are increasingly applied for the wastewater treatment and purification due to their high reactivity and degree of functionalization, large surface area, size-dependent properties etc. [12,13]. NPs, especially, the chemically synthesized titanium dioxide (TiO_2) has been extensively applied in the photocatalytic treatment of industrial wastewaters [14,15]. Nano-sized TiO_2-based photocatalytic treatment is a highly effective method for the degradation and detoxification of recalcitrant organic and inorganic pollutants from industrial wastewaters [16,17]. A general mechanism of TiO_2-based photocatalysis is shown in Fig. 3.1. The chemical synthesis of NPs under specific conditions require highly expensive and toxic and hazardous chemicals and their release in the environment creates a serious eco-toxicological concern [18]. Nonetheless, the green synthesis is a simple, eco-friendly and less toxic way of synthesizing NPs from biodegradable materials such as plant extracts, microbes and enzymes [18, 19].

However, the synthesis of NPs using plant extracts is the most useful strategy as it lessens the chance of associated contamination while reducing the reaction time and maintaining the cell structure [19]. Moreover, the application of green NPs for industrial wastewater treatment could be an excellent strategy to cope with environmental pollution. To date, only very few studies reported the application of green synthesized NPs in wastewater treatment [18, 20].

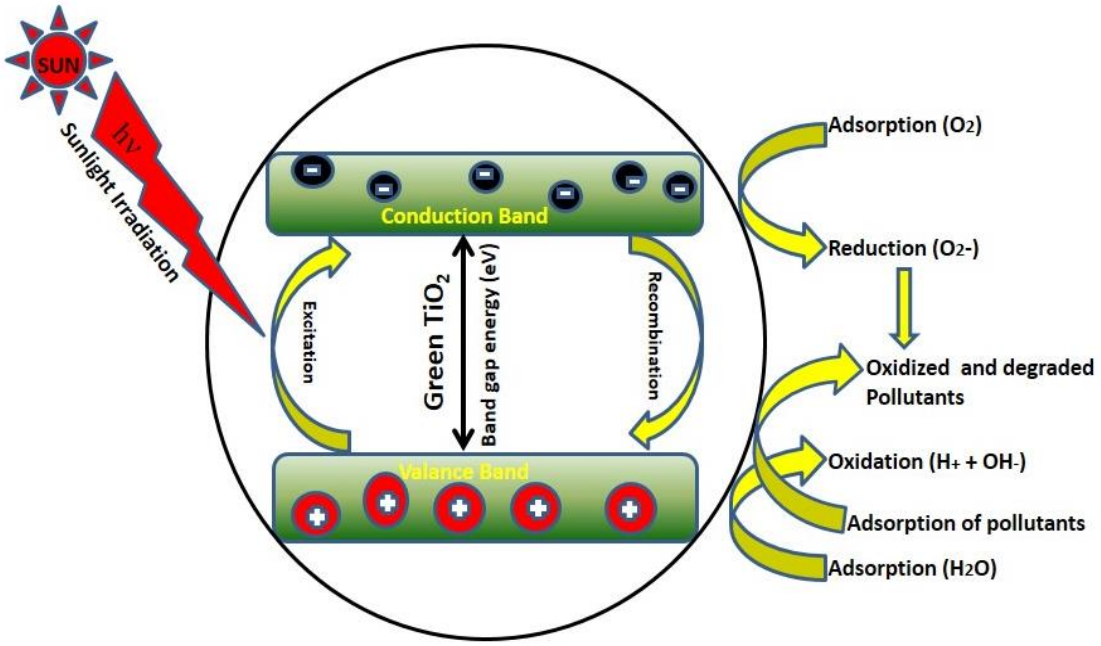

Fig. 3.1: General mechanism of photocatalysis.

However, green synthesized TiO_2 NPs for the solar photocatalytic treatment of TWW has not been applied so far. Therefore, in the present study, TiO_2 NPs was synthesized using leaf extract of a petro plant, Jatropha curcas L. using a simple green chemistry approach. Jatropha belongs to the family, Euphorbiaceae and widely cultivated as petro plants for the biodiesel production in many parts of the world (Fig. 3.2). Further, FESEM, EDS, XRD, UV-Vis spectroscopy, DLS, BET, BJH, and FTIR were employed to study the structural, optical and textual properties of the green synthesized TiO_2 NPs. Further, to evaluate the performance in wastewater treatment, the green synthesized TiO_2 NPs was first applied for the solar photocatalytic treatment of secondary treated

TWW. Present research work is graphically shown by the Fig. 3.3.

Fig. 3.2: Image of *Jatropha curcus* L. plant.

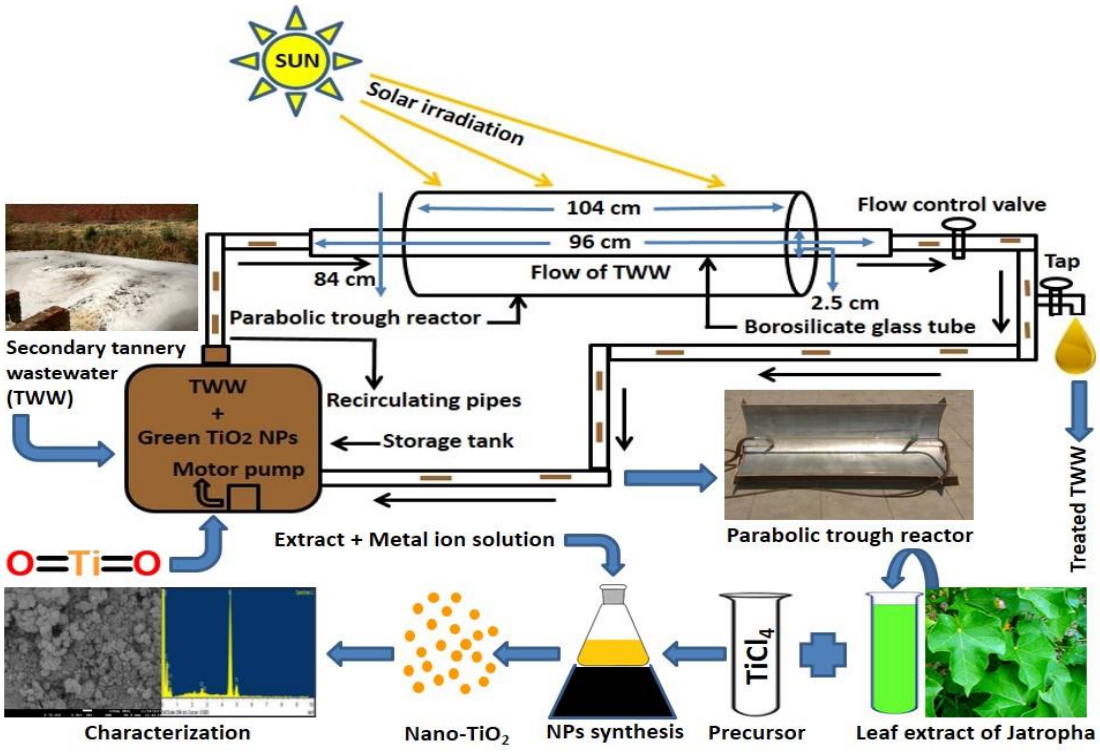

Fig. 3.3: Graphical representation of presented research work

3.2. Material and methods

3.2.1. Materials and chemicals used in experiments

Titanium chloride ($TiCl_4$, analytical grade, purity ≥99.85%) was used as a precursor directly without further purification for the synthesis of TiO_2 NPs and purchased from Fisher Scientific, U.K. The fresh leaves of Jatropha curcas were obtained from the author's university campus and utilized for the green synthesis of TiO_2 NPs. All the chemicals and reagents used in the physicochemical characterization of TWW were of analytical grade (purity ≥99%) and purchased from Sigma-Aldrich (St. Louis, MO, USA). Whatman GF/C filter papers (Whatman, England) of pore size 1.2 µm were used for the filtration of TWW and leaf extract. Double distilled (DD) water was used in all the experiments.

3.2.2. Green synthesis of TiO_2 NPs

Firstly, *Jatropha curcas* L. leaves were washed thoroughly with DD water to remove the associated dust particles and cut it into the very fine pieces and then dried in the presence of sunlight. 20.0 g of leaves of Jatropha curcas L. was immersed in the 100 ml of DD water and boiled at 80 °C for 40 min for the preparation of leaf extract. Further, the obtained leaf extract was kept for cooling at room temperature, filtered using Whatman GF/C filter paper (Whatman, England) and used for the green synthesis of TiO_2 NPs.

For the green synthesis of TiO_2 NPs, 80 ml of 0.50 M $TiCl_4$ was added to the 80 ml of filtered leaf extract in a ratio of 1:1 (v/v) with a continuous stirring at room temperature. A color change from transparent to whitish-brown in the solution was observed within 20 min after mixing together precursor and leaf extract due to the reduction of metallic ions (Ti^{4+}) which indicated the green synthesis of TiO_2 NPs. To obtain the precipitates of NPs, 15 ml of ammonia was added to the solution of NPs drop-wise under continuous

stirring at room temperature. Then, the obtained precipitates of NPs were separated out from the solution through filtration, followed by washing with ethyl alcohol to remove the ionic impurities. Afterward, the washed precipitates were air dried and calcined at 450 °C for 3 h in a muffle furnace and then finely grind in a crystal mortar pestle to obtain the final powder form of TiO_2 NPs. The possible reaction mechanism of green synthesis of TiO_2 NPs is illustrated in Fig. 3.4.

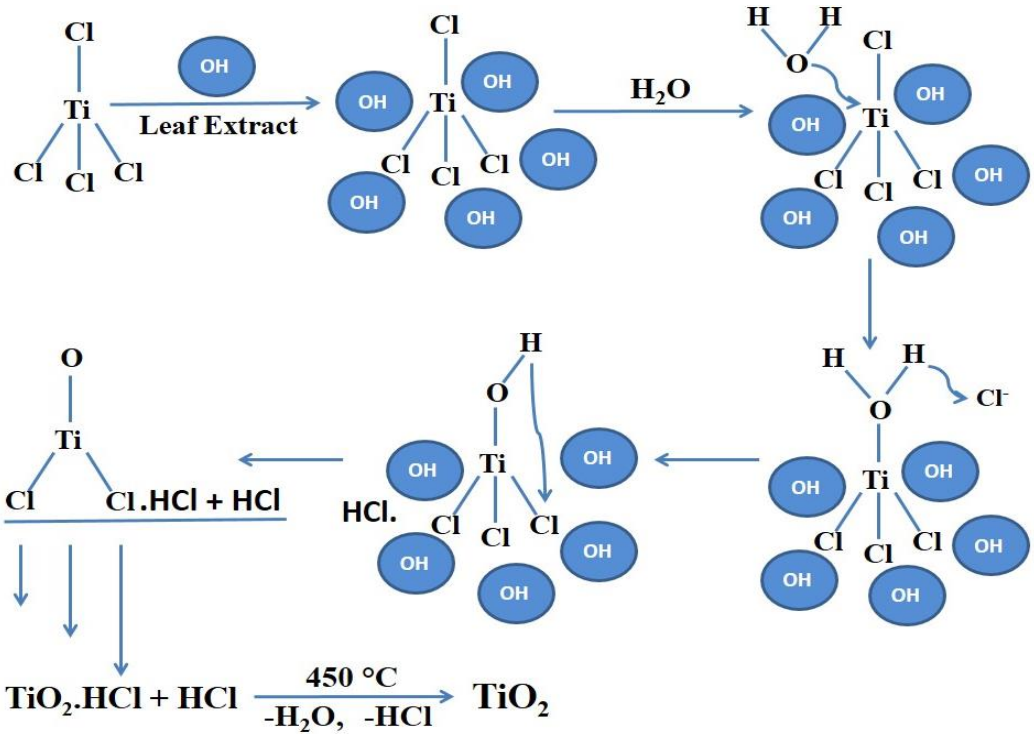

Fig. 3.4: The possible reaction mechanism for the formation of TiO_2 NPs in presence of hydroxyl group (-OH) of leaf extract of *Jatropha curcas L*. as capping agent.

3.2.3. Characterization of green synthesized TiO_2 NPs

Green synthesized TiO_2 NPs was characterized by powder X-ray Diffraction (XRD) to analyze its crystal structure and phase. The XRD pattern was recorded on X-ray diffractometer (Philips-X'Pert Pro MPD, The Netherlands) equipped with a Cu-Kα radiation (λ = 0.154 nm) within a 2θ range of 10°–80° at 40 kV/40 mA. The morphological characteristics and size of the green synthesized TiO_2 NPs were

determined by Field Emission Scanning Electron Microscopy (FESEM) (JSM-7610F, JEOL, Japan). The composition of the green synthesized TiO_2 NPs was determined by X-ray Energy-Dispersive Spectrometer (EDS) (Oxford, INCAx-act, Japan). In addition, the particles size distribution of green synthesized TiO_2 NPs was determined by Dynamic Light Scattering (DLS) (Zitasizer NanoZS-90, Malvern Instruments Ltd., U.K.). Fourier Transform-Infrared spectrometer (FTIR) (Model Nicolet 6700, Thermo Fisher Scientific, USA) was used to characterize the functional groups involved in the green synthesis of TiO_2 NPs. Brunauer-Emmett-Teller (BET) and Barret-Joyner-Halenda (BJH) analysis (BELSORP-MINI-II, Japan) was done to know the surface area, pore size distribution and pore volume of the green synthesized TiO_2 NPs. Furthermore, the optical properties of green synthesized TiO_2 NPs were analyzed by UV–Visible spectrophotometer (Evolution™-201, Thermo Fisher Scientific, USA).

3.2.4. Treatment of TWW by green synthesized TiO_2 NPs

3.2.4.1. TWW sample collection and its physicochemical characterization

TWW sample after the secondary (biological) treatment process was collected in a pre-sterilized clean container (capacity 20 L; Tarson Production Pvt. Ltd., USA) from the outlet of a Common Effluent Treatment Plant (CETP) of tannery industries located at Unnao (26.48 °N, 80.43 °E), Uttar Pradesh, India. The CETP is relied on the conventional activated sludge treatment process (CASTP) and used to treat 1.9 MLD of TWW against a design flow of 2.15 MLD. The CETP receive wastewater through the pipelines and tanks from a cluster of 21 LTs located in nearby areas, and the wastewater treatment is carried out around the year (365 days). The collected TWW sample was immediately transported to the laboratory and stored at 4 °C until the physicochemical analysis carried out. Further, TWW sample was analyzed for various physicochemical parameters to define the strength of pollution as per the standard

protocols outlined in “Standard Methods for Examination of Water and Wastewater” [21].

3.2.4.2. Reactor design and operating conditions

A self-designed and fabricated parabolic trough reactor (PTR) was employed for the solar photocatalytic treatment of real secondary treated TWW. The PTR was constructed using a highly lustrous stainless aluminum chrome plated parabolic trough of 104 cm length and 84 cm width. A UV transparent borosilicate glass tube of length 96 cm and an internal diameter of 2.5 cm was mounted over the trough with the help of strong holders. Rubber tubes were attached to both the sides of the glass tube to ensure a proper flow of TWW. Rubber tubes were further joined with a completely closed plastic tank (capacity 5 L) fitted with a submersible motor pump at the bottom to maintain a continuous circulation of wastewater throughout the solar photocatalytic treatment process. Then, the plastic tank was fed with TWW sample (5 L) and PTR was operated in presence of sunlight in a sunny day of summer (April) under clear sky conditions from the time period between 10:00 a.m. and 03:00 p.m. for the photocatalytic treatment of TWW. During photo-catalytic treatment, the average intensity of solar irradiation was 985 W/m^2 measured by Kusam Meco KM-SPM-530 Digital Solar Power Meter (KUSAM-MECO, India). The TWW sample was run for 5 h (300 min) with the green synthesized TiO_2 NPs as photocatalyst and the average temperature attained by the running TWW during the experimental run was 59 °C. For wastewater treatment, the flow rate was adjusted to 0.25 L/s. The schematic diagram and original picture of the PTR constructed for the photocatalytic degradation of TWW are presented in Fig. 3.5a,b.

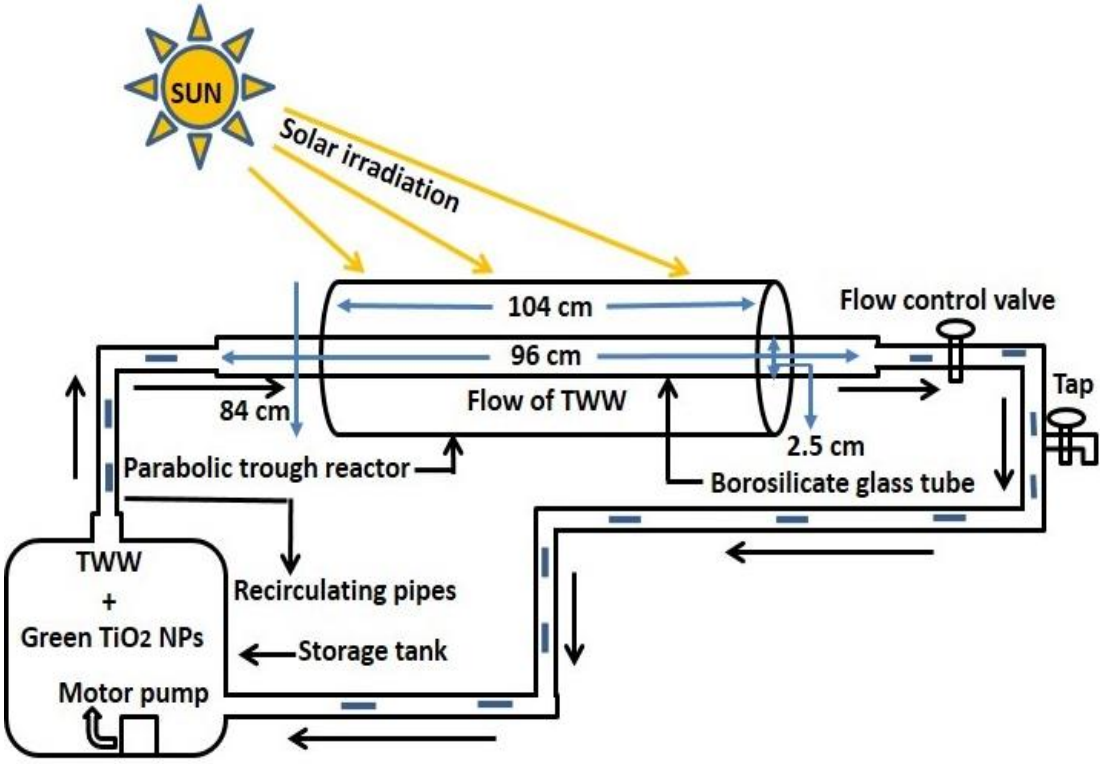

Fig. 3.5: (a) A schematic diagram of a parabolic trough reactor (PTR).

Fig. 3.5: (b) A pictorial diagram of PTR constructed for solar photocatalytic treatment of TWW.

3.2.4.3. Photocatalytic treatment of TWW

To evaluate the performance of the green synthesized TiO_2 NPs in wastewater treatment, 5 L of filtered secondary treated TWW without any pH adjustment was photocatalytically treated with the green synthesized TiO_2 NPs (5 g) for 5 h in PTR, which was directly exposed to sunlight. To provide the better sunlight exposure to borosilicate glass tube, PTR was oriented about a horizontal east-west axis to constantly minimize the angle of incidence and maximize the incident beam radiation for the effective photocatalytic treatment of TWW. After the photocatalytic treatment, TWW sample was taken out from PTR and kept for settling for 15 min to separate out the TiO_2 NPs. Afterward, the treated TWW sample was utilized to calculate the removal efficiencies for pollution parameters such as COD and Cr to define the pollution profile. In the present study, the solar photocatalytic treatment of TWW was carried out at the School for Environmental Sciences located in the author's university campus.

3.3. Results and Discussion

3.3.1. Characteristics of green synthesized TiO_2 NPs

The X-ray diffraction (XRD) pattern of the green synthesized TiO_2 NPs is shown in Fig. 3.6, which successfully unfolded its crystalline nature and anatase phase. The average crystallite size of the green synthesized TiO_2 NPs was calculated by Debye Scherrer's equation [22]:

$$d = 0.89\,\lambda/\beta\mathrm{Cos}\theta \qquad (3.1)$$

Where d is the average mean diameter of NPs, λ is the wavelength of X-ray radiation source, 0.89 is a constant crystalline shape factor, θ is the Bragg's diffraction angle, and β is the angular full width at half maximum (FWHM) of XRD peaks recorded at diffraction angle 2θ The average crystallite size of the green synthesized TiO_2 NPs was found to be 13 nm.

The XRD pattern of the green synthesized TiO_2 NPs showed various peaks in a wide range of 2θ angle ($10 < 2\theta < 80$) revealed that the distinct peaks recorded at 25.37°, 37.12°, 37.90°, 38.71°, 48.22°, 54.12°, 55.21°, 62.91°, 68.76°, 70.57° and 75.40° were well corresponded to the Miller indices (hkl) values, (1 0 1), (1 0 3), (0 0 4), (1 1 2), (2 0 0), (1 0 5), (2 1 1), (2 0 4), (1 1 6), (2 2 0) and (2 1 5), respectively, confirmed the anatase phase (calcined at 450 °C for 3 h) of the crystalline TiO_2 NPs. The obtained results were closely matched with the Joint Committee on Powder Diffraction Standards (Anatase XRD, JCPDS Card No. 78-2486) [23]. All the peaks corresponded to the characteristics facets of the tetragonal anatase phase of crystalline TiO_2 NPs with space group I41/amd and lattice parameters were a = b = 3.792 Å, c = 9.554 Å. However, any other peaks related to the impurity were not found. The sharp peaks clearly implying the high crystallinity of the nanosized-TiO_2, which is considered to be favorable for the photo-catalytic activity and directly related to the charge recombination rate. The high crystallinity lessens the amount of the trapping electrons, which act as the recombination centers for the photo-induced electrons-hole pairs [24]. Further, the sufficiently long lifetime of the electron-hole pairs corresponding to the high charge separation will give rise to a fairly large number of electrons and holes and thus, initiate the photocatalytic redox reactions.

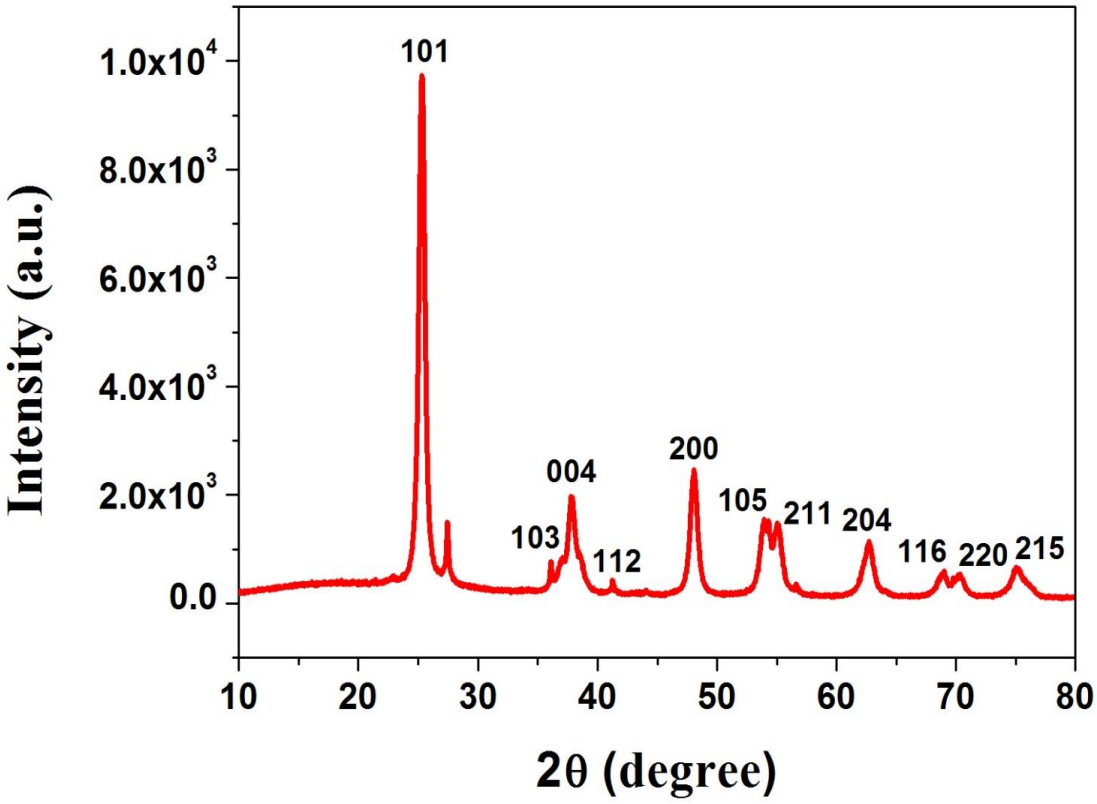

Fig. 3.6: X-ray diffraction pattern of green synthesized anatase TiO_2 NPs.

The FESEM analysis was performed to determine the shape and estimate average grain size of the green synthesized TiO_2 NPs. The FESEM images evidenced the successful green synthesis of spherical shaped TiO_2 NPs with a diameter ranging from 10 to 20 nm (Fig. 3.7a). It was clearly evident that a large number of small and distinct TiO_2 NPs were observed along with fewer relatively large sized agglomerated NPs as can be easily seen in the FESEM images [25]. The agglomeration of TiO_2 NPs was might be due to the low pH of the solution of TiO_2 NPs. However, the phytochemicals such as polyphenols, flavonoids, alkaloids, antioxidants, terpenoids, steroids, free amino acids and tannins present in the leaves of Jatropha curcas L. perhaps play a key role as capping agents, which enhanced the dispersion between NPs by reducing their agglomeration [26,27] and thus, could be very useful in the synthesis of a variety of NPs.

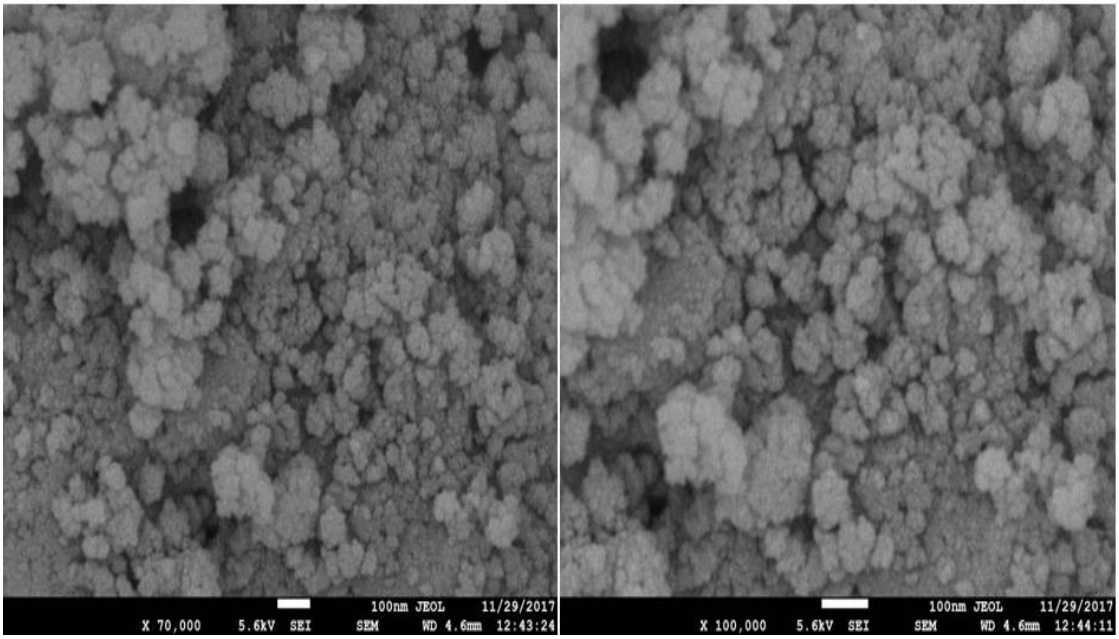

Fig. 3.7: (a) FESEM images of green synthesized TiO_2 NPs.

The X-ray Energy Dispersive Spectrometer (EDS) was employed to know the elemental composition of the green synthesized TiO_2 NPs [28]. The EDS spectrum is shown in Fig. 3.7b, which revealed the purity of sample as both titanium (Ti) and oxygen (O) is present in the sample with weight percentage, 34% and 23% and atomic percentage, 13% and 26%, respectively. This further confirmed the green synthesis of TiO_2 NPs. Further, the C and Cl were also present in the sample. The Cl peak was might be raised from chloride group present in the precursor (i.e. $TiCl_4$) used for the green synthesis of TiO_2 NPs; however, the C peak was might be due to the presence of phytochemicals present in the leaf extract of *Jatropha curcas* L.

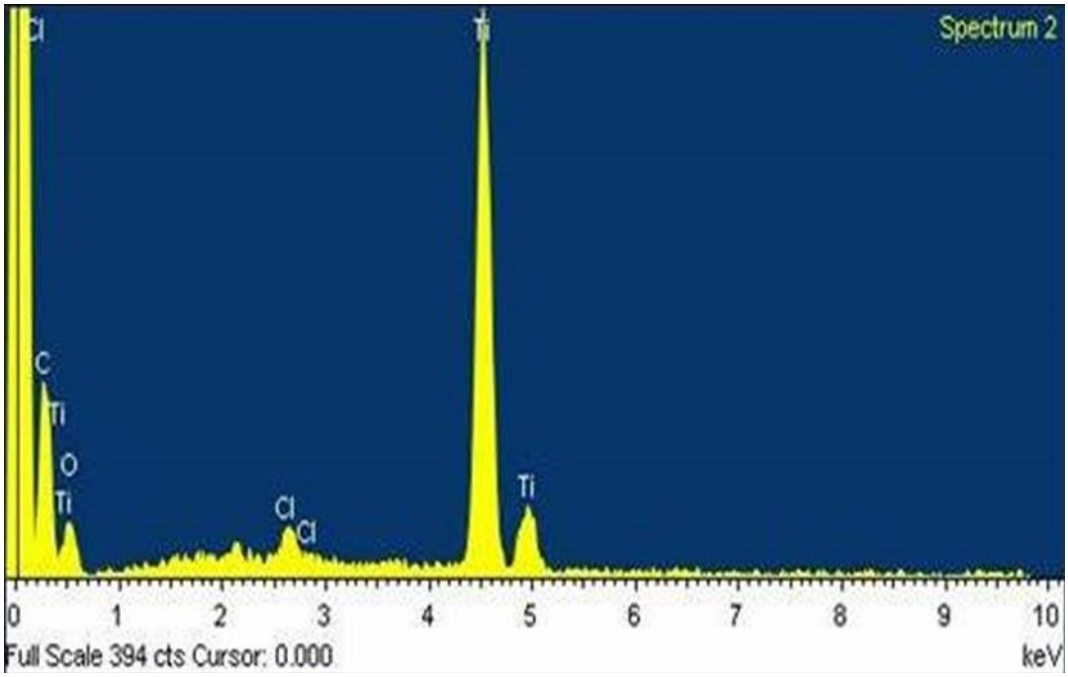

Fig. 3.7: (b) EDS spectrum of green synthesized TiO_2 NPs.

Moreover, FT-IR spectroscopy was also employed to identify the possible biomolecules on the basis of chemical groups present in the Jatropha curcus leaf extract (JCLE) responsible for the capping/reduction of metallic ions (Ti^{+4}) of the precursor, which play an important role in the synthesis of NPs. The FT-IR spectrum of JCLE is shown in Fig. 3.8a. A broadband at 3495 cm^{-1} showed the presence of a hydroxyl group in JCLE and that was might be due to the presence of phenols [29]. The existence of the phenolic group was probably due to the presence of polyphenolic tannins in JCLE, which might cap the surface of green synthesized TiO_2 NPs. A primary amine group was also present in the range of band 3257–3381 cm^{-1}. An intense peak at 2330 cm^{-1} showed CN stretching while a strong band at 1757 cm^{-1} was attributed to stretching vibrational frequency of C=O of anhydrides from the carbonyl group. A strong peak at 681 cm^{-1} was assigned to C-Cl. Further, a weak band at 1680 cm^{-1} indicated the presence of C=C of alkene group in JCLE [29].

A typical FT-IR spectrum of the green synthesized TiO_2 NPs recorded in the series of absorption band 500 cm^{-1} to 4000 cm^{-1} is shown in Fig. 3.8b. The band intensities in

the different regions of the spectrum recorded for the powdered TiO_2 NPs were analyzed. A broad peak at 3400 cm^{-1} and a small peak at 1640 cm^{-1} possibly attributed to the presence of the hydroxyl group and surface adsorbed water, respectively [14]. The hydroxyl group might be contributed to the enhancement of photocatalytic activity. When the amount of hydroxyl group increased on the surface of TiO_2 NPs, the OH^- largely increased which are responsible for the higher electron transportability and thus, enhanced the photocatalytic activity [30]. An absorption peak at 500–700 cm^{-1} may correspond to Ti–O stretching and Ti–O–Ti bridging stretching modes [31,32]. The absorption peak at 652 cm^{-1} possibly indicated the contribution of anatase phase of the green synthesized TiO_2 NPs as reported earlier [33]. However, no peak was recorded at 2900 cm^{-1} for C-H stretching band that ensured the removal of all the organic compounds from the sample during the calcination process.

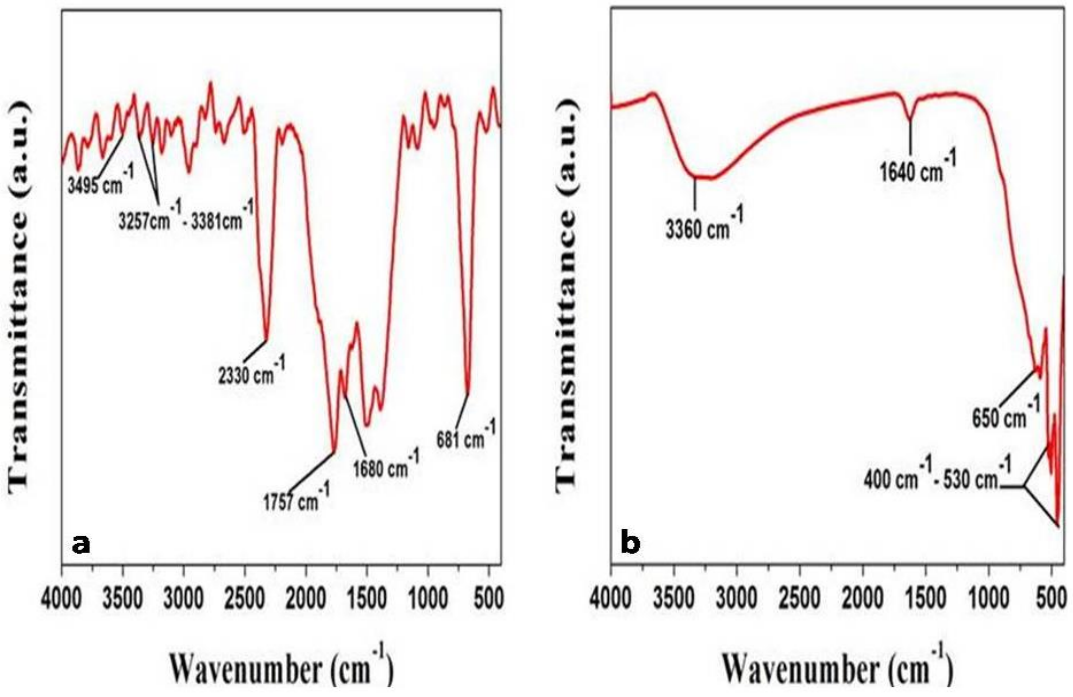

Fig. 3.8: (a) FT-IR spectra of leaf extracts of *Jactropha curcus* L. (b) green synthesized TiO_2 NPs.

To further study the optical properties and confirm the green synthesis of TiO_2 NPs, the analysis of the absorption spectra of the sample was also performed. The absorption spectrum of the green synthesized TiO_2 NPs is presented in Fig. 3.9a, which revealed a strong absorption peak at 336 nm within the absorption range from 200 to 800 nm that further provided the evidence of the green synthesis of metallic TiO_2 NPs. In the absorption spectra, a blue shift was observed when compared with the bulk TiO_2 NPs, which clearly indicated the widened band gap. In addition, the individual distribution pattern of the green synthesized TiO_2 NPs was confirmed by the sharp and intense peak recorded in the absorption spectra. However, the deviations observed in the peak value (absorption) in the present study was might be due to the interference caused by the impurities present in the solution of NPs as compared to the previous literature [31,32,33]. Furthermore, the band gap energy was determined according to Tauc equation [34]

$$\alpha(h\nu) = \beta(h\nu - E_g)^m \quad (3.2)$$

where, α is the extinction coefficient, β is the constant and has different values for different transitions, E_g is the energy gap, $h\nu$ is the photon energy and m denotes an exponent (m = 2) for an indirect allowed transition (plotted between $\alpha(h\nu)^{1/2}$ and $h\nu$); (m = 3) for an indirect forbidden transition (plotted between $\alpha(h\nu)^{1/3}$ and $h\nu$); (m = 1/2) for a direct allowed transition (plotted between $\alpha(h\nu)^2$ and $h\nu$); (m = 3/2) for a direct forbidden transition (plotted between $\alpha(h\nu)^{2/3}$ and $h\nu$). It is obvious that both the indirect and direct transition may occur in all the semiconductor materials. The band gap energy (Eg) may vary with the type of the transition up to 0.5 eV for the same semiconductor [35].

Tauc plot as shown in Fig. 3.9b,c showed the photon energy ($h\nu$) on the X-axis and a quantity $(\alpha h\nu)^2$, $(\alpha h\nu)^{1/2}$ on the Y-axis; and extrapolating the linear portion of the curve

to the X-axis yields the band gap energy of the green synthesized TiO_2 NPs. The obtained direct band gap energy was 3.68 eV whereas the indirect band gap energy was 3.28 eV, which is corroborated by those reported in the earlier studies [35]. Furthermore, the band gap energy was higher than that of the bulk TiO_2 NPs (3.2 eV) [35]. This indicated the strong quantum confinement, which may be due to the changes raised in the valence and conduction bands of the green synthesized TiO_2 NPs [32,36].

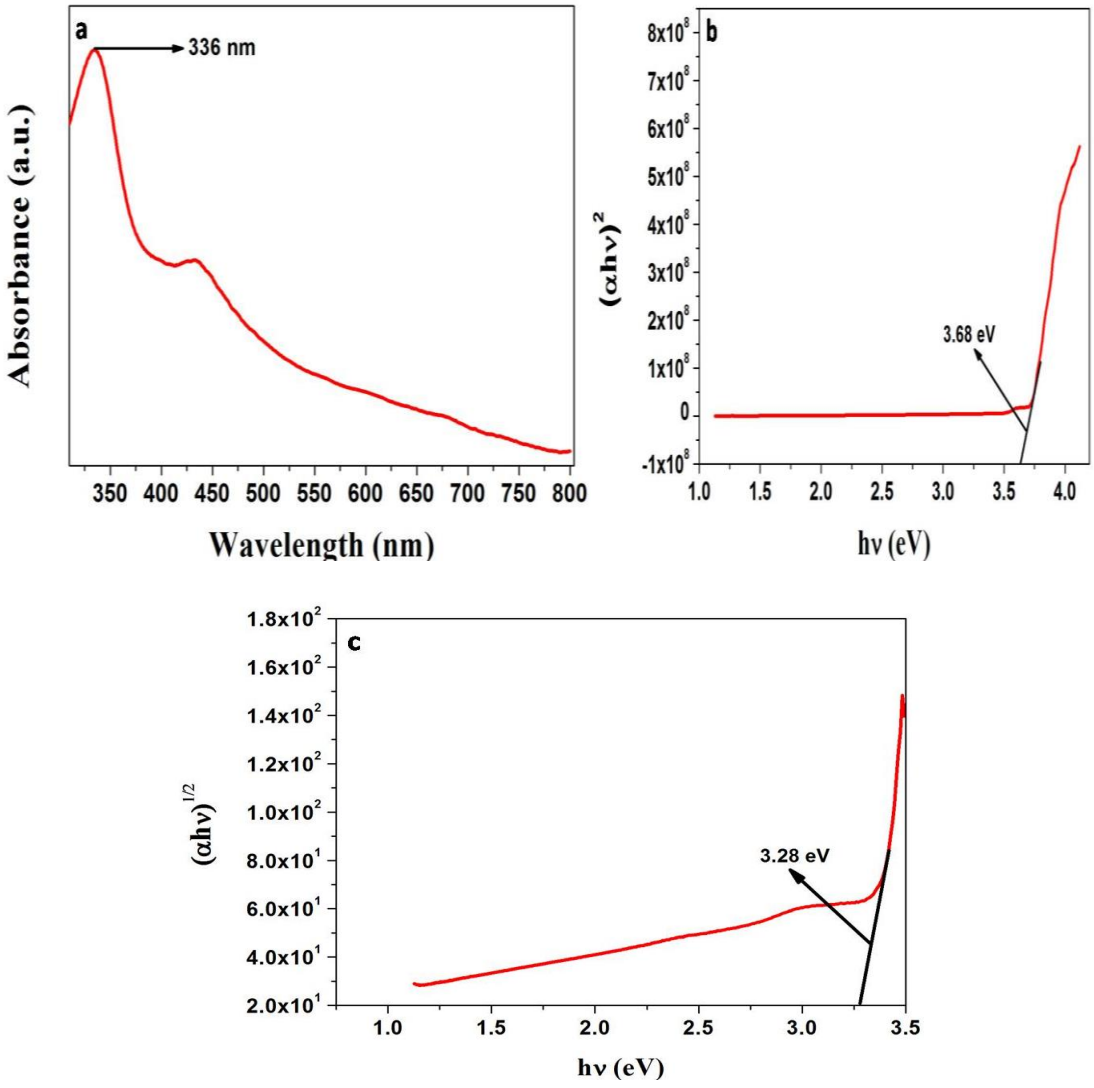

Fig. 3.9: (a) UV–Vis absorption spectrum (b) Graphical representation of Tauc plot $(\alpha h\nu)^2$ and (c) $(\alpha h\nu)^{1/2}$.

Dynamic light scattering (DLS) technique was used to determine the distribution of particle size of the green synthesized TiO_2 NPs. For this, the powdered TiO_2 NPs were

completely dissolved in HCl followed by ultrasonication to achieve the uniform distribution of NPs for the preparation of the representative solution, which was used to determine the particle size distribution. The DLS plot as shown in Fig. 3.10 revealed that a maximum intensity was obtained at the average particle size of 75 nm, which further provided the evidence of the green synthesis of nanosized TiO_2. This further justified the range of particle size of the green synthesized TiO_2 NPs as determined by SEM study.

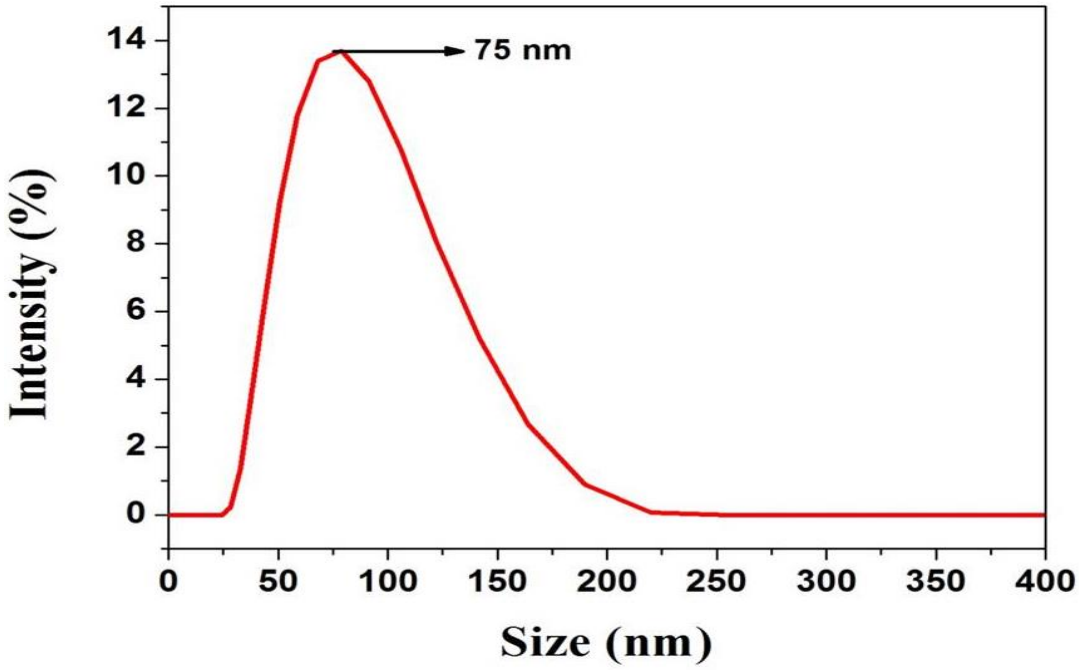

Fig. 3.10: Particle size distribution curve of green synthesized TiO_2 NPs by DLS.

Furthermore, N_2 adsorption-desorption isotherms over the sample of TiO_2 NPs were obtained using a surface area and pore size analyzer. The surface area of the green synthesized TiO_2 NPs was determined by the Brunauer-Emmett-Teller (BET) analysis whereas pore volume and pore size distribution for the green synthesized TiO_2 NPs were determined by the Barrett-Joyner-Halenda (BJH) analysis. As shown in Fig. 3.11a,b, the surface area (S_{BET}) of the green synthesized TiO_2 NPs was 27.038 m^2/g whereas the mean pore diameter and total pore volume of the green synthesized TiO_2 NPs was 19.100 nm and 0.1291 cm^3/g. Results confirmed that the green synthesized

TiO_2 NPs have mesoporous nature with the large surface area and thus, contains a number of active sites on the surface, which enhance the adsorption phenomenon and play a significant role in the removal of pollutants from wastewater during photocatalytic oxidation.

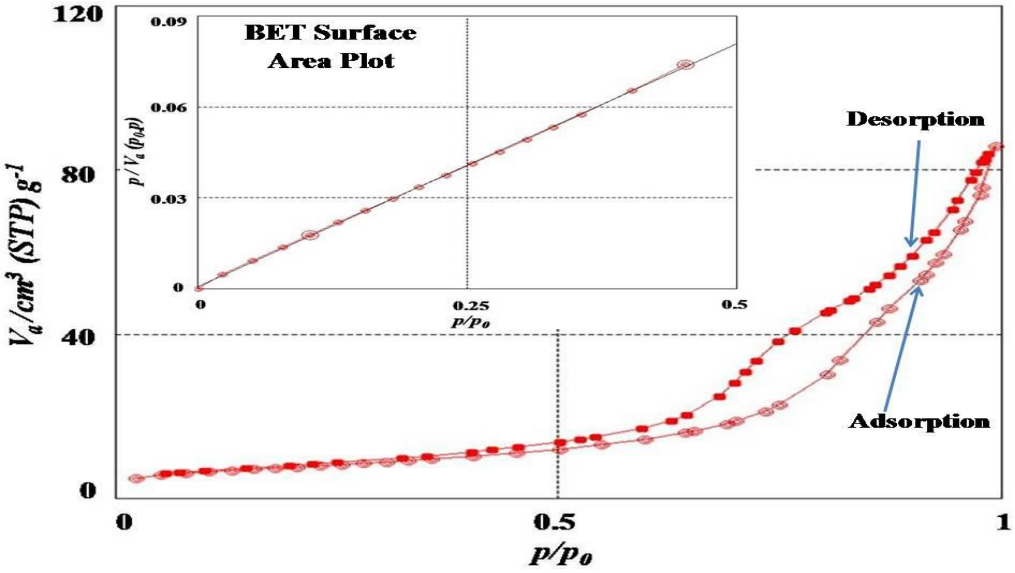

Fig. 3.11: (a) N_2 Adsorption/desorption isotherm of the green synthesized TiO_2 NPs.

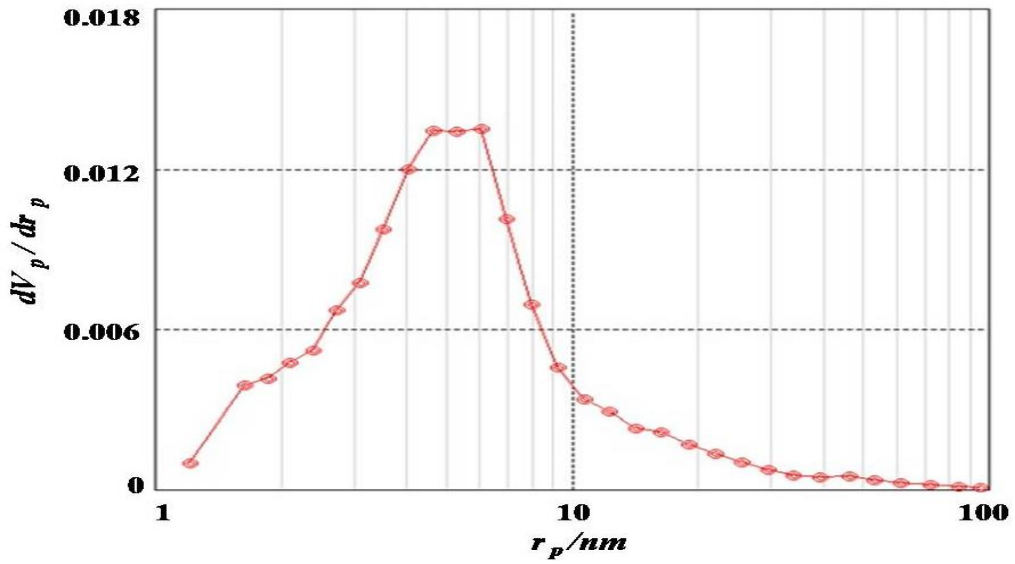

Fig. 3.11: (b) BJH plot of the green synthesized TiO_2 photocatalyst.

3.3.2. Performance evaluation of the green synthesized TiO_2 NPs for photocatalytic treatment of TWW and removal efficiencies

To evaluate the performance efficiency, green synthesized TiO_2 NPs was applied for the solar photocatalytic treatment of secondary treated TWW. The physicochemical characteristics of the secondary treated TWW are presented in Table 3.1. All the values recorded for the physicochemical parameters reported in the present study were higher than the recommended permissible limit of industrial discharge and thus, reflect the highly polluted nature of TWW even after the secondary (biological) treatment (Table 3.1).

Table 3.1. Physico-chemical characteristics of secondary treated tannery wastewater.

Physico-chemical parameter	Recorded values	Permissible limit for effluent discharge (USEPA 2002)
Color	Dark brown color	-
Odour	Objectionable	-
pH	8.2	-
Temperature (°C)	32	-
EC (mS $cm^{-1)}$	11.65	-
BOD (mgL^{-1})	436	40.00
COD (mgL^{-1})	1428	120.00
TDS (mgl^{-1})	4064	-
TSS (mgl^{-1})	2216	-
Phosphate (mgl^{-1})	118.66	-
Sulfate (mgl^{-1})	6.75	-
Nitrate (mgl^{-1})	14.05	-
Phenol (mgL^{-1})	8.68	0.50
Cr (mgL^{-1})	6.88	0.05

Further, the degradation of TWW is mainly analyzed in terms of reduction in Cr^{+6} and COD to define its pollution strength. It has been reported that the photoreduction of Cr^{+6} from wastewaters is significantly increased with the photooxidation of recalcitrant organic pollutants, which is analyzed in terms of COD reduction [37]. In the present study, after the solar photocatalytic treatment of TWW with the green synthesized TiO_2 NPs in PTR, the treated wastewater sample was used to calculate the Cr^{+6} and COD removal efficiency to determine the effectiveness of the photocatalytic treatment process according to the following equation:

$$\text{Removal Efficiency (\%)} = C_0 - C_t / C_0 \times 100 \quad (3.3)$$

Where, C_0 is the initial concentration of wastewater pollutants before the photocatalytic treatment and C_t is the residual concentration of wastewater pollutants after the photocatalytic treatment.

3.3.3. COD removal efficiency

In the present study, the COD value of TWW after the solar photo-catalytic treatment with green synthesized TiO_2 NPs was measured by open reflux method (Method No. 5220B) [21]. The COD value of the untreated TWW (control) was found to be 1428 mg L^{-1}, which was quite higher than the permissible limit (Table 3.1). The high COD value of TWW was might be due to the high organic loading and recalcitrant organic pollutants. TWW with high COD value is responsible for the disturbed ecological functioning of receiving water bodies and ultimately affects the aquatic life [1]. However, an appreciable removal in COD was achieved after the solar photocatalytic treatment of TWW with green synthesized TiO_2 NPs and the removal efficiency was found to be 82.26%. The degradation profile of COD is illustrated in Fig. 3.12 and the percent removal of COD from TWW was calculated according to Eq. (3.3).

The kinetics of COD degradation from TWW during solar photo-catalytic treatment

with TiO_2 semiconductor photocatalyst can be illustrated by the first-order reaction:

$$\ln C_0 / C_t = kt \quad (3.4)$$

Where, k is the rate constant (0.03179 min^{-1}), C_0 is the initial concentration of COD and Ct is the concentration of COD at the irradiation time (t). Fig. 3.13 describes the linear relationship of $\ln(C_0/C_t)$ versus irradiation time (t) for COD. The rate constant was determined for TiO_2 photocatalyst from the slope of the linear fitting line as shown in Fig. 3.13. As it can be seen, a good correlation to the first order reaction kinetics (r^2 > 0.96) was found. The photocatalytic behavior is correlated with the structural, morphological and optical properties of the prepared TiO_2. Further, due to the large surface area, more active sites are present on the surface of TiO_2 NPs which are responsible for the adsorption of pollutants.

Further, the presence of polyphenolic tannins in leaf extract of J. curcas was might be the reason for the enhancement in COD removal efficiency. The formation of Ti^{+4} was might be due to the formation of a complex between the titanium ions and phenolic group and electron transfer mechanism. Due to the complex nature of the green synthesized TiO_2 NPs, the chemical analysis of organic complex formation is very complicated; however, the literature depicting the interaction between the titanium ions and the phenolic group is not available so far. Further investigation is required to unfold the interaction between the titanium ions and phenolic group to clearly understand the COD removal mechanism.

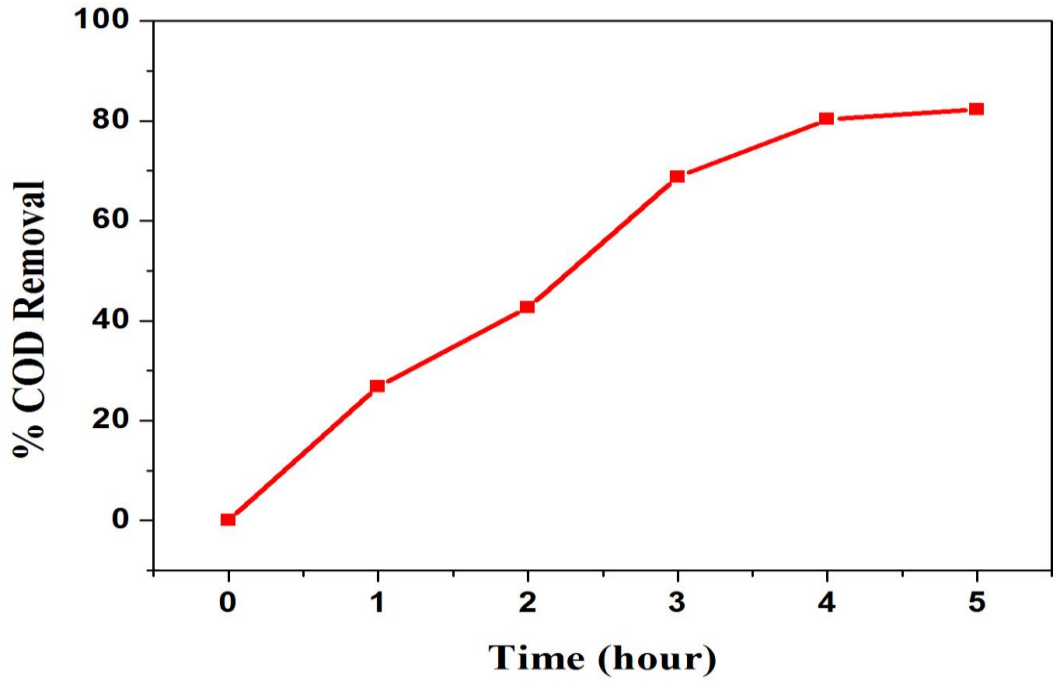

Fig. 3.12: COD degradation profile during solar photocatalytic treatment of TWW with green synthesized TiO_2 NPs.

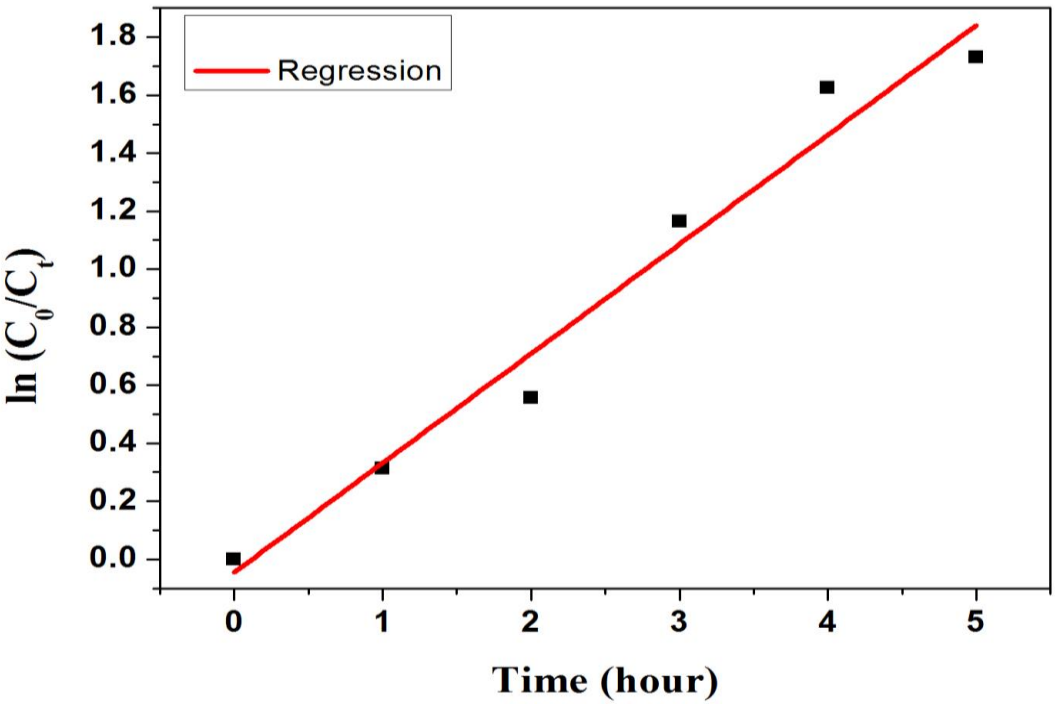

Fig. 3.13: Kinetic data for COD degradation during solar photocatalytic treatment of TWW with green synthesized TiO_2 NPs.

3.3.4. Cr removal efficiency

In the present study, green synthesized TiO_2 NPs was applied for the photocatalytic removal of Cr^{+6} from secondary treated TWW. The total Cr and Cr^{+6} content in the untreated TWW (control) were found to be 6.88 mg L^{-1} and 3.26 mg L^{-1}, which was quite higher than the permissible limit (Table 1). After the photocatalytic treatment, the remained Cr^{+6} in the photodegraded TWW was detected and quantified by 1,5-diphenyl carbazide (DPC) method spectrophotometrically by taking the absorbance at λ_{max} = 540 nm [10] and the Cr removal efficiency was found to be 76.48%. The degradation profile of COD is illustrated in Fig. 3.14 and the percent removal of COD from TWW was calculated according to Eq. 3.3.

The kinetics of COD degradation from TWW during solar photo-catalytic treatment with TiO_2 semiconductor photocatalyst can be illustrated by the first-order reaction (Eq. (4)) where k is the rate constant (0.0289 min^{-1}), C_0 is the initial concentration of Cr and Ct is the concentration of Cr at the irradiation time (t). Fig. 3.15 describes the linear relationship of $\ln(C_0/C_t)$ versus irradiation time (t) for Cr. The rate constant was determined for TiO_2 photocatalyst from the slope of the linear fitting line as shown in Fig. 15. As it can be seen, a good correlation to the first order reaction kinetics ($r^2 >$ 0.95) was found. The photocatalytic behavior is correlated with the structural, morphological and optical properties of the prepared TiO_2. Further, due to the large surface area, more active sites are present on the surface of TiO_2 NPs which are responsible for the adsorption of Cr from TWW during the photocatalytic oxidation. It can be easily observed from the reaction kinetics that the removal of Cr was slightly slow as compared to the COD from TWW during solar photocatalytic treatment.

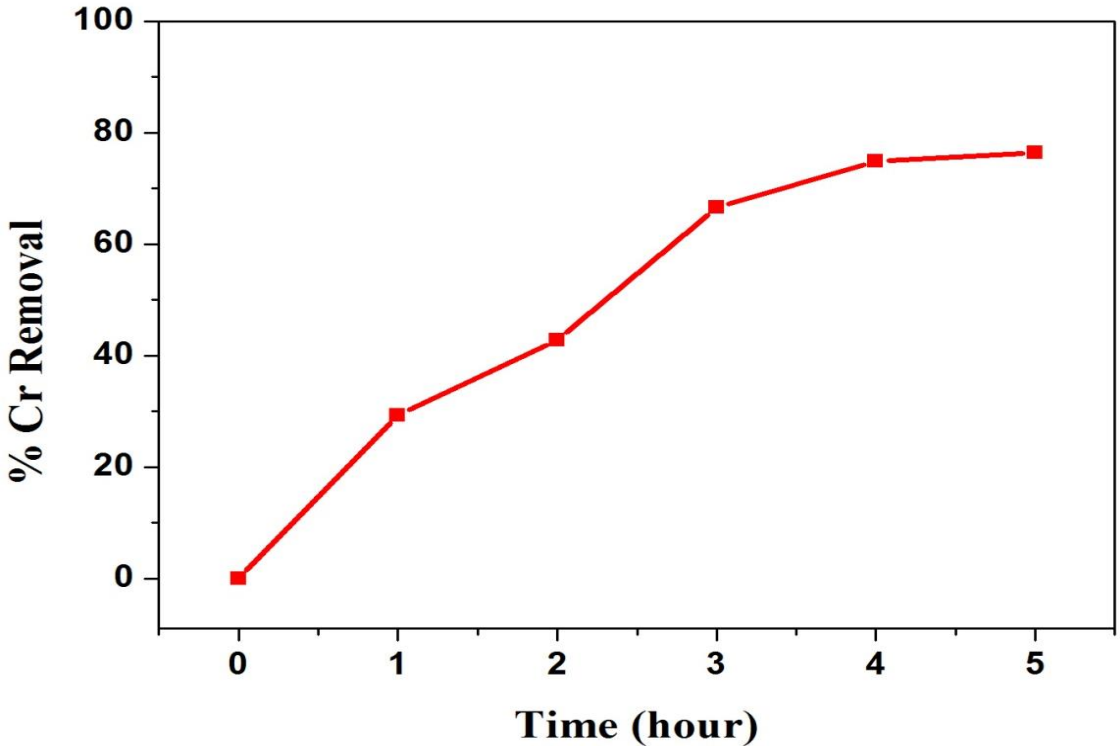

Fig. 3.14: Cr removal profile during solar photocatalytic treatment of TWW with green synthesized TiO_2 NPs.

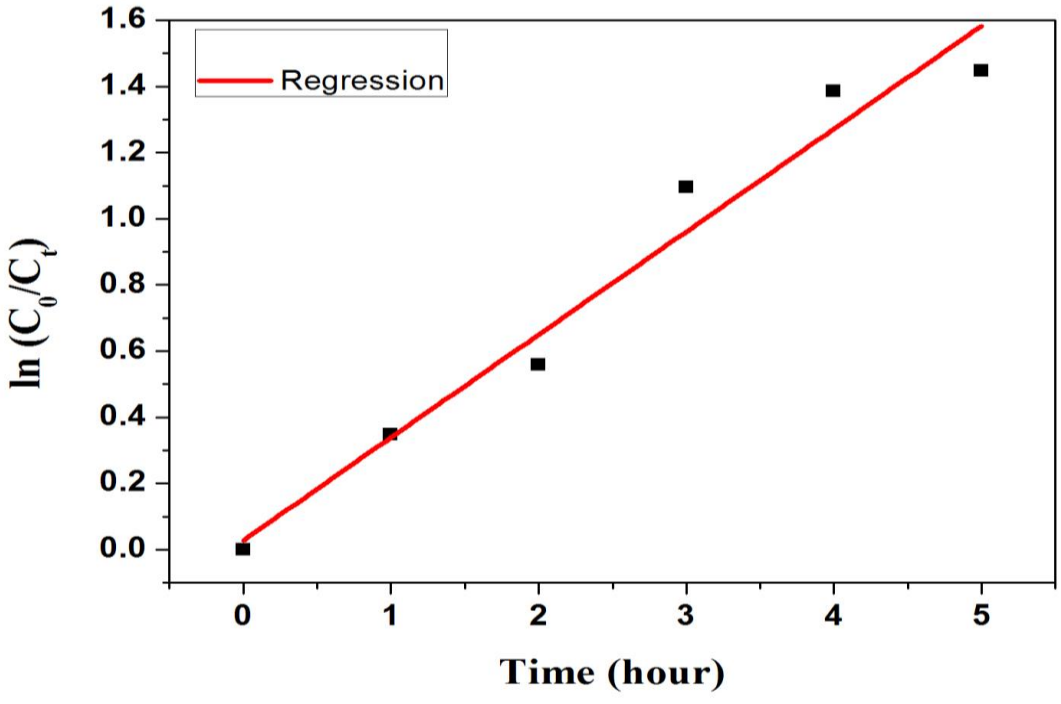

Fig. 3.15: Kinetic data for Cr removal during solar photocatalytic treatment of TWW with green synthesized TiO_2 NPs.

Further, the photocatalytic reduction of Cr^{+6} to Cr^{+3} along with photooxidation of organic pollutants can be easily understood by the following reaction mechanisms [38]:

$$TiO_2 + h\nu \rightarrow h^+ + e^- \quad (3.5)$$

$$Cr_2O_7^{2-} + 14H^+ + 6e^- \rightarrow 2Cr^{3+} + 7H_2O \quad (3.6)$$

$$2H_2O + 4h^+ \rightarrow O_2 + 4H^+ \quad (3.7)$$

$$H_2O + h^+ \rightarrow OH + H^+ \quad (3.8)$$

$$OH + \text{organics} \rightarrow CO_2 + H_2O \quad (3.9)$$

$$H^+ + \text{organics} \rightarrow CO_2 + H_2O \quad (3.10)$$

The key reason for the removal of Cr^{+6} from TWW was may be the adsorption due to an increase in the surface area of the green synthesized TiO_2 NPs as reported in previous studies [10,37]. FE-SEM and EDS analysis were done to confirm the adsorption of Cr^{+6} onto the surface of green synthesized TiO_2 NPs and record the changes in morphology after the solar photocatalytic treatment of TWW. The FE-SEM images clearly depicted the more rough and heterogeneous surface of the green synthesized TiO_2 NPs due to their enhanced agglomeration (size increased) after the photocatalytic oxidation of TWW and thus, provided the possibility for the adsorption of Cr^{+6} onto the surface of NPs [25] (Fig. 3.16a). Furthermore, the EDS analysis clearly evidenced the adsorption of Cr^{+6} onto the surface of green synthesized TiO_2 NPs as confirmed by the Cr peaks in the EDS spectra [10] (Fig. 3.16b). The elemental composition of green synthesized TiO_2 NPs after the solar photocatalytic treatment of TWW was found to be Ti = 22.19%, O = 60.35% and Cr = 2.40% (weight %). However, the impurities of Cl, Ca, Na, Mg, Si, and P peaks were also present in the sample as revealed by their respective peaks observed in the EDS spectra. The peaks that showed the impurities in the sample was might be due to their respective salts/chemicals (such as sodium chloride, magnesium oxide, calcium hydroxide, sodium tripolyphosphate and chrome-

silica syn-tans) used in rawhide/skins preservation, basification, liming and tanning process in LTs. Overall, the green synthesized TiO_2 NPs clearly demonstrated the tremendous potential for the photocatalytic removal of Cr^{+6} from TWW.

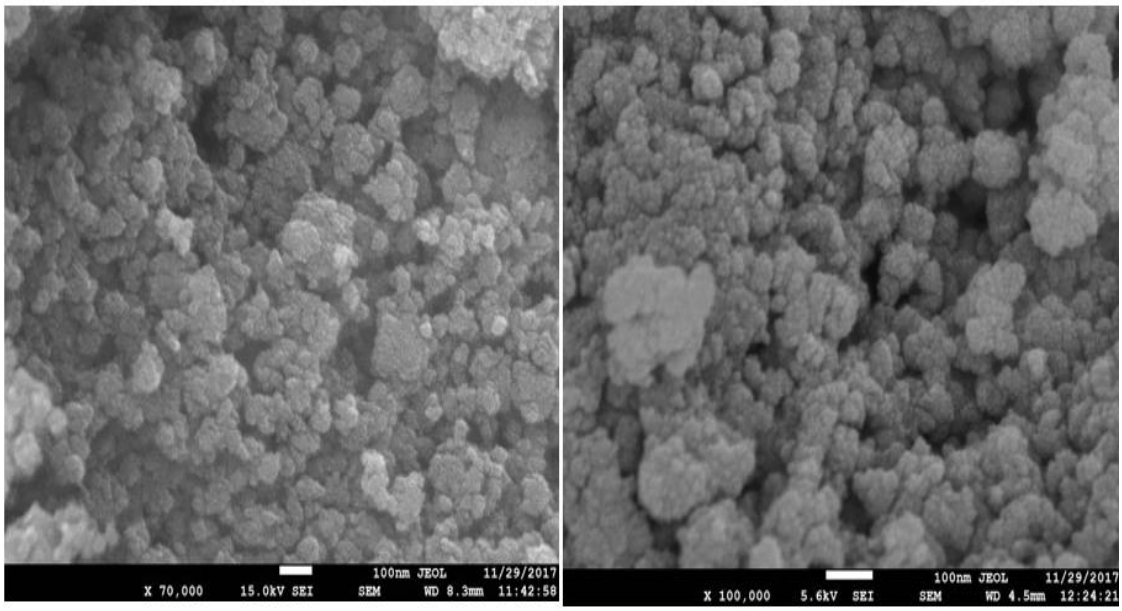

Fig. 3.16: (a) FE-SEM images of green synthesized TiO_2 NPs after photocatalytic treatment of TWW.

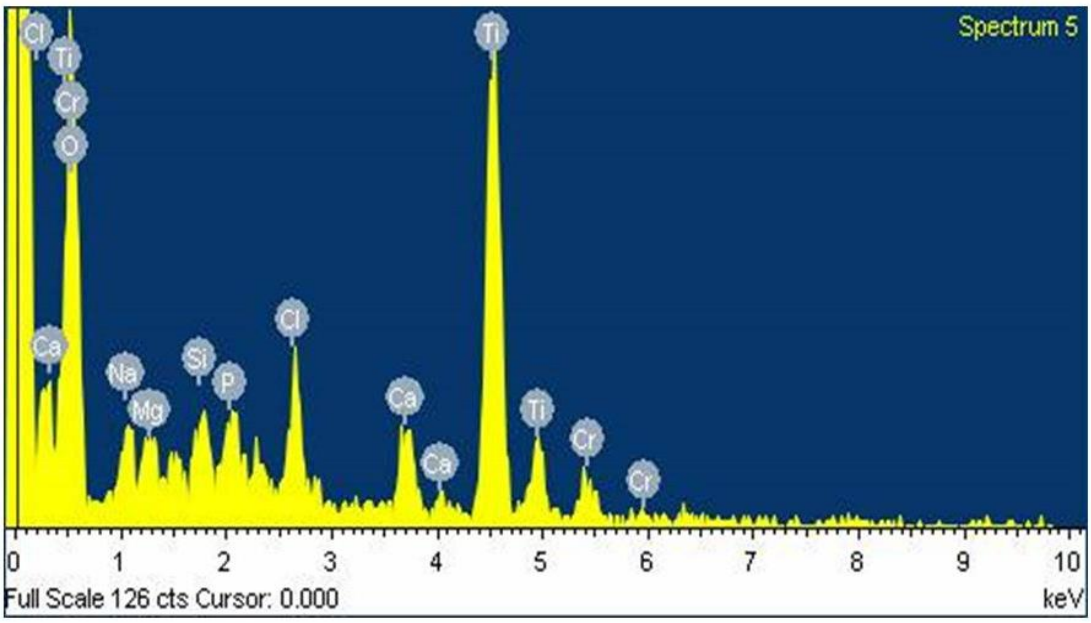

Fig. 3.16: (b) EDS spectrum of green synthesized TiO_2 NPs after photocatalytic treatment of TWW.

4. Conclusions

The present study was to synthesize the TiO_2 NPs using leaf extract of J. curcas L. and its performance evaluation for the first time in the solar photocatalytic treatment of TWW after the secondary treatment process. In the present study, a simple green chemistry method was employed for the green synthesis of TiO_2 NPs using the leaf extract of a biodiesel plant, Jatropha curcas L. and characterized by various techniques. The average crystallite size, surface area, pore size diameter and total pore volume of the green synthesized TiO_2 photocatalyst was 13 nm, 27.038 m^2/g, 19.100 nm and 0.1291 cm^3/g, respectively. The analysis of leaf extract revealed the presence of various phytochemicals such as phenols and tannins, which might be responsible for the reduction of metallic ions and acts as capping agents during the green synthesis of TiO_2 NPs and thus, stabilize the NPs. The reduction of metallic ions by the organic materials of leaf extract and green synthesis of TiO_2 NPs was confirmed by UV-Visible spectroscopy, FESEM, EDS, and FT-IR results. Further, the green synthesized TiO_2 NPs showed 82.26% and 76.48% removal of COD and Cr^{+6}, simultaneously, from real TWW after its solar photocatalytic treatment and thus, convincingly demonstrated the remarkable potential for wastewater treatment. The photocatalytic degradation of TWW obeys the first-order kinetics. The higher solar photocatalytic activity of the green synthesized TiO_2 NPs can be attributed to the nano-size, pure crystalline anatase phase, large amount surface hydroxyl groups and higher surface area. Finally, the green synthesis of TiO_2 NPs utilizing the extract of biodegradable and non-toxic *Jatropha curcas* L. leaves is a very promising approach. Jatropha curcas L. leaves are normally considered as waste material but are environment-friendly and easily available and thus, their utility in the green synthesis of TiO_2 NPs are amicable for the in-situ remediation of TWW or possibly for the other type of wastewater after the secondary treatment to

combat the environmental threats.

References

[1] G. Saxena, R. Chandra, R.N. Bharagava, Environmental pollution, toxicity pro file and treatment approaches for tannery wastewater and its chemical pollutants, Rev. Environ. Contam. Toxicol. 240 (2016) 3-69.

[2] R. Chandra, R.N. Bharagava, A. Kapley, H.J. Purohit, Bacterial diversity, organic pollutants and their metabolites in two aeration lagoons of common effluent treatment plant (CETP) during the degradation and detoxi fication of tannery wastewater, Bioresour. Technol. 102 (2011) 2333-2341.

[3] S. Aber, D. Salari, M.R. Parsa, Employing the Taguchi method to obtain the optimum conditions of coagulation- flocculation process in tannery wastewater treatment, Chem. Eng. J. 162 (2010) 127-134.

[4] O.P. Shukla, U.N. Rai, S. Dubey, Involvement and interaction of microbial communities in the transformation and stabilization of chromium during the composting of tannery e ffluent treated biomass of Vallisneria spiralis L. Bioresour. Technol. 100 (2009) 2198-2203.

[5] S. Dixit, A. Yadav, P.D. Dwivedi, M. Das, Toxic hazards of leather industry and technologies to combat threat: a review, J. Clean. Prod. 87 (2015) 39-49.

[6] G. Lofrano, G.E. Meric Zengin, D. Orhon, Chemical and biological treatment technologies for leather tannery chemicals and wastewaters: a review, Sci. Total Environ. 461-462 (2013) 265-281.

[7] A. Aich, A.R. Goswami, U.S. Roy, S.K. Mukhopadhyay, Ecotoxicological assessment of tannery e ffluent using guppy fish (Poecilia reticulata) as an experimental model: a biomarker study, J. Toxicol. Environ. Health A 78 (2015) 278 -286.

[8] V. Kumar, C. Majumdar, P. Roy, Effects of endocrine disrupting chemicals from

leather industry effluents on male reproductive system, J. Steroid Biochem. Mol. Biol. 111 (2008) 208-216.

[9] R. Chandra, R.N. Bharagava, S. Yadav, D. Mohan, Accumulation and distribution of toxic metals in wheat (Triticum aestivum L.) and Indian mustard (Brassica campestris L.) irrigated with distillery and tannery effluents, J. Hazard. Mater. 162 (2009) 1514-1521.

[10] K.M. Joshi, V.S. Shrivastava, Photocatalytic degradation of Chromium(VI) from wastewater using nanomaterials like TiO_2, ZnO, and CdS, Appl. Nanosci. 1 (2011) 147-155.

[11] S. Mishra, R.N. Bharagava, Toxic and genotoxic effects of hexavalent chromium in environment and its bioremediation strategies, J. Environ. Sci. Health, Part. C Environ. Carcinogen. Ecotoxicol. Rev. 34 (2016) 1-32.

[12] X. Guan, J. Chang, Z. Xu, Y. Chen, H. Fana, Remediation of chromium(III)-contaminated tannery e ffluents by using gallic acid-conjugated magnetite nano-particles, RSC Adv. 6 (2016) 29054-29063.

[13] X. Qu, P.J.J. Alvarez, Q. Li, Applications of nanotechnology in water and waste-water treatment, Water Res. 47 (2013) 3931-3946.

[14] M.Y. Ghaly, T.S. Jamil, I.E. El-Seesy, E.R. Souaya, R.A. Nasr, Treatment of highly polluted paper mill wastewater by solar photocatalytic oxidation with synthesized nano TiO_2, Chem. Eng. J. 168 (2011) 446-454.

[15] M.C. Bordes, M. Vicent, R. Moreno, J. Garcia-Montano, A. Serra, E. Sanchez, Application of plasma-sprayed TiO_2 coatings for industrial (tannery) wastewater treatment, Ceramic Int. 41 (2015) 14468-14474.

[16] M.A. Lazar, S. Varghese, S.S. Nair, Photocatalytic water treatment by titanium dioxide: recent updates, Catalysts. 2 (2012) 572 -601.

[17] W. Zhang, Y. Li, Y. Su, K. Mao, Wang, Q Effect of water composition on TiO_2 photocatalytic removal of endocrine disrupting compounds (EDCs) and estrogenic activity from secondary e ffluent, J. Hazard. Mater. 215 (2012) 252-258.

[18] C.P. Devatha, A.K. Thalla, S.Y. Katte, Green synthesis of iron nanoparticles using different leaf extracts for treatment of domestic waste water, J. Clean. Prod. 139 (2016) 1425-1435.

[19] B. Ajitha, P.S. Reddy, Biosynthesis of silvernanoparticles using Momordica charantia leaf broth; evaluation of their innate antimicrobial and catalytic activities, J. Photochem. Photobiol. B: Biol. 146 (2015) 1-9.

[20] T. Wang, X. Jin, Z. Chen, M. Megharaj, R. Naidu, Green synthesis of Fe nanoparticles using eucalyptus leaf extracts for treatment of eutrophic wastewater, Sci. Total Environ. 466-467 (2014) 210-213.

[21] APHA (American Public Health Association),, Standard Method for Examination of Water and Wastewater, 22nd ed., (2012) Washington DC.

[22] J.S.J. Hargreaves, Some considerations related to the use of the Scherrer equation in powder X-ray di ffraction as applied to heterogeneous catalysts, Catal. Struct. React. 2 (2016) 33-37.

[23] J. Chen, Li Zhang, NH_4Cl-assisted low temperature synthesis of anatase TiO_2 nanostructures from Ti powder, Mater. Lett. 63 (2009) 1797-1799.

[24] J.T. Carneiro, T.J. Savenije, J.A. Moulijn, G. Mul, How phase composition influences optoelectronic and photocatalytic properties of TiO_2, J. Phys. Chem. C 115 (2011) 2211-2217.

[25] S.S. Muniandy, N.H.M. Kaus, Z-Tao Jiang, M. Altarawneh, H.L. Lee, Green synthesis of mesoporous anatase TiO_2 nanoparticles and their photocatalytic activities, RSC Adv. 7 (2017) 48083.

[26] A.A. Asuk, M.A. Agiang, K. Dasofunjo, A.J. Willie, The biomedical signi ficance of the phytochemical, proximate and mineral compositions of the leaf, stem bark and root of Jatropha curcas, Asian Pac. J. Trop. Biomed. 5 (2015) 650-657.

[27] H. Bar, D.K. Bhui, G.P. Sahoo, P. Sarkar, S.P. De, A. Misra, Green synthesis of silver nanoparticles using latex of Jatropha curcas, Colloids Surf., A: Physicochem. Eng. Aspects 339 (2009) 134-139.

[28] G.V. Khade, M.B. Suwarnkar, N.L. Gavade, K.M. Garadkar, Green synthesis of TiO_2 and its photo catalytic activity, J. Mater. Sci.: Mater. Electron. 26 (2015) 3309 -3315.

[29] K.M. Kumar, B.K. Mandal, K.S. Kumar, P.S. Reddy, B. Sreedhar, Biobased green method to synthesize palladium and iron nanoparticles using Terminalia chebula aqueous extract, Spectrochimica Acta Part A: Mol. Biomol. Spectroscopy 102 (2013) 128-133.

[30] W. Li, D. Du, T. Yan, D. Kong, J. You, D. Li, Relationship between surface hydroxyl groups and liquid-phase photo catalytic activity of titanium dioxide, J. Colloid Interface Sci. 444 (2015) 42-48.

[31] A.M. Peiro, J. Peral, C. Domingo, X. Momenech, J.A. Ayllon, Low-temperature deposition of TiO_2 thin films with photocatalytic activity from colloidal anatase aqueous solutions, Chem. Mater. 13 (2011) 2567-2573.

[32] J. Yu, Y. Su, B. Cheng, M. Zhou, Effects of pH on the microstructures and photo-catalytic activity of mesoporous nanocrystalline titania powders prepared via hy-drothermal method, J. Mol. Catalysis A: Chem. 258 (2006) 104-112.

[33] K.E. Karakitsou, X.E. Verykios, Effects of altervalentcation doping of TiO_2 on its performance as a photocatalyst for water cleavage, J. Phys. Chem. 97 (1993) 1184 -1189.

[34] J.C. Tauc, The optical properties of solids, Amsterdam, North Holland, 1972. p. 372.

[35] R. Lopez, R. Gomez, Band-gap energy estimation from di ffuse re flectance measurements on sol-gel and commercial TiO_2: a comparative study, J. Sol-Gel Sci. Technol. 61 (2012) 1-7.

[36] C. Dette, M.A. PérezOsorio, C.S. Kley, P. Punke, C.E. Patrick, P. Jacobson, F. Giustino, S.J. Jung, K. Kern, TiO2 Anatase with a band gap in the visible region, Nano Lett. 14 (2014) 6533-6538.

[37] S.M.A. Moniema, M.E.M. Ali, T.A. Gad-Allaha, A.S.G. Khalil, M. Ulbricht, M.F. El-Shahat, M.A. Ashmawy, H.S. Ibrahima, Detoxi fication of hexavalent chromium in wastewater containing organic substances using simonkolleite-TiO_2 photocatalyst, Process Saf. Environ. Prot. 95 (2015) 247-254.

[38] M. Malakutian, F. Mansuri, Hexavalent chromium removal by titanium dioxide photocatalytic reduction and the effect of phenol and humic acid on its removal e fficiency, Int. J. Environ. Health Eng. 4 (2015) 1-8.

Chapter: 4

Green Synthesis of Copper Oxide Nanoparticles Using Leaf Extract of *Jatropha Curcas L.* for Cytotoxicity Test in Hepatocellular Liver Carcinoma Cell Line HepG2

4.1. Introduction

Cancer is a life vulnerable decease and has been a world-wide public health problem, caused serious health effects and manifested in diverging ways around the world. Cancer causes the one in seven deaths from all around the world and it also causes more deaths than AIDS, tuberculosis and malaria. According to a report of International Agency for Research on Cancer (IARC), near about 14.1 million new cancer cases were identified across the world which covers about 82% of the world's population which is a very serious concern. Estimated total cancer deaths in 2012 were 8.2 million from worldwide but it is a more serious concern to economically developing countries because 5.3 million deaths were estimated in these countries [1]. According to the report, by 2030, it can be predicted that worldwide load is going to be increased to 21.7 million new cancer cases and 13 million cancer deaths merely due to the advancement and aging of the population [2]. In economically developing countries, the three most commonly diagnosed cancers are liver, lung and stomach in males and breast, cervix uteri, and lung in females. Therefore, the cancer causes the economic burden on developing countries as its very costly medical treatment [3].

HepG2 is an immortalized human liver cancer cell line. This cell line derived from the liver tissue of a 15-year-old Caucasian American male who had a well-differentiated hepatocellular carcinoma which is fifth most-common cancer worldwide [4]. HepG2 cells can be grownup productively at an enormous rate and able to secrete

many plasma proteins such as fibrinogen, α-fetoprotein, fibronectin, plasminogen, albumin etc. They can be stimulated with human growth hormones [5]. According to Ma and Yu 2006, Liver cancer was the number three cause of cancer mortality. A total of 598,412 deaths (416,926 male and 81,486 female) were attributed to liver cancer in 2002. Chemotherapy is a technique in which various cytotoxic drugs have been used to destroy the cancer cells but the existing cytotoxic drugs or agents used for liver cancer treatment are found to be expensive and inefficient because they induce severe side effects due to their toxicity in noncancerous tissues [6].

Nanoscience and Nanotechnology are motivated by the synthesis of particles having various sizes and morphology at nanoscale. The morphology intensely affects on their broadly varying properties. Much attention has been attracted to nanoparticles on account of their unique properties and energetic application which are strongly influenced by their size, morphology and structure [7]. In recent times, it is becoming beneficial in drug delivery process for the treatment of several diseases and disorders. Amongst various synthesized nanoparticles, transition metal oxide nanoparticles such as copper oxide nanoparticles due to its unique optical, mechanical, thermal, conduction and catalytic properties have diverse biological applications [8]. Copper oxide is a P-type semiconductor material having narrow band gap energy, is very stable in nano-configuration [9, 10]. Nanoparticles of copper oxide have unique and very valuable applications, usually in electronics and optoelectronics [11]. These particles can be used as catalyst, superconducting materials, thermoelectric materials, glass, ceramic resistors, magnetic storage media, gas sensors and photoconductors [12-15]. Various types of synthesis of metallic oxide nanomaterials such as sonochemical method [16], sol-gel technique [17], one-step solid-state reaction method at room temperature [18], electrochemical method [19], thermal decomposition of precursors [20] and co-

implantation of metal and oxygen ions [21], precipitation method [22], chemical vapour deposition [23], thermal decomposition [24] hydrothermal method are reported [25]. These conventional nonbiological (chemical and physical) processes for the synthesis copper oxide nanoparticles are expensive, inefficient and require high energy and temperature and for some cases, these methods generate toxic and hazardous materials. Due to these toxic effects of conventional methods, researchers focused on the biological approach and preferred green synthesis. For the development of an eco-friendly, biocompatible and nontoxic process for nanoparticle synthesis, green chemistry approaches continuously gaining intense interest among researchers and scientists. Green synthesized metal oxide Nanoparticles have more interest due to their unique optical, mechanical, chemical and electrical properties, such as increased electrical conductivity, thermal conductivity, catalytic activity and antibacterial activity [19, 25].

Biosynthesis of nanoparticles comprises various approaches such as parts of plants, yeast, bacteria and fungi but plants are most efficient approach because of its easiest and eco-friendly nature. Recently green synthesis of different nanoparticles using plants are reported for example *Gundelia tournefortii* [26] *Gloriosa superba* [27] *neem* [28], *alfalfa* [29], *Cinnamomum camphora* [30], *Emblica officinalis* [31], *lemon grass* [32], *tamarind* [33] *and Euphorbia tirucalli* [34] have been around reported. Green synthesis is used in reducing metal ions into nanoparticles by biomolecules (alkaloids, flavanoids, phenols, tannins, quinines, terpenoids etc.) present in plant extract. This method of reduction of metal ions to base metal is quick, simple and efficiently calibrated. Water soluble metabolites which are presented in plants work as a reducing agent.

In this research work, we have mainly focused on the green process to successfully prepare copper oxide nanoparticles with controlled shape, sizes to find some of the optical and medicinal properties for different applications for the development of society. Copper oxide nanoparticles synthesized by leaf extract of *Jatropha Curcus L.* were characterized by XRD (X-Ray diffraction), SEM, EDX, UV- Visible spectroscopy, FTIR (Fourier transform infrared spectroscopy). Further, synthesized material tested for catalytic activity for degradation of methylene blue dye and analysed the photoluminescence property of synthesized nanoparticles. Graphical representation of presented research work has been shown in Fig.4.1.

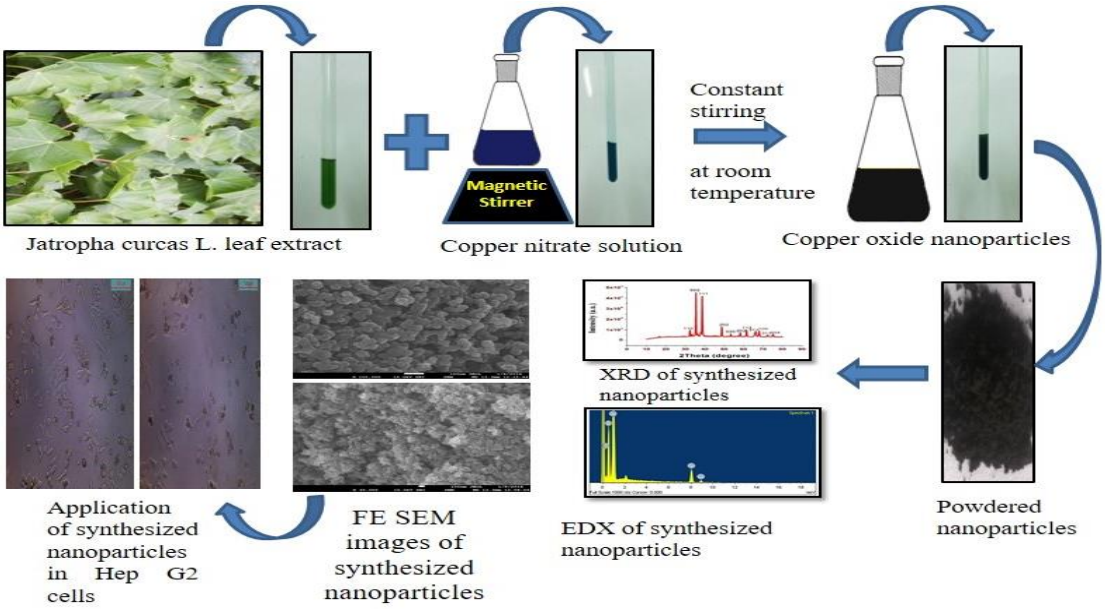

Fig. 4.1: Graphical representation of presented research work

4.2. Materials and Method

4.2.1. Materials and characterization techniques

Copper (II) Nitrate and Ammonia from Fisher Scientific (U.K.) were used in the experiments for the synthesis of copper oxide nanoparticles. Chemicals were of analytical reagent grade purity and ethanol was used in the whole experiment.

The crystal structure, surface morphology and composition of the synthesized nanoparticles were examined with powder X-Ray diffraction (XRD), scanning electron microscopy (SEM), and energy-dispersive spectrometry (EDX). SEM images were captured on an LEO 435 VP instrument operated at 25 kV; EDX was carried out by JEOL JXA-8100 EPMA. XRD pattern was recorded using X-ray diffractometer (Phillips X Pert model) equipped with Cu K_α radiation (λ = 0.1542 nm) within the 2θ range of 10°-80°. With the help of UV- Visible spectroscopy (EVOLUTION-201) the band gap energy of synthesized nanoparticles was deliberated.

HepG2 cells (3 x 10^4 per well), grown in 6-well plates in DMEM supplemented with 10% FBS for 24 h, were treated with copper oxide nanoparticles. Morphological changes were observed with an inverted microscope (OLYMPUS IX 70, Olympus Optical Co. Ltd., Sibuya-ku, Tokyo, Japan) and images were acquired.

4.2.2. Preparation of *Jatropha curcas L.* leaf extract

Fresh leaves of *Jatropha curcas L.* were washed thoroughly several times with biodegradable and distilled water to remove the dust particles and other unwanted impurities and cut it into fine pieces**.** 15 g of the leaves were mixed with 120 ml of ethanol and heated at 80 ^{0}C for 50 minutes. The resulting extract was cooled at room temperature and what man filter paper no.1 was used for filtration of the solution.

4.2.3. Synthesis of copper oxide nanoparticles

In a typical synthesis, 100 ml of 0.2 M copper (II) Nitrate ethanolic solution added first to leaf extract in ratio 1:1 with continuous stirring at room temperature. Subsequently 20 ml of 25% ammonia solution slowly added under stirring for the precipitation. A change in the color of the solution was observed during the stirring process. The color change of solution from blue to black confirms the nanoparticles formation. The obtained precipitate was washed with ethanol to remove the impurity of

all the ions and dried for 24 hours at room temperature. After the calcination of precipitation at 800^0C in the furnace, black powder of copper oxide nanoparticles was obtained.

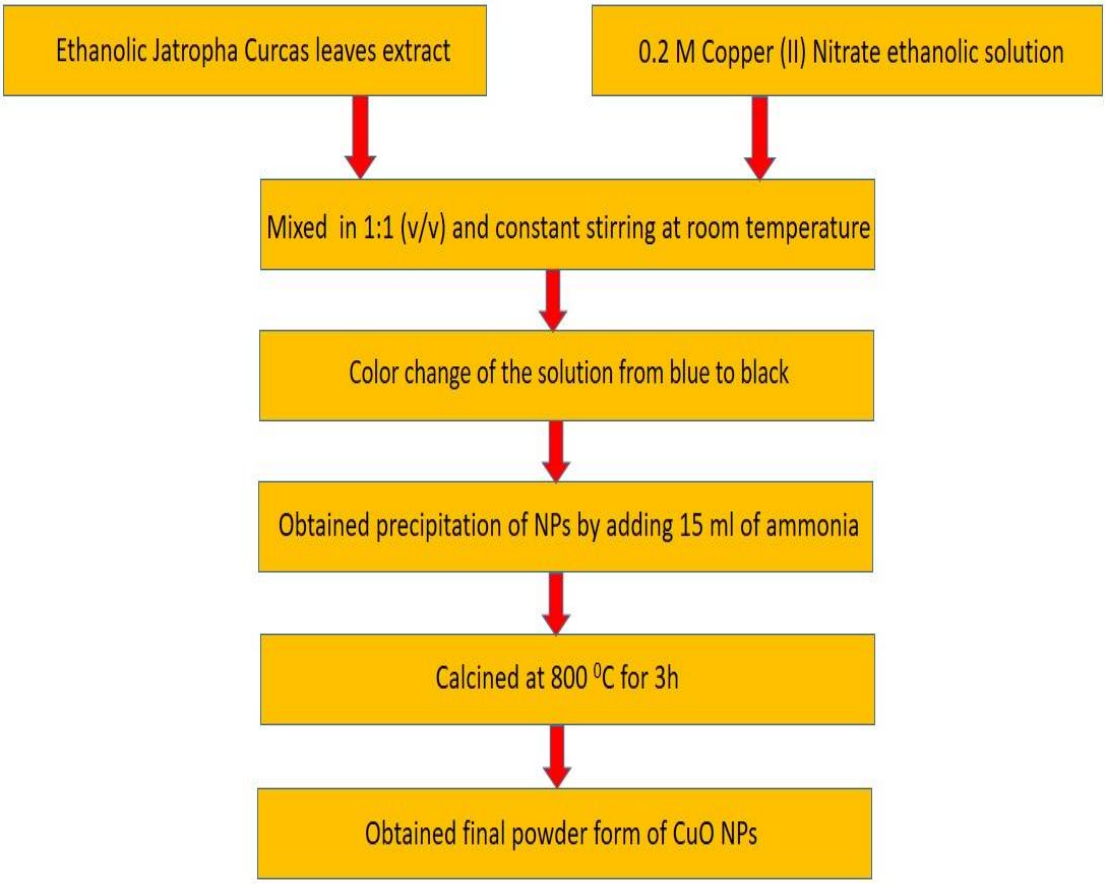

Fig. 4.2: Green synthesis of CuO nanoparticles using leaves extract of *Jatropha curcas L.*

4.2.4. Cell culture and treatment

Human hepatocellular liver carcinoma cell line (HepG2), utilized in the relevant studies and was purchased from the National Centre for Cell Sciences (NCCS, Pune, India). These cell lines were maintained in Dulbecco's Modified Eagle's Medium (DMEM) (Invitrogen, USA), supplemented with 10% fetal bovine serum (Gibco BRL, Gaithersburg, MD), L-glutamine, and antibiotics (penicillin, 100 U ml^{-1} and streptomycin, 50 mg ml^{-1}). Cells were cultured at 37 ºC in 95% air and 5% CO_2

humidified incubators. Cells were typically grown to 60–70% of confluency, washed in phosphate-buffered saline (PBS) and placed into the serum-free medium (DMEM containing 0.1% bovine serum albumin) overnight prior to treatments. Sodium arsenite and arsenite tagged IONPs were dissolved with glass-distilled water to desired concentrations and passed through 0.45 mm Millipore filters (Millipore India Pvt. Ltd., Bangalore, India) to remove particulate matter and freshly prepared for each experiment.

4.2.5. Cell viability assay

Cell viability assay was performed using MTT dye. Briefly, 1 x 10^5 cells were seeded per well in 100 ml of medium in 96-well microtiter plates (Nunc, Roskilde, Denmark). Cells grown for 24 h were exposed to copper oxide nanoparticles at a various dose. After 24 h of incubation, the medium was aspirated; MTT solution (1.2 mg ml^{-1}) added to each well and incubated for 4 h at 37 ºC. For solubilization of the formazan crystals formed, DMSO (100 ml) was added to each well and optical density was measured at wavelength 595 nm (EMax Precision Micro Plate Reader, Molecular Devices, USA). The absorbance correlates linearly to the number of living cells in culture. The percent cell survival was calculated as: survival = (HepG2 test/HepG2 control) x 100%. Dose-response bar diagrams were drawn, and IC_{50} value, the concentration that inhibits 50% of the growth of cells, was calculated.

4.3. Results and Discussion

4.3.1. Characterization of green synthesized CuO nanoparticles

Synthesized copper oxide nanoparticles characterized by X-ray Analysis for revealing the crystalline nature of synthesized nanoparticles. As shown in Fig. 4.3, diffraction peaks recommend that synthesized material has the good crystallinity and it shows the significance of experimental procedure on the nucleation the crystal. The XRD pattern

shows the peak position corresponding to 2θ values of 32.40^0, 35.50^0, 38.72^0, 48.77^0, 53.45^0, 58.27, 61.54^0, 66.08^0, 68.02^0 and 72.40^0 with (hkl) values of (110), (002), (111), (202), (020), (202), (113), (311), (220) and (311). These values of planes are closely matched with (JCPDS CARD NO- 45-0937). Characteristic peaks of copper oxide seem in XRD pattern, indicating the purity of our sample. The average crystallite size of nanoparticles was calculated by the Debye-Scherer formula,

$$D = .89\lambda/\beta Cos\theta$$

Where, λ (1.54Å) is the wavelength of X-Rays, θ Bragg's diffraction angle and β is the full width at half maximum. The calculated size of the crystallite size was found to be 45 nm.

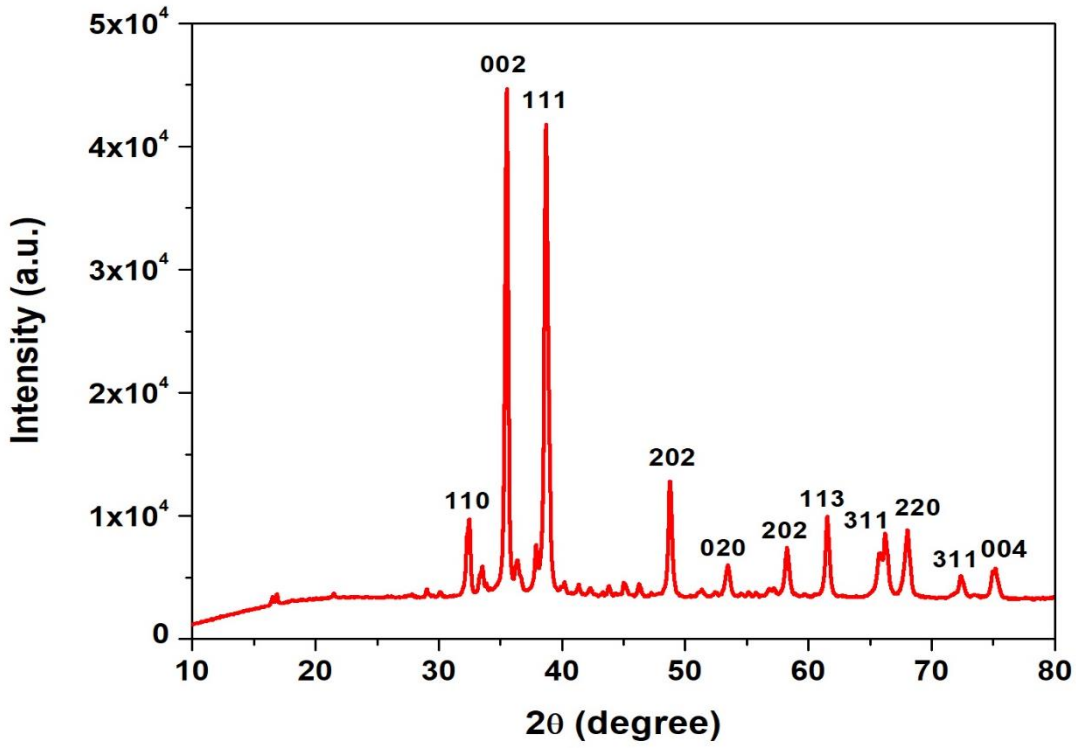

Fig. 4.3: XRD Pattern of green synthesized copper oxide nanoparticles

SEM images of the copper oxide nanoparticles are shown in Fig. 4.4. As can be seen from SEM images; the particles were found to be spherical in the range 50-200 nm. In

Fig.4.5, the EDX micrograph of the copper oxide reveals the purity of the sample. Both copper (Cu) and Oxygen (O) are present in the sample.

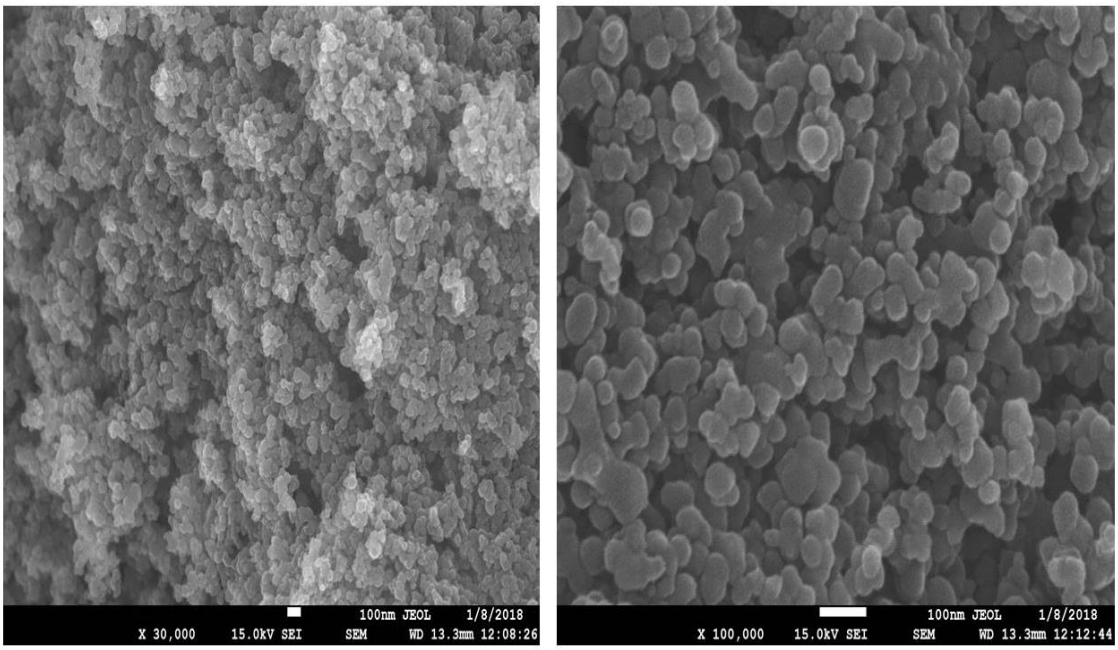

Fig. 4.4: FE-SEM images of green synthesized copper oxide nanoparticles

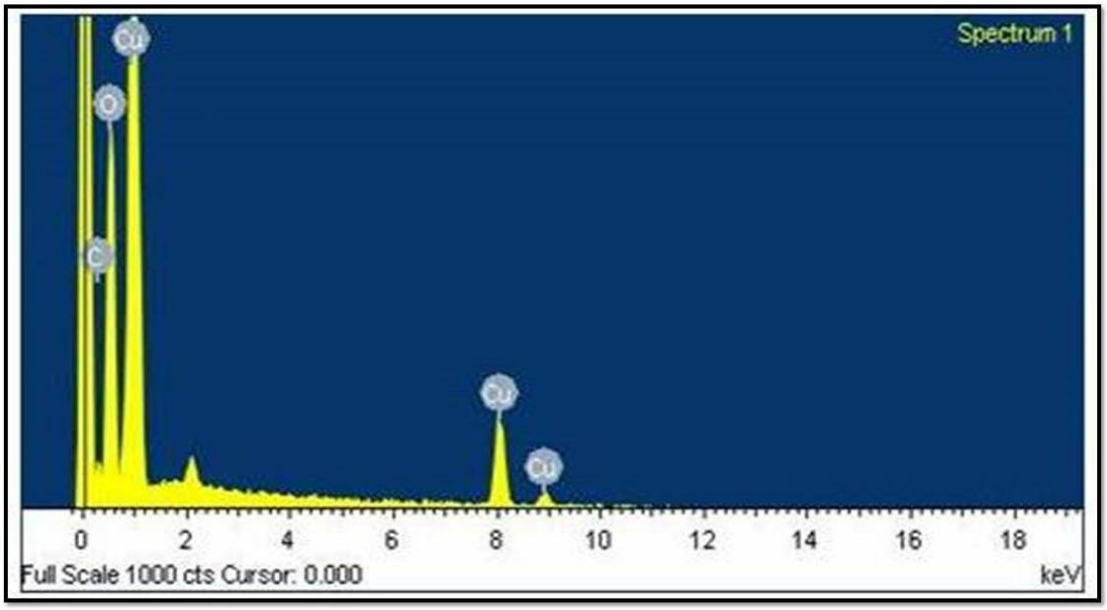

Fig. 4.5: EDX spectra of green synthesized copper oxide nanoparticles

For UV-Visible analysis of synthesized CuO NPs, the synthesized material in powder form was dispersed in hydrochloric acid. Spectra analysis reveals the optical property

of the synthesized copper oxide NPs and confirms their presence. The spectrum of the copper oxide nanoparticles is shown in Fig. 4.6 (a).The surface plasmon absorption peak was found around 450 nm. The surface plasmon absorption in the metal oxide nanoparticles is due to the collective oscillation of the free conduction band electrons which is excited by the incident electromagnetic radiation. This type of resonance is seen when the wavelength of the incident light far exceeds the particle diameter [35]. The UV-visible absorption spectrum was clearly indicating the widening of band gap. Using the Tauc equation, the energy band gap of material can be determined [36].

$$\alpha(h\nu)=B(h\nu-Eg)^{m} \qquad 4.1$$

Where, B is constant and has different values for different type of transitions. E_g is the energy gap and hv is the photon energy, m denotes an exponent which have values ½, 3/2, 2 and 3 depending on the electronic transition [37]. Tauc plot as shown in Fig. 4.6 (b) has the photon energy ($h\nu$) on the X axis and $(\alpha h\nu)^2$ on the Y axis. Extrapolating the linear portion of the curve to the X-axis yields the energy band gap of the material. This is found to be 2.4 eV. This value is higher than that of bulk copper oxide which has near about 1.7 eV energy band gap.

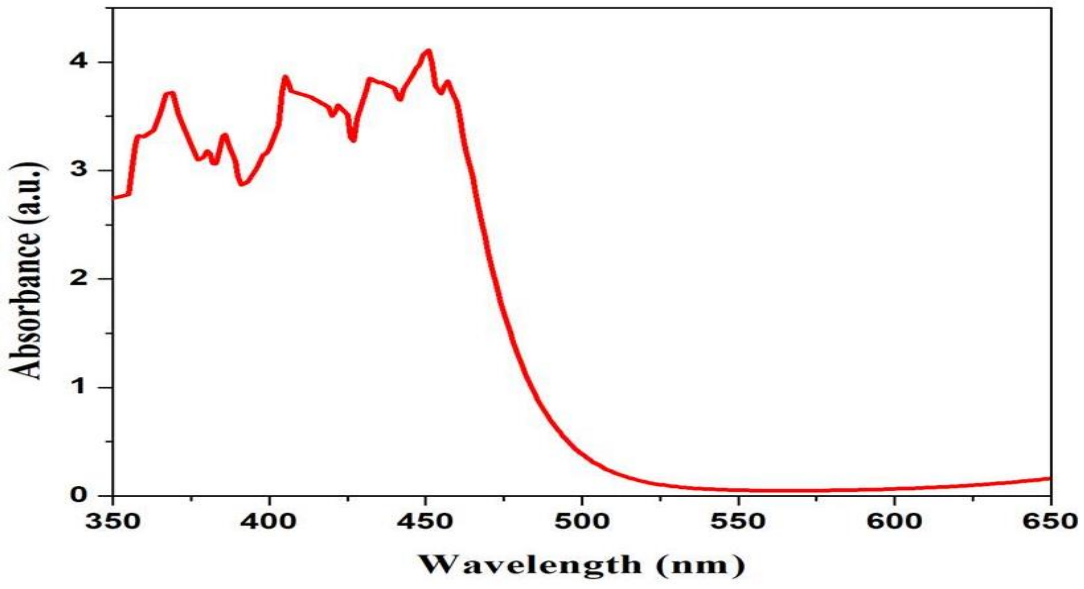

Fig. 4.6: (a) Absorption spectra of green synthesized copper oxide nanoparticles

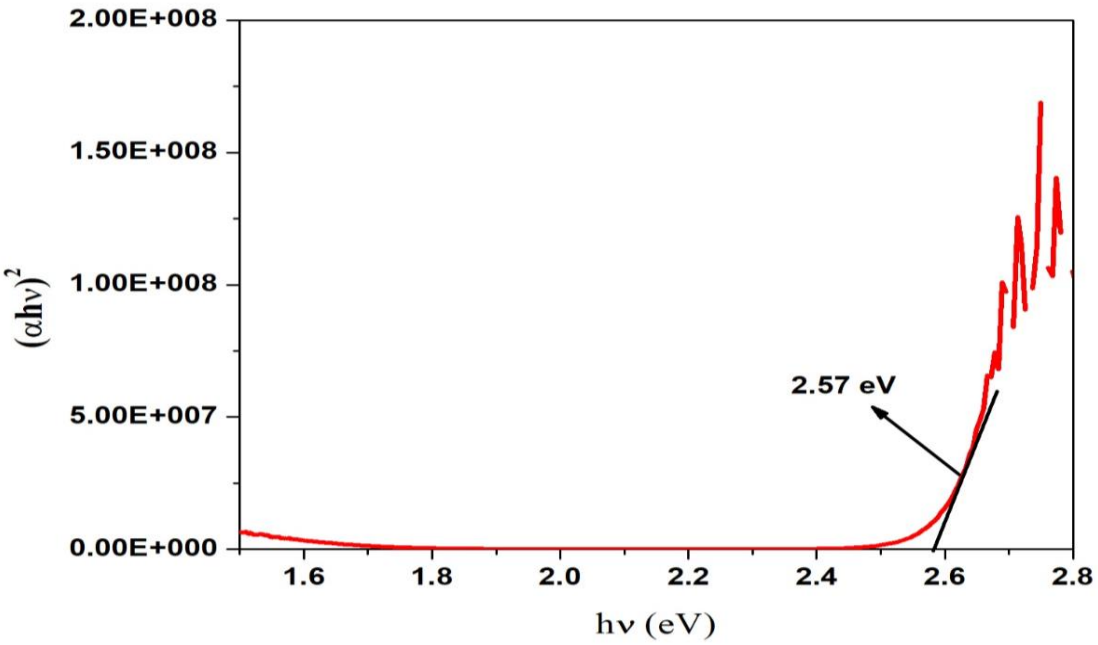

Fig. 4.6: (b) Tauc plot of green synthesized copper oxide nanoparticles

The FTIR spectra of synthesized copper oxide NPs was recorded to identify the functional groups present in sample is shown by Fig. 4.7. The FTIR spectrum exhibits peaks and bands in the range 4000-500 cm^{-1}. The peak at 683 cm^{-1} is due to the characteristic vibration mode of CuO [38]. The appearance of the strong peak at 850 cm^{-1} demonstrates the existence of carbonyl group (C-H). The peak observed at 1440 cm^{-1} shows stretching in the C-O bonding. Carbonyl group has appeared in the spectra at 1688 cm^{-1} which play a significant role in the reduction of cupric chloride ions. Moreover, the peak at 3026 cm^{-1} shows the stretching of C-H bonding. An intense peak at 3465 cm^{-1} possibly attributed to the presence of the hydroxyl group [39].

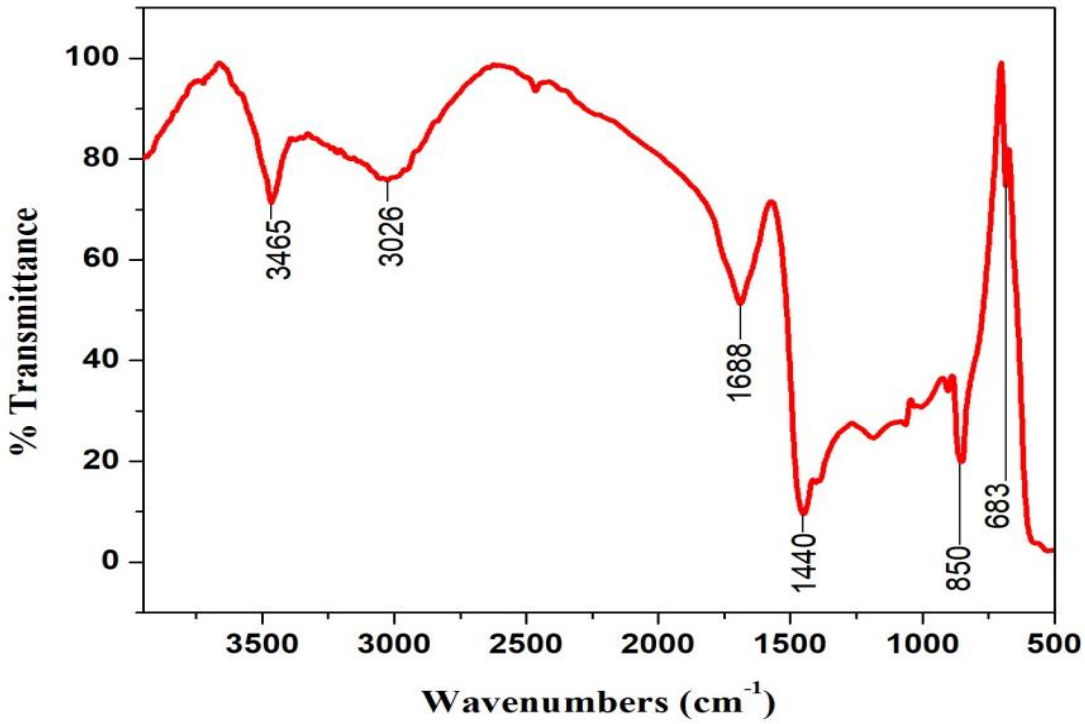

Fig. 4.7: FTIR spectra of green synthesized copper oxide nanoparticles

N_2 adsorption-desorption isotherms on the sample of CuO NPs was found using a surface area and pore size analyzer. The surface area of the green synthesized CuO NPs was evaluated by the Brunauer-Emmett-Teller (BET) analysis whereas pore volume and pore size distribution for the green synthesized CuO NPs were evaluated by the Barrett-Joyner-Halenda (BJH) analysis.

The surface area (S_{BET}) of the green synthesized CuO NPs was 18.23 m^2/g whereas the mean pore diameter and total pore volume of the green synthesized CuO NPs was 70.630 nm and 0.1291 cm^3/g as shown in Fig.4.8 a, b.

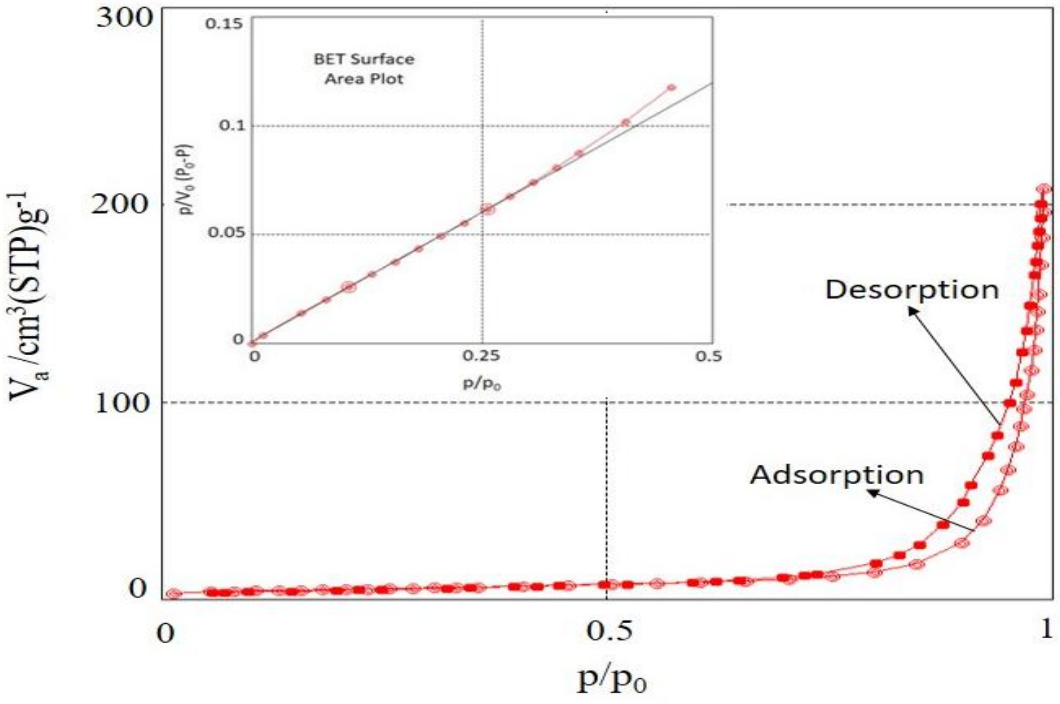

Fig. 4.8: (a) N_2 Adsorption/desorption isotherm of the green synthesized CuO NPs.

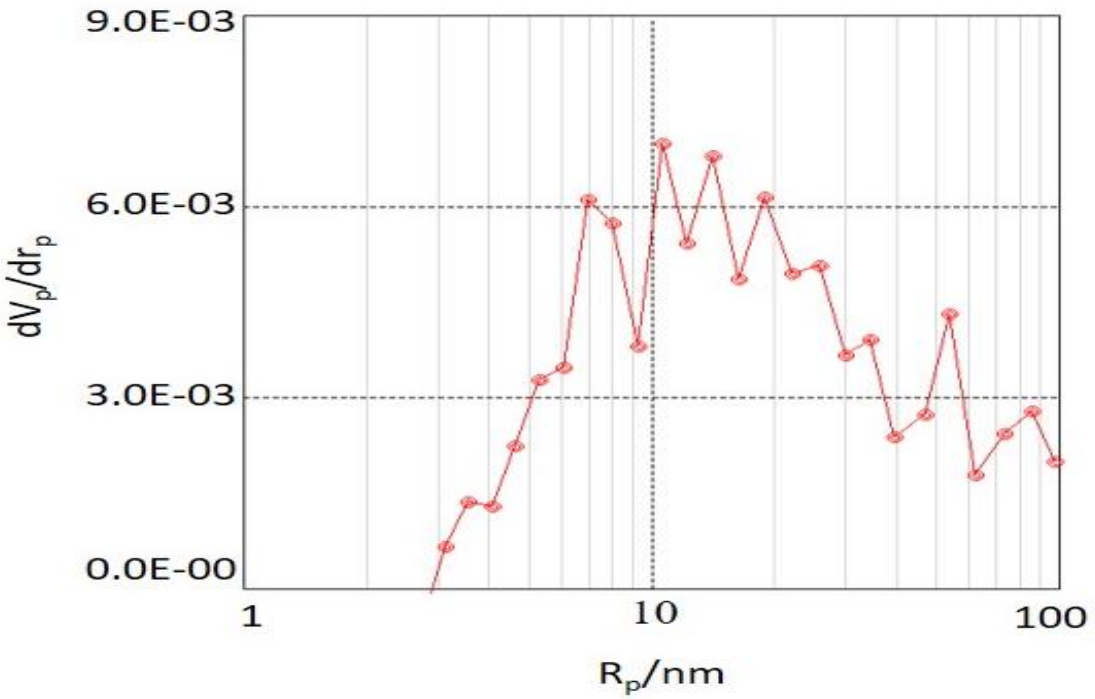

Fig. 4.8: (b) BJH plot of the green synthesized CuO NPs.

4.3.2. Assessment of cell morphology

The cell morphology study of HepG2 cells in presence of the copper oxide nanoparticles in different concentrations was observed under a confocal microscope. In presence of copper oxide nanoparticles, the characteristic apoptotic changes like cell rounding and cell shrinkage were found with the concentration above 10 μM for 24 h, whereas control cells alone did not show any morphological changes as shown in Fig.4.9.

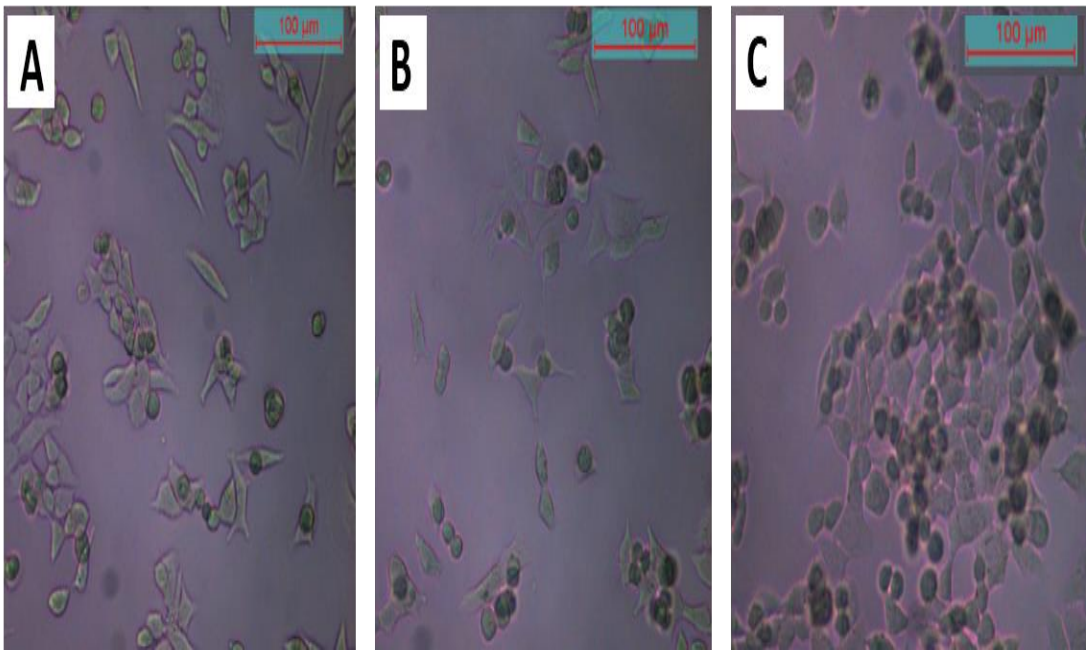

Fig. 4.9: Cellular morphology of HepG2 cells alone (A), treated for 24 h with10 μM copper oxide nanoparticle (B) and 20 μM CuO NPs (C)

4.3.3. Cytotoxicity of CuO nanoparticles

The biological activity of copper oxide nanoparticles was assessed using human hepatocellular cell line (HepG2) in the presence and absence of the copper oxide nanoparticles. The cell viability assay exhibited that copper oxide nanoparticles at 5 μM shows no appreciable change in cell cytotoxicity but when administered at higher dose of 20 μM, results in remarkably increase in cytotoxicity which is due to the ability of copper oxide nanoparticles to penetration of cell membrane and to bind the CuO

nanoparticles with the cellular biomolecules [40, 41]. This leads to the disruption of cellular trafficking and finally cells go to the apoptosis and cell death. After all it showed IC_{50} value at 45 μM Fig. 4.10.

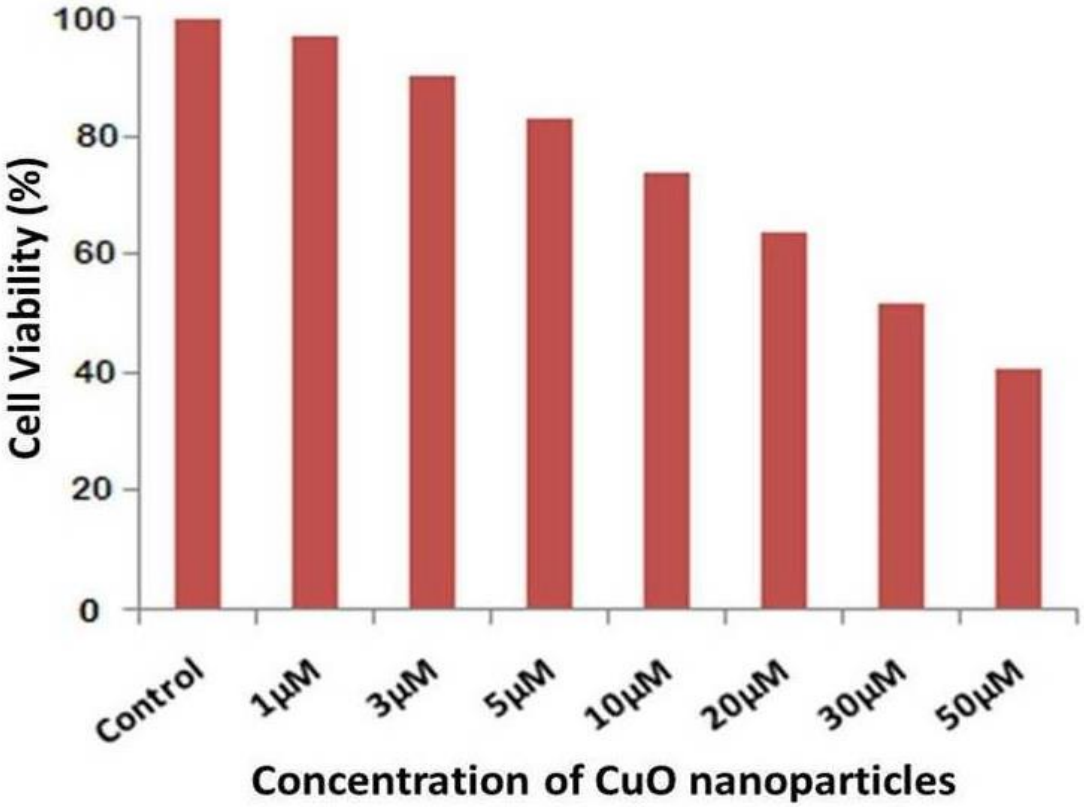

Fig. 4.10: Effect of copper oxide nanoparticle on HepG2 cell viability at different concentration of copper oxide nanoparticles.

4.4. Conclusions

Synthesis of copper oxide nanoparticles by *Jatropha curcas L.* leaf extract involve biochemical reactions wherein biological molecules react with the material surface for the reduction of metallic ions. The synthesized nanoparticles are stable with suitable morphologies and characteristics. The exploitation of these nanoparticles in the field of drug delivery has a great importance in the field of drug targeting since it has quite good transport properties and cell membrane penetration power. Moreover, it has to some extent cancer cell killing ability which is reflected in the cell viability assay.

References

[1] L.A. Torre, F. Bray, R.L. Siegel, J. Ferlay, J. Lortet-Tieulent, A. Jemal, Global cancer statistics 2012, CA: Cancer J clinic. 65 (2015) 87-108.

[2] C. Martel, J. Ferlay, S. Franceschi, J. Vignat, F. Bray, D. Forman, Dr M. Plummer, Global burden of cancers attributable to infections in 2008: a review and synthetic analysis, Lancet Oncol.13(2012) 607-615.

[3] A. Jemal, F. Bray, M.M. Center, J. Ferlay, E. Ward, D. Forman, Global cancer statistics, CA: a cancer J. for clinic. 61(2011) 69-90.

[4] J.A.M. Cocadiz, C.C.Y. Lim, J.T. Dalet, M.T.A. Barzaga, F.M. Heralde III, CD133, MUC1 and KRT19 chromosomal rearrangements and Gene expressions as potential biomarkers for liver cancer, Int. J. Medical Res. Health Sci. 6(9) (2017) 21-31.

[5] M.C. Liu, S. Yu, J. Sy, C.M. Redman, F. Lipmann, Tyrosine sulfation of proteins from the human hepatoma cell line HepG2, Proc. Natl. Acad. Sci. USA. 82 (1985) 7160-7164.

[6] Stephanie E. Combs, Thomas E. Schmid, Peter Vaupel, Gabriele Multhoff, Stress Response Leading to Resistance in Glioblastoma-The Need for Innovative Radiotherapy (iRT) Concepts. Cancers. 8 (2016) 15.

[7] S.A. Khan, S. Shahid, M.R. Sajid, F. Noreen, S. Kanwal, Biogenic synthesis of CuO nanoparticles and their biomedical applications: a current review, Int. J. Adv. Res. 5 (2017) 925-946.

[8] R. Guin, S. Banu A, G.A. Kurian, Synthesis of copper oxide nanoparticles using Desmodium Gangeticum aqueous root extract, Int. J. Pharm. Pharm. Sci. 7(1) (2014) 60-65.

[9] P.P.N. Vijay Kumar, U. Shameem, P. Kollu, R.L. Kalyani, S.V.N. Pammi, Green synthesis of copper oxide nanoparticles using Aloe vera leaf extract and its

antibacterial activity against Fish bacterial pathogens, Bio Nano Sci. 5 (2015)135-139.

[10] H. Wang, J.Z. Xu, J.J. Zhu, H.Y. Chen, Preparation of CuO nanoparticles by microwave irradiation, J. of Crystal Growth. 244 (2002) 88-94.

[11] T. H. Tran and V. T. Nguyen, Copper Oxide Nanomaterials Prepared by Solution Methods, Some Properties, and Potential Applications: A Brief Review, Int. Sch. Res. Notic. 2014 (2014) 14.

[12] A. Chowdhuri, V. Gupta, K. Sreenivas, R. Kumar, S. Mozumdar, P. Patanjali, Response speed of SnO_2-based H_2S gas sensors with CuO nanoparticles, Appl. Phys. Lett. 884 (2004) 1180.

[13] C. Wang, X.Q. Fu, X.Y. Xue, Y.G. Wang, T.H. Wang, Surface accumulation conduction controlled sensing characteristic of p-type CuO nanorods induced by oxygen adsorption, Nanotechnology. 18 (2007)145506.

[14] K.H. Muller, High-Tc Supper Conductors and Related Materials, vol. 86, Kluwer Academic, Dordrecht, The Netherlands, (2001), ISBN: 978-3-319-52675-1.

[15] H. Siddiqui, M.S. Qureshi, F.Z. Haque, Effect of copper precursor salts: Facile and sustainable synthesis of controlled shaped copper oxide nanoparticles, Optik. 127 (2016) 4726-4730.

[16] R.V. Kumar, Y. Diamant, A. Gedanken, Sonochemical Synthesis and Characterization of Nanometer-Size Transition Metal Oxides from Metal Acetates Chem. Mater. 12 (2000) 2301-2305.

[17] A.A. Eliseev, A.V. Lukashin, A.A. Vertegel, L.I. Heifets, A.I. Zhirov, Y.D. Tretyakov, Complexes of Cu(II) with polyvinyl alcohol as precursors for the preparation of CuO/SiO_2 nanocomposites, Mater. Res. Innov. 3 (2000) 308-312.

[18] J.F. Xu, W. Ji, Z.X. Shen, S. H. Tang, X.R. Ye, D.Z. Jia, X.Q. Xin, Preparation and Characterization of CuO Nanocrystals J. Solid State Chem. 147 (2000) 516-519.

[19] K. Borgohain, J. B. Singh, M.V. Rama Rao, T. Shripathi, S. Mahamuni, Quantum size effects in CuO nanoparticles, Phys. Rev. 61 (2000) 11093.

[20] J.Q. Yu, Z. Xu, D.Z. Jia, J. Chin., Decontamination procedure of CEES on the surface of CuO NPs, Func. Mater. Inst. 5 (1999) 267-273.

[21] S. Nakao, M. Ikeyama, T. Mizota, P. Jin, M. Tazawa, Y. Miyagawa, S. Miyagawa, S. Wang, L. Wang, Rep. Res. Cent. Ion Beam Technol., Hosei Univ. Suppl., 18(2000) 153.

[22] J. Zhu, D. Li, H. Chen, X. Yang, L. Lu, X. Wang, Highly dispersed CuO nanoparticles prepared by a novel quick-precipitation method, Materials Letters. 58 (2004) 3324-3327.

[23] A.A. Ponce, K.J. Klabunde, Chemical and catalytic activity of copper nanoparticles prepared via metal vapor synthesis, Journal of Molecular Catalysis A: Chemical. 225 (2005) 1-6.

[24] M. Salavati, F. Davar, Synthesis of copper and copper (1) oxide nanoparticles by thermal decomposition of a new precursor Materials letters. 63 (2009) 441- 443.

[25] F. Teng, W. Yaob, Y. Zheng, Y. Teng, T. Xu, S. Liang, Y. Zh, Synthesis of flower like CuO nanostructures as a sensitive sensor for catalysis, sens. and Act. B. 134 (2008) 761-768.

[26] A. Ali, H. Zafar, M. Zia, I. Ul Haq, A.R. Phull, J.S. Ali, A. Hussain, Synthesis, characterization, applications, and challenges of iron oxide nanoparticles, Nanotechnol. Sci. Appl. 9 (2016) 49-67.

[27] M. Nasrollahzadeh, M. Mahamb, S. Mohammad Sajadi, Green synthesis of CuO nanoparticles by aqueous extract of Gundelia tournefortii and evaluation of their catalytic activity for the synthesis of N-monosubstituted ureas and reduction of 4-nitrophenol, Journal of Colloid and Int. Sci. 455 (2015) 245-253.

[28] H. Raja Naika, K. Lingaraju, K. Manjunath, D. Kumar, G. Nagaraju, D. Suresh, H. Nagabhushana, Green synthesis of CuO nanoparticles using *Gloriosa superba* L. extract and their antibacterial activity, J. of Taibah Univ. for Sci. 9 (2015) 7-12.

[29] S. Shiv Shankar, A. Rai, A. Ahmad, M. Sastry, Rapid synthesis of Au, Ag, and bimetallic Au core-Ag shell nanoparticles using Neem (*Azadirachta indica*) leaf broth, J. Colloid Interface Sci. 275 (2004) 496-502.

[30] J.L. Gardea-Torresdey, J.G. Parsons, E. Gornez, J. Videa, H.E. Troiani, P. Santiagol, Formation and Growth of Au Nanoparticles inside Live Alfalfa Plants Nano Lett. 2 (2002) 397-401.

[31] J. Huang, Q. Li, D. Sun, Y. Lu, Y. Su, X. Yang, H. Wang, Y. Wang, W. Shao, N. He, J. Hong, Biosynthesis of silver and gold nanoparticles by novel sundried Cinnamomum camphora leaf C. Chen, Nanotechnology. 18 (2007) 105104-105115.

[32] B. Ankamwar, D. Chinmay, A. Absar, S. Murali, Biosynthesis of Gold and Silver Nanoparticles Using Emblica Officinalis Fruit Extract, Their Phase Transfer and Transmetallation in an Organic Solution, J. Nanosci. Nanotechnol. 5 (2005) 1665-1671.

[33] S.S. Shankar, A. Rai, B. Ankamwar, A. Ahmad, M. Sastry, Biological synthesis of triangular gold nanoprisms, Nat. Mater. 3 (2004) 482-488.

[34] B. Ankamwar, M. Chaudhary, S. Murali, Synthesis and Reactivity in Inorganic, Metal-Organic, and Nano-Metal Chemistry, Nano-Metal Chem. 35 (2005) 19-26.

[35] B.S. Ravikumar, H. Nagabhushana, D.V. Sunitha, S.C. Sharma, B.M. Nagabhushana, C. Shivakumara, J. Alloys Compd. 585 (2014) 561-571.

[36] S. Dhaneshwar, V. Patel, D. Patil, G. Meena, Studies on synthesis, stability, release and pharmacodynamic profile of a novel diacerein-thymol prodrug**,** Bio. & Med. Chem. Lett. 23 (2013) 55-61.

[37] J. C. Tauc, optical properties of solids (Amsterdam: North Holland) (1972) 372.

[38] R. Bhatt, I. Bhaumik , S. Ganesamoorthy, A. K. Karnal, M. K. Swami, H. S. Patel, P. K. Gupta, Urbach tail and bandgap analysis in near stoichiometric $LiNbO_3$ crystals Physics Status Solidi A. 209 (2012) 176-180.

[39] V. Vellora, T. Padil, M. Cernik, Green synthesis of copper oxide nanoparticles using gum karaya as a biotemplate and their antibacterial application**,** Int. J. Nanomed. 8 (2013) 889-898**.**

[40] M.Y. Ghaly, T.S. Jamil, I.E. El-Seesy, E.R. Souaya, R.A. Nasr, Treatment of highly polluted paper mill wastewater by solar photocatalytic oxidation with synthesized nano TiO_2, Chem. Eng. J. 168 (2011) 446-454.

[41] P. Jean-Pascal, D. Jacques, A. Jean-Nicolas, J. Mejia, E. Boilan, F. Noel, Maude F., C. Demazy, S. Lucas, C. Saout, O. Toussaint, Copper(II) oxide nanoparticles penetrate into HepG2 cells, exert cytotoxicity via oxidative stress and induce pro-inflammatory response, Nanoscale. 4(2012) 7168.

[42] Y. Wang, G.A. Winfred, H. Hwang, G.Y. Clement, H. Yu, B.T. Paul, A study of the mechanism of in vitro cytotoxicity of metal oxide nanoparticles using catfish primary hepatocytes and human HepG2 cells, Sci. Total Env. 409 (2011) 4753-4762.

Chapter: 5

Coriander Extract Mediated Green Synthesis of Zinc Oxide Nanoparticles and Their Structural, Optical and Antibacterial Properties

5.1. Introduction

In past few decades, generation of bacterial infection in industrial sectors including environmental, food, personal care products, synthetic textiles, packaging, healthcare, clinics; and public health threat due to emergence of resistance to antibiotics with their excess uses in bacteria have received worldwide attention of scientific community to develop new age antimicrobial agents, formulations and methods. Metal oxide nanoparticles exhibit remarkable biological applications and are of great interest for both fundamental research and technological development [1-8].

Several investigators are trying to develop the proper growth and processing techniques for the synthesis and to manipulate the features of metal oxide nanoparticles (NPs). Among the metal oxides, zinc oxide is a promising multifunctional material has stimulated intensive research interest due to its unique optical, electrical and chemical properties which are well exemplified by the number of previous articles. Having a large band gap (3.3 eV), large exciton binding energy, good transparency and high electron mobility, it is very useful material for the optoelectronic applications [3, 4]. It is worth noting that zinc oxide nanoparticles can be used in various applications such as biotechnology, drug delivery, medical, optical devices, DNA labeling, biomolecular detection, diagnostics [5] optoelectronics, nanogenerators, biosensors, solar cells, photocatalysts lubricants, rubber, photodetectors, cement ceramics sensors etc.,[6,7]**.** Furthermore, because of their large surface area these nanoparticles are used in

wastewater treatment [8] and in the removal of impurities like arsenic and sulphur from water or wastewaters [9]. There are a number of chemical and physical methods reported in the literature for the preparation of nanoparticles of different sizes, shapes, and compositions which require high temperature, pressure, expensive and toxic chemicals, hazardous reagents and nonpolar solvents, imposes an inordinate challenge before materials scientist [10, 11]. To overcome the limitations of these conventional methods, green synthesis has emerged as an eco-friendly alternative for the low-cost development of nanoparticles, which are highly efficient and biocompatible and can be used in a variety of applications [12-14]. It has been previously reported that among the different biological synthesis methods of nanoparticles plant-mediated synthesis are rapid, potentially advantageous and have more stability in various shape and size than the other organisms, as the microorganisms based synthesis is not of industrial viability due to necessity of multiple purification steps, highly aseptic conditions and their maintenance [15, 16].

A large number of plants have been reported in recent years for the synthesis of nanoparticles from the extract of various parts of plants such as eucalyptus hybrid, *Coriandrum sativum*, cycas, sorghum bicolor, *Azadiracthta indica*, *Cassia auriculata*, Camelliasinensis, Aloevera, Calotropisgigantea, *Nelumbo nucifera*, *Ocimum sanctum* and many more [17-25]. In this manuscript, ZnO nanoparticles were synthesized and stabilized using *Coriandrum sativum* (annual herb) leaf extract by the bioreduction method without using any harmful reducing and capping agent, and also different applications have been reported. Image of *Coriandrum sativum* leaves has shown in Fig. 5.1 *Coriandrum sativum* is a medicinal plant also known as “dhania” belongs to family Apiaceae [26, 27].

Fig. 5.1: Image of *Coriandrum sativum* leaves

5.2. Experimental Methods

5.2.1. Materials

Zinc acetate dihydrate and sodium hydroxide from Fisher Scientific (U.K.) were used in the experiments for the synthesis of zinc oxide nanoparticles. All the chemicals were of analytical reagent grade purity.

5.2.2. Preparation of *Coriandrum sativum* leaf extract

Fresh leaves of *Coriandrum sativum* were washed thoroughly several times with biodegradable and distilled water to remove the dust particles and other unwanted impurities and cut it into fine pieces**.** 30 g of the leaves were mixed with 120 mL of ethanol and heated at 80 °C for 30 minutes. The resulting extract was cooled at room temperature and filtered by Whatman filter paper no.1 [18].

5.2.3. Synthesis of zinc oxide nanoparticles

In a typical synthesis, 100 mL of 0.1 M zinc acetate dihydrate was added first to leaf extract in ratio 1:1 with continuous stirring at room temperature for complete dissolution. Subsequently 20 mL of 1.0 M NaOH solution was slowly added under stirring to increase the pH value and in turn for the precipitation [18]. A progressive change in the color of the solution was observed during the stirring process and the

change from sturdy brown to yellowish white confirms the nanoparticles formation. The obtained precipitate was washed with ethanol to remove the impurity of all the ions produced during the reaction and dried for 4 hours at room temperature. After the calcination of precipitation at 400 °C in the furnace, the yellowish white powder was obtained.

5.2.4. Characterization of zinc oxide nanoparticles

The crystal structure of the synthesized nanoparticles was examined with powder X-ray diffraction (XRD) and the pattern was recorded using X-ray diffractometer (Phillips X Pert model) equipped with CuKα radiation (λ = 0.1542 nm) within the 2θ range of 10°–70°. Morphological characteristics, size and composition of nanoparticles were determined by scanning electron microscopy (SEM) equipped with the X-Ray energy-dispersive spectrometry (EDX). SEM images were captured on an LEO 435 VP instrument operated at 25 kV; EDX was carried out by JEOL JXA-8100 EPMA. To obtain further information as well to verify the size and shape of nanoparticles, transmission electron microscope (TEM- 200 KV, TECNAI G2, S-TWIN, FEI, Holland) was employed. Size distribution of particles was examined by the Zitasizer NanoZS-90. Fourier transform infrared spectroscopy analysis was performed by Broker FTIR alpha model to theorize the functional groups involved in the synthesis. The optical properties of synthesized nanoparticles were deliberated with the help of UV- visible spectroscope (EVOLUTION-201).

5.2.5. Antimicrobial activity of zinc oxide nanoparticles

Herein, Agar well diffusion method was used to assess the antimicrobial activity of synthesized nanoparticles [28, 29]. For this purpose, bacteria *Escherichia coli* were employed as the test organism. In a typical process, 25 mL of nutrient agar was poured into sterile Petri plate. The plates were allowed to solidify and then 100 µL of 24 hrs

culture of *E. coli* was spread on the petri plate. Sterile cork borer was used to make the wells in the plate. Zinc oxide nanoparticles solution was prepared at a concentration of 100, 200, 300 and 400 mg/mL. About 100 µL of prepared solution were loaded in the wells. Thereafter, antimicrobial activity was screened quantitatively by recording the diameter of inhibitor zones plate after incubation for 24 hrs at 30 °C.

5.3. Results and Discussion

In the green synthesis of zinc oxide nanoparticles, biochemical reactions are involved, wherein biological molecules react with the precursor leading to a reduction of metallic ions. *Coriandrum sativum* leaf extract contains minerals and vitamin contents including calcium, phosphorus, iron, sodium and also oxalic acid, 2- decenoic acid, capric acid, tridecanoic acid, undecanoic acid and E-11 tetra decanoic acid in larger amount which are responsible for reduction process [30]. Moreover, characterization of green synthesized ZnO nanoparticles by various techniques unfolds their structural and optical properties.

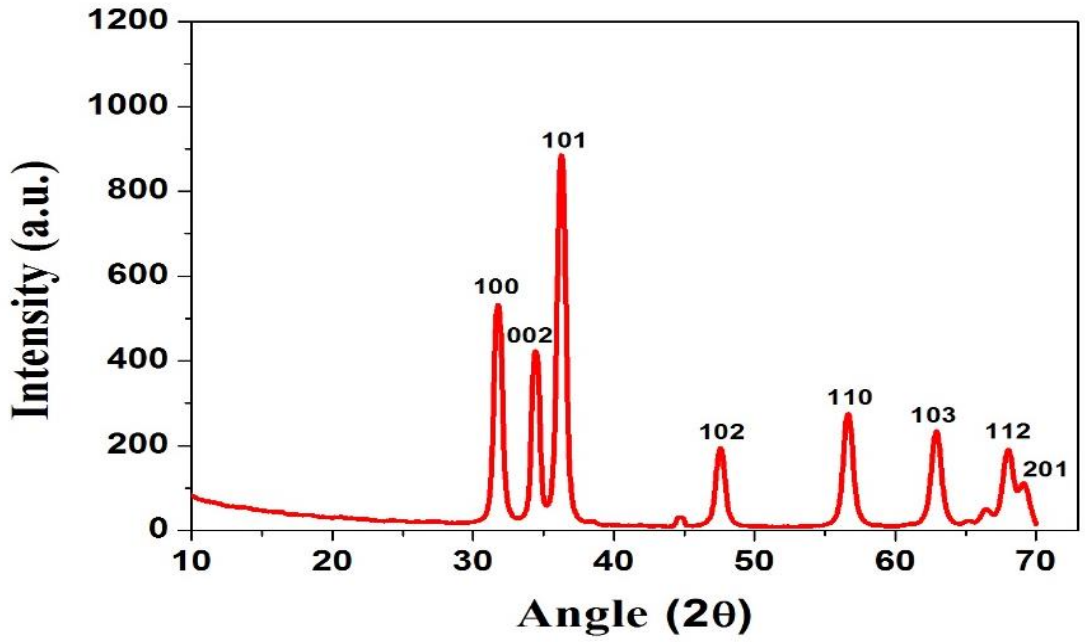

Fig. 5.2: XRD pattern of Zinc Oxide NPs

XRD pattern of synthesized sample is shown in Fig. 5.2. The sharp and narrow

diffraction peaks suggest that synthesized product has the good crystallinity with relatively larger crystallites, and signifies the effects of experimental conditions on the nucleation and growth of the crystal. The XRD patterns shows the noticeable peaks corresponding to 2θ values of 31.64°, 34.43°, 36.29°, 47.75°, 56.51°, 62.90°, 67.98° and 69.23°. The prominent peaks correspond to (hkl) values of (100), (002), (101), (102), (110), (103), (112), (112) and (201). These plane values are closely matched with wurtzite structure of ZnO [31]. Additionally, no characteristic peaks other than the ZnO appears which in turn specify the high purity of our sample. The average crystalline size of nanoparticles was estimated using the Debye-Scherer formula [32], $D = 0.89\ \lambda / \beta\ Cos\theta$, where, λ(1.54 Å) is the wavelength of X-ray, θ being Bragg's diffraction angle and β is the full width at half maximum. The calculated value of crystalline size was found to be 60 nm, which obviously supports the SEM and TEM results.

Typical SEM images of the ZnO nanoparticles are shown in Fig.5.3. SEM images revealed that the particles are well shaped and spherical in the size range 30-150 nm, and there is fairly large number of individual small nanoparticles along with very few agglomerated relatively bigger particles. As depicted in Fig. 5.4, the EDX micrograph of the ZnO reveals the purity of the sample. Both zinc (Zn) and oxygen (O) are present in the sample with weight percentage 90.86% and 9.14% successively; and atomic percentage 70.88% and 29.12% proves that the prepared ZnO is essentially free from impurities.

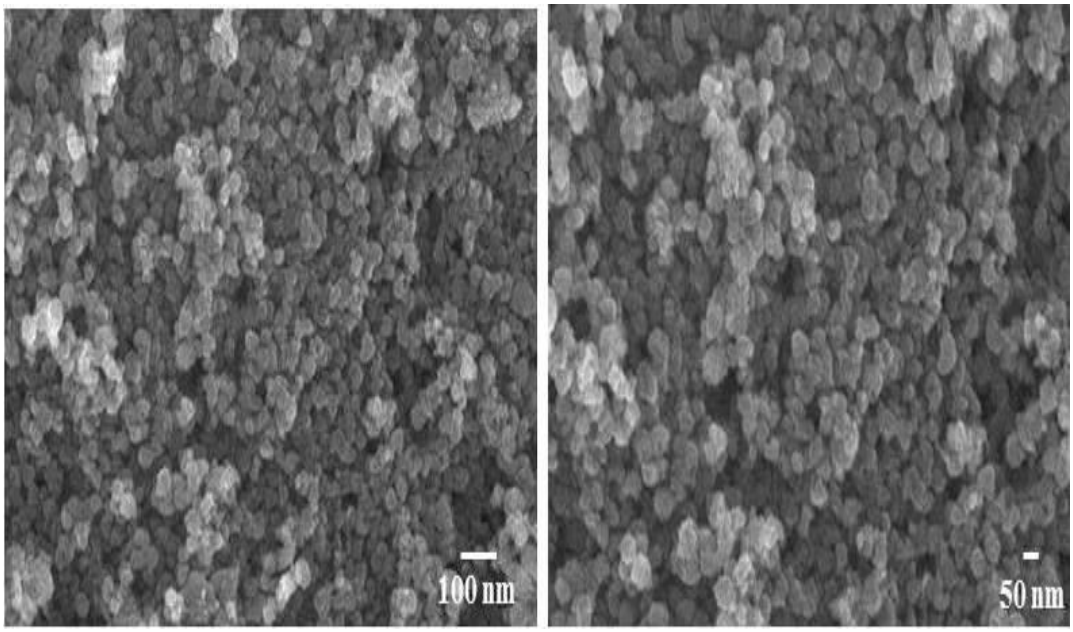

Fig. 5.3: SEM images of ZnO NPs

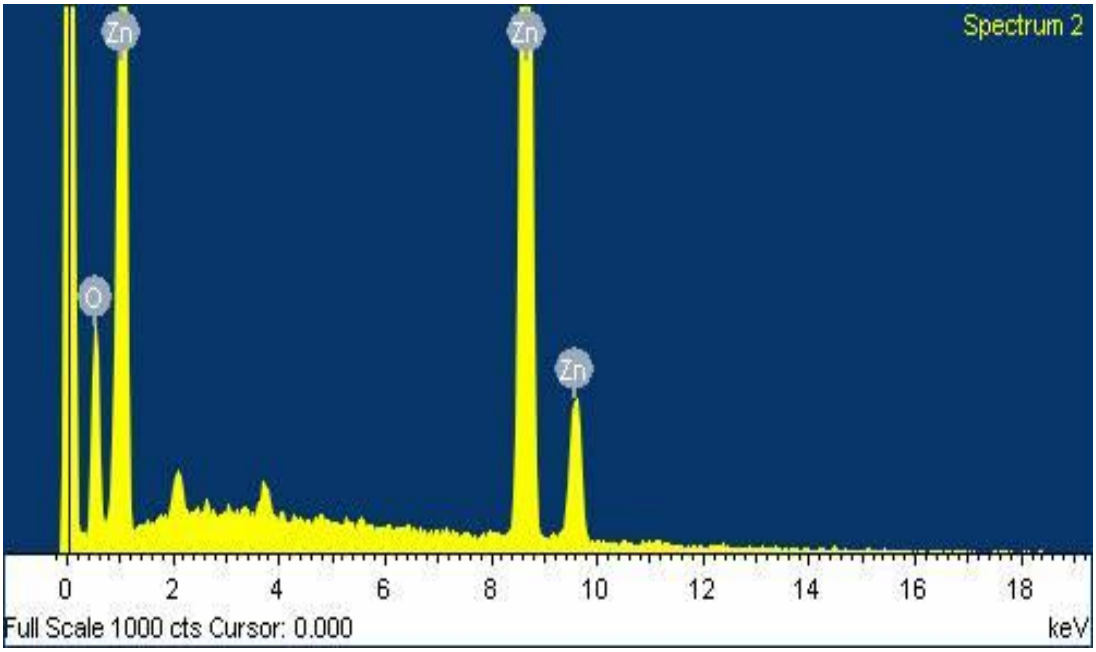

Fig. 5.4: EDX spectra of aqueous extract of coriandrum ZnO NPs revealed by green synthesis method

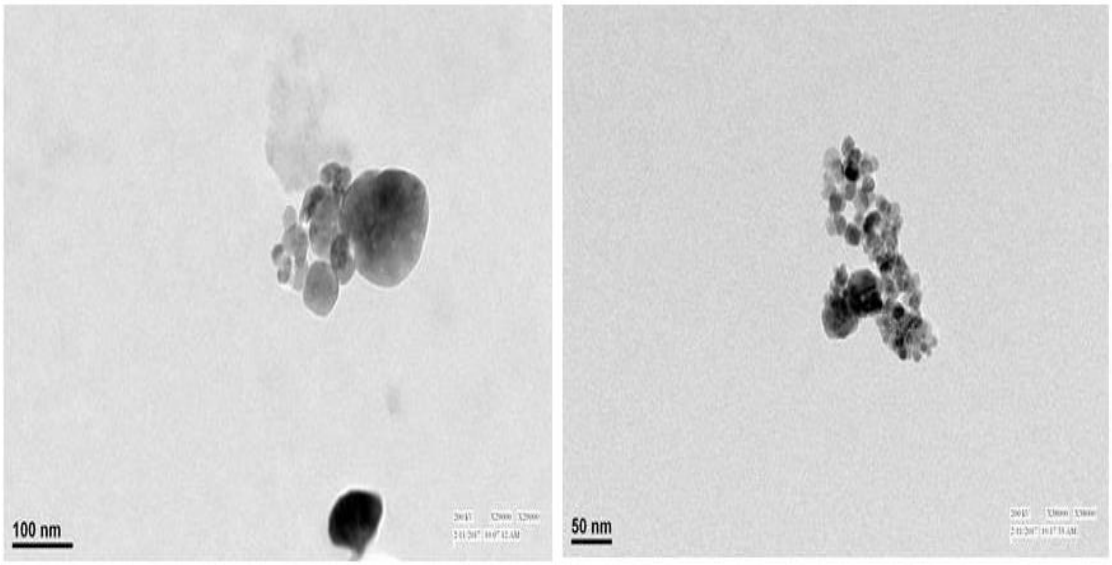

Fig. 5.5: TEM images of synthesized zinc oxide nanoparticles by coriandrum leaf extract

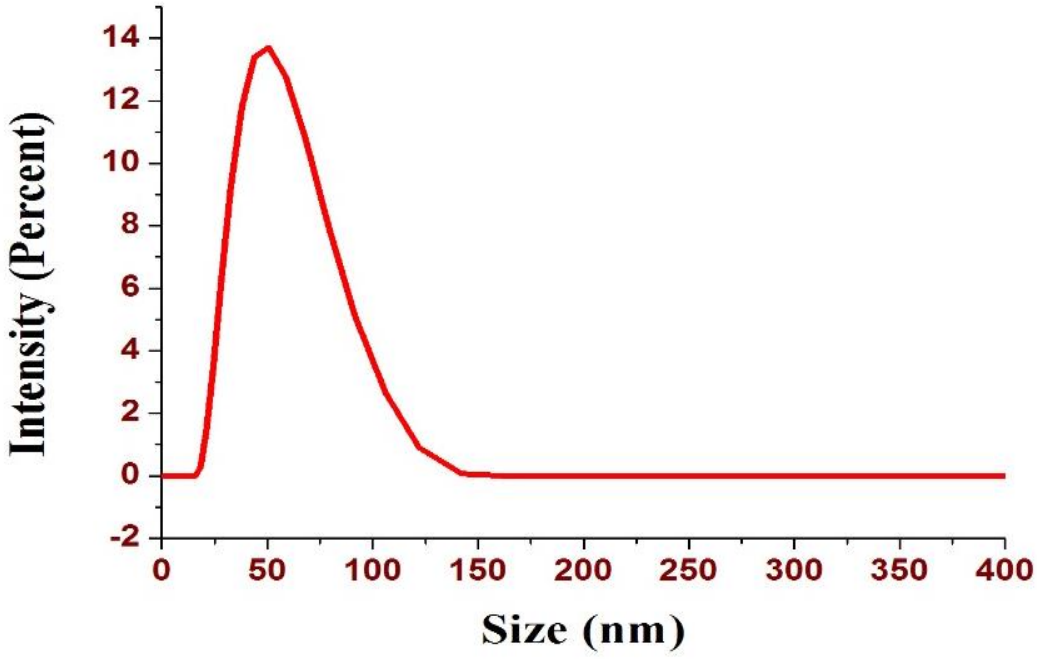

Fig. 5.6: Particle size distribution of synthesized ZnO nanoparticles by coriandrum leaf extract

TEM images are shown in Fig. 5.5 too confirm the nanosize and spherical morphology of zinc oxide prepared, as indicated in SEM images. Average particle size estimated to

40 nm, which nearly matched with the crystalline size of zinc oxide nanoparticles determined from the XRD analysis.

To determine the distribution of particle size in the synthesized sample, we have used dynamic light scattering technique. To ensure this, synthesized ZnO nanoparticles in powder form were fully dissolved in hydrochloric acid for the preparation of representative solution followed by ultrasonication for uniform distribution of nanoparticles. Fig. 5.6 shows the size distribution of the dispersed nanoparticles. The image reveals a maximum intensity at the average particle size of 55 nm, and thereby results suggest that the synthesized ZnO is in nanosize form. Here, the difference in the average particle size obtained by DLS and TEM images may clearly be seen. The slightly larger diameter given by DLS may be attributed to the presence of a few aggregates of nanoparticles.

Fig. 5.7 shows the FTIR spectra of green synthesized ZnO nanoparticles. The spectra were recorded in the series of absorption band 4000 cm^{-1} to 500 cm^{-1}. The band at 3500 cm^{-1} is possibly attributed to the O-H stretching of hydroxyl group, whereas the peak observed at 1630 cm^{-1} identifies the presence of asymmetrical stretching of COO^- (carboxylate) of Zn [33]. The broad peak at 1029 cm^{-1} occurs due to the stretching vibration between C-N bonds of amine [34]. Moreover, absorption band at 548 cm^{-1} identifies the occurrence of ZnO nanoparticles [35]. Thus, it can be observed from the FTIR spectrum that *Coriandrum sativum* leaf extract is significantly rich in different chemical groups such as –OH, –COOH and amine. Further, hydroxyl group probably due to the presence of phenols [36]. The presence of phenols probably indicates the existence of polyphenolic tannins which also prevent aggregation, play an important role in the reduction and stabilization of ZnO nanoparticles. Thus, the physicochemical properties of *Coriandrum sativum* act as a bio template that prevents agglomeration.

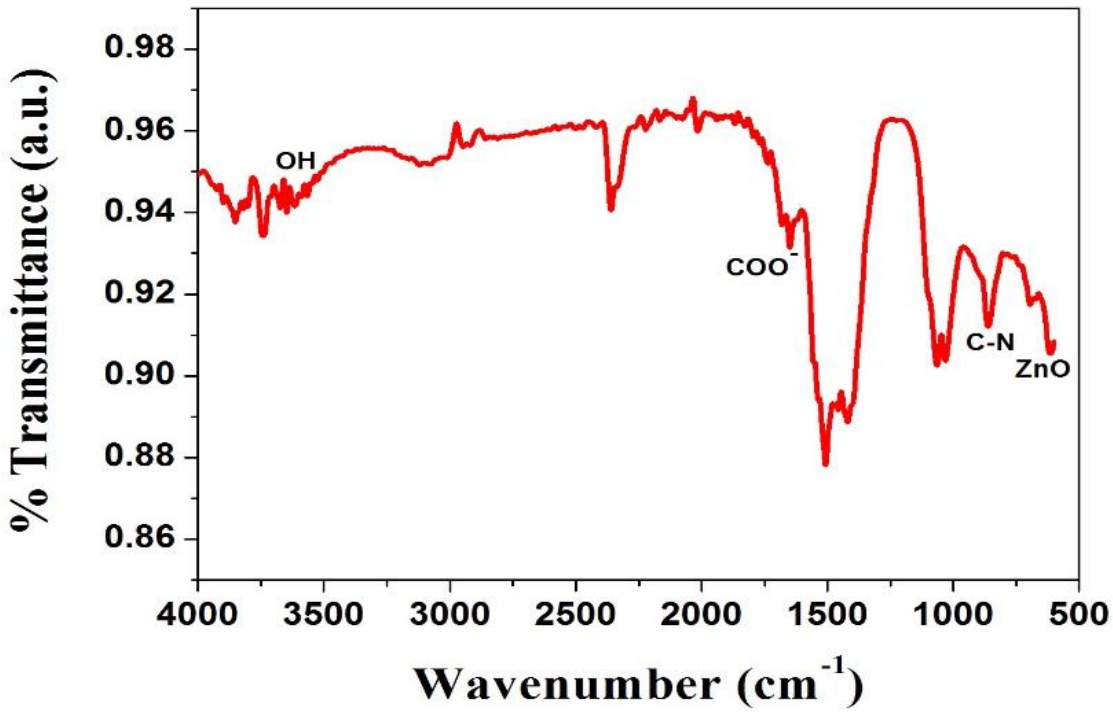

Fig. 5.7: FTIR of ZnO nanoparticles synthesized using coriandrum leaf extract

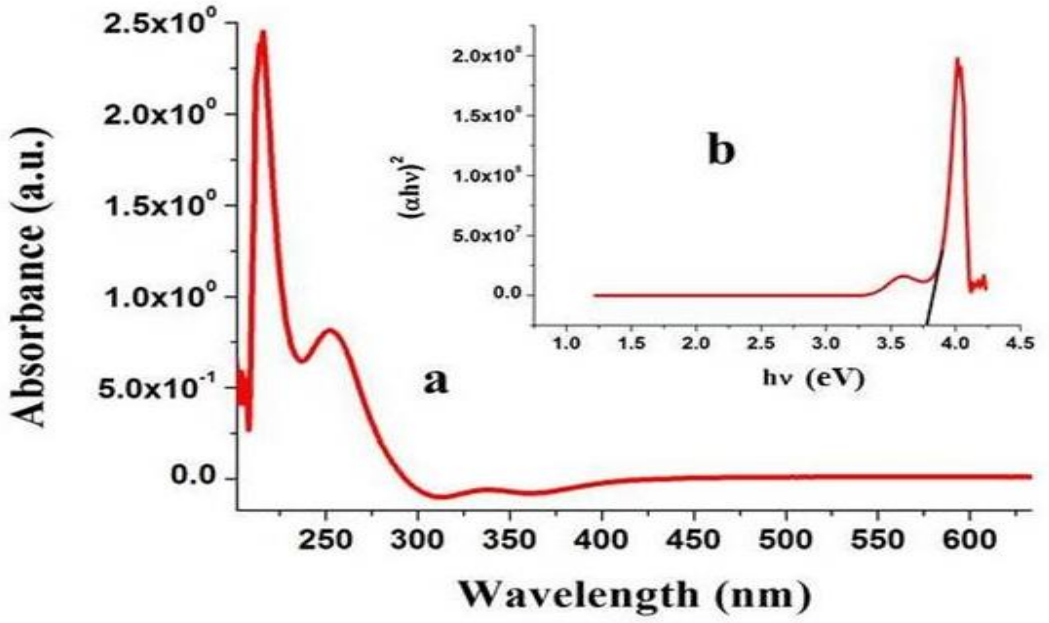

Fig. 5.8: (a) Absorption spectrum of ZnO nanoparticles **(b)** Tauc plot of ZnO

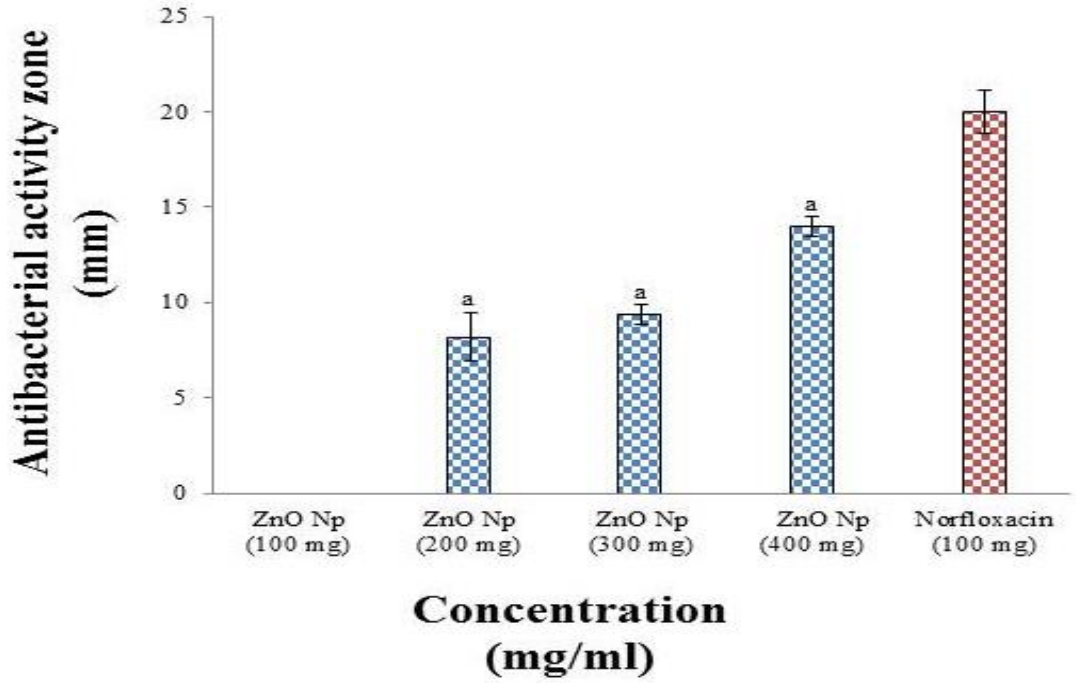

Fig. 5.9: Antibacterial activity (zone of inhibition, mm) of zinc oxide nanoparticle solution against pathogenic Escherichia coli. (ZnO NPs = Zinc oxide nanoparticle; Average value given is mean of three replicates with standard deviation and significant value were predicted by using ANOVA (a $p < 0.01$, b $p < 0.05$) by comparing data of each concentration of ZnO NPs with 100mg Norfloxacin).

Absorption spectra analysis of the synthesized sample was performed to study the optical property and to confirm the presence of ZnO nanoparticles. This spectrum is displayed in Fig. 5.8(a). A perusal of Fig. 8(a) reveals a strong absorption peak at 272 nm within the absorption range 200-650 nm, which further confer ZnO nanoparticles formation [37]. When compared to bulk ZnO (369 nm), the observed blue shift clearly indicate a widening of band gap. Intense and sharp absorption further reveals the individual distribution of the nanoparticles. The band gap energy was determined using Tauc equation $\alpha h\nu = B (h\nu - E_g)^m$ for direct band gap material [38], where, α is the absorption coefficient for direct band gap material, B is constant and

has different values for different transitions. E_g is the energy gap and hv is the photon energy while m denotes an exponent which have values ½, 3/2, 2 and 3 depending on the electronic transition [39]. Tauc plot as shown in Fig. 5.8(b) has the photon energy (hν) on the X-axis and a quantity $(\alpha\ h\nu)^2$ on the Y-axis; and extrapolating the linear portion of the curve to the X-axis yields the energy band gap of the material. The gap was found to be 3.8 eV which is comparable to the values obtained by others [40-43]. Moreover, our calculated value is higher than that of bulk ZnO (3.3 eV), which indicates that the as prepared ZnO nanoparticles to exhibit strong quantum confinement by modifying valence and conduction bands of ZnO semiconductor.

The observed sizes of the inhibition zones are illustrated in Fig. 5.9, which specifies that synthesized zinc oxide nanoparticles exhibit antibacterial activity against *E. coli*. *E. coli*, a gram negative bacterium which produces predominantly extended-spectrum beta-lactamases enzymes which contribute to tolerance or resistance to many antibiotic drugs such as penicillin, cephalosporin and carbapenems etc. [44]. The results of antibacterial activities of our samples were compared with standard antibiotic norfloxacin (100 mg). From the column graph, it is fascinating to note that ZnO nanoparticles exhibited strong toxicity to bacteria except at the concentration 100 mg/mL. With increasing concentration of NPs, zone of inhibition increases and is maximum at the concentration of 400 mg/mL; which shows efficient and comparable antibacterial activity as the norfloxacin. These results are consistent with the literature. Though there are several mechanisms are attributed to the bactericidal activity of ZnO nanoparticles, the exact mechanism is not known and is still under debate. Nevertheless, the possible mechanism for the bactericidal activity, explained as follows, involves the factors including mainly reactive oxygen species (ROS) and the release of Zn ion [45-49]. It has been found in the literature that the activity depends upon crystallite size,

morphology, composition, specific surface and phase of crystalline material [48]. Because of larger surface area than the bulk and distinguishable porosity as the particle size reduces, greater number of reactive oxygen species (ROS), namely O_2^-, hydrogen peroxide (H_2O_2), OH^-, and organic hydroperoxides are generated due to small crystallites, which in turn are considered responsible for the damage of cellular composition such as lipids, phosphorus-containing elements (DNA) and disabling of proteins by oxidative stress [50, 51]. It should be noted that oxidative stress results when reactive oxygen species production surpasses the capability of antioxidant defence of the cell [51].

Moreover, it is written somewhere [52] that the ZnO nanoparticles have positive zeta potential. Owing to this, nanoparticles provide enhanced particle surface reactivity and adherence with the microbial pathogens; and so surface properties also affect the interactions with the cell walls of the bacteria by allowing easy penetration into the bacteria. The exposure of nanoparticles to the surface of bacteria or accumulation of nanoparticles in the cell or even in the cytoplasm inhibit several functions in the cell thereby inducing structural abnormalities such as distraction of cellular function or deformation or rupture or blebs in membranes, leading eventually to death of bacterial cells [53, 54]. It is therefore evident from the above analysis that the interplay between the membrane biology of the pathogen and chemical and physical properties of medium appears to be a most important aspect of bactericidal properties.

5.4. Conclusions

In summary, synthesized zinc oxide nanoparticles by *Coriundrum sativum* have significant shape and size, which were confirmed by SEM, XRD and TEM techniques, also with greatly reduced toxicity than the chemical and physical synthesis methods. FTIR and EDS showed the chemical contents and purity of the sample. TEM results

demonstrate the presence of spherical nanoparticles of average particle size 40 nm, whereas dynamic light scattering examination shows average particle size of 55 nm. Green synthesized ZnO NPs exhibit useful and potent antibacterial activity against the test bacteria *E. coli*. The interplay between the membrane biology of the pathogen and chemical and physical properties of medium appears to be most important aspect of bactericidal properties. Conclusively, green method provides progression over chemical and physical method and synthesized material by this approach will not be used only in engineering field but also in drug delivery advantageously.

References

[1] T. Bora, J. Dutta, Applications of nanotechnology in wastewater treatment-a review, Nanosci. Nanotechnol. 14 (2014) 613-626.

[2] Z. Fan, X. Huang, C. Tan, Thin metal nanostructures: synthesis, properties and applications, Chem. Sci. 6 (2015) 95-11.

[3] S. Ansilin, J. Kavya Nair, C. Aswathy, V. Rama, J. Peter, J. Jeyachynthaya Persis, Green synthesis and characterisation of copper oxide nanoparticles using Azadirachta indica (neem) leaf aqueous extract, J. Nanosci. Tech. 2 (2016) 221-223.

[4] Z. Fan, G.L. Jia, Zinc oxide nanostructures: synthesis and properties, J. Nanosci. Nanotech. 5 (2005) 1561-1573.

[5] M. Singhal, V. Chhabra, P. Kang, D.O. Shah, Synthesis of ZnO nanoparticles for varistor application using Zn-substituted aerosol OT microemulsion, Mat. Res. Bull. 32 (1997) 239-247.

[6] C.W. Bunn, The lattice-dimensions of zinc oxide, Proc. Phy. Soc. Lon. 47 (1935) 835-842.

[7] X.L. Cheng, H. Zhao, L.H. Huo, S. Gao, J.G. Zhao, ZnO nano particulate thin film: preparation, characterization and gas-sensing properties, Sens. Acutat. B Chem. 102 (2004) 248-252.

[8] S. Barua, S.K. Pal, J. Dutta, Nanostructured zinc oxide for water treatment, Nanosci. Nanotech. Asia 2 (2012) 290-102.

[9] D.K. Tiwari, J. Behari, P. Sen, Application of nanoparticles in waste water treatment, World App. Sci. J. 3 (2008) 417-433.

[10] M. Singh, S. Manikandan, A.K. Kumaraguru, Nanoparticles: A new technology with wide applications, Res. J. Nanosci. Nanotech. 1 (2011) 1-11.

[11] S. Ahmed, M. Ahmad, S. Ikram, A review on plants extract mediated synthesis of silver nanoparticles for antimicrobial applications: a green expertise, J. Adv. Res. 7 (2016) 17-28.

[12] K.S. Kavitha, S. Baker, D. Rakshith, H.U. Kavitha, H.C.Y. Rao, B. P. Harini, S. Satish, Plants as green source towards synthesis of nanoparticles, Int. Res. J. Bio. Sci. 2 (2013) 66-76.

[13] S. Roy, T.K. Das, Plant mediated green synthesis of silver nanoparticles-A review, Int. J. Plant Bio. Res. 3 (2015) 1-10.

[14] N. Jain, A. Bhargava, S. Majumdar, J. Panwar, Extracellular biosynthesis and characterization of silver nanoparticles using Aspergillus flavus, Nanoscale 3 (2011) 635-641.

[15] S. Iravani, B. Zolfaghari, Green Synthesis of silver nanoparticles using pinuseldarica bark extract, Bio. Res. Int. 2013 (2013) 1-5.

[16] B.S. Kim, J.Y. Song, Biological synthesis of gold and silver nanoparticles using plant leaf extracts and antimicrobial applications, in biocatalysis and biomolecular engineering, John Wiley & Sons, New York, (2010).

[17] M. Dubey, S. Bhadauria, B.S. Kushwah, Green synthesis of nano silver particles from extract of Eucalyptus hybrida (Safeda) leaf, Dig. J. Nanomat. Biostruc. 4 (2009) 537-543.

[18] R. Sathyavathi, M.B. Krishna, S.V. Rao, R. Saritha, D.N. Rao, Silver has the advantage of having broad antimicrobial biosynthesis of silver nanoparticles using Coriandrum sativum leaf extract activities against gram-negative and gram-positive bacteria and their application in nonlinear optics, Adv. Sci. Lett. 3 (2010) 1-6.

[19] A.K. Jha, K. Prasad, Green synthesis of silver nanoparticles using resistance, the antimicrobial activity of silver nanoparticles cycas leaf, Int. J. Green Nanotech. Phy.

Chem. 1 (2010) 110-117.

[20] R.A. Leela, K.A.M. Vivekanandan, Tapping the unexploited plant resources for the synthesis of silver against other bacterial species, Afri. J. Biotech. 7 (2008) 3162-3165.

[21] S.S. Shankar, A. Rai, A. Ahmad, M. Sastry, Rapid synthesis of Au, Ag, and bimetallic Au core-Ag shell nanoparticles using Neem (Azadirachta indica) leaf broth, J. Coll. Inter. Sci. 275 (2004) 496–502.

[22] P. Ramesh, A. Rajendran, M. Meenakshi Sundaram, Green synthesis of zinc oxide nanoparticles using flower extract Cassia auriculata, J. Nanosci. Nanotech. 2 (2014) 41-45.

[23] G. Sangeetha, S. Rajeshwari, R. Venckatesh, Green synthesis of zinc oxide nanoparticles by aloe barbadensis miller leaf extract: structure and optical properties, Prog. Nat. Sci. Mat. Int. 22 (2011) 693-700.

[24] C. Vidya, S. Hiremath, M.N. Chandraprabh, M.A.L. Antonyraj, I. Venugopal, A. Jain, K. Bansal, Green synthesis of ZnO nanoparticles by Calotropis gigantea, Int. J. Curr. Eng. Tech. 23 (2013) 118-120.

[25] D. Gnana Sangeetha, D.S. Thambavani, One pot synthesis of zinc oxide nanoparticles via chemical and green method, Res. J. Mat. Sci. 1 (2013) 1-8.

[26] A. Verma, S.N. Pandeya, S.K. Yadav, S. Singh, P. Soni, A review on Coriandrum sativum: an ayurvedic medicinal herb of happiness, J. Phar. Bioall. Sci. 1 (2011) 28- 48.

[27] S. Ramezani, M. Rahmanian, R. Jahanbin, F. Mohajeri, M.R. Rezaei, B. Solaimani, Diurnal changes essential oil content of coriander (Coriundrum sativum L.) aerial parts from Iran, Res. J. Bio. Sci. 4 (2009) 277-281.

[28] A. Smania, F.D. Monache, E.D.F.A. Smania, R.S. Cuneo, Antibacterial activity of

steroidal compounds isolated from *Ganoderma applanatum* (Pers.) Pat (*Aphyllophoro mycetideae*) fruit body, Int. J Med Mushrooms 1 (1999) 325-330.

[29] A.J. Das, R. Kumar, S.P. Goutam, S.S. Sagar, Sunlight irradiation induced synthesis of silver nanoparticles using glycolipid biosurfactant and exploring the antibacterial activity, J. Bioeng. Biomed. Sci. 6 (2016) 1-5.

[30] M.N.I. Bhuiyan, J. Begum, M. Sultana, Chemical composition of leaf and seed essential oil of *Coriandrum sativum* L, Bang. J. Pharma. 4 (2009) 150-153.

[31] JCPDS Card No. 36-1451.

[32] J.S.J. Hargreaves, Some considerations related to the use of the Scherrer equation in powder X-ray diffraction as applied to heterogeneous catalysts, Cata. Struc. React. 2 (2016) 33-37.

[33] Z. Tao, X. Yu, J. Liu, L. Yang, S. Yang, A facile synthesis and photoluminescence of porous S doped ZnO architectures, J. Alloys Comp. 459 (2008) 395-398.

[34] G. Xiong, U. Pal, J.G. Serrano, K.B. Ucer, R.T. Williams, Photoluminescence and FTIR study of ZnO nanoparticles: the impurity and defect perspective, Physica. Status Sol. 3 (2006) 3577-3581.

[35] P. Ramesh, A. Rajendran, A. Subramanian, Synthesis of zinc oxide nanoparticle from fruit of *Citrus aurantifolia* by chemical and green method, Asian J. Phytomed. Clin. Res. 22 (2014) 189-195.

[36] K.M. Kumar, B.K. Mandal, K.S. Kumar, P.S .Reddy, B. Sreedhar, Biobased green method to synthesize palladium and iron nanoparticles using *Terminalia chebula* aqueous extract, Spectrochim. Acta A: Mol. Biomol. Spect. 102 (2013) 128-33.

[37] Y.H. Ni, X.W. Wei, J.M. Hong, Y. Ye, Hydrothermal preparation and optical properties of ZnO nanorods, Mater. Sci. Eng. B. 121 (2005) 42-47.

[38] J.C. Tauc, Optical properties of solids, Elsevier, Amsterdam, North Holland, 1972.

[39] R. Bhatt, I. Bhaumik, S. Ganesamoorthy, A.K. Karnal, M.K. Swami, H.S. Patel, P.K. Gupta, Urbach tail and band gap analysis in near stoichiometric $LiNbO_3$ crystals, Physica Status Solidi A. 209 (2012) 176-180.

[40] S. Talam, S.R. Karumuri, N. Gunnam, Synthesis, characterization, and spectroscopic properties of ZnO nanoparticles, Int. Scholar. Res. Notice. 2012 (2012) 1-5.

[41] M.S. Samuel, L. Bose, K.C. George, Optical properties of ZnO nanoparticles, SB Academic Rev. 16 (2009) 57-65.

[42] F.K. Shan, G.X. Liu, W.J. Lee, B.C. Shin, Stokes shift, blue shift and red shift of ZnO-based thin films deposited by pulsed-laser deposition, J. Cryst. Growth. 291 (2006) 328-333.

[43] R. Rusdi, A.A. Rahman, N.S. Mohamed, N. Kamarudin, N. Kamarulzaman, Preparation and band gap energies of ZnO nanotubes, nanorods and spherical nanostructures, Powder Technol. 210 (2011)18-22.

[44] S. Shaikh, J. Fatima, S. Shakil, S.M.D. Rizvi, M.A. Kamal, Antibiotic resistance and extended spectrum beta-lactamases: Types, epidemiology and treatment, Saudi J. Bio. Sci. 22 (2015) 90-101.

[45] T. Xia, M. Kovochich, M. Liong, L.M. Adler, B. Gilbert, H. Shi, JI. Yeh, J.I. Zink, A.E. Nel, Comparison of the mechanism of toxicity of zinc oxide and cerium oxide nanoparticles based on dissolution and oxidative stress properties, ACS Nano. 2 (2008) 2121-2134.

[46] J. Sawai, S. Shoji, H. Igarashi, A. Hashimoto, T. Kokugan, M. Shimizu, H. Kojima, Hydrogen peroxide as an antibacterial factor in zinc oxide powder slurry, J. Ferm. Bioeng. 86 (1998) 521-522.

[47] H. Yang, C. Liu, D. Yang, H. Zhang, Z.J. Xi, Comparative study of cytotoxicity,

oxidative stress and genotoxicity induced by four typical nanomaterials: the role of particle size, shape and composition, J. App. Toxico. 29 (2009) 69-78.

[48] V. Berry, A. Gole, S. Kundu, C.J. Murphy, R.F. Saraf, Deposition of CTAB-terminated nanorods on bacteria to form highly conducting hybrid systems, Am. Chem. Soc. 127 (2005) 17600-17601.

[49] A. Sirelkhatim, S. Mahmud, A. Seeni, N.H.M. Kaus, L.C. Ann, S.K.M. Bakhori, H. Hasan, D. Mohamad, Review on zinc oxide nanoparticles: antibacterial activity and toxicity mechanism, Nano-Micro Lett. 7 (2015) 219-242.

[50] X. Bai, L. Li, H. Liu, L. Tan, T. Liu, X. Meng, Solvothermal synthesis of ZnO nanoparticles and anti-infection application in vivo, ACS Appl. Mater. Interf. 7 (2015) 1308-1317.

[51] G. Storz, J.A. Imlay, Oxidative stress, Curr. Opin. Microbiol. 2 (1999) 188-194.

[52] M. Arakha, M. Saleem, B.C. Mallick, S. Jha, The effects of interfacial potential on antimicrobial propensity of ZnO nanoparticle, Sci. Rep. 5 (2015) 1-10.

[53] L. Zhang, Y. Jiang, Y. Ding, M. Povey, D.J. York, Investigation into the antibacterial behaviour of suspensions of ZnO nanoparticles (ZnO nanofluids), Nanopart. Res. 9 (2007) 479-489.

[54] P.K. Stoimenov, R.L. Klinger, G.L. Marchin, K.J. Klabunde, Metal oxide nanoparticles as bactericidal agents, Langmuir. 18 (2002) 6679-6686.

Chapter: 6

Synthesis of Nanosized Iron Oxide by Leaf Extract of Coriandrum Sativum and its Antimicrobial Properties

6.1. Introduction

In recent decades, nanomaterials have extensive effect in areas of physics, chemical science, electronics, optics, materials science, biomedical science and many more [1, 2]. The upsurge in infectious diseases and indiscriminate use of antimicrobial drugs around the globe has lead to the emergence of different types of multi-drug resistant bacterial strains to traditional antibiotics, which in turn has become a serious concern for the public health [3-6]. Consequently, for obvious trepidations, it has become vital to explore new and promising antibacterial agents with synergistic properties to abate the actions of such pathogens. Nanoscale metal oxide materials offer unique advantages over other types of materials and their sizes make them ideal candidates for the tailoring of surface properties, production of functional nanostructures and devising novel applications. Among metal oxide nanoparticles, iron oxide has earned a great deal of attention of scientific community due to their multivalent oxidation forms as wustite (FeO), magnetite (Fe_3O_4), maghemite (γ-Fe_2O_3) and hematite (α-Fe_2O_3) in the atmosphere [7]. They have various potential applications in spintronics, agricultural, magnetic refrigeration, gas sensing, ferrofluids, catalysts [8, 9] and in many biomedical applications such as tissue repair, targeted drug delivery, hyperthermia, cellular therapy and magnetic resonance imaging owing to their multifunctional properties [10-12].

Furthermore, NPs also play a crucial role in environmental remediation cycles and remove organic and inorganic pollutants from polluted water and wastewater such as

heavy metals lead, chromium, arsenic and organic dyes, methylene blue and methyl orange- mostly contributed by large-scale urbanization, fertilizers and industrialization [13]. Higher surface area of iron oxide at nano range increases their surface energy, effectiveness, catalytic reactivity and other properties.

A variety of methods with varying degree of success have been reported for the synthesis of iron oxide nanoparticles [14]. In these reported methods, some are very popular in spite of their expense and harmful starting materials, high energy requirements or specialized equipment. To evade these inadequacies of conventional methods, we have focused on sustainable alternative technique using a green, safe, cost-effective and eco-friendly method based on biological systems namely, plant. Nanoparticles synthesis using plant extracts is often termed as green synthesis. Remarkably, in biosynthesis, metal ions are reduced into their nanoparticles by the broad range of biomolecules (alkaloids, flavonoids, phenols, tannins, quinines, terpenoids etc.) [15]. Functional groups present in plant metabolites which provides effective metal-reducing agents for a potent coating on the metal nanoparticles in a single step [16]. In addition, they are generating much interest as a capping/stabilizing agent.

Considering the vast potentiality of plants as sources, we have used leaf extract of *Coriandrum sativum* for bioconversion of iron ions to nanoparticles. Coriander is a medicinal plant, also known as cilantro, is commonly available in India. It has therapeutic properties like aphrodisiac, carminative, depurative, digestive, analgesi fungicidal, revitalizing, antispasmodic, stomachic and stimulant [17-19]. In a recent study, it has been shown that essential oil in coriander inhibits gram-positive bacteria *E. coli*, *Staphylococcus aureus*, *Pseudomonas aeruginosa and Enterococcus faecalis* [20]. Though, the preparation of iron oxide nanoparticles using plant extracts has

already been mentioned in the literature [21, 22], to the best of our knowledge, none has reported *Coriandrum sativum* mediated synthesis of iron oxide nanoparticles. The present investigation, therefore, is aimed to synthesize iron oxide nanoparticles from *Coriandrum sativum* leaves extract and extensive characterization of these NPs by using standard spectroscopic techniques, and to evaluate its antibacterial activity against a bacterium *E. coli.*

6.2. Materials and Methods

6.2.1. Materials and chemicals used

For the synthesis of iron oxide nanoparticles, ferric chloride (analytical grade, purity ≥96%) purchased from Thermo Fisher Scientific, India was used as the starting material. Sodium hydroxide pellets (NaOH) used for the precipitation of iron oxide NPs and were purchased from Thermo Fisher Scientific, India. Double distilled (DD) water was used in the whole experiment. All the chemicals were of analytical grade and were used without further purification.

6.2.2. Green synthesis of iron oxide nanoparticles

The scheme of the green synthesis of iron oxide nanoparticles by leaves of *Coriandrum sativum* has been presented in Fig.6.1 Initially, 30 gm. fresh and healthy leaves of *Coriandrum sativum* were washed thoroughly twice/thrice with DD water and cut it into fine pieces**.** Washed leaves of *Coriandrum sativum* were transported in 100 ml of DD water in an Erlenmeyer flask and heated at 80^0C for 50 minutes. The resulting leaf extract was filtered with Whatman filter paper no.1 to get a clear solution. Further, leaf extract and 0.2 M ferric chloride ($FeCl_3$) solution were mixed in the volume ratio 1:1. The color change of the solution from pale yellow to light brown took place at room temperature within 20 minutes after the mixing the precursor and leaf extract solution due to the reduction of metallic ions, which showed the green synthesis of iron

oxide NPs. To attain the precipitates of NPs, 20 ml of 2M NaOH solution was added to the precursor and leaf extract solution drop-wise under continuous stirring at room temperature. Then, the obtained precipitate of iron oxide NPs was separated out from the solution through filtration, followed by washing with ethyl alcohol to remove the ionic impurities. Subsequently, the washed precipitate was air dried and annealed at 450 °C for 2 h in a muffle furnace, and then finely ground in a crystal mortar pestle to get the iron oxide NPs in powder form [13].

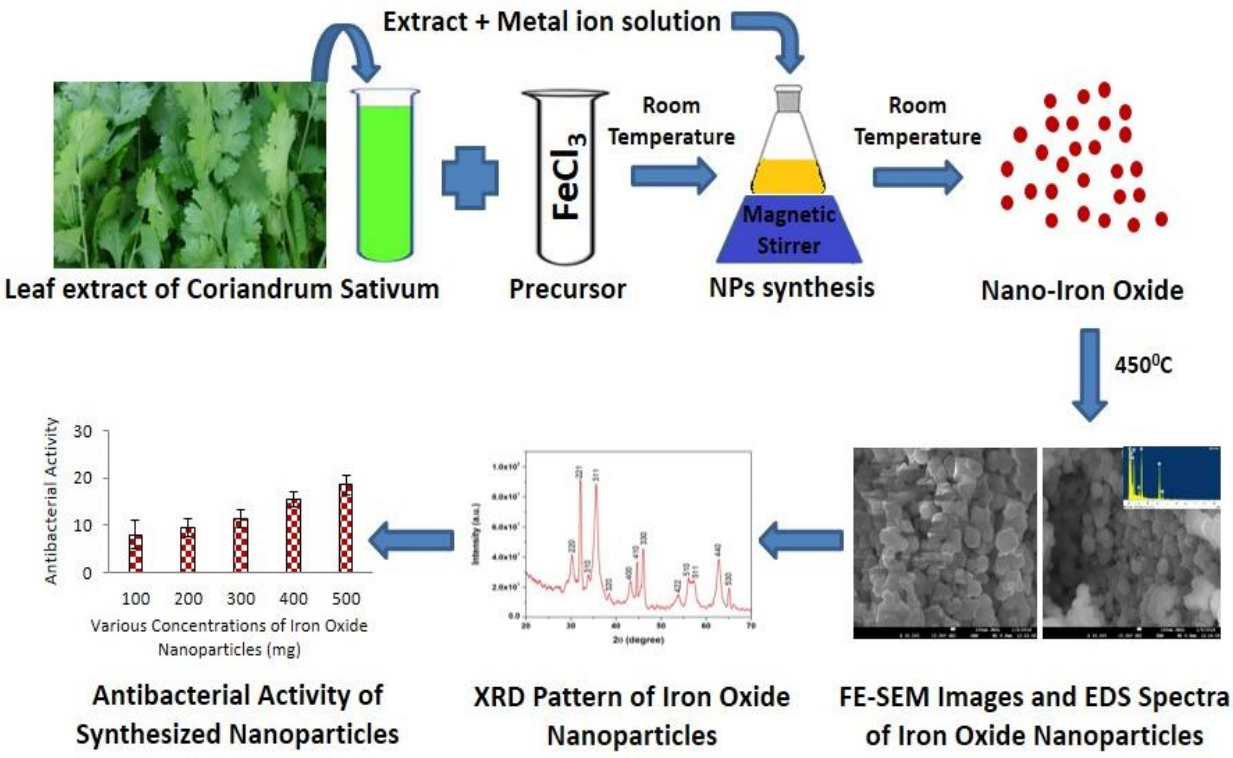

Fig. 6.1: Diagram for the green synthesis of iron oxide NPs using Coriandrum sativum leaf extract

The mechanism of the iron oxide NPs formation from the leaf extract involves reduction of metallic ions due to functional groups present in the leaf extract. The compounds present in Coriandrum sativum leaf with considerable amount are mainly 2-decenoic acid, tridecenoic acid, E-11 tetradecenoic acid, capric acid, undecenoic acid [23], which act as capping/reducing agent for the generation of iron oxide NPs.

6.2.3. Antibacterial activity of iron oxide nanoparticles

The antibacterial activity of synthesized NPs was determined by the agar well diffusion method [24, 25]. Briefly, in this method, nutrient agar was poured into sterile Petri plate and allowed to solidify 100 μL of 24 hrs. *Escherichia coli* culture was spread on the Petri plate. Thereafter, wells were made using a sterile cork borer. Various concentration of iron oxide nanoparticles solution (100, 200, 300,400 and 500 mg/mL) were loaded into each well. Afterward, antibacterial activity zone was measured after 24 hrs.

6.3. Characterization

For the identification of phase and crystallinity of the product, XRD pattern was recorded using X-ray diffractometer (Phillips X Pert model) equipped with Cu K_α radiation (λ = 0.1542 nm) within the 2θ range of 20°–70°. The morphology and size of the green synthesized iron oxide NPs were determined by Field Emission Scanning Electron Microscopy (FESEM) (JSM-7610F, JEOL, Japan). The composition of the green synthesized Iron oxide NPs was determined by X-ray Energy-Dispersive Spectrometer (EDX) (Oxford, INCAx-act, Japan). Fourier Transform-Infrared (FTIR) spectrometer (Model Nicolet 6700, Thermo Fisher Scientific, USA) was used to characterize the functional groups present in the synthesized iron oxide nanoparticles. The band gap energy of synthesized nanoparticles was measured with the help of UV-visible spectroscopy (EVOLUTION-201).

6.4. Results and Discussion

XRD pattern obtained for synthesized iron oxide nanoparticles sample is shown in Fig.2 (a). It is evident from the XRD pattern that the major diffraction peaks exist at 2θ values of 30.24^0, 32.11^0, 33.81^0, 35.61^0, 38.50^0, 43.24^0, 44.76,46.07^0, 53.84^0, 56.08^0 and 57.29^0, 62.78^0 and 65.12^0 which correspond to Fe_2O_3 nanoparticles

associated with the planes (220), (221), (310), (311), (320), (400), (410), (330), (422), (510), (511), (440) and (530) respectively, which is found to be in good agreement with JCPDS card no. 39-1346, as shown in Fig.6.2 [28]. All planes were evaluated corresponding to 2θ values by peak indexing from interplanar spacing [29]. The crystallite size was estimated using Debye-Scherrer's formula [30].

$$D = k\lambda / \beta Cos\theta \qquad (1)$$

Where λ is the wavelength of X-ray (Cu K_α is 1.542 Å), θ is the Bragg diffraction angle, k is shape factor and β is the full width at half maximum (FWHM). Using the Scherrer formula, the calculated average crystallite size of the synthesized product was found to be 80 nm.

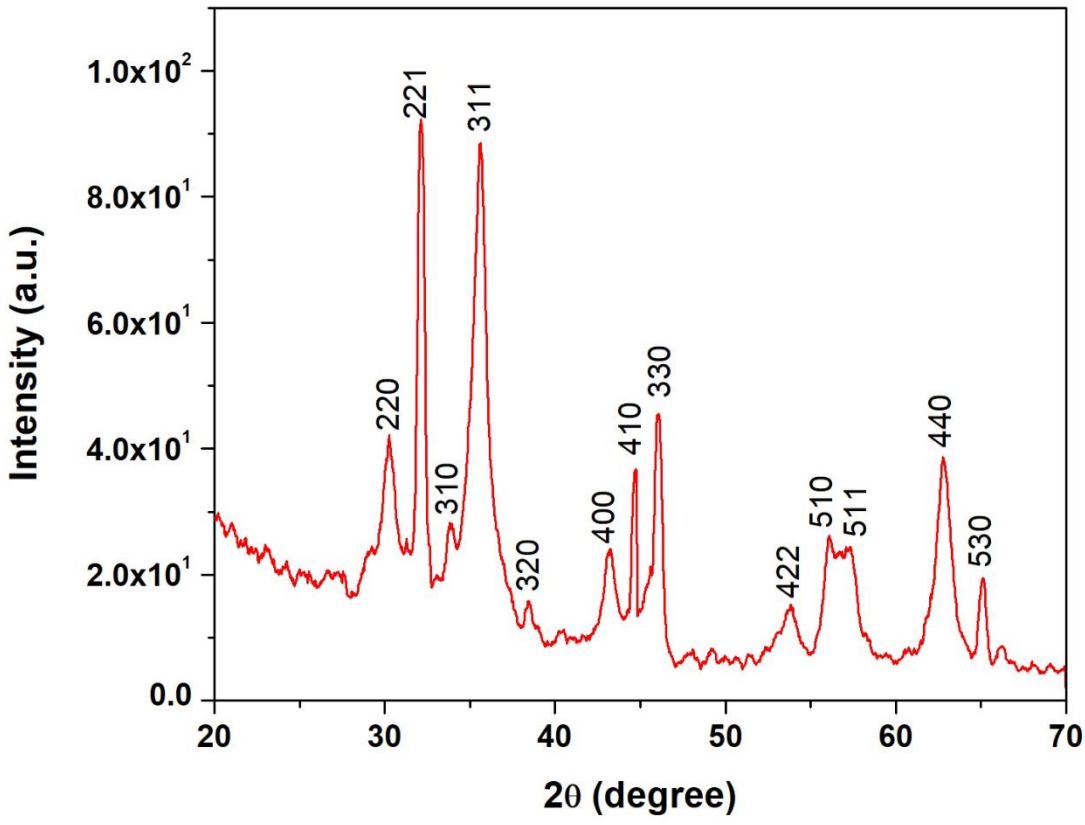

Fig. 6.2: XRD pattern of iron oxide nanoparticles

The FE-SEM analysis was performed to determine the morphology of the synthesized iron oxide nanoparticles and is shown in Fig.6.3.These images

demonstrated the successful synthesis of spherically shaped iron oxide NPs with a diameter ranging from 10-150 nm. A large number of small iron oxide NPs were observed along with fewer somewhat large sized agglomerated NPs [13**]**. The agglomeration of iron oxide NPs might be due to the low pH of the solution as well as due to the interaction among magnetic nanoparticles [32].

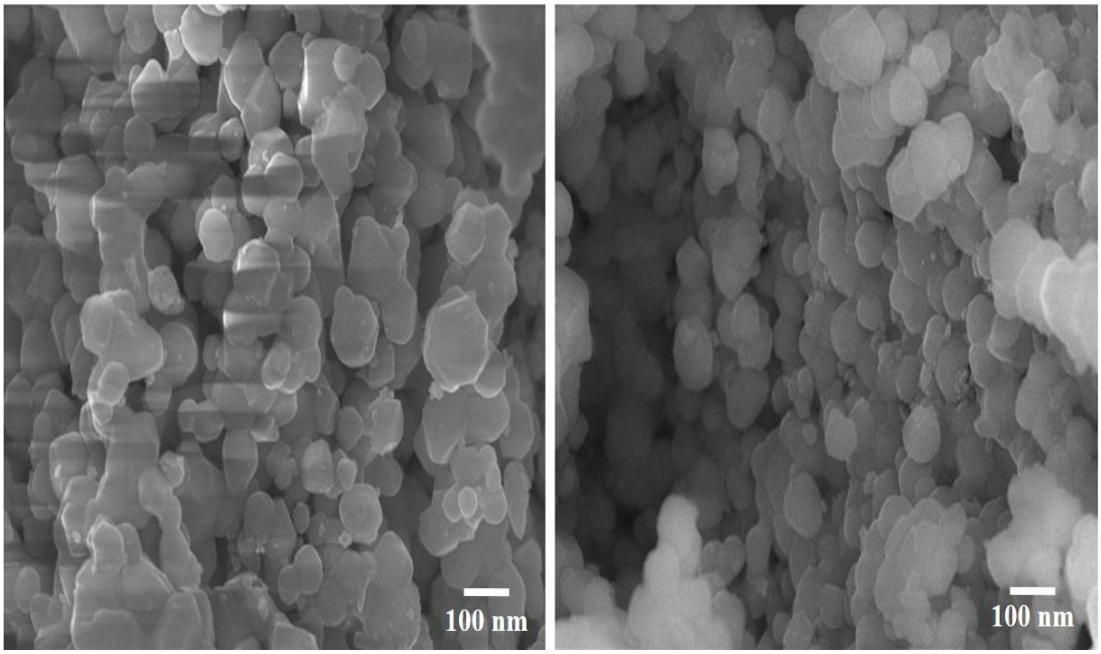

Fig. 6.3: FE-SEM images of green synthesized iron oxide nanoparticles

The chemical compositions of the synthesized sample were examined by X-ray Energy Dispersive (EDS) spectra and are displayed in Fig.6.4. The spectra reveal the composition of the sample and endorse the presence of iron (Fe) and Oxygen (O) in the sample. The EDS spectrum as shown in Fig.6.6, revealed the purity of sample as both Iron (Fe) and oxygen (O) are present in the sample.

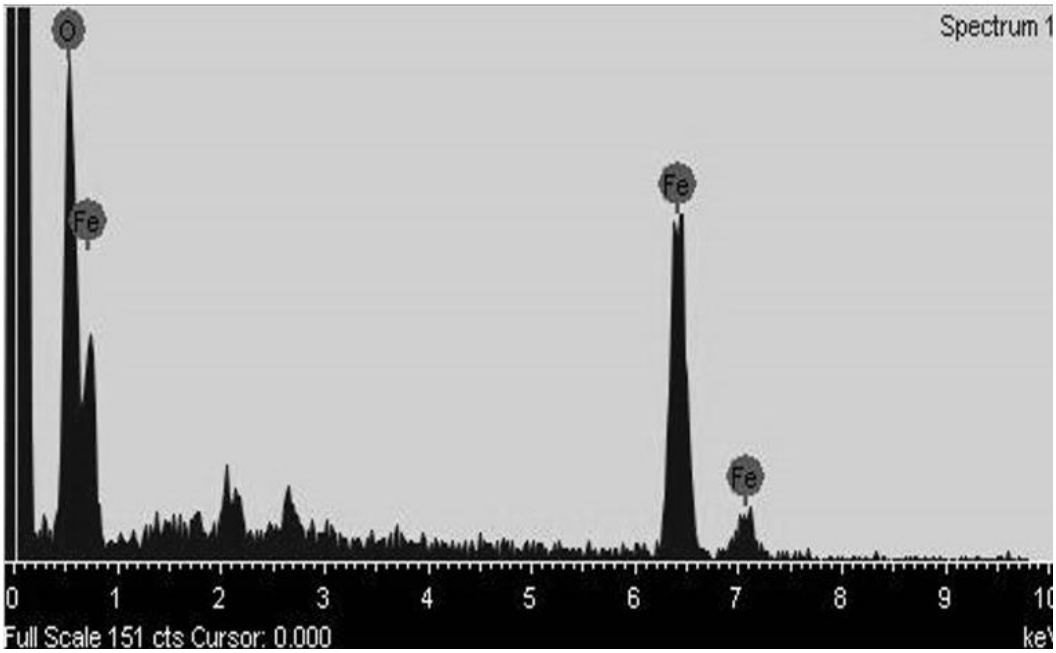

Fig. 6.4: EDS spectra of powder of green synthesized iron oxide nanoparticles

The FTIR spectra of the sample (Fig.6.5) were recorded to identify the functional groups present in the plant extract, which are accountable for the synthesis of nanoparticles. The spectrum exhibits peaks in the range 4000-500 cm^{-1}. The band observed at 2929 cm^{-1} shows stretching in the C-H bonding [34]. The appearance of the strong band at 1650 cm^{-1} demonstrates the existence of carbonyl group (C=O) [35, 36]. It is noteworthy that carbonyl group has a significant role in the reduction of ferric chloride ions. In addition, the peak at 2260-2300 cm^{-1} implies the presence of alkyne group (C≡C) in the sample. In addition, the broad peak at 1030 cm^{-1} is related to aliphatic C-N stretching. Absorption peak around 860 cm^{-1} is attributed to twisting of NH_2 group. Further, the peak at 630 cm^{-1} is due to the characteristic vibration of Fe-O bonds of γ -Fe2O3 nanoparticles [36-38]. Thus, it can be deduced that FTIR spectra elucidate the presence of organic groups in the plant extract, which are able to prevent the agglomeration process during the formation of nanoparticles.

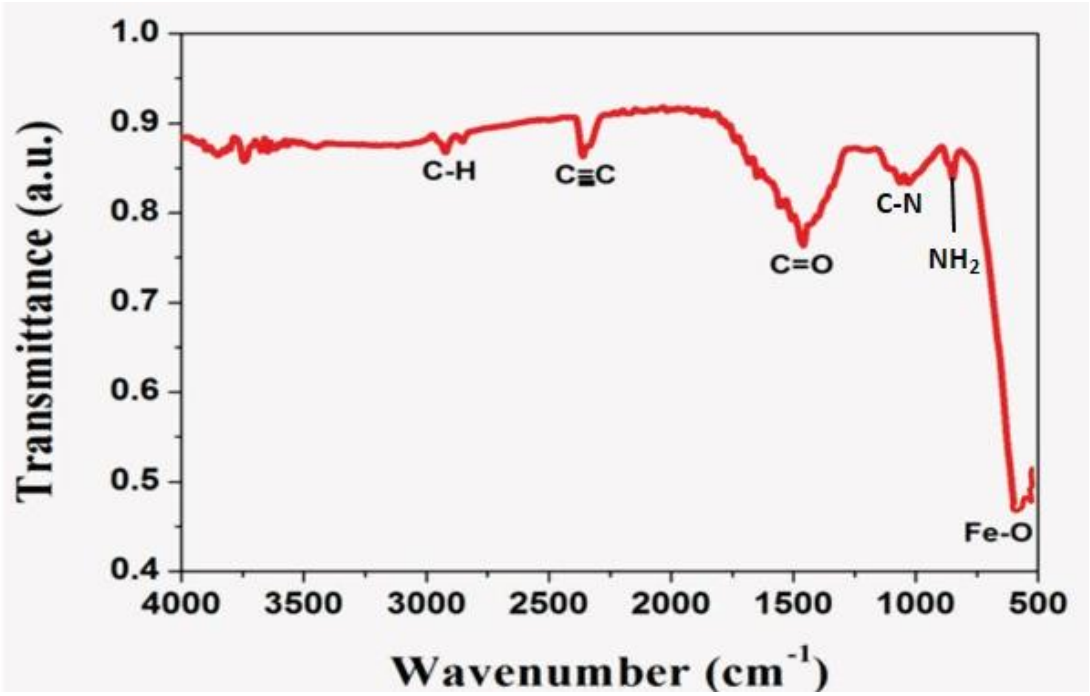

Fig. 6.5: FTIR spectra of green synthesized iron oxide nanoparticles

The UV-Vis absorption spectra of synthesized powder were recorded in the wavelength range 200 -1200 nm. The recorded spectrum is shown in Fig. 6.6(a), as shown in the figure, the peak at 210 nm reveals the prominent exciton band. The energy band gap has been determined using the tauc relation [39]. It is a convenient way of studying the optical absorption spectrum of a material. According to this relation

$$\alpha(h\nu)=B(h\nu-E_g)^n \qquad 6.3$$

where, α is the absorption coefficient, B is proportionality constant and has different values for different transitions, E_g *is* the energy band gap of sample material, *hν* is the photon energy and n is an exponent which assumes the values ½, 3/2, 2 and 3 depending on the electronic transition. For calculating direct band gap n=1/2 is substituted, whereas for indirect bandgap n=2 is substituted in above equation. To determine the direct band gap of the synthesized material, the graph of $(\alpha h\nu)^2$ versus *hν* has been plotted [39, 40]. The obtained Tauc plot is shown in Fig.6.6 (b).

Extrapolating the linear portion of the curve to the X-axis yields the band gap of the synthesized iron oxide nanoparticles. The evaluated band gap of iron oxide nanoparticles in this way was found to be 3.0eV, which is greater than that of bulk Fe_2O_3 (2.2 eV). Herein, band gap widening is clearly a prominent effect of quantum confinement. The obtained band gap in our study is well supported by previously reported literature [41, 42].

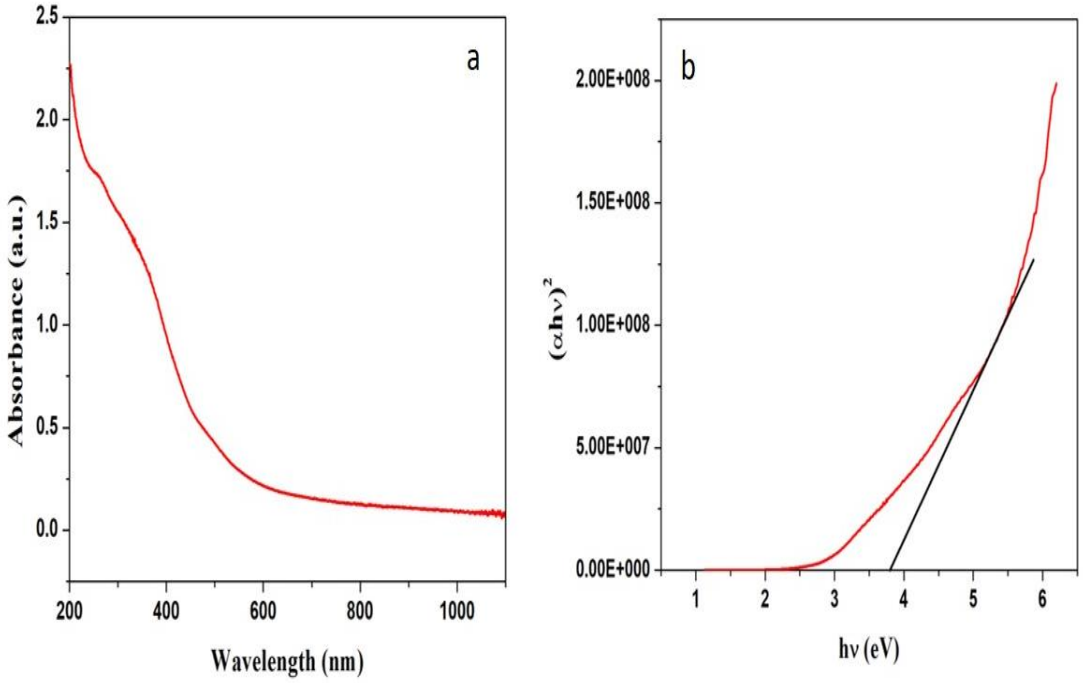

Fig. 6.6: UV absorption spectra **(a)** and Tauc plot **(b)** of green synthesized iron oxide nanoparticles

In recent years, concerns about the emergence of drug-resistant pathogenic bacteria have lead to the development of new antimicrobial agents. Various researches on iron oxide nanoparticles have demonstrated that they revealed antibacterial effect against gram-negative and gram-positive bacteria [43]. In this work, Agar well diffusion method was performed for screening the antimicrobial activity of synthesized nanoparticles. For the purpose, 20 ml of sterilized nutrient Agar was poured into sterile petri plate; after solidification, 100 µL of 24 h culture of *Escherichia*

coli was swabbed on each petri plates. Wells of 10 mm diameter were made in each plates using sterile cork borer. Now, iron oxide nanoparticles solution was prepared at a concentration of 100, 200,300,400 and 500 mg/ml. Subsequently, about 100 μL of different prepared solution were added to the wells. The plates were incubated at 30º C for 24 hours. After incubation the diameter of inhibitor zones was measured in mm and recorded. Fig.6.10 reflects that the iron oxide nanoparticles have antibacterial activity against *E. coli* and the activity increases with the increased concentration of nanoparticles. The possible reason for the bactericidal activity of iron oxide nanoparticles might be due to the presence of reactive oxygen species (ROS) generated by different nanoparticles [44]. Secondly, chemical interaction between iron oxide nanoparticles and membrane proteins or the outer bilayer of bacteria may be attributed to the antibacterial activity of nanoparticles. The hydrogen peroxide produced enters the cell membrane of bacteria and inhibits them [45]. Apart from this, another mechanism that the metal nanoparticles might adapt to kill bacteria is that the iron oxide nanoparticles possessing positive charges attack the bacteria having the negative charges which form the electromagnetic attraction between the bacteria and the nanoparticles [46]. This formation causes the bacteria to get oxidized and finally kill them.

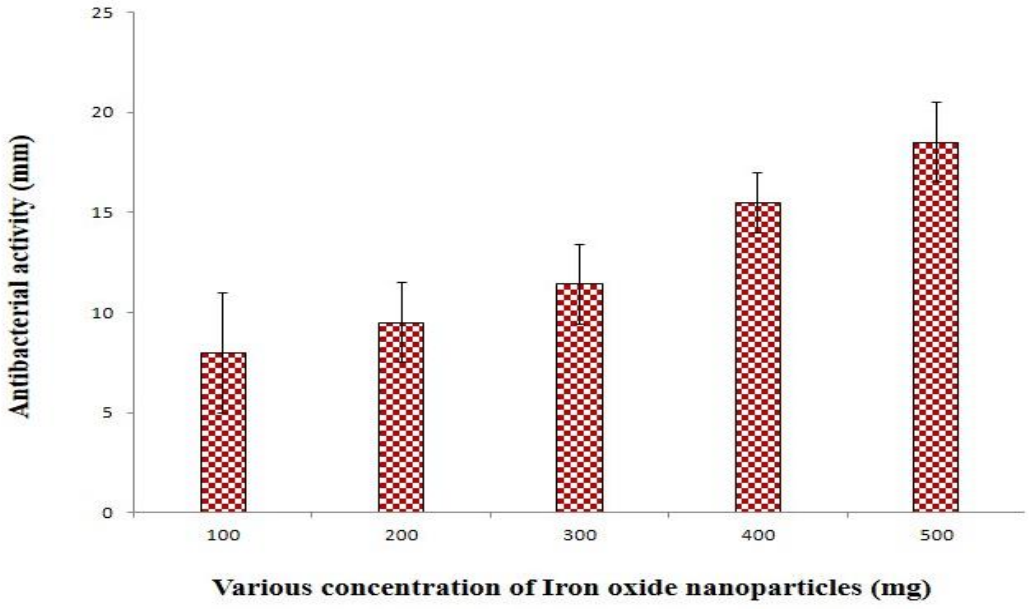

Fig. 6.7: Antibacterial activity (zone of inhibition, mm) of iron oxide nanoparticles solution against pathogenic *Escherichia coli*.

6.5. Conclusions

In the present study, iron oxide NPs were successfully synthesized utilizing the leaf extract of *Coriandrum sativum* through simple, low-cost and environmentally benign green chemistry route, and their structural, surface morphological, and optical properties were investigated. The average crystallite size of iron oxide NPs from XRD pattern was found to be 80 nm. Iron oxide NPs with diameter of 10–150 nm were confirmed from the FESEM images. FTIR spectrum analysis suggests that the carbonyl group present in leaf extract play a significant role in the reduction of ferric chloride ions. Furthermore, from antimicrobial activities evaluation against pathogenic bacteria *Escherichia coli*, it was found that synthesized iron oxide nanoparticles possess significant antimicrobial properties. The strongest efficiency was obtained at a dose 500 mg/ml of NPs. In this way, the prepared iron oxide NPs are amicable for the development of nanoparticles based antimicrobial drugs for the protection of public health.

References

[1] S. Shah, S. Dasgupta, M. Chakraborty, R. Vadakkekara, M. Hajoori, Green synthesis of iron nanoparticles using plant extracts, int. j. bio. & pharma. res. 6 (2014) 549-552.

[2] S. Duan, R. Wang, Bimetallic nanostructures with magnetic and noble metals and their physicochemical applications, Progress in Natural Science: Materials Int. 23 (2) (2013) 113-126.

[3] J.J. Vijaya, N. Jayaprakash, K. Kombaiaha, K. Kaviyarasu, L.J. Kennedy, R.J Ramalingam, H.A. Al-Lohedan, V.M. Mansoor-Ali, M. Maaza, Bioreduction potentials of dried root of *Zingiber officinale* for a simple green synthesis of silver nanoparticles: antibacterial studies, Journal of Photochemistry & Photobiology B: Bio. 177 (2017) 62-68.

[4] M. Ramesh, M. Anbuvannan, G. Viruthagiri, Green synthesis of ZnO nanoparticles using Solanum nigrum leaf extractand their antibacterial activity, Spectrochimica Acta Part A: Molecular and Bio. Spec. 136 (2015) 864-870.

[5] G. Sharmila, M.F. Fathima, S. Haries, S. Geetha, N.M. Kumar, C. Muthukumaran, Green synthesis, characterizationand antibacterial efficacy of palladium nanoparticles synthesized using Filicium decipiens leaf extract, J. of Molecular Struc. 1138 (2017) 35-40.

[6] H. Huawe, T. Gang, W. Yejing, C. Rui, C. G. Peng, C. Liqun, Z. Hua, Z. Ping, X. Qingyou, In situ green synthesis and characterization of sericin-silver nanoparticle composite with effective antibacterial activity and good biocompatibility, Mat. Sci. and Eng.: C. 80 (2017) 509-516.

[7] U. Hafeli, W. Schutt, J. Teller, M. Zborowski, Scientific and Clinical Applications of Magnetic Carriers, New York, Plenum, (1997), ISBN 978-1-4757-6482-6.

[8] L.C. Hsu, Y.Y. Li, C.G. Lo, C.W. Huang, G. Chern, Thermal growth and magnetic characterization of α-Fe_2O_3 nanowires, Journal of Physics D: App. Phy. 41 (2008) 185003.

[9] J.J. Guoa, R. Wanga, W.W. Tjiu, J. Pan, T. Liu, Synthesis of Fe nanoparticles @ grapheme composites for environmental applications, J. Hazard Mater. (63-73) (2012) 225-226.

[10] B. Dobosz, R. Krzyminiewski, G. Schroeder, J. Kurczewska, Electron paramagnetic resonance as an effective method for a characterization of functionalized iron oxide, Journal of Physics and Chemistry of Solid. 75(5) (2014) 594-598.

[11] D.K. Kim, Y. Zhang, W. Voit, K.V. Rao, J. Kehr, B. Bjelke, *M.* Mohamed, Superparamagnetic iron oxide nanoparticles for bio-medical applications, Scripta Mate. 44 (2001) 1713-1717.

[12] S. Saha, Bhunia, Synthesis of Fe_2O_3 Nanoparticles and Study of its Structural, Optical Properties, J. of Phy. Sci. 17 (2013) 191-195.

[13] S. P. Goutam, G. Saxena, V. Singh, A.K. Yadav, R.N. Bharagava, K.B. Thapa, Green synthesis of TiO_2 nanoparticles using leaf extract of *Jatropha curcas* L. for photocatalytic degradation of tannery wastewater, Chem. Eng. J. 336 (2018) 386-396.

[14] H.A. Salam, P. Rajiv, M.Kamaraj, P. Jagadeeswaran, S. Gunalan, R. Sivaraj, Plants: green route for nanoparticle synthesis, International Research Journal of Bio. Sci. 1(5) (2012) 85-90.

[15] S. Sun, C.B. Murray, D. Weller, L. Folks, A. Moser, Monodisperse FePt nanoparticles and ferromagnetic FePt nanocrystal superlattices, Science. 287(5460) (2000) 1989-1992.

[16] A. Carrubba, R. Torre, A.D. Prima, F. Saiano, G. Alonzo, Statistical analyses on the essential oil of Italian Coriander (*Coriandrum sativum* L.) fruits of different ages and origins, J. of Essential Oil Res. 14(6) (2002) 389-396.

[17] S. Ramezani, M. Rahamanian, R. Jahanbin, F. Mohajeri, M.R. Rezaeiand, B. Solaimani, Diurnal changes in essential oil content of Coriander (*Coriander sativum* L.) areal parts from Iran, Res. J. of Bio. Sci. 4 (2009) 277-281.

[18] N.A. Afifi, A. Ramadan, E.A. El-Kashoury, H.A. El-Banna, Some pharmacological activities of essential oils of certain umbelliferous fruits, Veterinary Medical Journal Giza. 42 (1994) 85-92.

[19] M. Mahdavi, F. Namvar, M. Bin Ahmad, R. Mohamad, Green biosynthesis and characterization of magnetic iron oxide (Fe_3O_4) nanoparticles using seaweed (*Sargassum muticum*) aqueous extract, Molecules. 18 (2013) 5954-5964.

[20] S. Filomena, F. Susana, A. Queiroz Joao, C. Domingues Fernanda, Coriander (*Coriandrum sativum* L.) essential oil: its antibacterial activity and mode of action evaluated by flow cytometry, J. of Med. Microbio. 60 (2011) 1479-1486.

[21] T. Shahwan, S. Abu Sirriah, M. Nairat, Green synthesis of iron nanoparticles and their application as a Fenton-like catalyst for the degradation of aqueous cationic and anionic dyes, Chem. Eng. J. 172(1) (2011) 258-266.

[22] L. Huang, X. Weng, Z. Chen, M. Megharaj, R. Naidu, Green synthesis of iron nanoparticles by various tea extracts: Comparative study of the reactivity, Spectrochimica Acta Part A: Mole. and Bio. Spect. 130 (2014) 295-301.

[23] Md. N. I. Bhuiyan, J. Begum, M. Sultana, Chemical composition of leaf and seed essential oil of Coriandrum sativum L. from Bangladesh, Bangladesh J. Pharm. 4 (2009) 150-153.

[24] A. Jr. Smania, F.D. Monache, E.D.F.A. Smania, R.S. Cuneo, Antibacterial activity of steroidal compounds isolated from Ganoderma applanatum (Pers.) Pat. (Aphyllophoromycetideae) Fruit Body, Inter. J. of Med. Mush. 1(4) (1999) 325-330.

[25] A.J. Das, R. Kumar, S.P. Goutam, S.S. Sagar, Sunlight Irradiation Induced Synthesis of Silver Nanoparticles using Glycolipid Bio-surfactant and Exploring the Antibacterial Activity, J. of Bio. & Bio. Sci. 6(5) (2016) 1-5.

[26] T. Theivasanthi, G. Venkadamanickam, M. Palanivelu, M. Alagar, Nano sized Powder of Jackfruit Seed: Spectroscopic and Anti-microbial Investigative Approach, Nano Bio. & Eng. 3(4) (2011) 1-6.

[27] H. Ping, Z. Shengen, W. Hua, P. De'an, T. Jianjun, T. Zhi, Alex A. Volinsky, Heat treatment effects on Fe_3O_4 nanoparticles structure and magnetic properties prepared by carbothermal reduction, J. of Alloys and Comp. 509(5) (2011) 2316-2319.

[28] W. Syinski, G. Mc Carthy, North Dakota state university, Fargo, North Dakota, USA, ICDD, Grant-in-aid (1990).

[29] P. Debye and P. Scherrer, Interferenzen an regellosen Teilchen im Rontgenlicht Teil III, Phys. Zeitschr. 18 (1917) 291-301.

[30] G.K. Williamson, W.H. Hall, X-ray line broadening from filed aluminum and wolfram, Acta Metall. 1 (1953) 22-31.

[31] P. Kour, S.K. Sinha, Studies of Sr^{2+} ion substitution on ferroelectric and piezoelectric properties of PZT nanocrystalline, Ceramica. 59 (2013) 34-38.

[32] S. Arokiyaraj, M. Saravanan, N.K. Udayaprakash, M. Valanarasu, B. Vijayakumar, S. Vincent, Enhanced antibacterial activity of iron oxide magnetic

nanoparticles treated with *Argemone mexicana* L. leaf extract: An in vitro study, Materials Res. Bulletin. 48(9) (2013) 3323-3327.

[33] W. Wu, Q. He, C. Jiang, Magnetic iron oxide nanoparticles: synthesis and surface functionalization Strategies, Nanoscale Res. Letters. 3 (2008) 397.

[34] G.S. Uthaya Kumar, J. Chanduru, S.A. Sivasubramanian, Asian J. of Biomed. and Pharma. Sci. 3(24) (2013), 12.

[35] R.B.G. Camara, L.S. Costa, G.P. Fidelis, L.T.D.B. Nobre, N.D. Santos, S.L. Cordeiro, M.S.S.P. Costa, L.G. Alves, H.A.O. Rocha, Heterofucans from the Brown Seaweed *Canistrocarpus cervicornis* with anticoagulant and antioxidant activities, Marine Drug. 9 (1) (2011) 124-138.

[36] P. Cambier, Infrared study of goethites of varying crystallinity and particle size: I. interpretation of OH and lattice vibration frequencies, Clay Minerals. 21 (1986) 191-200.

[37] B. Kumar, S. Kumari, L. Cumbal, A. Debut, Biogenic synthesis of iron oxide nanoparticles for 2-arylbenzimidazole fabrication, J. of Saudi Chem. Soc. 18(4) (2014) 364-369.

[38] S.V. Ganachari, V.K. Joshi, R. Bhat, R. Deshpande, B. Salimath, N.V.S. Rao, A. Venkataraman, Large scale synthesis and characterization of γ-Fe_2O_3 nanoparticles by self-propagating low temperature combustion method, International Journal of Science Research. 1(2) (2012) 77-79.

[39] J.C. Tauc, Optical Properties of Solids, *(*Amsterdam*:* North-Holland*)* 372 (1972)**.**

[40] S. Talam, S.R. Karumuri, N. Gunnam, Synthesis, Characterization, and Spectroscopic Properties of ZnO Nanoparticles, ISRN Nanotecnology. 2012 (2012) 1-6.

[41] M.F. Al-Kuhaili, M. Saleem, S.M.A. Durrani, Optical properties of iron oxide (α-Fe_2O_3) thin films deposited by the reactive evaporation of iron, Journal of Alloys and Compounds. 521 (2012) 178-182.

[42] A.J. Deotale, R.V. Nandedkar, Correlation between Particle Size, Strain and Band Gap of Iron Oxide Nanoparticles, Materials Today: Proceedings. 3 (2016) 2069-2076.

[43] T. Naseem, M.A. Farrukh, Antibacterial activity of green synthesis of iron nanoparticles using *Lawsonia inermis* and *Gardenia jasminoides* leaves extract, J. of Chem. 2015 (2015) 1-7.

[44] O. Yamamoto, Influence of particle size on the antibacterial activity of zinc oxide, Int. J. of Inorg. Materials. 3(7) (2001) 643-646.

[45] Y.T. Prabhu, K.V. Rao, B.S. Kumari, V.S.S. Kumar, T. Pavani, Synthesis of Fe_3O_4 nanoparticles and its antibacterial application, Int. Nano Letters. 5(2) (2015) 85-92.

[46] S. Rezaei-Zarchi, A. Javed, M.J. Ghani, S. Soufian, F.B. Firouzabadi, A.B. Moghaddam, S.H. Mirjalili, Comparative study of antimicrobial activities of TiO_2 and CdO nanoparticles against the pathogenic strain of *Escherichia coli*, Iranian J. of Path. 5(2) (2010) 83-89.

Chapter 7

Conclusions and Future Prospects

7.1 Conclusions

In this research work, metal oxide nanoparticles (TiO_2, CuO, ZnO and Fe_2O_3) were synthesized using plant leaf extract. Structural and optical properties of synthesized nanoparticles were anaylysed with the help of UV-Visible spectrophotometer, Field Emission Scanning Electron Microscopy (FESEM), X-ray Energy Dispersive Spectroscopy (EDS), Fourier Transform Infrared (FT-IR) spectroscopy, X-ray Diffraction (XRD), Dynamic Light Scattering (DLS), Brunauer-Emmett-Teller (BET) and Barret-Joyner-Halenda (BJH) analysis. Green synthesized nanoparticles were used to perform the experiment for their environmental and biomedical applications. On the basis of the obtained results during the reserch work, This study have some key conclusions which are summarized as follows:

(1) Present study suggest that the plant mediated methods of synthesizing metal oxide nanoparticles have proved to be one of the best methods till date. This is due to its cost effective , simple, efficient and eco-friendly nature.

(2) In present research work, experimental results showed an appreciable reduction in chemical oxygen demand (COD) and chromium (Cr) content of TWW treated with green synthesized TiO2 NPs during the photocatalytic treatment and thus, convincingly demonstrated the tremendous potential for wastewater treatment and brings a new direction to the development of nanomaterial-based next-generation wastewater treatment technologies to solve the problem of environmental pollution associated with industrial wastewaters.

(3) Green synthesized copper oxide nanoparticles using plant extract exhibited as good anticancer agent when conducted in-vitro cytotoxicological studies on hepatocellular carcinoma HepG2 cancer cell. The results shows that the green synthesized copper oxide nanoparticles can be used for the treatment of cancer which is the major threat to modern human society. Green synthesized CuO NPs showed the significant results on mammalian cell through killing of cancer cells without any evil effect on hepatocytes. So the CuO NPs synthesized by green chemistry approached, can be successfully applied for the treatment of liver cancer since it has sufficient transport properties and cell membrane penetration power.

(4) In this research work, FTIR results proved that bioamolecules from jatropha curcas leaf extract are responsible for bioreduction of titanium cholride and the leaf extract act as reducing and capping agents for the titanium di oxide nanoparticles which preventing the agglomeration of the nanoparticles and thereby stabilizing the nanoparticles.

(5) Present investigation also suggests that the green synthesized zinc oxide nanoparticles and iron oxide nanoparticles exerting in-vitro toxic effect on human bacterial pathogens Antibacterial studies. The Antimicrobial properties of synthesized nanoparticles were assessed against the bacterial species Escherichia coli and were found effective. Antibacterial efficacy of the prepared nano particles against the pathogenic bacteria E. coli reveals that the zinc oxide nanoparticles and iron oxide nanoparticles have considerably significant antibacterial potential.

7.2 Future prospcts

A number of new possibilities have come into account in relation to the use of green nanomaterials, owing to their biocompatibility and effectiveness. Key future prospects of the research work are summarized as follows:

(1) Green synthesized nanomaterials could emerge as future cancer therapeutics in the near future.

(2) More understanding of underlying reaction mechanisms of green approaches, better characterization techniques and data analysis will construct a solid foundation for ecofriendly and sustainable nanotechnology via green synthesis.

(3) In future, green synthesized nanomaterials can be utilized in adsorption of metal ion for the wastewater treatment purpose.

(4) Green synthesized nano materials also can be used as antimicrobial agent against various pathogenic bacteria.

(5) The efforts to improve the property profile of green synthesized nanomaterials still going on and hope that the overall performance in terms of wastewater treatment and antimicrobial activity will be further enhanced.

LIST OF PUBLICATIONS

Published Research papers:

1. **Surya Pratap Goutam**, Gaurav Saxena, Varunika Singh, Anil Kumar Yadav, Ram Naresh Bharagava, Khem B Thapa, Green synthesis of TiO_2 nanoparticles using leaf extract of Jatropha curcas L. for photocatalytic degradation of tannery wastewater, Chemical Engineering Journal. 336 (2018)386-396.
2. **Surya Pratap Goutam,** Anil Kumar Yadav, Amar Jyoti Das, "Coriander Extract Mediated Green Synthesis of Zinc Oxide Nanoparticles and their Structural, Optical and Antibacterial Properties", Journal of Nanoscience and Technology, 3 (2017), 249-252.
3. A.J. Das, R. Kumar, **Surya Pratap Goutam**, S.S. Sagar, Sunlight Irradiation Induced Synthesis of Silver Nanoparticles using Bio-surfactant and Exploring the Antibacterial Activity, J Bioengineer & Biomedical Sci. 6 (2016) 1-5.
4. **Surya Pratap Goutam**, Sarvesh Kumar Avinashi, Manju Yadav, Diptarka Roy, Rajkamal Shastri, Green Synthesis and Characterization of Characterization of Aluminium Oxide Nanoparticles Using Leaf Extract of Rosa, Advanced Science, Engineering and Medicine. 10 (2018)1-4.
5. Shikha Srivastava, **Surya Pratap Goutam**, Richa Srivastava, A. K. Yadav, B. C. Yadav, Synthesis of Titanium Dioxide (TiO_2) via Sol-Gel Method and Fabrication of Dye-Sensitized Solar Cell, Advanced Science, Engineering and Medicine. 10 (2018)1-4.
6. Rajkamal Shastri, Devesh Kumar, **Surya Pratap Goutam**, RR Yadav, Anil Kumar Yadav.Size Dependent structural , electronic and vibrational properties of CdmSn (m+n=2-6) nanoclusturs: A DFT study, International Journal of Advanced Research. 3 (2015) 787-798.

Book Chapters:

1. **Surya Pratap Goutam**, Gaurav Saxena, Diptarka Roy, Anil Kumar Yadav, Ram Naresh Bharagava, An invited book chapter entitled "Green Synthesis of Nanoparticles and their Applications in Water and Wastewater Treatment" for an edited book "Bioremediation of Industrial Waste for Environmental Safety-Volume I: Industrial Waste and its Management" has been accepted and contracted to publish by "Springer Nature" Singapore.
2. Gaurav Saxena, **Surya Pratap Goutam**, Akash Mishra, Sikandar I. Mulla, Ram Naresh Bharagava, Book chapter entitled "Emerging and Ecofriendly Technologies for Removal of Organic and Inorganic Pollutants from Industrial Wastewaters" for an edited book "Bioremediation of Industrial Waste for Environmental Safety-Volume II: Industrial Waste and its Management" has been accepted and contracted to publish by "Springer Nature" Singapore.

Communicated Research Papers:

1. **Surya Pratap Goutam,** Kamlesh Pandey, Anil Kumar Yadav, Rajesh Kumar, Amar Jyoti Das, Raj Kamal Shastri, Synthesis of Nanosized Iron Oxide by Leaf Extract of Coriandrum Sativum and their Antimicrobial Properties.
2. **Surya Pratap Goutam,** Diptarka Roy, Samir Mandal, Arijit Maiti, Jayita dan, Anil Kumar Yadav, Green Synthesis of Copper Oxide Nanoparticles Using Leaf Extract of Jatropha Curcas L. for Cytotoxicity Test in Hepatocellular Liver Carcinoma Cell Line HepG2.

Conferences (Oral/Poster) Presentations:

1. International Pharmaceutical conference-2015 on "Nano-formulations and Translational research: Small Getting Bigger" organized by Department of Pharmaceutical Sciences Babasaheb Bhimrao Ambedkar University, Lucknow, Uttar Pradesh, India on 2nd and 3rd February 2015.
2. Second International Conference, **Kathmandu** Symposia on Advanced Materials - 2014 (KASAM-2014), September 7-10, 2014 held in **Kathmandu, Nepal**.

3. 2nd Lucknow Science Congress, March 27-28, 2014, Babasaheb Bhimrao Ambedkar University, Lucknow, Leveraging Science and Innovation for development.
4. International Conference on Nanoscience and Nanotechnology-2013, November, 18-20, 2013, organized by Department of Applied Physics, School For physical sciences, Babasaheb Bhimrao Ambedkar University (A Central University) Vidya Vihar, Rae Bareilly Road, Lucknow-226025, Uttar Pradesh, India.
5. 6th IJAA-JSPS International Conference on "Contemporary Advances of Science and Technology (IC-CAST-2015), organized by Banaras Hindu University, Varanasi, India, during August 7-9, 2015.
6. 103rd Indian Science Congress held at University of Mysore from January 3-7, 2016.
7. 104th Indian Science Congress held at S.V. University Tirupati from January 3-7, 2017.
8. National Conference on "Application of high pressure "Techniques and novel materials in the frontiers of science" organized by National Centre of Experimental Mineralogy and Petrology, the University of Allahabad during October 25-26, 2013.
9. International conference on nanoscience and nanotechnology (ICNN-2017) organized by department of applied physics, school for physical sciences, Babasaheb Bhimrao Ambedkar University (A Central University), Lucknow-226025.
10. Characterization and Functionalization of nanomaterials (CFN-2015) Department of Physics, Banaras Hindu University, Varanasi-221005 (India), March-09-13, 2015, under UG networking program.
11. International Symposia on Advances in Materials Characterization (ISAMC-2014) July 14, 2014 organized by Department of Applied Physics, School For Physical Sciences, Babasaheb Bhimrao Ambedkar University (A Central University) Vidya Vihar, Raebareli Road, Lucknow-226025, Uttar Pradesh, India.

Chemical Engineering Journal 336 (2018) 386–396

Contents lists available at ScienceDirect

Chemical Engineering Journal

journal homepage: www.elsevier.com/locate/cej

Green synthesis of TiO_2 nanoparticles using leaf extract of *Jatropha curcas* L. for photocatalytic degradation of tannery wastewater

Surya Pratap Goutam[a], Gaurav Saxena[b], Varunika Singh[c], Anil Kumar Yadav[a,*], Ram Naresh Bharagava[b], Khem B. Thapa[a]

[a] *Advanced Materials Research Laboratory, Department of Applied Physics (DAP), School for Physical Sciences (SPS), Babasaheb Bhimrao Ambedkar University (A Central University), Vidya Vihar, Raebareli Road, Lucknow 226 025, Uttar Pradesh, India*

[b] *Laboratory for Bioremediation and Metagenomics Research (LBMR), Department of Environmental Microbiology (DEM), Babasaheb Bhimrao Ambedkar University (A Central University), Vidya Vihar, Raebareli Road, Lucknow 226 025, Uttar Pradesh, India*

[c] *Solar Energy Laboratory for Experimental Studies, Department of Environmental Sciences (DES), School for Environmental Sciences (SES), Babasaheb Bhimrao Ambedkar University (A Central University), Vidya Vihar, Raebareli Road, Lucknow 226 025, Uttar Pradesh, India*

GRAPHICAL ABSTRACT

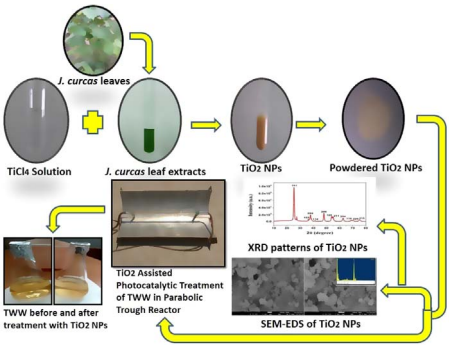

ARTICLE INFO

Keywords:
Green synthesis
Titanium dioxide
Tannery wastewater
Photocatalysis
Chromium
Chemical oxygen demand

ABSTRACT

Green synthesis is a simple, eco-friendly and emerging approach of synthesizing nanoparticles (NPs) and currently, attracting scientific community from around the world. The objective of the present study was to synthesize green titanium dioxide (TiO_2) NPs and evaluate its performance for the photocatalytic treatment of TWW after the secondary (biological) treatment process. TiO_2 NPs was synthesized using leaf extract of the biodiesel plant, *Jatropha curcas* L. in a one-step at room temperature to examine its treatability for tannery wastewater (TWW). Moreover, the green synthesized TiO_2 NPs was further characterized by UV–Visible spectrophotometer, Field Emission Scanning Electron Microscopy (FESEM), X-ray Energy Dispersive Spectroscopy (EDS), Fourier Transform Infrared (FT-IR) spectroscopy, X-ray Diffraction (XRD), Dynamic Light Scattering (DLS), Brunauer-Emmett-Teller (BET) and Barret-Joyner-Halenda (BJH) analysis. Results confirmed the synthesis and anatase phase of the spherical TiO_2 NPs and also unfold the presence of phytochemicals in leaf extract, which might involve in the capping/stabilization of NPs. Further, the green synthesized TiO_2 NPs was applied for the first time to testify its potential for the simultaneous removal of chemical oxygen demand (COD) and chromium (Cr) from secondary treated TWW. During the photocatalytic treatment of wastewater in a self-designed and fabricated Parabolic Trough Reactor (PTR), 82.26% removal of COD and 76.48% removal of Cr from TWW was achieved upon the treatment with green synthesize TiO_2 NPs, and thus, successfully employed for the

* Corresponding author.
E-mail address: akyadavbbau@gmail.com (A.K. Yadav).

https://doi.org/10.1016/j.cej.2017.12.029
Received 29 September 2017; Received in revised form 2 December 2017; Accepted 6 December 2017
Available online 07 December 2017
1385-8947/

J. Nanosci. Tech. - Volume 3 Issue 1 (2017) 249–252

Share Your Innovations through JACS Directory

Journal of Nanoscience and Technology

Visit Journal at http://www.jacsdirectory.com/jnst

ISSN: 2455-0191

Coriander Extract Mediated Green Synthesis of Zinc Oxide Nanoparticles and Their Structural, Optical and Antibacterial Properties

Surya Pratap Goutam[1], Anil Kumar Yadav[1,*], Amar Jyoti Das[2]

[1]*Advanced Materials Research Laboratory, Department of Applied Physics (DAP), Babasaheb Bhimrao Ambedkar University, Lucknow – 226 025, UP, India.*
[2]*Department of Environmental Microbiology, Babasaheb Bhimrao Ambedkar University, Lucknow – 226 025, UP, India.*

ARTICLE DETAILS

Article history:
Received 07 September 2017
Accepted 15 September 2017
Available online 02 October 2017

Keywords:
Coriandrum sativum
Zinc Oxide Nanoparticles
TEM
XRD
Antibacterial Activity

ABSTRACT

In this work, synthesis, morpho-structural characterization, optical and antibacterial properties of zinc oxide nanoparticles have been reported. Zinc oxide nanoparticles were prepared at room temperature via green route using *Coriandrum sativum* leaf extract. The product was characterized by X-ray diffraction (XRD), Transmission electron microscopy (TEM), Fourier transform infrared spectroscopy (FTIR), Scanning electron microscopy (SEM) with energy dispersive X-ray analysis (EDX) and UV-Visible spectroscopy to ascertain its formation. Morphology study indicates spherical nature of the nanoparticles and the formation of zinc oxide nanoparticles was confirmed by EDX. XRD analysis showed crystalline nature of the ZnO with wurtzite structure having average crystallite size of 60 nm which was also corroborated by SEM and TEM analyses. Furthermore, the estimated band gap was 3.8 eV as determined by UV-Visible spectral analysis. Antibacterial efficacy of the prepared nano particles against the pathogenic bacteria E. coli reveals that the ZnO nanoparticles have considerably higher antibacterial potential and is possibly due to a combination of events. Besides, the outcomes of the synthesis certainly contribute to the developing a better understanding of simple, low-cost, green and nontoxic synthesis method and growing the knowledge base needed to design a suitable antibacterial materials and framework for advanced and wise applications.

1. Introduction

In past few decades, generation of bacterial infection in industrial sectors including environmental, food, personal care products, synthetic textiles, packaging, healthcare, clinics, ;and public health threat due to emergence of resistance to antibiotics with their excess uses in bacteria have received worldwide attention of scientific community to develop new age antimicrobial agents, formulations and methods. Metal oxide nanoparticles exhibit remarkable biological applications and are of great interest for both fundamental research and technological development [1-8]. Several investigators are trying to develop the proper growth and processing techniques for the synthesis and to manipulate the features of metal oxide nanoparticles (Nps). Among the metal oxides, zinc oxide being a promising multifunctional material has stimulated intensive research interest due to its unique optical, electrical and chemical properties which is well exemplified by the number of previous articles. Having a large band gap (3.3 eV), large exciton binding energy, good transparency and high electron mobility, it is very useful material for the optoelectronic applications [3, 4]. It is worth noting that zinc oxide nanoparticles can be used in various applications such as biotechnology, drug delivery, medical, optical devices, DNA labelling, bio molecular detection, diagnostics [5] optoelectronics, nanogenerators, biosensors, solar cells, photocatalysts lubricants, rubber, photo detectors, cement ceramics sensors etc.,[6,7]. Furthermore, because of their large surface area these nanoparticles are used in waste water treatment [8] and in the removal of impurities like arsenic and sulphur from water or waste waters [9]. There are a number of chemical and physical methods reported in literatures for the preparation of nanoparticles of different sizes, shapes, and compositions which require high temperature, pressure, extremely expensive and toxic chemicals, hazardous reagents and nonpolar solvents, imposes an inordinate challenge before materials scientist [10, 11]. To overcome the limitations of these conventional methods, green synthesis has been emerged as an ecofriendly alternative for low-cost development of nanoparticles, which are highly efficient and biocompatible and can be used in a variety of applications [12-14]. It has been previously reported that among the different biological synthesis methods of nanoparticles plant-mediated synthesis are rapid, potentially advantageous and have more stability in various shape and size than the other organisms, as the microorganisms based synthesis is not of industrial viability due to necessity of multiple purification steps, highly aseptic conditions and their maintenance [15, 16]. A large number of plants have been reported in recent years for the synthesis of nanoparticles from the extract of various parts of plants such as eucalyptus hybrid, *Coriandrum sativum*, cycas, sorghum bicolor, *Azadiracthta indica*, *Cassia auriculata*, Camelliasinensis, Aloevera, Calotropisgigantea, *Nelumbo nucifera*, *Ocimum sanctum* and many more [17-25]. In this manuscript, ZnO nanoparticles were synthesized and stabilized using *Coriandrum sativum* (annual herb) leaf extract by the bio reduction method without using any harmful reducing and capping agent, and also different applications have been reported. Image of *Coriandrum sativum* leaves has shown in Fig. 1. *Coriandrum sativum* is a medicinal plant also known as “dhania” belongs to family Apiaceae [26, 27].

Fig. 1 Image of *Coriander sativum* leaves

2. Experimental Methods

2.1 Materials

Zinc acetate dihydrate and sodium hydroxide from Fisher Scientific (U.K.) were used in the experiments for the synthesis of zinc oxide nanoparticles. All the chemicals were of analytical reagent grade purity.

*Corresponding Author
Email Address: akyadavbbau@gmail.com (Anil Kumar Yadav)

Cite this Article as: Surya Pratap Goutam, Anil Kumar Yadav, Amar Jyoti Das, Coriander extract mediated green synthesis of zinc oxide nanoparticles and their structural, optical and antibacterial properties, J. Nanosci. Tech. 3(1) (2017) 249–252.

Journal of Bioengineering & Biomedical Science

Das et al., J Bioengineer & Biomedical Sci 2016, 6:5
DOI: 10.4172/2155-9538.1000208

Research article OMICS International

Sunlight Irradiation Induced Synthesis of Silver Nanoparticles using Glycolipid Bio-surfactant and Exploring the Antibacterial Activity

Amar Jyoti Das[1], **Rajesh Kumar**[1*], **Surya Pratap Goutam**[2] **and Sadhana Singh Sagar**[1]

[1]*Rhizospheric Biology Laboratory, Department of Environmental Microbiology, School for Environmental Sciences, India*

[2]*Department of Applied Physics, School of Physical sciences, Babasaheb Bhimrao Ambedkar (A Central) University, Vidya Vihar, Raibareli Road, Lucknow, India*

[*]**Corresponding author:** Rajesh Kumar, Rhizospheric Biology Laboratory, Department of Environmental Microbiology, School for Environmental Sciences, Babasaheb Bhimrao Ambedkar (A Central) University, Vidya Vihar, Raibareli Road, Lucknow-226 025 India, Tel: +91 9621329477; E-mail: rajesh_dem@bbau.ac.in

Received date: October 22, 2016; **Accepted date:** November 07, 2016; **Published date:** November 15, 2016

Abstract

In the present study, sunlight irradiation induced strategy for the rapid green synthesis of silver nanoparticles (AgNPs), is reported for the first time using glycolipid bio-surfactant. On exposing a mixture of silver nitrate solution and glycolipid bio-surfactant in the ratio 3:1 to sunlight, stable silver nanoparticles were obtained within few minutes. The glycolipid bio-surfactant acts as both reducing and stabilizing agents in the synthesis of nanoparticles. The nanoparticles synthesized were characterized using UV–Vis spectrophotometer, scanning electron microscopy and FTIR. Synthesized nanoparticles were in the range of 70-90 nm with spherical shape. The absorption spectroscopy indicates the band gap of silver nanoparticles was 3.4 eV. Further, the antibacterial activity assay of the synthesized nanoparticle exhibits as potential antibacterial agents. Hence, the present study demonstrates that biologically synthesized nanoparticle could be employed for developing antibacterial drug.

Keywords: Silver nanoparticles; Glycolipid bio-surfactant; Photo induced; Antibacterial agent

Introduction

Photo elicited reduction of nanoparticle strategies method gaining wide attention in recent years because of the subsequent advantages as the methods are more competitive and cost effective, controlled reduction of metal ions can be done without using excess of reducing agent and radiation is absorbed regardless of the radiation is absorbed in spite of the presence light absorbing solutes and products [1,2]. Biosurfactant are rising as a possible nanoparticles stabilizing agent, due to their non-toxic and eco-friendly nature. Silver nanoparticles (AgNPs), united of nanomaterial's of noble metals, have intensive applications in several fields. They are widely used as an additive for numerous materials and products including plastics, glass, cement, ceramics, lubricants, rubber, adhesives, paints, pigments, ointments etc. They can also be used for antistatic materials, antibacterial materials, biosensor materials and cryogenic superconducting materials [3,4]. Hence, in the present study attempt has been made for synthesis of silver nanoparticles using glycolipid bio-surfactant utilizing sunlight as the irradiation source.

Materials and Methods

Bio-surfactant production

Bio-surfactant used in the present study was produced by *Pseudomonas sp*. This strain was isolated from petroleum oil contaminated soil and stored in our laboratory at 4°C. For screening the bio-surfactant production different test were performed. Hemolytic assay was performed by streaking the bacterial strain onto blood agar plate [5,6]. Drop collapse test was performed in a 96-microwell plate [7]. Oil displacement test was determined by following the method of Ohno et al. [8]. For bio-surfactant production seventy two hours grown bacterial culture in mineral salt medium (composition g/l $MgSO_4$ -0.5, $(NH_4)_2SO_4$ -1, $NaNO_3$ -2.5, Na_2HPO_4 -6, K_2HPO_4-1.0, $FeCl_3$ -0.1, KH_2PO_4-1.0, $CaCl_2$ -0.01, $MnSO_4$ -0.005, dextrose -15) was centrifuged at 10,000 rpm, 4°C temperature for 20 minutes. Culture supernatant (crude bio-surfactant) obtained was transferred to empty beakers and stored at 4°C temperature.

Detection of glycolipids by phenol H_2SO_4 method

Glycolipids production was detected according to the method Dubois et al. [9]. Briefly, 1 ml of 5% phenol was added to small amount of crude bio-surfactant. To above mixture, 4 ml of concentrated H_2SO_4 was added drop by drop. Colour change was observed; development of yellow to orange color indicated the presence of glycolipids.

Synthesis of silver nanoparticles

For the synthesis of silver nanoparticles, 2ml of crude bio-surfactant was mixed with 6 ml of 0.001 M of silver nitrate solution. The reaction mixture was then placed in direct sunlight on a bright sunny day for different time periods to determine the minimum interaction time [10]. Same volume of silver nitrate solution is considered as control. The study was carried out in the summer months of May to June at, Lucknow, India having the temperature of ranging from 42°C to 45°C. After 25 to 30 minutes of reaction in sunlight changes in colour of the samples indicates the synthesis of nanoparticles. After then change in color of the solution the reaction mixture containing the nanoparticles was centrifuged for 10 min at 10,000 rpm and pellet received was re-dispersed in deionized water [10].